A thesis presented to the Faculty of Science

Doctoral Thesis

Astrophysical and cosmological constraints on parameters of hypothetical particles

VSEVOLOD SYVOLAP

sivolapseva@gmail.com

Supervisor: Dr. Prof. Oleg Ruchayskiy

April, 2021

"The nitrogen in our DNA, the calcium in our teeth, the iron in our blood, the carbon in our apple pies were made in the interiors of collapsing stars. We are made of starstuff."

Carl Sagan, 1980

"Nature uses only the longest threads to weave her patterns, so that each small piece of her fabric reveals the organization of the entire tapestry."

Richard P. Feynman

Abstract

The Standard Model of particle physics describes the properties of the most fundamental constituents of matter – elementary particles. This model has been put to numerous consistency tests and all its major predictions have been experimentally confirmed. Nevertheless it has been firmly established that several *observed* phenomena do not find their explanation within the Standard Model. Among these phenomena are: the origin of neutrino masses and of neutrino oscillations; a mechanism of violation of matter-antimatter symmetry in the early Universe; and the existence of dark matter. These phenomena mean that the list of fundamental particles will extended one day beyond the 17 particles known today.

It is possible that new particles may have masses similar to those of known elementary particles and very weak interaction strength (otherwise they would have been discovered long ago). Dedicated experiments with high intensity of interactions and sensitive detectors are required to discover these *feebly interacting particles*. Such particles can also be copiously produced in cosmic environments where temperatures and matter densities are enormous as compared to laboratory experiment. This thesis analyses cosmic bounds for a particular class of such feebly interacting particles – sterile neutrinos (or "heavy neutral leptons").

In the first part of the thesis a new mechanism of sterile neutrino production in the interiors of exploding supernovae is considered. This mechanism drastically increases the efficiency of production. Surprisingly this does not lead to stringent bounds on sterile neutrino parameters, given the scarcity of the observational data and many "unknowns" about the details of supernovae explosion.

In the second part of the thesis, the interaction of sterile neutrinos with primeval plasma is analysed. The presence of extra particle species in the primordial plasma changes the dynamics of the Universe and in particular affects the yield of primordial Helium-4 – second most abundant chemical element in the Universe. The thesis discusses a novel effect that arises from sterile neutrino interaction with primordial plasma. This effect significantly changes the existing bounds on the properties of sterile neutrinos that stood untouched for 20 years. Using the same machinery the influence of sterile neutrinos on the global expansion of the Universe is analysed. The limits on the lifetime of sterile neutrinos from the measurements of the anisotropies of Cosmic Microwave Background are derived. It is also demonstrated that while sterile neutrinos can reduce the observed tension between the Hubble constant measurements from late-time and early-time probes, it cannot fully alleviate this tension.

The final part of the thesis analyses how the parameter space, accessible to the future intensity frontier experiments changes in view of our new results.

Abstrakt

Standardmodellen for partikelfysik beskriver de mest egenskaber grundlæggende bestanddele af stof - elementære partikler. Denne model er blevet sat til adskillige konsistensforsøg, og alle dens vigtigste forudsigelser er blevet bekræftet eksperimentelt. Ikke desto mindre er det fastslået, at flere observerede fænomener ikke finder deres forklaring inden for standardmodellen. Blandt disse fænomener er: oprindelsen af neutrino-masser og af neutrino-svingninger en mekanisme til krænkelse af materie-antimaterie-symmetri i det tidlige univers; og eksistensen af mørkt stof. Disse fænomener betyder, at listen over grundlæggende partikler udvides en dag ud over de 17 partikler, der er kendt i dag.

Det er muligt, at nye partikler kan have masser svarende til kendte elementære partikler og meget svag interaktionsstyrke (ellers ville de være blevet opdaget for længe siden). Der kræves dedikerede eksperimenter med høj intensitet af interaktioner og følsomme detektorer for at opdage disse svagt interagerende partikler. Sådanne partikler kan også produceres rigeligt i kosmiske omgivelser, hvor temperaturer og stofdensiteter er enorme sammenlignet med laboratorieeksperimenter. Denne afhandling analyserer kosmiske grænser for en bestemt klasse af sådanne svagt interagerende partikler - sterile neutrinoer (eller " tunge neutrale leptoner ").

I den første del af afhandlingen overvejes en ny mekanisme til steril neutrino-produktion i det indre af eksploderende supernovaer. Denne mekanisme øger produktionseffektiviteten drastisk. Overraskende nok fører dette ikke til strenge grænser for sterile neutrino-parametre i betragtning af knapheden på observationsdataene og mange " ukendte " om detaljerne i eksplosion af supernovaer.

I anden del af afhandlingen analyseres interaktionen mellem sterile neutrinoer med ural plasma. Tilstedeværelsen af ekstra partikelarter i urplasmaet ændrer universets dynamik og påvirker især udbyttet af ur Helium-4 - det næstmest forekommende kemiske element i universet. Specialet diskuterer en ny effekt, der stammer fra steril neutrino-interaktion med urplasma. Denne effekt ændrer markant de eksisterende grænser for egenskaberne ved sterile neutrinoer, der stod uberørt i 20 år. Ved hjælp af det samme maskineri analyseres sterile neutrinos indflydelse på den globale ekspansion af universet. Grænserne for levetid for sterile neutrinoer fra målingerne af anisotropierne af kosmisk mikrobølgebaggrund er afledt. Det er også demonstreret, at mens sterile neutrinoer kan reducere den observerede spænding mellem Hubble-konstante målinger fra sene tidlige og tidlige tidssonder, kan det ikke lindre denne spænding fuldt ud.

Den sidste del af afhandlingen analyserer, hvordan parameterrummet, der er tilgængeligt for fremtidige intensitetsgrænseeksperimenter, ændrer sig i lyset af vores nye resultater.

Contents

List of publications

- Alexey Boyarsky, Maksym Ovchynnikov, Nashwan Sabti, **Vsevolod Syvolap**, "When FIMPs Decay into Neutrinos: The Neff Story", 2103.09831 , Submited to Phys.Rev.D

- Kyrylo Bondarenko, Alexey Boyarsky, Juraj Klaric, Oleksii Mikulenko, Oleg Ruchayskiy, **Vsevolod Syvolap**, Inar Timiryasov "An allowed window for heavy neutral leptons below the kaon mass", 2101.09255 ,

- Alexey Boyarsky, Maksym Ovchynnikov, Oleg Ruchayskiy, **Vsevolod Syvolap**, "Improved BBN constraints on Heavy Neutral Leptons 2008.00749 submitted to Phys.Rev.Letters

- Vsevolod Syvolap, Oleg Ruchayskiy, Alexey Boyarsky, "Resonance production of keV sterile neutrinos in core-collapse supernovae and lepton number diffusion" 1909.06320, Submitted for Phys.Rev.D "

Introduction

1.1 Need for new physics beyond the Standard Model

The Standard Model has been enormously successful in providing a self-consistent picture of elementary particle physics and interactions. It has passed many consistency tests in earth-based collider experiments. However the complete set of observables including cosmological and astrophysical observations still speaks of its incompleteness. Such inconsistencies between the Standard Model (SM) and the observable data are usually referred to as *Beyond Standard Model* (BSM). Such unexplained phenomena include: *the existence of dark matter; the origin of neutrino masses; matter-antimatter asymmetry of the Universe; the origin of dark energy*. Besides these phenomena, there exist potential experimental evidence for new physics whose statistical significance is insufficient at the time of writing to call them "BSM phenomena" (*e.g.* anomalous magnetic moment of muon [10]). In addition to observational evidence, there are deep theoretical questions related to the origin and structure of the SM, so called "*fine-tuning problems*", including in particular the strong CP problem; the difference between electroweak and Planck scales, as well as our inability to consider gravity on equal field-theoretical footing with other interactions, *etc*. Finally, SM possesses a number of unexpected and unexplained relations between different parameters such as *e.g.* Koide formula [188] or [81]. While not a problem *per se* it may be hinting at some common origin of the seemingly random parameters of the SM.

In this thesis we are concentrating on the first three *observational* problems that are the most unambiguous hints that new particles and interactions should exist.

1.1.1 Dark matter

The term *dark matter* (DM) [213] refers to a broad set of astrophysical and cosmological observations, including [55, 173]:

- Rotational curves of galaxies [49] – radial distribution of velocities of stars rotating around the galactic center can not be explained by the observed (*luminous*) matter distribution in galaxy assuming classical Newton gravity

- Bullet cluster observations (*e.g.* [171, 85, 72]) – a unique observation of two colliding clusters of galaxies passing through each other. Hot gas components of both clusters are emitting X-rays, making the gas visible. Interactions between the gas components of two clusters cause the gas distribution to be shifted from the centers of gravity of the corresponding clusters. At the same time, according to the gravitational lensing maps, the mass distribution follows that of the collisionless stars. This indicates that most of the galaxy clusters' mass comes from some collisionless substance.

- Cosmic microwave background observations [15] indicate that while photons and baryons were still a coupled substance, some unknown structure was experiencing the Jeans instability, collapsing into primordial overdensities. This substances is not coupled to photons/baryons and therefore does not experience pressure. The cosmological numerical simulations of large scale structure and of galaxy formation confirm that such processes would occur very differently from what we observe now if only baryonic matter[1] was present.

All of these phenomena can be explained by postulating the presence of some kind of "hidden" matter – something that is sufficiently massive and does not

---

[1] In cosmology by baryonic matter one means any forms of the usual matter: atoms, electrons, ions

interact with ordinary matter. No SM particles (not even neutrinos) can serve as dark matter. Therefore a new particle – a dark matter candidate – has to be postulated.[2]

For a particle to be a viable dark matter candidate, it should obey the following properties:

1. Dark matter should be present in the Universe from the early times, when the structure formation started and survive until nowadays, affecting the evolution of the Universe and its structure throughout cosmic historis. Hence, the life-time of dark matter particle has to be of the order or longer than the age of the Universe $\tau_{\mathrm{DM}} \gtrsim t_{\mathrm{univ}} \sim 10^{10}$ y. Note, that there might still be stable or (slowly) decaying DM particles.

2. According to the simulations of structure formation ([238, 189]) DM particles have to be non-relativistic, when formation started. The structures are then formed in the bottom-up manner (the smallest structures collapse first). This is one of the reasons why active neutrinos could not constitute DM. For a specific DM generation mechanism this can constrain the DM mass.

3. In the case of fermion dark matter, there is a robust bound on the minimal mass of DM from the phase-space considerations [68]. The Pauli exclusion principle does not allow fermions to occupy the same state in the phase space, hence there is a limit on total number density of DM particles [220].

With all those restrictions there is still a lot of space for different parameters of hypotetical particles that could serve as a DM candidate.

---

[2]An alternative, non-particle, hypothesis could be modification of the laws of gravity and/or of Newtonian dynamics (see *e.g.* [112, 84] for review). Such a modification, however, is not able to account for all the observed phenomena especially taking into account necessity to explain the Bullet cluster structures [84]. Hence we will stick with the particle dark matter hypothesis.

1.1.2 Neutrino masses and neutrino oscillations

Neutrino oscillations – transition of neutrinos of one flavour to another, $\nu_e \leftrightarrow \nu_\mu \leftrightarrow \nu_\tau$ – have been observed by many experiments, including Solar neutrinos [83], atmospheric neutrinos ([114]), reactor neutrinos detection [28, 22, 103] and neutrinos from accelerator experiments ([13, 9, 161]). Oscilaltion phenomenon requires at least two of three neutrinos to have a mass (for a review see [242]). The standard treatment of particle oscillation in quantum mechanics tells that the flavour (charge) states (ν_e, ν_μ, ν_τ) not to have a definite mass. While the states that do have one, need to be mixed from three flavour states. A mixing pattern between different flavours is encoded into a PMNS (Pontecorvo-Maki-Nakagawa-Sakata) matrix [159, 177, 178]. The only way to have neutrino mass term within the SM is to introduce a 5-dim non-renormalizable operator ("Weinberg operator" [228]). This means that SM becomes an effective field theory and the presence of higher-dimentional operator is an indication of new physics (in analogy of Fermi theory of weak interactions), possibly at high energies. This means that new particles are required to make neutrinos massive.

1.1.3 Baryon asymemtry in the Universe

The Standard Model does not distinguish particles over antiparticles. Yet in the universe we observe an asymmetry between matter and antimatter. While historically first antiparticles were detected in cosmic rays [29], we understand today that all antimatter that we observe (see *e.g.* [19] are produced in cosmic ray interactions rather than being primordial). Thus, we do not detect any primordial antimatter or antiparticle structures. Given the standard cosmological history, this is possible only if there was a small asymmetry between particles and antiparticles in the universe.

The quantitative measure of the asymmetry, defining how much particle number density exceeds the antiparticle number related to photons – baryon-to-photon ration – has a very low value [14]

$$\eta_B \equiv \frac{n_b - n_{\bar{b}}}{n_\gamma} \approx (6.05 \pm 0.07) \times 10^{-10} \qquad (1.1)$$

which states, that at the earliest stages of Universe evolution, there was only 1 particle more, than anti-particle for each billion of them. It should be noted, that this relation is applicable for the *baryon matter* and charged leptons, which number density is tightened by the electro-neutrality of the Universe, as those types of matter we can directly observe with large accuracy. But this can not be applied for neutrinos, the cosmological neutrino background $C\nu B$ can in principle have sizeable asymmetry between neutrinos and antineutrinos as for now it is unobservable due to extremely low energies of relic neutrinos. This problem can not be solved within the SM [80] and any new physics is required to satisfy three *Sakharov conditions* [195], to be a valid solution.

1.2 Three frontiers of exploration

The beyond-the-Standard-Model phenomena (as outlined above) are well established and indicate that new particles (and maybe even new types of interactions) should exist. At the same time, there are no clear indication as to what kinds of particles/interactions can be responsible for resolution of these BSM phenomena. Of course, there are so called "experimental anomalies" (discrepancies/mismatches at $3 - 4\sigma$ level between experiments or between data and prediction)[3] and each of them may become a new established signal beyond-the-Standard model. But even if these or other experimental anomalies will become well-established BSM phenomena, we will not be able to tell what particles are behind them.

Broadly speaking, new particles have escaped our detections either because they are too heavy (with masses higher than the energy reach of the LHC) or because they interaction strength is smaller than that of weak interactions. Such super-weakly (these days the name "*feebly*" gets used more and more, see e.g. [17]) do not necessarily need to be heavy to stay undetected. The situation is graphically depicted in Figure 1.1 — where a schematic space of "mass vs. interaction" is shown. All known particles are then gathered in the left upper corner of the parameter space, indicating that they are interacting at least weakly. GeV, MeV or even keV-scale particles, interacting with the SM sector with a sufficiently suppressed interaction strength, could have escaped

---

[3]At the time of writing one can mention *Hubble tension* in cosmology [93]; anomalous magnetic moment of muon [10]; violation of lepton universality in B-meson decays [1].

our detectors unnoticed (or has never been produced in sufficient quantities to be distinguished from SM backgrounds). They can occupy region below the diagonal line. In spite of being feebly interacting they still can be the ones, responsible for resolution of the BSM phenomena.

Different kinds of experiments are required to search for particles of different masses and interaction strengthes. The existing approaches can roughly be combined into several groups.

1. **Energy frontier** – increasing the energy of particle collisions beyond that of the Large Hadron Collider. New heavy particles can be *discovered* in this way. Potential future experiments include FCC-hh [3], CLIC [82], CEPC [100] and ILC [43], see the European Strategy for Particle physics report [107] for discussion of their comparative science reach, capabilities, etc.

2. **Intensity frontier** – increasing intensity of collisions and/or creating detectors sensitive to rare events. This can be done both within the scopes of existing experiments (as *e.g.* during the high-luminosity phase of the LHC [199] or NA62 [160]), with the new dedicated experiments (see the list in *e.g.* [47, 107]).

3. **Cosmic frontier** is different from the previous two approaches, because in this case the "experiments" themselves are not human-made and therefore the "experimental environments" are not controllable. On the other hand, cosmic frontier enables for us physical conditions unimaginable on Earth and therefore their use can be complementary to the ground-based experiments.

This thesis explores limits on hypothetical feebly interacting particles coming from cosmic frontier. The obtained results allow to constrain particle physics models and even have consequences for the future particle physics experiments at intensity frontier. This demonstrates the complementarity of three frontiers and the power of the cosmic frontier exploration.
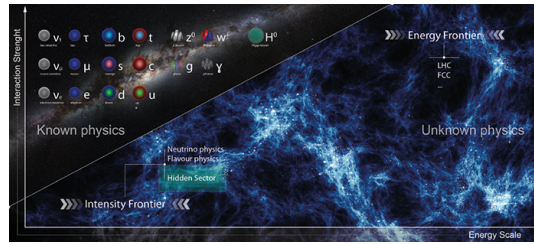
Figure 1.1: Known and unknown particles. All SM particles have masses below $200\,\mathrm{GeV}$ and interact at least via weak interaction. New particles may either be (much) heavier – moving rightwards on the above figure – or may have weaker-than-weak interaction strength with the SM particles – moving downwards in Figure above. Image credit: Richard Jacobsson and Daniel Dominguez. CERN Courier. February 2016.
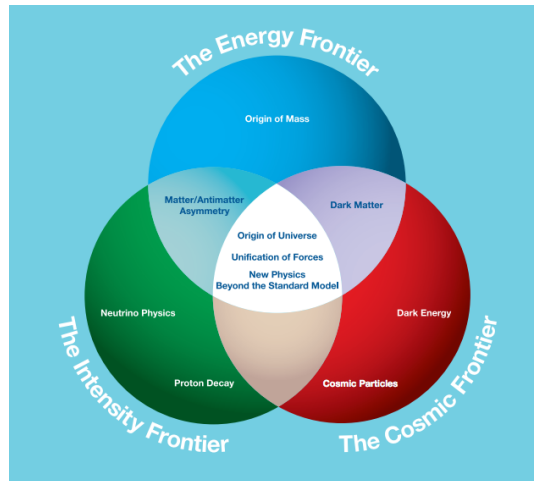
Figure 1.2: To enable discoveries of new particles, all of the three frontiers should be pushed forward. *Energy frontier* is advanced by increasing the energy of colliding particles, beyond that attained at the Large Hadron Collider in CERN. *Intensity Frontier* is pushed by experiments with high intensity particle beams and sensitive large detectors, tuned for searching for rare events. The high intensity beams do not necessarily need to have high energy of particles, as many viable BSM models predict new particles below GeV scale. Finally, the *Cosmic Frontier* uses cosmic environments as "poor man's accelerators". Energies, intensities, temperatures, densities, etc. reachable in these environments are often superior to those in the human-made laboratories. Unfortunately, cosmic "experiments" are beyond our control and we have to analyse the data, trying to marginalize over vast variety of astrophysical and cosmological "unknowns". Figure from [132] is taken for illustrative purposes, variety of options for each frontier are far greater than depicted, see *e.g.* [107].

Heavy neutral leptons

2.1 General properties

One of the promising extension of the Standard Model, capable of incorporating neutrino oscillations is the model with several right-handed neutral particles, that are singlets with respect to the SM gauge group $SU_c(3) \times SU(2) \times U_Y(1)$ [163, 237, 119, 165, 198, 197]. These particles play a role of right-helicity partners of active $(\nu_e, \nu_\tau, \nu_\mu)$ neutrinos. Owing to the absence of SM gauge charges they are called *sterile neutrinos*. The simplest Lagrangian of the theory (called *type I seesaw* model) has the form[1] (for reviews see *e.g.* [71, 25, 242]):

$$\mathcal{L}_{\nu MSM} = \mathcal{L}_{SM} + i\bar{N}_I \partial_\mu \gamma^\mu N_I - \left(\frac{M_I}{2} \bar{N}_I^c N_I + F_{\alpha I} \bar{l}_\alpha N_I \tilde{\Phi} + h.c. \right) \qquad (2.1)$$

Where $\mathcal{L}_{SM}$ is the Standart model Lagrangian, l_α - left-handed lepton doublets (α enumerates lepton generations so runs through values e, μ, τ), M_I - three Majorana masses, $\tilde{\Phi}_i = \epsilon_{ij}\Phi_j$ – the conjugated Higgs doublet that allows to "distinguish" neutrino from the charged lepton component in l_α, N_I are several *right*-chiral fermion fields, $(I = 1, 2, \ldots, \mathcal{N})$. The matrix $F_{\alpha I}$ is the $3 \times \mathcal{N}$ matrix of (in general complex) Yukawa couplings. The symbol N_I^c means *charge-conjugation* of the spinor N_I and thus the term $\bar{N}_I^c N_I$ denotes the Majorana mass term that can be added to the theory because spinors N_I carry no charges. The sum over indexes I, α is assumed.

---

[1]Here and in following we will use Heaviside system, where $\hbar = c = k = 1$.

Sterile neutrinos N_I interact with the SM sector only through mixing with active neutrinos as they are not coupled to any gauge boson. Mixing with active neutrinos is governed by Yukawa interaction terms $F_{\alpha I}\bar{l}_\alpha N_I \tilde{\Phi}$.

The Lagrangian (2.1) has $7\mathcal{N} - 3$ independent real parameters, $\mathcal{N}$ Majorana masses M_I and $6\mathcal{N} - 3$ dimentionless elements of Yukawa matrix $F_{\alpha I}$ (angles and phases) – parameters, that define mixing properties.

After the electroweak $SU(2) \times U(1) \to U(1)$ symmetry breaking, the Yukawa interaction terms turn into the ordinary Dirac mass:

$$F_{\alpha I}\bar{l}_\alpha N_I \tilde{\Phi} \to \frac{F_{\alpha I}v}{\sqrt{2}}\bar{\nu}_\alpha N_I \tag{2.2}$$

where $v = 246\,\text{GeV}$ is the vacuum expectation of the Higgs field. We can therefore introduce the matrix of Dirac masses $M_D = F_{\alpha I} \cdot \frac{v}{\sqrt{2}}$. the Yukawa couplings can be chosen smaller compared to the Majorana masses M_I.

The ratio of the Dirac to Majorana masses defines the mixing strength between sterile and active neutrinos, called *mixing angle*

$$\Theta_{\alpha I} \equiv \frac{v^2 |F_{\alpha I}|^2}{M_I^2}, \qquad \theta_I^2 \equiv \sum_{\alpha = e, \mu, \tau} \frac{v^2 |F_{\alpha I}|^2}{M_I^2} \tag{2.3}$$

For $|F_{\alpha I}v| \ll |M_I|$ one finds after the diagonalization of the mass matrix in Eq. (2.1), 3 light mass eigenstates ν_i with masses m_1, m_2, m_3 and $\mathcal{N}$ heavy mass eigenstates (that we will call by the same name, N_I) with masses $\approx M_1, \ldots, M_{\mathcal{N}}$. As a consequence, the flavor eigenstates (SM or *active* neutrinos) ν_α can be expressed as a linear combination of the $3 + \mathcal{N}$ *mass eigenstates* of the Lagrangian (2.1):

$$\nu_\alpha = \sum_{i=1}^{3} V_{\alpha i}^{\text{PMNS}} \nu_i + \sum_{I=1}^{\mathcal{N}} \Theta_{\alpha I} N_I^c, \tag{2.4}$$

where V^{PMNS} is the PMNS matrix [56, 111] and $\Theta_{\alpha I}$ are similar *mixing angles* between SM and sterile neutrinos.

The active neutrino mass matrix is given then by the famous *seesaw formulat*:

$$(m_\nu)_{\alpha\,\beta} = -\sum_{I=1}^{\mathcal{N}} (M_D)_{\alpha I} \frac{1}{M_I} (M_D^T)_{I\beta} \tag{2.5}$$

and the light masses $m_1 \ldots m_3$ are its eigenstates.

Similarly, the heavy mass eigenstates, having Majorana masses approximately equal to M_I contain small *admixture* of SM neutrinos ν_α (proportional to the same $\Theta_{\alpha I}$).[2] and therefore they inherit "neutrino-like" interactions (analogs of charged and neutral currents of weak interactions), suppressed by $\Theta_{\alpha I} \ll 1$.

2.1.1 Naming conventions

New particles N_I have many names. Owing to the way they were introduced they are called *right handed neutrinos*. Owing to the absence of gauge charges they are called *sterile neutrinos*. Due to the fact that they possess neutrino-like interactions they sometimes are called *heavy (Majorana) neutrinos* or *heavy neutral leptons* (HNLs). Strictly speaking the name HNL or "heavy Majorana neutrino" should be reserved for the mass eigenstate, while the name "sterile neutrino" should be used for the flavour states, but this distinction is rarely observed and the naming conventions rather depend on the field: cosmologists and neutrino physicists usually speak about "sterile neutrino"s, while particle physicists refer to "heavy neutral leptons". We will use both names interchangeably, having this distinctions in mind.

2.2 How sterile neutrinos can alleviate BSM problems

Neutrino experiments have measured two neutrino mass splittings [111], meaning that at least two of the 3 neutrino masses are non-zero. For $\mathcal{N} \geq 2$ the Lagrangian (2.1) has more free parameters that can be fixed by neutrino oscillation experiments. Therefore, it can comfortably explain neutrino masses and oscillations and some of the parameters *remain unfixed*. In particular, masses M_I are not constrained by the neutrino data, owing to the seesaw relation (2.5) where we can always rescale $M_D \to z M_D$ simultaneously with $M_I \to z^2 M_I$ without changing the matrix $m_{\alpha\,\beta}$. The number of free parameters

---

[2]With some abuse of notation we call both sterile (flavour) eigenstates and heavy mass eigenstates N_I. This is justified by the fact that the two states coincide (up to $\mathcal{O}(\Theta_{\alpha I})$ corrections.

for $\mathcal{N} = 2$ is equal to 4 (2 HNL Majorana masses, 1 CP phase and 1 ratio of Yukawa terms). The number of free parameters for $\mathcal{N} = 3$ is equal to 9 and includes apart from 3 HNL Majorana masses some ratios of Yukawa couplings, owing for example to the symmetry of the seesaw relation (2.5): $F_{\alpha\,I} \to F_{\alpha\,J}(M_I/M_J)^{1/2}$ for $I \neq J$.

The HNL masses can be fixed from purely "pragmatic" considerations – each mass range demands its own search strategy [see *e.g.* 209, 39, 25]. Thus for each mass range one can analyse available experiments and determine whether seesaw predictions can be tested.

Although seesaw mechanism does not impose the limits on the mass directly, the Majorana mass can be constrained by extra theoretical considerations. As HNLs interact with the Higgs boson, the corresponding quantum corrections to the Higgs mass from HNLs running in the loops, together with the seesaw formula leads to the upper limit $M_I \sim 10^7$ GeV [224]

It is much more attractive, however, to ask whether HNls can solve more than one existing BSM problem. It is interesting to consider this probability not only from the point of view of our attempt to keep a model of elementary particle physics as simple as possible, but also because it imposes some additional restrictions on the parameters of new particles. We are focused on the three of the above-mentioned BSM – neutrino oscillations, baryon asymmetry of the Universe, and dark matter. Each of them can be either solved or alleviated with the help of HNLs.

- **Neutrino oscillations.** As already mentioned, neutrino oscillation data requires $\mathcal{N} \geq 2$ HNLs. For a fixed Majorana mass, the value of the Yukawa coupling can be estimated to be

$$|F|^2 \approx \frac{\sqrt{\Delta m^2_{\text{atm}}} M_I}{v^2} \sim 2 \times 10^{-15} \frac{M_I}{\text{GeV}} \qquad (2.6)$$

For HNLs beyond the electroweak scale if means $|F|^2 \lesssim 10^{-13}$. The estimate (2.6) would hold for $\mathcal{N} = 1$. In case of $\mathcal{N} > 1$ it serves as the lower bound on Yukawas of sterile neutrinos. Indeed, a pair of HNLs can be combined into a quasi-Dirac fermion with approximately conserved generalized lepton number [201, 143]. In the limit of degenerate in mass HNL pair, neutrino masses are exactly zero even for Yukawa couplings

$\mathcal{O}(1)$. The situation becomes more complicated for $\mathcal{N} = 3$ [125] or if one takes into account fine-tuning between various parameters [234, 164, 73, 123, 201, 143, 4, 190, 118, 102].

- **Dark matter.** The idea that sterile neutrino can serve as viable dark matter candidate goes back to 1990s [94, 204], see [61] for review. Sterile neutrinos in the seesaw model are *decaying dark matter candidates* [98, 8]. There are two main decay channels of sterile neutrino:

$$N \to \gamma + \nu_i, \qquad N \to \nu_i + \nu_j + \bar{\nu}_j \qquad (2.7)$$

with decay width [71, 101]:

$$\Gamma_{N \to 3\nu} = \frac{G_F^2 M_I^2}{96\pi^3} \theta^2 = \frac{1}{4.7 \times 10^{10} \text{sec}} \left(\frac{M_I}{50 \text{ keV}} \right)^5 \theta^2 \qquad (2.8)$$

and subdominant (loop mediated) radiative decay

$$\Gamma_{N \to \gamma\nu} = \frac{9\alpha G_F^2 M_I^2}{256\pi^4} \theta^2 = \frac{1}{1.45 \times 10^{13} \text{sec}} \left(\frac{M_I}{50 \text{ keV}} \right)^5 \theta^2 \qquad (2.9)$$

where $theta^2 = \sum_\alpha \theta_\alpha^2$ and θ_α is given by (2.3). While the dark matter particles should necessarily live longer than the lifetime of the Universe, which translates into the bound

$$\theta^2 < 1.1 \times 10^{-7} \left(\frac{50 \text{ keV}}{M_I} \right)^5 \qquad (2.10)$$

The main constrain comes, however, from the radiative decay channel (2.9), see [61] for review.

The production of sterile neutrinos in the early universe [98, 7, 37, 36, 150, 121] can proceed in different regimes at temperatures $T \gtrsim 10 - 100$ MeV, depending on the presence or absence of lepton asymmetry in the Universe. Their abundance will be presented as either thermal or non-thermal relic, decoupled at high temperatures and evolving as free particles since then.

- **Baryon asymmetry of the Universe.** To generate the baryon asymmetry, several Sakharov conditions [195] must be met – *(i)* Baryon number should be violated, *(ii)* C-symmetry and CP-symmetry should be violated,

and *(iii)* corresponding interactions should be out of thermal equilibrium. In the SM there is no baryon-number violating processes at temperature below the electroweak scale $T_{EW} \sim 10^2 \, \text{GeV}$. But for higher temperature, there exist *sphaleron processes* [149] that lead to non-conservation of total baryon plus lepton numbers $B + L \neq const$, although the difference is conserved $B - L = const$. Two other conditions are *not* satisfied in the Standard Model [200] for the experimentally observed value of the Higgs boson.

The presence of HNLs changes the situation qualitatively, leading to *leptogenesis* [115]. In leptogenesis scenarios lepton number is violated and sphalerons transfer it to baryon number. The violation of the lepton number in the early Universe can occur due to Majorana nature of HNLs [91] (which is operational only for sufficiently large HNL masses [90]). For the lower (GeV or even MeV scales HNL masses) CP-violating HNL oscillations as the source of lepton number violation [24, 35, 38], for the recent status see [105, 144]. To generate the observable baryon asymmetry two HNLs should be sufficiently degenerate in mass $M_2, M_3 \gg |M_2 - M_3|$ [105, 144].

2.3 Neutrino minimal Standard Model

Among many parameter choices of seesaw Lagrangian there is a special one where parameters of the particles are chosen in such a way as to explain *all three BSM problems*. The model with this choice of parameters received the name νMSM (*Neutrino Minimal Standard Model*). Namely, it turns out that the same two HNLs can explain neutrino oscillation and generate matter-antimatter asymmetry of the Universe. The third HNL then plays the role of dark matter particle, whose production depends on the properties of other two particles.

Below we discuss in more details its structure and potential observational constraints on its properties.

Matrix $F_{\alpha I}$ in (2.1) can be parametrized as [38, 35]

$$F = \tilde{K}_L f_d \tilde{K}_R^\dagger, \qquad \tilde{K}_L = K_L P_\alpha, \quad \tilde{K}_R = K_R P_\beta \qquad (2.11)$$

where we separate 3 diagonal Yukawa couplings

$$f_d = \text{diag}(f_1, f_2, f_3), \qquad (2.12)$$

Majorana phases:

$$P_{\alpha/\beta} = \text{diag}(e^{i\alpha_1/\beta_1}, e^{i\alpha_2/\beta_2}, 1) \qquad (2.13)$$

and the mixing matrix

$$K_L/R = \begin{pmatrix} 1 & 0 & 0 \\ 0 & c_{L/R}^{23} & s_{L/R}^{23} \\ 0 & -s_{L/R}^{23} & c_{L/R}^{23} \end{pmatrix} \begin{pmatrix} c_{L/R}^{13} & 0 & s_{L/R}^{13} \\ 0 & 1 & 0 \\ -s_{L/R}^{13} & 0 & c_{L/R}^{13} \end{pmatrix} \begin{pmatrix} c_{L/R}^{12} & s_{L/R}^{12} & 0 \\ -s_{L/R}^{12} & c_{L/R}^{12} & 0 \\ 0 & 0 & 1 \end{pmatrix} \qquad (2.14)$$

where $c_{L/R}^{ij}, s_{L/R}^{ij}$ stands for $\cos(\theta_{L/R}^{ij}), \sin(\theta_{L/R}^{ij})$ The typical pick of masses are chosen in that way, so the lightest of them is that $M_1 \sim$ keV, and it will be the main candidate to play the role of dark matter if the mixing angle (= interaction strength) is small so has large life-time. Two others are much heavier - with masses $M_{2,3} \sim 100\,\text{MeV}$ or even $\sim$ few GeV. They are almost degenerate, $|M_2 - M_3| \ll M_2$. Those two heavy sterile neutrinos are chosen in that way, so they can describe process of neutrino oscillations and to provide observed baryon asymmetry of the Universe. This would be the mass ranges we focus in our study.

2.3.1 Current and expected constraints on the νMSM parameters

There are three main sources of constraint (current and planned) on the HNL parameters – earth-based experiments, astrophysical and cosmological constraints. Let us focus first on HNLs with masses $M_2, M_3 \gtrsim 50$ MeV. Two main types of earth-based experiments are *missing energy experiments* searching for invisible decay channel of relatively long living mesons π/K and *displaced vertices experiments* searching for appearance of SM particles as a result of previously produced HNL decay. The first type of experiments can constrain HNLs with mass smaller, than K-meson $m_N < m_K$ and give a constraint in

terms of pure flavour mixing U_e or U_μ (U_τ remains undetectable, as tau-lepton is too massive to be produced in decays of such mesons $m_K \ll m_\tau$). Existing experiments: PIENU [18], TRIUMPH [74] ($\pi \to e$), KEK [236], NA62 [87, 127] ($K \to e/\mu$), E949 [34] ($K \to \mu$), while the second type of experiments is sensitive for also combinations of mixings (as it includes production and decay of HNL than can proceed through different mixing channels) but they are less restrictive. Corresponding experiments are PS-191 [54, 53], CHARM [52], NuTeV [221] as well as DELPHI [12]. The combined existing experimental bounds arefor both U_e^2 and U_μ^2 mixings are presented on Fig. 2.1.
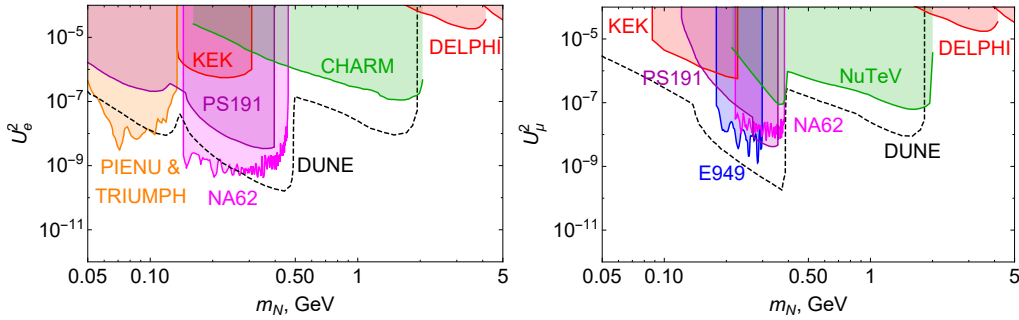
Figure 2.1: Accelerator bounds for mixing cases of U_e^2 (left panel) and U_μ^2 (right panel) for the HNL mass below 5 GeV. For comparison, estimated sensitivity of DUNE experiment [86] is given with dashed line. Figure taken from [60]

We will discuss the constraints from BBN and abundances of the light elements later on in corresponding Chapter. This is an important source of cosmological constraints ([193, 99, 194]) on parameters of HNLs as accuracy of the measurements of light element abundances serves as one of the pillars of modern cosmology.

Compound constrained region of parameter space from BBN, baryogenesis, existing experiments and expected parameter space for future SHiP experiment [21] has been analysed in [60] for the case of two heavy neutral leptons providing a conservative coverage of parameter space that is either already or will be constrained (Fig. 2.2) for the scenarios of two hierarchies - normal and inverted.

Constraints for the keV-mass sterile neutrinos may come from different sources. Some of them may be relaxed, if we consider additional extensions to the SM, besides the HNLs. As in that case, sterile neutrinos do not have to be 100
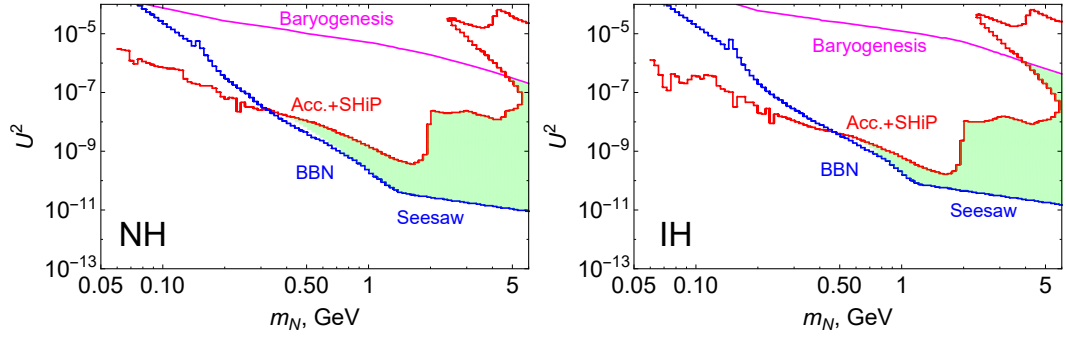
Figure 2.2: Parameter space of the models with two HNLs that is constrained from existing experiments data and cosmological arguments such as constraints from BBN and baryogenesis requirements together with prospective results from SHiP experiment. Green area corresponds to points in parameter space, that is fully consistent with all of mentioned bounds, hence not affecting abundances of light elements at significant level, can generate correct baryon asymmetry and can be responsible for neutrino oscillation data for either normal (NI) or inverted (IH) hierarchy.

percent of the density of dark matter. The most robust lower bound for the *DM sterile neutrinos* comes from the *phase-space limits*. Since they are fermions and due to Pauli principle, two of them can not occupy the same phase-space state, there is a lower limit on their mass - Tremaine-Gunn bound [220]. Depending on the production mechanism, velocity distribution and their dynamics, this bound may vary, but in general it allows neutrinos with masses $M_I \gtrsim 1$ keV ([68]).

Another source is the *X-Ray constraints*. As we mentioned, sterile neutrinos is an example of decaying DM. 2-body decay into neutrino and photon potentially lead to a narrow line in a spectra, observed from object with large density of DM. The initial energy of the photon $E_\gamma = M_I/2$ would give a correction to spectra of such objects. X-ray searches aim to find a narrow peak in telescope data. Searches proceeds in spectra of central region of dwarph spheroidal galaxies (Ursa Minos, Draco) and Andromeda galaxy. The main searches were performed, using data of *XMM-NEWTON* [63, 65, 64, 227], *INTERGAL* [62, 239], *Chandra* [70, 6, 187], *Suzaku* [156]. There are other sources of indirect observational constraint like from Lyman-α or from structure formation. Besides such observations, there are direct searches of Dark matter or double beta-decays which can be also used for constraining the parameters of sterile neutrinos – XENON100 [32], XENON1T [31], DARWIN [2], KATRIN [230], see [79]. The bounds are presented at Fig.**??**. Besides those bounds, there exist presumptive bounds on the keV mass sterile neutrinos from study of their

effect on the supernovae explosion. But such bounds are not strict yet, so we do not present them at above plots. We will discuss this question in more details in Sec. 3
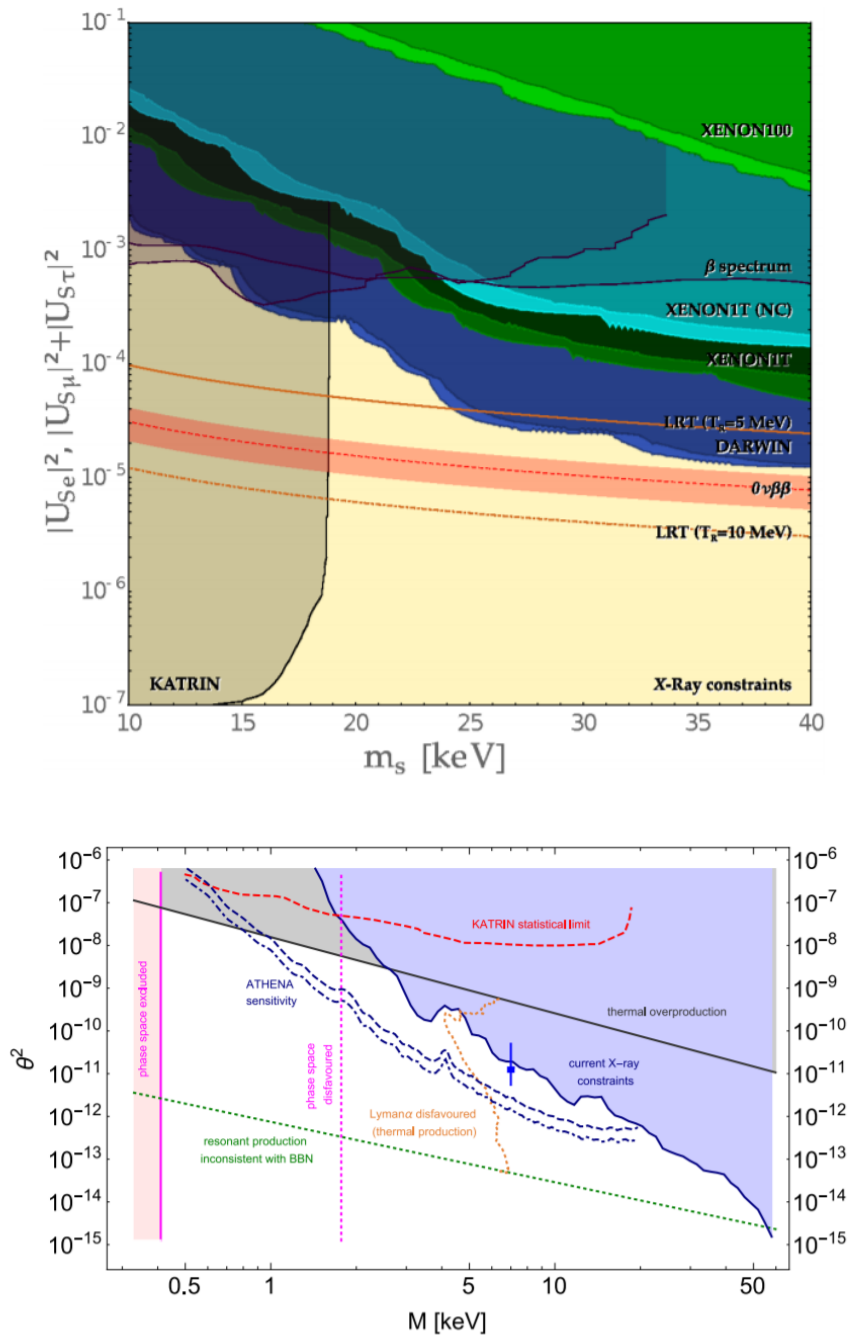
Figure 2.3: Plots, representing existing and expected constraints on the parameters of keV-mass sterile neutrino from different sources - experimental direct detection *top panel* or DM-based constraints *bottom panel*.Plots taken from [61]

Supernovae constraints on sterile netruino parameters

<div align="right">

3

</div>

Although neutrinos play an important role in a huge variety of astrophysical phenomena, including the evolution of all stars at almost every stage of their life, among all of them, neutrinos are probably the most prominent in supernova explosions - one of the brightest and the most energetic phenomenon we can observe. Supernovae explosion is a final stage of a massive star when it runs out of fuel, that can support nuclear reaction in its core. The gravitational force becomes stronger than the one from the pressure of the plasma and the outer layers of the star begin to fall on its core. Such an increase of gravitational binding energy is followed by a significant jump of the temperature and the density of the star media up to orders of magnitude, reaching nuclear density and MeV-temperatures in the core. At a certain moment, the fall of the layers stops, and the shock wave inside the star, bouncing from the central core, begins to rapidly propagate in the opposite direction. This leads to a supernova explosion, during which neutrinos are believed to play an extremely important role in energy transition inside the star. This process is followed by a drastic increase of brightness of the star and intense emission of both photon and neutrino radiation, with great superiority of the latter during the short time. Such conditions are close to the ones, that can be present in the early Universe and they are perfect for the study of the potential effect of novel particles, especially HNLs as they are mixed exactly with neutrinos.

3.1   Observational data

Even though supernova explosions have been observed for a long time, almost all of them corresponded to very distant events. Because of this, only the emission of photons could be effectively observed while detection of the neutrino flux was impossible. The only one close event was the observation of SN 1987a, which exploded in the Large Magellanic Cloud - a dwarf satellite
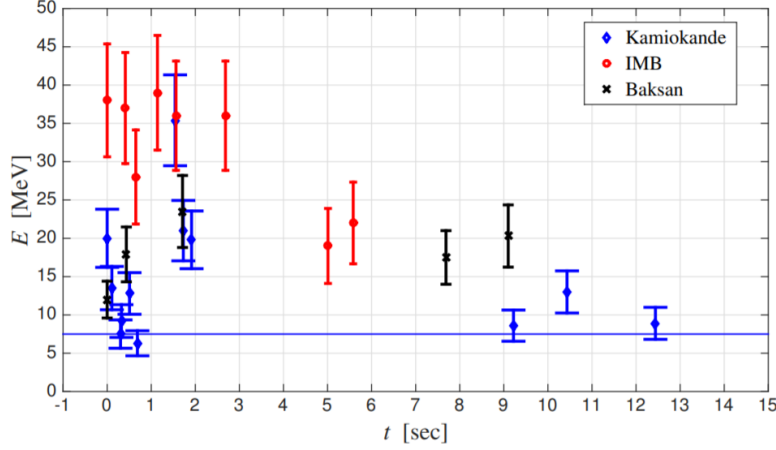
Figure 3.1: Neutrino detection events corresponding to SN1987a explosion. Data from three experiments (IMB, Kamiokande II, and Baksan) is aligned in such a way that the first event on each detector corresponds to $t = 0$. No synchronization in detectors clocks does not allow to accurately arrange in time events from different detectors, but only within one experiment, hence the full data set may be shifted. The horizontal line corresponds to the energy threshold in the Kamiokande II experiment analysis. Figure taken from [58]

galaxy of the Milky Way at a distance of around 50 kPc away. Three detectors have reported simultaneous detection of a series of events corresponding to a neutrino flux from explosion of supernovae - IMB [212], Kamiokande II [133] and Baksan scintillator telescope [26]. Time-aligned events from those three detectors are shown at 3.1. Besides those three, there was another detection of few neutrino events on the Mont Blanc neutrino observatory [16] which preceded the other three experiments observations by about 4-5 hours. This fact and that Mont Blanc was designed to capture neutrinos from closer (~ 10 kPc) core-collapse SN events, prevents these results to be associated with the SN1987A and they are commonly treated just as a background fluctuation. The observed neutrino flux is in total given as a sequence of ~ 20 events of $\bar{\nu}_e$ detection with energy $E_\nu \sim 10$ MeV. The number of events is not enough to reproduce the emission spectrum with details like exact shape, but it still tells about several features:

- The duration of the emission can not be longer, than $\Delta t_{\text{dur}} \approx 10$ s, as it follows from Kamiokande and Baksan results. Although on these results three last events are separated, they do not belong to other potential sources with high confidence. At the same time, not all IMB events are completely trustful as the two last ones are too close to the experiment

threshold. Hence, although the total duration is quite established, there is a possibility, that the emission was not continuous, but had a gap between events at $t \sim 1 - 2$ sec after first detection and events at $t \sim 10$ s.

- The energy of neutrinos were at the level of $E_{\bar{\nu}_e} \lesssim 40$ MeV giving the expected temperature of the area of emission $T \sim 10$ MeV.

- Bayesian analysis of the observed events in an assumption of different shapes of the spectrum, estimates the total energy output in form of electron anti-neutrinos as $E_{\bar{\nu}_e \, \text{tot}} \sim 0.5 \cdot 10^{53}$ erg. Commonly assumed flacour equipartition in neutrino emission (same energy release in each of neutrino/anti-neutrino flavors) predicts total energy release at the level of $E_{\text{tot}} \sim 3 \cdot 10^{53}$ erg. [157]

3.2   SN explosion model

A supernova explosion is an incredibly complex physical system that requires a huge amount of computation to study and simulate. Correspondent research is carried out by many different groups ([136, 78, 166, 138, 223, 75, 48, 58, 45, 216]) which typically includes different 1-D, 2-D and 3-D numeric simulations of the explosion, which requires solving of a complicated MHD system of equations together with neutrino transport equations. Commonly accepted model of core-collapse supernovae and corresponding neutrino emission can be described in the following steps [137]:

- **Onset of Core Collapse** - Contraction of the stellar core under increasing pressure leads to an increase of temperature inside. Photons became hot enough to start disintegration of nuclei of the iron group leading to plasma of free nucleons.

- **Trapped neutrinos** - with the increase of matter density above $\rho \sim 10^{11}$ g cm^{-3}, neutrino mean free path becomes smaller, than the size of the stellar core. It causes them to become trapped inside the core. Their interaction with nucleons together with electron capture by nucleons produce a large population of neutrinos inside the core.

- **Core bounce** matter density inside the core continue to increase, reaching the nuclear values $\rho \sim 10^{14}$ g cm^{-3}. From this point on, the nuclear forces resist the subsequent contraction as they significantly increase the incompressibility of the core. The external layers of the star, previously falling on the core, now bounce off it with generating a shock wave propagating outwards.

- $\bar{\nu}_e$ **burst** Electrons, previously present in star medium and trapped in the core are intensively captured and converted into $\bar{\nu}_e$

$$p + e^- \rightarrow n + \nu_e \tag{3.1}$$

. It generates a population of neutrinos higher than a thermal equilibrium population (for zero lepton asymmetry), as trapped electrons correspond to a large lepton number captured inside the core. Those neutrinos, since also trapped could not leave the core fast until shock leads to sufficiently low densities, such that neutrinos can diffuse through the star media. At this moment, a large fraction of electron anti-neutrinos finds their way out, leading to the short-time burst emission of $\bar{\nu}_e$ and considerable loss of electron lepton number inside the core media. Pair production of neutrinos in a hot plasma leads to re-population of neutrinos of all flavors.

- **Shock stalling and revival** During the propagation through the stellar media, shock loses its energy in the dissociation of heavy nuclei. It is enough to stall the propagation and for the successful explosion, energy transition to the shockwave is required. Neutrinos could be a good agent for this, transferring the energy via processes of neutrino/anti-neutrino capture on nucleons

$$\nu_e + n \rightarrow p + e^-, \qquad \bar{\nu}_e + p \rightarrow n + e^+ \tag{3.2}$$
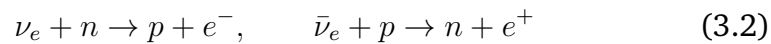
During the time, needed for shock revival, the stellar matter continues to collapse on the core, increasing its temperature and further emission of neutrinos.

- **Proto-neutron star cooling** Already after the initial $\bar{\nu}_e$ burst, neutrino emission from the SN started, actively cooling the SN media during the
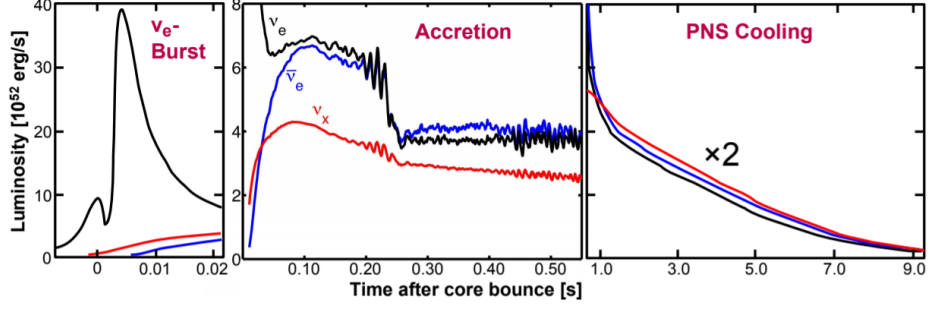
Figure 3.2: Neutrino emission rates as calculated in 20 $M_\odot$ star SN explosion [216, 137]. Three panels of the plot from left to right corresponds to three subsequent phases of neutrino emission - $\bar{\nu}_e$ burst, accretion and Kelvin-Helmholtz cooling. Approximately half of the total energy is emitted during the first second of explosion in burst and accretion phases.

accretion and subsequent Kelvin-helmholtz cooling phase when the star emits remaining gravitational binding energy. Unlike the $\bar{\nu}_e$ burst, during this phase neutrinos of all flavours are emitted with the approximately same rate. A simple estimate, using the diffusion approach for neutrinos propagation gives the timescale of the remaining cooling [77]

$$\tau_{E,\,\text{loss}} \sim \frac{3R_{\text{ns}^2}}{\pi^2 c \lambda_{\text{mfp}}} \frac{E_{\text{th}^0}}{2E_\nu^0} \sim 10 \text{ s} \tag{3.3}$$

where $R_{\text{ns}} \approx 10$ km - the radius of the remaining neutron star, λ_{mfp} - neutrino mean free path

$$\lambda_{\text{mfp}} = \frac{1}{n_n \langle \sigma v \rangle_\nu} \sim 10 \text{ cm} \left(\frac{E}{100 \text{ MeV}}\right)^{-2} \left(\frac{M_{\text{ns}}}{1.5 M_\odot}\right)^{-1} \left(\frac{R_{\text{ns}}}{10 \text{ km}}\right)^3 \tag{3.4}$$

and $\frac{E_{\text{th}^0}}{2E_\nu^0}$ - ratio of thermal energies of neutrino and nucleons.

Schematic representation of the explosion phases are show on Fig. 3.3 and example of neutrino emission luminocity dependence on time is shown on Fig. 3.2.

Since neutrinos diffuse through the supernovae medium before being emitted, they are not freely propagating from the very beginning of their production. Rather than that, at some moment they become free due to a drop of proto-neutron density - the radius of neutrino-sphere. This radius can be different
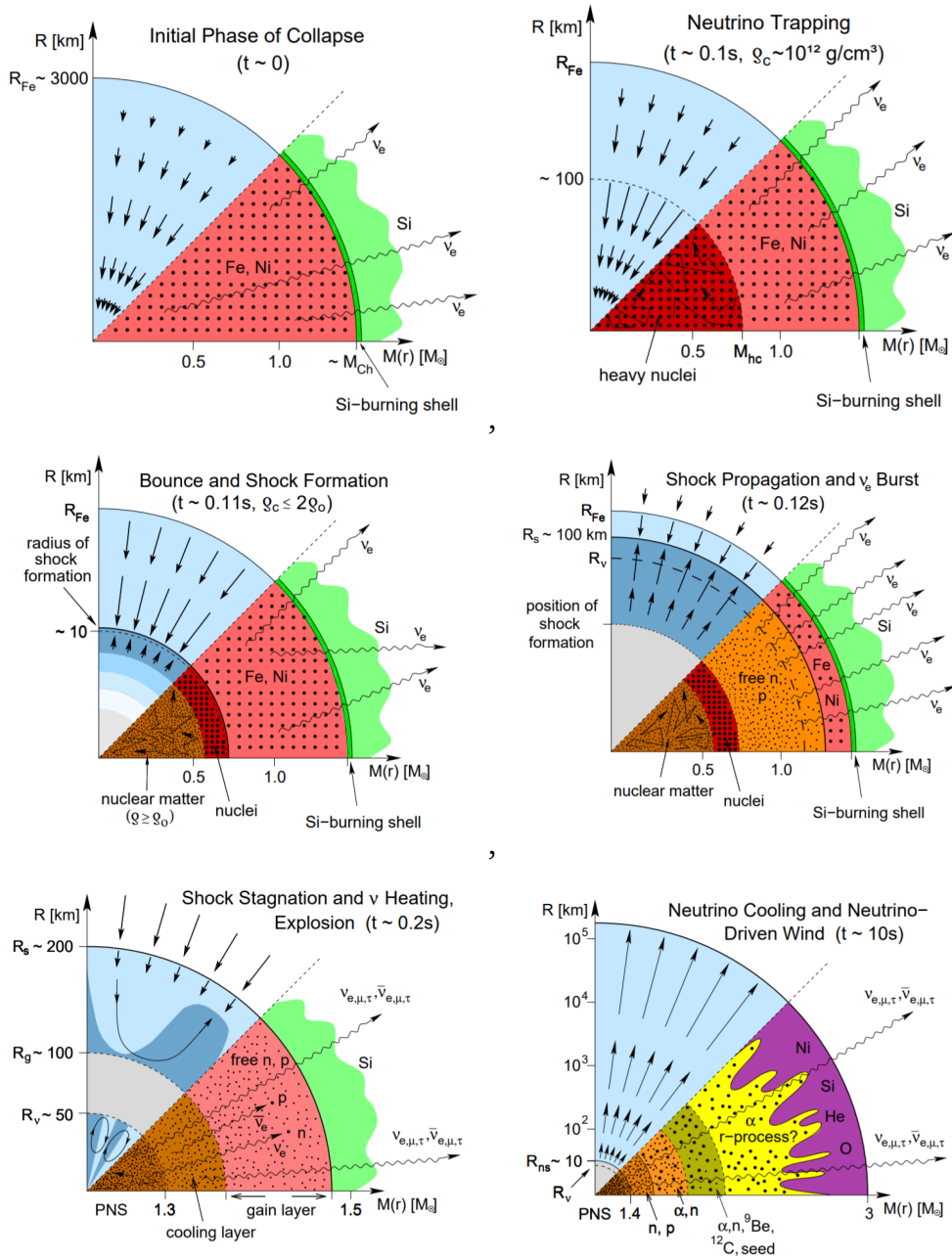
Figure 3.3: Schematic diagrams of the SN pre- and during the collapse evolution. Each diagram correspond to one of six described phases from top left to bottom right. Here parameters $R_{Fe}, R_S, R_\nu, R_g, R_{ns}$ correspond to radii of : iron core, shock, neutrinosphere, gain (separation between heating and cooling from neutrinos) and proto-neutron star respectively. $M_{Ch} \approx 1.4 M_\odot$ is a Chandrasekhar mass, M_{hc} - mass of the inner core, ρ_c - is the density in the center and $\rho_0 \approx 3 \cdot 10^{14}$ g cm^{-3} - characteristic nuclear density Figure taken from the [137]

for neutrinos of different energies, hence the resulting spectra of emitted neutrinos will not be perfectly thermal but rather "pinched" [141, 142]:

$$f_\nu(E) = \frac{(1+\alpha)^{3+\alpha}}{\Gamma(3+\alpha)} \left(\frac{E}{\langle E \rangle} \right)^\alpha exp \left(-(1+\alpha) \frac{E}{\langle E \rangle} \right) \qquad (3.5)$$

where α - pinching parameter, describing the discrepancy between this spectra and typical thermal distribution and can vary depending on the model and flavor in the range ($\alpha \approx$ 2-11) and $\langle E \rangle$ - average energy of neutrinos.

The total energy, released in SN explosion would be given by the difference of gravitational binding energy of progenitor and remnant. The absolute value of this energy for the progenitor would be much smaller than of the remnant $E_{\rm bind} \ll 10^{53}$ erg, since the remnant is a much more compact object, making it completely dependent on the latter. In general, there are two options for SN remnants - neutron star and black hole. While in the first case this value can be calculated for different neutron star EoS [207] (leading to different density profiles) or at least estimated from the simple model of a constant density sphere, which is a reasonable approximation, in the case of a black hole there is no definite binding energy. Hence the total energy deposit may be unknown. The previously described SN explosion model and corresponding neutrino emission properties rely on the assumption of having a neutron star as a remnant. In the case of a black hole, although the beginning phases of evolution may coincide with the neutron star option it can be significantly different later as if collapse to BH starts, it will cut the emission of neutrinos and will begin to completely determine the subsequent evolution of the system.

3.3 Simple model for estimates

We aim to demonstrate the effect of back-reaction from the build-up of the lepton asymmetry on the resonant production of sterile neutrinos and demonstrate, that uncertainties in the SN parameters are present in different numeric models of the SN explosion can be crucial for a possibility to set any constraints on novel particles. As we will describe in more detail, the sterile neutrino emission depends on the spatial and temporal distribution of density of baryons ρ_B, temperature, lepton asymmetries of electrons, and neutrinos of electron and other flavors Y_e, Y_{ν_α}. To obtain such quantities one has to run a corresponding numeric simulation solving the MHD/transport system of equations. Different numerical approaches, including 2- and 3-D simulations to the supernova give broadly consistent results (see e.g. the comparison of codes and approximations in [139, 170]). The differences of the SN media

parameters within different codes and the same progenitor mass are typical $\mathcal{O}(10\%)$. In the case of different progenitor stars, distinctions between the value of temperature profile in numeric simulation sometimes may reach a considerably high level (see the comparison of temperatures at $r \sim R_{\mathrm{ns}}$ at Fig. 3.5) even with other assumptions to be equivalent. Note, that it does not mean the same significant difference in potential observation of neutrinos flux as it is determined mostly by the temperature of the neutrino-sphere and if two numeric models have this value coinciding, both of them may be as good to simulate the SN1987A explosion[1], hiding their discrepancies behind the non-transparency wall of too dense plasma. Nevertheless, this does not mean that such a medium will be opaque for sterile neutrinos. And quite the opposite, we will see, that sterile neutrinos production may be significantly affected by even small (compared to the potential difference between numeric models) changes of parameters of the SN media, leading to significant changes in the number of produced sterile neutrinos (see Appendix 3.6.1) for giving mass and mixing angle.

Therefore, we will not establish any constraints or limits on the sterile neutrinos on purpose and demonstrate that the current state of the art of both existing observations and theoretical understanding does not allow to provide any robust constraints.

In our calculations, we will use two models of SN explosion - fiducial SN model, which is a result of numerical treatment of hydrodynamic simulation [218] of the progenitor star with a mass of $18.6 M_\odot$ and SFHo nuclear equation of state [206]. The gravitational mass of the explosion remnant is a neutron star with a mass $1.4 M_\odot$. And for the tests and a simplified picture, we will use a toy model which is represented via time-constant profiles of density, temperatures, and some of the lepton numbers. The parameters of the toy model will only roughly correspond to temperature and density orders of magnitude and their radial profile behavior.

To simplify the analytical treatment of the problem and to achieve the result, that is easily reproducible, instead of using the full simulation with time-evolution we approximate the temporal evolution of our background SN model by three snapshots of simulation taken at different post-bound times

---

[1]The progenitor of the SN1987A is a blue supergiant star Sk $-62°202$ [122] whose mass is expected to be in the range of $15 - 20 M_\odot$ [229].

$t_\mathrm{pb} = 0.05, 0.5, 1$ sec, see Fig. 3.4. We adopted the same model as was used e.g. in [211, 210]. We will consider, that the profile does not change during a one-time interval. At times $t_\mathrm{pb} > 1$ sec, the temperature begin to drop significantly as the accretion phase ends. That is why we do not take into account times $t > 1\,\mathrm{sec}$. The values of the correspondent (profiles of matter density, temperature, and asymmetries) are shown in Fig. 3.4 for both fiducial and toy models. We also follow [211, 210] and assume, that active neutrinos have an equilibrium spectrum given by the temperature from the snapshot.
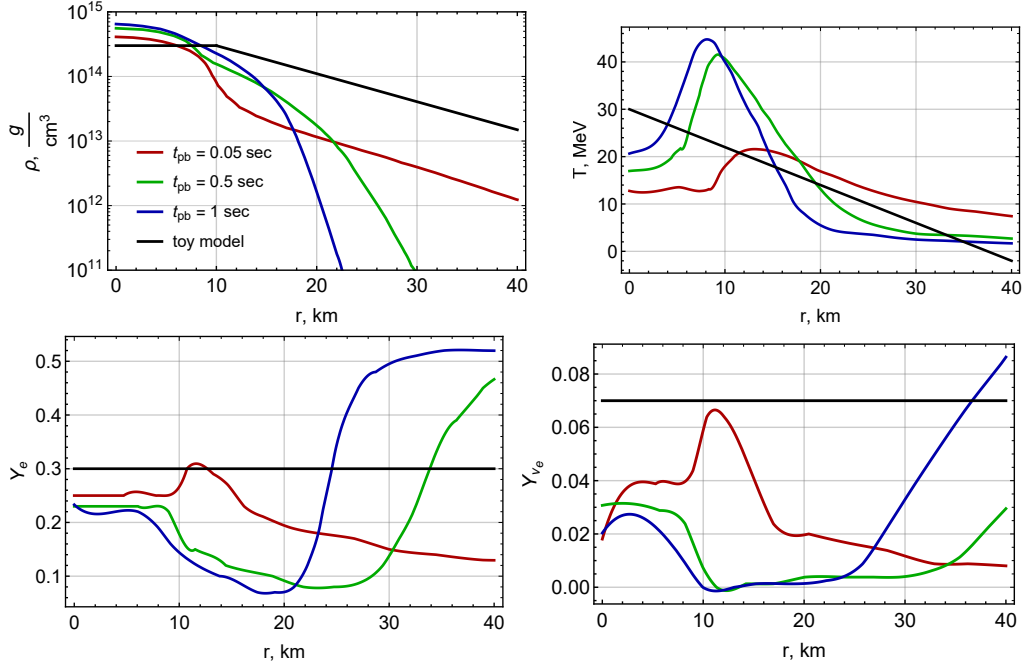
Figure 3.4: Radial profiles of density, temperature, electron and electron neutrino asymmetries, taken as snapshots from 1D hydrodynamic simulations of the 18.6 $M_\odot$ supernovae explosion [218]. Post-bounce times are $t_\mathrm{pb} = 0.05, 0.5, 1$ s Black lines show the (time-independent) profiles in our toy model. ALthough the differences between fiducial and toy model may look significant, it still captures well the main result and related effects.

For the toy model we adopt the following conditions. Baryon density has a constant value inside the supernova core ($r < R_\mathrm{core}$) and decrease exponentially outside the core,

$$\rho_B = \rho_0 \exp\left[-\frac{r - R_\mathrm{core}}{R_\mathrm{core}}\right], \quad r > R_\mathrm{core} \tag{3.6}$$

Temperature has a linear behaviour, decreasing from T_max at $r = 0$ to T_min at $r = 50$ km and. Proton number fraction remains constant and it is just a simplification for our model (note that does not necessarily mean that we
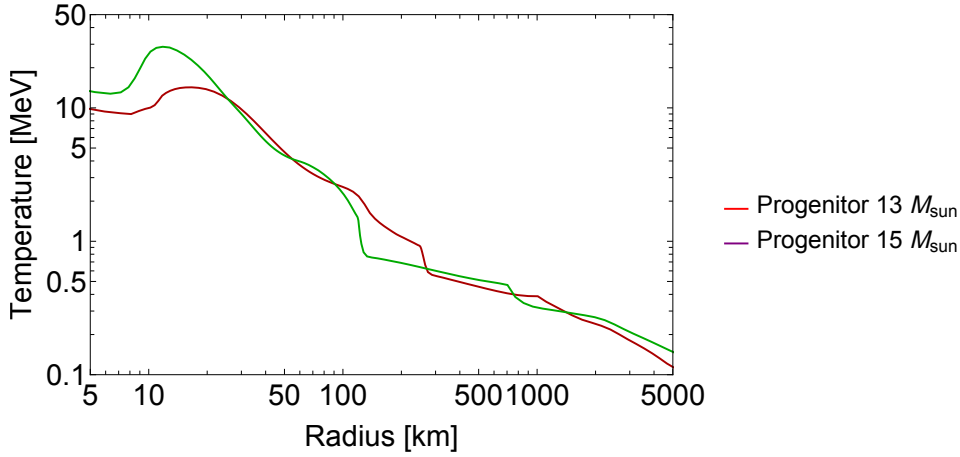
Figure 3.5: Dependence of the temperature profiles (and in particular of the maximal temperature, T_{max}) on the mass of progenitors. Both temperature profiles are for the same post-bounce time $t_{\mathrm{pb}} \simeq 250\,\mathrm{msec}$ and obtained as a result of simulations with the same numerical code [154]. The plots are shown for two different progenitor models with main sequence masses of $13 M_\odot$ [167] and $15 M_\odot$ [232] that provided the initial conditions for the corresponding runs. The uncertainty in the determination of the mass of the progenitor of the SN1987A is $15 - 20 M_\odot$ [see e.g. 229].

Core radius	$R_{\mathrm{core}} = 10\mathrm{km}$
Max. Temperature	$T_{\mathrm{max}} = 30\,\mathrm{MeV}$
Min. Temperature	$T_{\mathrm{min}} = 3\,\mathrm{MeV}$
Baryon core density	$\rho_0 = 3 \times 10^{14} \frac{\mathrm{g}}{\mathrm{cm}^3}$
Baryon core number density	$N_0 = 10^{38}\,\mathrm{cm}^{-3}$
Proton fraction	$Y_p = 0.3$

Table 3.1: Parameters of the toy model of the supernova adopted in this section. Temperature is chosen to decrease linearly from T_{max} at $r = 0$ to T_{min} at $r = 50\mathrm{km}$ and is also constant during the first second.

define the number of electrons as there may be the change of population of other charge massive leptons). Numerical values of the relevant parameters are specified in Table 3.1.

3.4 It it possible to set a robust constraint on BSM particle from SN1987A explosion?

If we assume the existence of any new BSM particles, they could affect a supernova explosion in different ways. The simplest of them is producing an additional cooling channel for the star. As was mentioned, estimate (3.3) predicts the cooling time of the order of 10 sec, and it can not be decreased significantly, as neutrinos are trapped inside the SN core. But new particles, like sterile neutrinos, may have significantly weaker interactions with media and hence, free-streaming out of SN core. This cooling channel is limited rather by the rate of neutrino production than by their mean free path. In this picture, the addition of new particles would lead to the shortening of the duration of neutrino emission. It is therefore used as so-called "energy-loss argument" *e.g.* [183, 181, 184, 101]. introduced by G.Raffelt and commonly used to set an order-of-magnitude constraint on new particles. Author in [183] studied a simplified cooling model of the SN in presence of axions and have found, that the shortening of neutrino pulse duration may become inconsistent with the SN1987a observations if the energy loss rate per unit mass via new channel exceeds

$$\epsilon_m \lesssim 1.0 \times 10^{19} \text{ erg g}^{-1} \text{ s}^{-1} \tag{3.7}$$

which can be also rewritten as energy loss rate per unit volume

$$\epsilon_v \lesssim 3.0 \times 10^{33} \text{ erg cm}^{-3} \text{ s}^{-1} \tag{3.8}$$

assuming the SN core matter density $\rho = 3.0 \cdot 10^{14}$ g cm^{-3}. For an object with mass $\mathcal{M} = 1.5 \cdot M_\odot$ it would correspond to limit of total energy loss rate from new channel

$$\mathcal{E}_{\text{total}} \lesssim 10^{53} \text{ erg s}^{-1} \tag{3.9}$$

There were a lot of studies of sterile neutrino production in the past years for a different mass range from eV to GeV [140, 182, 175, 203, 169, 148, 97, 99, 98, 7, 116, 46, 130, 131, 147, 117, 215, 185, 233, 225, 241, 226, 33, 186, 235]. Almost all of them (except for *e.g.* [7, 185, 241, 33, 211, 210]) were focused on the study of electron flavour mixing and the energy-loss argument was used quite widely to constraint the parameters of sterile

neutrinos. Though, we believe, that even when the rate of energy loss rate is close to 10^{53} erg, *this does not lead to the bounds that are both strong and robust.* Indeed, applicability of this constraint requires several conditions and the first of them is that the observation of neutrino flux from SN1987A was indeed an observation of a continuous cooling process and not anything else, which may be the case if the remnant of the SN1987A is a black hole instead of the neutron star. Such possibility is allowed, as the remnant of the SN1987A has not been found yet [27], although it does not mean, that the neutron star is not hidden somewhere [110, 27] . It was proposed in [75, 48, 58, 45], that the observation of the SN1987A could be a result of *(i)* delayed formation of a black hole giving the initial seconds of neutrino pulse and *(ii)* emission of neutrinos from the accretion disc. Such a scenario, if not refused, can make such constraint inapplicable.

Even if the remnant of a star is a NS, its parameters are not precisely known. Those, the energy deposit, that should be available for emission during explosion is also not well restricted:

$$E_{\mathrm{NS}} \approx 6.3 \times 10^{53}\, \mathrm{erg} \left(\frac{\mathcal{C}}{0.6} \right) \left(\frac{M_{\mathrm{NS}}}{2M_\odot} \right)^2 \left(\frac{10\mathrm{km}}{R_{\mathrm{NS}}} \right) \qquad (3.10)$$

with the numeric coefficient $\mathcal{C} \approx 0.6$ [152, 153, 137], depending on the details of mass distribution in the NS. The estimates made for the remnant allow the range of masses of a neutron star $M_{\mathrm{NS}} \simeq 1.7 - 1.9 M_\odot$, see [27] for review, while the radius of the NS can depend on different EoS. Those uncertainties mean, that total energy released in an explosion may vary up to a factor of 1.5 which is already on the level of the energy-loss rate constraint. Taking all this into account, we believe, that for now, it is impossible to provide a *robust* constraint on the SN parameters.

3.5   HNLs production in supernovae

3.5.1 Collision and resonant production mechanisms

Propagation of neutrinos in homogeneous media Dense and hot supernovae medium is an intense source of all neutrino flavors. Once produced, they propagate through supernovae medium without free escaping. During this propagation, neutrinos interact with media and this affects neutrino self-energy that can be expressed as a correction to self-energy. This correction leads to a change in the neutrino oscillation properties, potentially enhancing the mixing between active (ν_e, ν_μ, ν_τ) and sterile flavor. Let us consider a simple scenario of one active neutrino flavor, mixed with one sterile.

$$\begin{pmatrix} \nu_a \\ \nu_b \end{pmatrix} = \begin{pmatrix} \cos\theta & -\sin\theta \\ \sin\theta & \cos\theta \end{pmatrix} \begin{pmatrix} \nu \\ \nu_s \end{pmatrix} \tag{3.11}$$

here ν_a, ν_b are eigenstates of free Hamiltionian - mass states, corresponding to masses m_a, m_b respectively. Taking, that at moment $t = 0$, a pure flavour state ν was produced with momentum p, this mixing leads to a well-known formula for neutrino oscillation probability

$$P_{\nu\to\nu_s}(r) = \sin^2(2\theta)\sin^2\left(\frac{\Delta M^2}{4p}r\right) \tag{3.12}$$

where $\Delta M = m_a - m_b$. If the uncertainty of area of initial neutrino production is larger, than $R^{-1} \sim \frac{\Delta M^2}{4p}$, than the result can be averaged over distance, giving constant probability of finding a sterile neutrino

$$\langle P_{\nu\to\nu_s} \rangle \to \frac{1}{2} \cdot \sin^2(2\theta) \approx 2\theta^2 \tag{3.13}$$

if mixing angle $\theta \ll 1$. Now, consider the case of medium with constant number density. In this case, dispersion relation for neutrino is affected by interacting with surrounding particles.

$$i\gamma^0\partial_0 \to i\gamma^0\partial_0 - V_{\text{eff}}\gamma^0 \tag{3.14}$$

here V_{eff} - correction for self energy (effective potential) that depends on the energy of neutrino and population of plasma. Different particle species gives different contributions to the value of V_{eff}: ([151],[168])

- Neutrinos of the different flavor - only Z-boson interactions:

$$V_{eff}^{\nu_x \nu_y} = \pm\sqrt{2}G_F(n_\nu - n_{\bar{\nu}}) \tag{3.15}$$

- Neutrinos of the same flavor - both W- and Z-boson interactions:

$$V_{eff}^{\nu_x \nu_x} = \pm 2\sqrt{2}G_F(n_\nu - n_{\bar{\nu}}) + \frac{8\sqrt{2}G_F p}{3m_Z^2}(\langle E_\nu \rangle n_\nu + \langle E_{\bar{\nu}} \rangle n_{\bar{\nu}}) \tag{3.16}$$

- Protons background:

$$V_{\text{eff}}^{\nu_x p} = \pm\frac{1}{\sqrt{2}}G_F(n_{\bar{p}} - n_p)(1 - 4\sin^2\theta_w) \tag{3.17}$$

- Neutrons background:

$$V_{\text{eff}}^{\nu_x n} = \pm\frac{1}{\sqrt{2}}G_F(n_n - n_{\bar{n}}) \tag{3.18}$$

- Charged leptons background of the same flavor:

$$V_{\text{eff}}^{\nu_x l_x} = \pm\sqrt{2}G_F(\frac{1}{2} + 2\sin^2\theta_w)(n_l - n_{\bar{l}}) + \frac{8\sqrt{2}G_F \cdot p}{3m_Z^2}(\langle E_l \rangle n_l + \langle E_{\bar{l}} \rangle n_{\bar{l}}) \tag{3.19}$$

- Charged leptons background of the different flavor:

$$V_{\text{eff}}^{\nu_x l_y} = \pm G_F(1 - 4\sin^2\theta_w)(n_l - n_{\bar{l}})/\sqrt{2} \tag{3.20}$$

here θ_w - Weinberg angle, $n_l, n_\nu, n_{p/n}$ number densities of leptons, neutrinos, protons and neutrons respectively. $\langle E_x \rangle$ - average energy of the correspondent particle of species x.

In general, contribution to effective potential can be separated into two terms - proportional to the asymmetry between particles and anti-particles and independent of it. The second term has an additional suppression due to the mass of either W- or Z- boson as it appears due to the second-order of

magnitude contribution of the bosonic propagator. At temperatures $T \ll m_W$ it might give a very small correction but since the asymmetry of plasma is another external parameter, which might be arbitrarily small, we can not completely neglect it. This correction is applied for active neutrino flavor, while the similar correction for sterile flavor is suppressed via small mixing angle. Neutrinos obey Dirac equation and as a consequence - Klein-Gordon equation. When particles are ultra-relativistic, their equation of motion could be rewritten as (see *e.g.* the book [181, Chap. 8]):

$$
i\frac{d}{dt}\begin{pmatrix} \nu_x \\ \nu_s \end{pmatrix} = \mathcal{H}_{\text{eff}}\begin{pmatrix} \nu_x \\ \nu_s \end{pmatrix}
\tag{3.21}
$$

where the "effective Hamiltonian" is

$$
\mathcal{H}_{\text{eff}} = \frac{m_s^2}{4E}\begin{pmatrix} -\cos 2\theta_0 & \sin 2\theta_0 \\ \sin 2\theta_0 & \cos 2\theta_0 \end{pmatrix} + \begin{pmatrix} V_{\text{eff}} & 0 \\ 0 & 0 \end{pmatrix}.
\tag{3.22}
$$

Here V_{eff} is the effective potential of ν_x m_s is the mass of sterile neutrino, E is its energy ($m_s \ll E$) and we have neglected masses of the active neutrinos; θ_0 is the vacuum active-sterile mixing angle. This effective potential leads to the change of mixing angle ([5]):

$$
\sin^2 2\theta_m = \frac{\Delta_s(p)\sin^2 2\theta}{\Delta_s(p)\sin^2 2\theta + (\Delta_s(p)\cos 2\theta + V_{\text{eff}})^2}
\tag{3.23}
$$

Together with mixing angle, oscillation probability (3.13) is also changed:

$$
\langle P_{\nu \to \nu_s} \rangle \approx \frac{1}{2}\frac{\Delta_s(p)\sin^2 2\theta}{\Delta_s(p)\sin^2 2\theta + D^2(p) + (\Delta_s(p)\cos 2\theta + V_{\text{eff}})^2}
\tag{3.24}
$$

where $D(p)$ - damping factor due to neutrinos interaction correspondent to probability that its wave function would collapse to a pure state. It is defined, as

$$
D(p) = \Gamma_{\text{int}}^{\nu_x}/2
\tag{3.25}
$$

where Γ_{int} - interaction rate of neutrinos with flavour "x" in plasma. Also here, and for further notations we have introduced parameter

$$
\Delta_s = \frac{m_s^2}{2p}
\tag{3.26}
$$

When $V_{\text{eff}} = 0$ the eigenvalues of the Hamiltonian (3.22) are $\pm\frac{1}{2}\Delta_s$ and the vacuum active-sterile oscillation length is given by π/Δ_s. If the interaction

rate is not high damping can be neglected, then matter mixing angle for small vacuum mixing values takes a simple form:

$$\tan 2\theta \simeq 2\theta_0 \frac{\Delta_s}{\Delta_s + V_{\text{eff}}} + \mathcal{O}(\theta_0^2) \tag{3.27}$$

Let us concentrate on the case without damping, as it would be our main scenario. From Eqn. (3.23) or (3.27) one can see, that depending on the value and sign of effective potential, matter mixing angle can be either suppressed or amplified. If the value of V_{eff} is positive, mixing angle is additionaly suppressed and this would not be the case of interest for now. But if it achieve negative values, mixing angle increases. When the condition

$$\Delta_s(E) + V_{\text{eff}}(r) = 0 \tag{3.28}$$

is satisfied, one has a resonance and $\theta_{\text{res}} \to \frac{\pi}{4}$ - maximum mixing case when both neutrino flavors enter the mass state in same proportions. For a specific value of V_{eff} there always exist an energy for which resonance occurs:

$$E_{\text{res}} = \frac{m_s^2}{|V_{\text{eff}}|} \tag{3.29}$$

Note, that in case of damping, there exist a maximum value for probability of conversion. Instead of resonance value $\langle P_{\nu \to \nu_s} \rangle \to 1/2$ we have

$$\langle P_{\nu \to \nu_s} \rangle \approx \frac{1}{2} \frac{\Delta_s(p) \sin^2 2\theta}{\Delta_s(p) \sin^2 2\theta + D^2(p)} \tag{3.30}$$

Significance of the resonance can be understood if we look at eigenvalues of the Hamiltonian (3.22). Its diagonalization gives two eigenvalues $E_{a,b}$ such that

$$E_{a,b} = \frac{V_{\text{eff}}}{2} \pm \sqrt{(\Delta_s + V_{\text{eff}})^2 + 4\Delta_s^2 \theta_0^2} \tag{3.31}$$

Corresponding for two eigenfunctions (mass eigenstates) $\nu_{a,b}$. At the resonance, the difference $E_a - E_b$ becomes smallest given by $\Delta E = 2\Delta_s \theta_0$ so the smaller the vacuum mixing angle, the closer energy levels approach. In the opposite case, when V_{eff} has positive value, the gap between energy levels only increase in media.

In case, if resonance is available, sterile neutrinos can be copiously produced in such media due to a significantly increased probability of oscillation. **Prop-**

agation of neutrinos in inhomogeneous media Now, let us consider the case of media with variable density. Naively, we should only substitute the constant potential with its variable form in the expressions of mixing angle (3.23) and conversion probability (3.24). It is not completely true, though. The equation of propagation of neutrinos in the media remains similar, but now with hamiltonian, that is a function of coordinate.

$$i\frac{d}{dr}\begin{pmatrix}\bar{\nu}_x\\\nu_s\end{pmatrix} = \mathcal{H}_{\text{eff}}(r)\begin{pmatrix}\bar{\nu}_x\\\nu_s\end{pmatrix} \tag{3.32}$$

where the "effective Hamiltonian" is

$$\mathcal{H}_{\text{eff}}(r) = \frac{m_s^2}{4E}\begin{pmatrix}-\cos 2\theta_0 & \sin 2\theta_0\\\sin 2\theta_0 & \cos 2\theta_0\end{pmatrix} + \begin{pmatrix}V_{\text{eff}}(r) & 0\\0 & 0\end{pmatrix}. \tag{3.33}$$

Notice that $[\mathcal{H}_{\text{eff}}(r), \mathcal{H}_{\text{eff}}(r')] \neq 0$ for $\theta_0 \neq 0$ and therefore exact solution of Eq. (3.21) is complicated. Moreover, eigenstates of such Hamiltonian are no more plane waves in whole space. But in the case of slowly varying media $|\nabla \log V_{\text{eff}}| \ll \Delta_s$ one can, however, solve this equation in the adiabatic limit. To this end one diagonalizes (3.33) at every point by the matrix $U(r)$, given by

$$U(r) = \begin{pmatrix}\cos\theta(r) & \sin\theta(r)\\-\sin\theta(r) & \cos\theta(r)\end{pmatrix} \tag{3.34}$$

So we consider the eigenstates as a plane waves locally at every point. With mixing angle defined by (3.23), up to change of constant V_{eff} to the variable one. In the medium with variable density the states $\nu_{a,b}$ propagate according to the equation, similar to Eq. (3.21):

$$i\frac{d}{dr}\begin{pmatrix}\nu_a\\\nu_b\end{pmatrix} = \begin{pmatrix}E_a(r) & i\theta'(r)\\-i\theta'(r) & E_b(r)\end{pmatrix}\begin{pmatrix}\nu_a\\\nu_b\end{pmatrix} \tag{3.35}$$

Non-diagonal elements appear since we define ν_a, ν_b as plane waves, that are eigenstates of Hamiltonian only locally, but during propagation, they are changing. The off-diagonal elements in the r.h.s. are equal to $-IU^\dagger\partial_r U$ and are responsible for the transition between different mass "eigenstates" (local) that would be absent for $\theta' = 0$. Media with slowly varying density would cause such a slow change of local eigenvalues, that the wave function of propagating neutrinos would be able to "adjust" at every point adiabatically without transiting to another state. Note, that it still allows a significant change
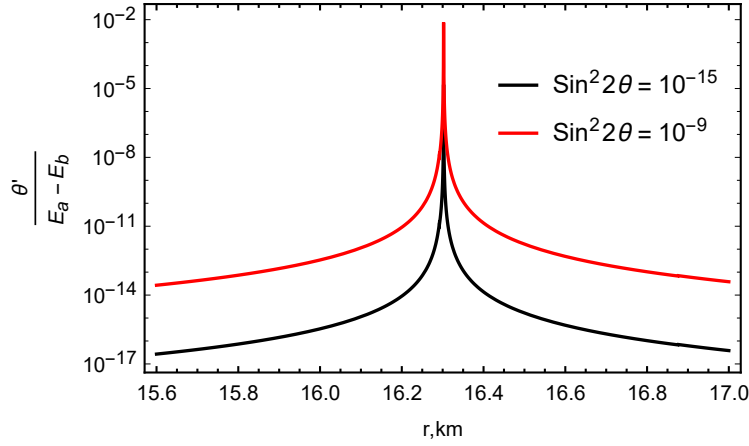
Figure 3.6: Dependence of the adiabaticity parameter $\gamma = \frac{\theta'}{E_a - E_b}$ on radius (Eq. (5.4)). We took the neutrino energy equals $E = 40$ MeV, sterile neutrino mass $m_s = 10$ keV. In the narrow region around resonance ($R_{\rm res} \simeq 16.3\,{\rm km}$ for the current parameters) mixing angle is varying significantly and hence, values of the adiabaticity parameter can reach large values there. While outside of the resonance, it may be negligibly small. For even smaller vacuum mixing angle, the value of this parameter can be larger than 1. It shows that for such a small mixing angles conversion indeed goes non-adiabatically while for larger values it is $\ll 1$ everywhere, so the conversion is totally adiabatic

.

of mixing angle at a large distance. This feature would lead to a well-known MSW effect ([162],[231]). Let us introduce a parameter of non-adiabaticity, γ:

$$\gamma \equiv \frac{\theta'(r)}{E_a(r) - E_b(r)} \tag{3.36}$$

The ratio of the off-diagonal and the difference of diagonal elements is a useful parameter in a two-level system determining, if a transition between those two levels is possible. The fully adiabatic scenario, when no transition occurs, corresponds to $\gamma \to 0$ which is achieved by either slowly varying matter density or large gap between local energy levels. Neglecting of such transition is a case, for example, that occurs for neutrinos, propagating in the Sun due to its relatively small density gradient. When γ becomes of the order of unity, we can not neglect transitions. Since the mixing angle at resonance can get large values, it turns out, that resonance value of parameter γ might significantly increase and become different from zero in some narrow region. We follow notations of [33] defining this region as where $\theta(r)$ changes from $\sin^2 2\theta = 1$ to $\sin^2 2\theta = \frac{1}{2}$ (*i.e.* $\frac{\pi}{8} \leq \theta(r) \leq \frac{3\pi}{8}$) we get its width $R_{\rm width} =$
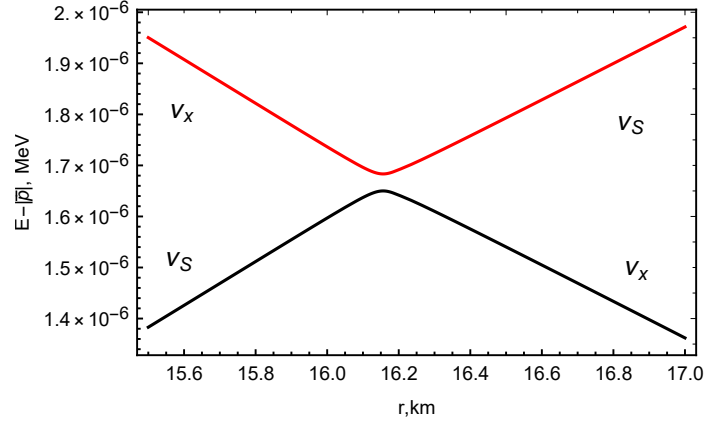
Figure 3.7: Energy levels E_a(black), E_b(red) of the system, depending on the radius. Mixing angle is chosen as $\sin^2 2\theta = 10^{-3}$, mass $m_s = 10$ keV, momentum $p = 30$ MeV. The y-axis shows $m_{a,b}/2E$. The closest distance between energy levels is at the resonance where the transition between the levels is the most likely. This plot demontrates, how a neutrino, produced as an active one inside the SN core, if remaining on the same mass state (no jumps between branches on plot), will become a sterile neutrino, when propagating out of the SN

$2\sin(2\theta_0)/\big(\log V_{\text{eff}}(R_{\text{res}})\big)'$. The non-adiabaticity parameter is maximal at the resonance and can be expressed through the width of the resonance

$$\gamma = \frac{1}{\pi}\frac{L_{\text{osc}}}{R_{\text{width}}} \tag{3.37}$$

where L_{osc} is the oscillation length at resonance

$$L_{\text{osc}} = \frac{2\pi}{|V_{\text{eff}}^{\text{res}}|\sin 2\theta_0}. \tag{3.38}$$

Now, assume at some point $r = 0$ active neutrino was produced and it freely propagates in media. If it crosses the resonance at some moment, the transition between mass states can occur. Since the relation between mass and flavor states is known at every point, this can be rethought as a transition between different flavor state combinations. In an extreme scenario of adiabatic transition, when neutrino propagates from the area with maximum mixing angle $\theta \to \pi/2$ ($|V_{\text{eff}}| \gg \Delta_s$) to a small vacuum value, it would correspond for transition between two pure flavor states - a situation similar to MSW effect. But since the non-adiabaticity, after passing the resonance neutrino would consist of two mass states with different proportions. If no more resonance area appears, they would propagate adiabatically. According to this scenario,

the probability of transition between flavor states ν_x and ν_s after crossing the resonance is given by [172]

$$P_{x \to s} = \frac{1}{2} - \left(\frac{1}{2} - P_{\mathrm{na}} \right) \cos 2\theta_{\mathrm{in}} \cos 2\theta_{\mathrm{out}} \qquad (3.39)$$

where θ_{in} – mixing angle, at the point of neutrino state creation and θ_{out} – mixing angle at the point of detection. P_{na} is a probability of transition between mass eigenstates due to non-adiabatic change of V_{eff}. Note, that this formula is meaningful only if propagation through resonance occurred. In the opposite case, P_{na} should be set to zero unless propagation is non-adiabatic everywhere. In the case, when R_{width} is much smaller than the characteristic scale, over which V_{eff} is changing, the effective potential can be approximated as a linear function of $(r - R_{\mathrm{res}})$ around the resonance. In this case, the Landau-Zener formula appears

$$P_{\mathrm{na}} = \exp\left[-\frac{\pi}{2\gamma} \right]. \qquad (3.40)$$

If such linear approximation won't be applicable, expression will be more complicated. For a variety assumptions about profile, it could be given in form (see *e. g.* Ch.8 of [181])

$$P_{\mathrm{na}} = \frac{\exp\left(-\pi F / (2\gamma) \right) - \exp\left(-\pi F' / (2\gamma) \right)}{1 - \exp(-\pi F' / (2\gamma))} \qquad (3.41)$$

Here $F' = F / \sin^2 \theta_0$ and F - parameter, that depends on density profile. For exponential dependence of effective potential $F = 1 - \tan(\theta_0)$. The more general case was studied in [129] where more general form of transition probability was found. For our purpose, the linear case (3.40) would be enough. **Propagation of neutrinos in supernovae** We limit ourselves for the

case of pure mixing when a sterile neutrino is mixed with one active flavor. Let us now consider a specific case of supernovae environment to study neutrino production. According to the description of the supernovae explosion in 3.2, the media interesting for us consists of protons, neutrons, electron-positron pairs, and neutrinos of all flavors. The population of muons is relatively small or negligible depending on the exact temperature of the media. The effective potential for such media is given by

- For electron flavor neutrinos:

$$V_{\text{eff}}^{\nu_e,\bar{\nu}_e}(r) = \mp \frac{G_F}{\sqrt{2}} N_b \left(-2Y_e + Y_n - 4Y_{\nu_e} - 2Y_{\nu_\tau} - 2Y_{\nu_\mu} \right). \qquad (3.42)$$

- For muon flavor neutrinos:

$$V_{\text{eff}}^{\nu_\mu,\bar{\nu}_\mu}(r) = \pm \frac{G_F}{\sqrt{2}} N_b \left(Y_n - 2Y_{\nu_e} - 2Y_{\nu_\tau} - 4Y_{\nu_\mu} - 2Y_\mu \right), \qquad (3.43)$$

- For tau-flavor neutrinos:

$$V_{\text{eff}}^{\nu_\tau,\bar{\nu}_\tau}(r) = \pm \frac{G_F}{\sqrt{2}} N_b \left(Y_n - 2Y_{\nu_e} - 4Y_{\nu_\tau} - 2Y_{\nu_\mu} \right), \qquad (3.44)$$

and the factor in front of the asymmetry terms is

$$\frac{G_F}{\sqrt{2}} N_b = 11.4\,\text{eV} \frac{N_b}{N_0} \qquad (3.45)$$

so the typical value of the correction to neutrino self-energy in the SN core is ~ 10 eV $\ll m_s$. Here $N_0 = 3 \cdot 10^{14}$ g/cm^3, $Y_i \equiv \frac{N_i - N_{\bar{i}}}{N_b}$ is the asymmetry in i^{th} particle ($i = \{n, p, e, \mu, \tau, \nu_e, \nu_\mu, \nu_\tau\}$), N_b is the baryons number density, the upper sign is for neutrinos, the lower sign - for anti-neutrinos. In the two latter cases, sign of effective potential does not change while in the case of electron flavor mixing it might change. Value of the effective potential for e- and $\mu/\tau-$ mixing is presented at Fig. 3.8 We will focus on the case
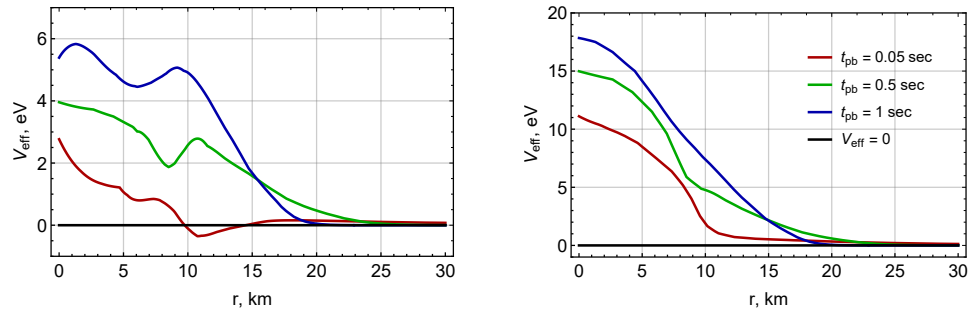
Figure 3.8: Value of the effective potential of neutrino, propagating in the SN media in case of its mixing with electron (**left panel**) and μ/τ (**right panel**) flavours. The result is calculated for three snapshots we use in our fiducial model 3.2. Parameters Y_{ν_μ} and Y_{ν_τ} are set to zero. While in the case of μ/τ mixing, the function for the potential is monotonic and never crosses zero value, electron flavour is much more complicated.
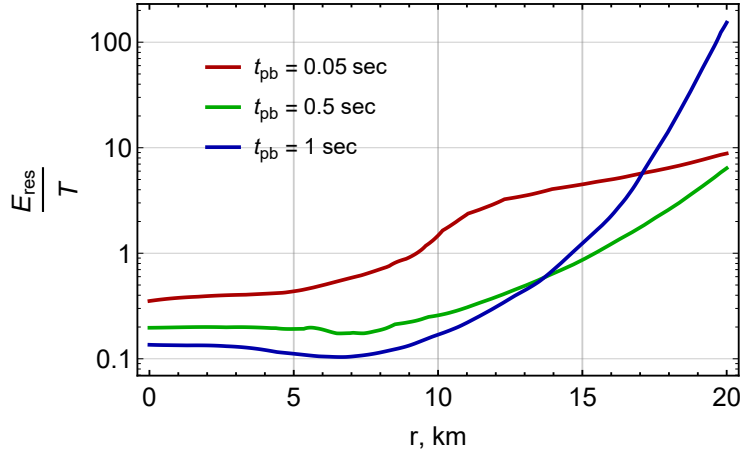
Figure 3.9: Ratio of the resonant energy satisfying the condition (3.28) to temperature at corresponding radius for μ/τ-flavour mixing at different times and radii. we have used the mass $m_s = 10$ keV here. When this ratio becomes $E_{\text{res}}/T \gg 1$, it corresponds to exponentially suppressed population of neutrinos, available for conversion and hence, its low rate. It becomes the reason, why the production proceeds efficiently only at radii $r \approx 10 - 20$ km.

of muon/tau-mixing. For them, only anti-neutrinos can undergo resonance condition (3.28) so only their production might be enhanced in the SN. At every point, there is a neutrino energy, which satisfies the resonance condition establishes a relation between the anti-neutrino energy and the radius of the resonance, R_{res}:

$$V_{\text{eff}}(R_{\text{res}}) = \frac{m_s^2}{2E_{\text{res}}} \tag{3.46}$$

Ratio of the resonance energy to temperature at each radius is demonstrated at Fig. 3.9. There are two production mechanisms to be considered - collision production and resonance conversion. Both of these mechanisms were already studied in the past for neutrinos of different flavors and sterile neutrinos ranging in masses from eV to GeV [140, 182, 175, 203, 169, 148, 97, 99, 98, 7, 116, 46, 130, 131, 147, 117, 215, 185, 233, 225, 241, 226, 33, 186, 235, 33, 7, 185, 241, 211, 210]. Let us briefly describe both of them.

- **Collisional production** takes into account, that if an active neutrino was produced, then during its propagation it can oscillate to sterile flavor. Then, if interaction occurs, the wave function of neutrino collapses to either active or sterile flavor (with probability, given by Eqn. (3.24)). This allows sterile neutrinos to be produced in every $2 \rightarrow 2$ reaction

involving neutrinos in a final state. This volume production can be described via equation ([204, 185, 208])

$$\frac{dn_s}{dtdE} = \frac{\Gamma_x}{2}\langle P_{\nu \to \nu_s}\rangle\frac{dn_x}{dE} \qquad (3.47)$$

where $\frac{dn_s}{dE}$ and $\frac{dn_x}{dE}$ - energy spectra of sterile and active flavor neutrinos, Γ_x- interaction rate of x -flavor neutrinos in the SN plasma. In the area, close to the point, where resonant condition 3.28 is satisfied, sterile neutrinos can be effectively produced. Contrary to the active neutrinos, they are not trapped inside the SN and can freely escape. But as was pointed out in [185], at the very resonance, large mixing angles makes also sterile neutrinos trapped, so the exact area of production is not the resonance point but area around it. Every point of the star volume corresponds to some resonance energy, and resulting spectra is completely non-thermal, determined by the value of effective potential at each point and population of neutrinos with corresponding energy. The most effective this production is in the SN core where the densities $\rho \sim 10^{14}$ g/ cm^3 and temperatures $T \sim$ few$\cdot 10$ MeV, are highest, leading to the largest values of interaction rate. To fins the total production rate, equation 3.47 must be integrated over whole star volume during the time of explosion:

$$\frac{dN_s}{dE} = \int_t dt \int_V 4\pi r^2 \frac{\Gamma_x}{2}(r)\langle P_{\nu \to \nu_s}(r)\rangle\frac{dn_x(r)}{dE} \qquad (3.48)$$

This final spectrum can be used to calculate the energy emission from supernovae, by integrating over energies. Such production mechanism can be present in both homogeneous and inhomogeneous media - hence it will be relevant for both the SN core, which can be approximated with constant density sphere, and the outer layers with variable density

- **Resonance conversion** is a production mechanism, available only in the inhomogeneous media and is very similar to the MSW effect. The mixing angle of neutrinos in the SN is given by

$$\tan 2\theta(r) \simeq 2\theta_0 \frac{\Delta_s}{\Delta_s + V_{\text{eff}}(r)} + \mathcal{O}(\theta_0^2) \qquad (3.49)$$

From Eq. (3.49) one sees that deep inside the SN, where $\Delta_s < |V_{\text{eff}}(r_{\text{in}})|$ and $V_{\text{eff}} < 0$, one has $\tan 2\theta_{\text{in}} \to -0 \Leftrightarrow \theta_{\text{in}} \to \frac{\pi}{2}$, because θ is confined

to $0 \leq \theta \leq \frac{\pi}{2}$. Active neutrino is produced in the central part of the SN, hence it can be considered as a pure mass state. It starts propagating adiabatically out of the SN. If the energy of neutrino is not too low, at some point it crosses the resonance where pure mass state may be converted into combination of two mass states, each of them propagating adiabatically again after the resonance. Almost immediately after the resonance effective mixing angle decreases to values relatively close to vacuum $\theta_0 \ll 1$ so correspondent mass states can be associated with flavor states each. If the transition was adiabatic everywhere, than every neutrino, that crosses the resonance would be converted to sterile at infinity. Instead, we have a conversion probability of active neutrino to sterile neutrino

$$P_{x \to s} = 1 - \exp\left[-\frac{\pi}{2\gamma}\right]. \tag{3.50}$$

for the case of small vacuum mixing angle $\theta_0 \ll 1$. In the MSW effect case, such a mechanism governed the conversion of electron flavor neutrinos produced inside the sun in nuclear reactions into muon neutrinos. The conversion, in that case, was fully adiabatic, but the vacuum mixing angle is not small, hence electron neutrinos are converted not into pure muon flavor but a linear combination of all flavors. Compared to volume collisional production, when neutrino of different energies may be converted to sterile at every point of the SN, but with different probability, resonant conversion scenario is closer to surface emission, as neutrinos with energy E are being converted and emitted only from a surface, for which condition 3.46 is true. An example of P_{res} values are presented at Fig. 3.10 Figure 3.7 illustrates the above considerations. Energy levels $E_a(r)$ and $E_b(r)$ do not cross. The value $E_a - E_b$ reaches its minimum as $r \to R_{\text{res}}$. In the case of fully adiabatic propagation (*i.e.* change of the radius) one remains on the same energy level $E_a(r)$ or $E_b(r)$. As a result, a state $\langle \nu_x |$ that is *mostly* $\langle \nu_a |$ deep inside the star would remain *mostly* $|\nu_a\rangle$ everywhere and would exit the star as mostly sterile state $|\nu_s\rangle$. The probability of such a process for $\theta_0 \ll 1$ is given by $P_{x \to s}^{\text{adiab}} \sim \cos^2 \theta_0 \to 1$ – the result familiar from the MSW effect in the Sun. This can be seen from Eq. (3.50) when the parameter of non-adiabaticity $\gamma \to 0$. Last detail is the probability for neutrino to interact during crossing the resonance region. If it does, its wave function is collapsed producing either pure active neutrino or sterile neutrino which corresponds to previously discussed collisional production. Taking this
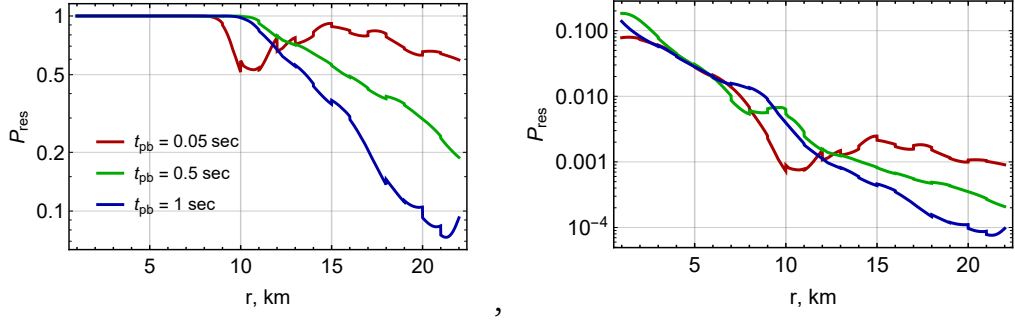
Figure 3.10: Dependence of the resonant conversion probability 3.50 on the radius, calculated for $U^2 = 10^{-11}$ (**left panel**) and $U^2 = 10^{-14}$ (**right panel**). Behaviour of the conversion probability corresponds to the rate of V_{eff} change. At small radii $R \lesssim 10$ km, core density varies slowly, leading to the most adiabatically transition, at larger radii, effective potential begin to drop rapidly (see Fig. 3.8) and the transition becomes non-adiabatic. It is seen, that at the beginning of the explosion, when the gradient of matter density is not large, conversion probability is much larger, than at later times, giving up to order-of-magnitude difference.

into account, the number of ν_s with energy E, resonantly produced by the time t and travelling into the solid angle $d\Omega$ is given by (we assume that $E \approx |\vec{p}|$, *i.e.* sterile neutrinos are ultra-relativistic):

$$\frac{d^2 N_s(t, E)}{dE\, d\Omega} = \int_0^t 4\pi R_{\text{res}}^2(E) E^2 \bar{f}_x^{\text{out}}\Big(t', R_{\text{res}}(E), E\Big) P_{x \to s}(E) e^{-R_{\text{width}}/\lambda_{\text{mfp}}} dt'.$$

(3.51)

here, $R_{\text{res}}(E)$ is the radius, at which resonance condition is satisfied for anti-neutrinos with the energy E, f_x^{out} - outgoing flux of active neutrinos of flavor x, factor $e^{-R_{\text{width}}/\lambda_{\text{mfp}}}$ stands for probability of active neutrino not to interact during crossing the resonance. We will focus on studying this scenario for the case of muon and tau mixing.

3.5.2 Back reaction of neutrino production, active neutrino population evolution during sterile neutrinos emission

Depletion and re-population of active neutrinos.

Sterile neutrinos production mechanism described above, for both resonant and collision conversion, acts effectively only on x- flavor anti-neutrinos.

During the neutrino conversion process, the population of anti-neutrinos at each resonance radius is being depleted, while the population of active neutrinos remains almost unchanged, as the production via vacuum mixing angle is negligible. Consider neutrino with energy E_ν and corresponding resonant radius for such neutrinos R_{res}. Before the production starts, if this radius is close to the core, the population of neutrinos has an equilibrium value $n_{\nu_x} \sim T^3$ given by FD spectrum in correspondence to the SN model. We can estimate the total energy density stored in thermal neutrinos in the SN volume:

$$E_{\nu,\text{therm}} = \int 3.15 \cdot T(r) \cdot n_{\nu_x}(T(r)) d^3 r \sim 10^{51} \text{erg} \qquad (3.52)$$

Resulting value is two orders of magnitude smaller, than estimated total emitted energy. Also, sterile neutrinos, as we will see, can indeed lead to energy emission at the level of $\mathcal{E}_{\text{max}} \approx 10^{53} \text{erg s}^{-1}$. If there was no re-population processes, all neutrinos would be washed-out of the supernovae during conversion process with the timescale $\tau_{\nu_s,\text{prod}} = E_{\nu,\text{therm}}/\mathcal{E}_{\text{max}} \sim 10^{-2}$ s. But the similar processes, that keep neutrinos in equilibrium also lead to refilling of thermal population - processes like nucleon-neutrino scattering

$$\bar{\nu}_x + N \rightarrow \bar{\nu}_x + N \qquad (3.53)$$

return the shape of neutrino distribution to equilibrium form, though it does not change the number of neutrinos at correspondent resonance radii. Together with it, intense nucleon-nucleon bremsstrahlung produces neutrino-antineutrino pairs

$$N + N \rightarrow N + N + \bar{\nu}_x + \nu_x, \qquad (3.54)$$

that can refill the "lost neutrinos". The reaction rates of the processes (3.53)–(3.54) are faster than sterile neutrino conversion rate [219]. It allows to assume the local thermal equilibrium for neutrinos during the sterile neutrinos production and hence, always use the FD distribution for f_{ν_x}. Note, that the rate of the process (3.54) depends on the distribution function of neutrinos due to Pauli blocking $\Gamma_{NN \rightarrow NN\nu\bar{\nu}} \sim (1 - f_{\nu_x})(1 - f_{\bar{\nu}_x})$. Since the conversion process does not affect the population of neutrinos ν_x, reaction (3.54) can create much more neutrinos than was present before the start of conversion. It would lead to slowing down the rate of the process (3.54) and hence, not complete refilling of neutrinos that were converted to HNLs. For the local

equilibrium case, it will be described by adding a lepton chemical potential for neutrino FD distributions:

$$\bar{f}_x(E, r, t) = \frac{1}{(2\pi)^3} \frac{1}{\exp\left[\frac{E + \mu_x(r,t)}{T(r)}\right] + 1} \tag{3.55}$$

(with $\mu_x \to -\mu_x$ for neutrino distribution function). *The evolution of the neutrino population is hence fully encoded into the evolution of the chemical potential μ_x and the value of the temperature of the supernovae.* This additional source of asymmetry between particles/anti-particles would be displayed in the change of V_{eff}. If in the SM scenario asymmetries for x-flavor is negligible [185], for the case of sterile neutrinos. Correction for the effective potential may become noticeable. The effect on the potential V_{eff} and, therefore, the resonance energy (3.46) via the change of the lepton number Y_x would definitely affect the production rate of sterile neutrinos. It is seen from the expression for resonance energy (3.46) that with the growth of Y_x the resonance energy increases, so that the number density of active anti-neutrinos with energy $E \geq E_{\text{res}}$ diminishes. If the asymmetry reaches the value of

$$Y_{\nu_\tau}^{\max} \approx \frac{1 - Y_e - 2Y_{\nu_e} - 2Y_{\nu_\mu}}{4} \tag{3.56}$$

or, in the case of muon mixing

$$Y_{\nu_\mu}^{\max} \approx \frac{1 - Y_e - Y_\mu - 2Y_{\nu_e} - 2Y_{\nu_\tau}}{4} \tag{3.57}$$

, the resulting resonance energy becomes infinite. Here in the latter case, we have included term with asymmetry of $\mu^\pm$ as in the case of very large lepton symmetries which, muons may be also present in plasma (while they remain negligible in the $\tau-$mixing case). It is a result of the increase of average energy of neutrinos in the presence of effective potential - larger number densities force neutrinos to occupy higher energy states and making them able to produce muons in reactions:

$$\nu_\mu + n \to p + \mu^- \tag{3.58}$$

$$\nu_\mu + e^- \to \mu^- + \nu_e \tag{3.59}$$

$$\nu_\mu + \bar{\nu}_e \to \mu^- + e^+ \tag{3.60}$$

leading to potential non-negligible population of μ^-. Similar reactions are possible for anti-neutrinos and anti-muons, but the number density of $\bar{\nu}_\mu$

is smaller in this asymmetry regime and they have slightly smaller energy, leading to less abundant production of μ^+. Because of this, muon lepton number asymmetry will be stored not only in neutrinos, but in muons as well, affecting also the number density of neutrons/protons through the electro-neutrality condition. The population of $\tau^\pm$ leptons remains negligible for because of their large mass. Hence we see, that the back-reaction effect of the production of sterile neutrinos - change of ν_x population, affects production rate through two quantities - a decrease of effective potential and decrease of anti-neutrinos number density available for conversion. Both of them lead to a decrease in the production of sterile neutrinos. **Diffusion of the lepton**

number The inhomogeneous chemical potential $\mu_x(r,t)$ triggers the lepton
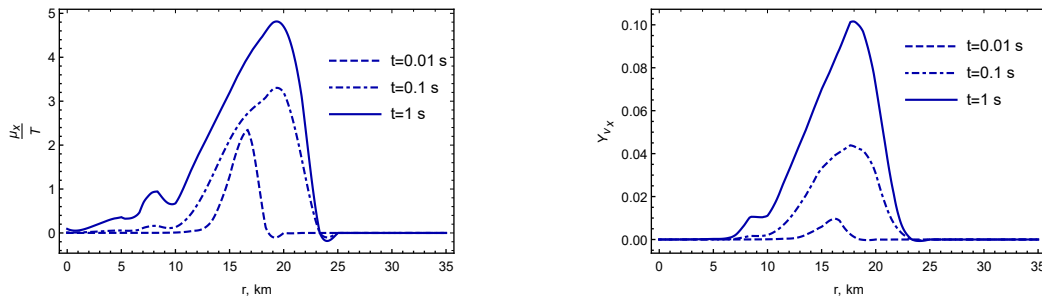
Figure 3.11: The same as for Fig. 3.12, but without diffusion. In absence of asymmetry, change of asymmetry and related chemical potential proceeds independently on every radius. In the absence of diffusion, which can redistribute the large number density of neutrinos to less populated regions of the star, the maximum asymmetry is sufficiently larger. The value of V_{eff} can not change the sign in this case as once the asymmetry reaches a critical value, that set V_{eff} to zero, resonance energy becomes infinite, completely turning off the production. The peak position is changing with time slightly due to the change of resonance condition eq. (3.46) with the build-up of the asymmetry Y as well as with the change of parameters of SN.

number diffusion processes. *Neutrinos* (whose number exceeds greatly that of anti-neutrinos) diffuse away and the reactions like (3.54) then replenish population of anti-neutrinos A typical time scale for the diffusion over the distance R is $t_{\text{diff}} = \frac{R^2}{\lambda_{\text{mfp}}}$, where λ_{mfp} is the mean free path of (anti)neutrinos of x-flavour. The neutrino mean free path depends on the neutrino energy and matter density. A straightforward computation of neutrino scattering in a medium of non-relativistic nucleons gives $\lambda_{\text{mfp}} \sim \frac{\pi}{G_F^2 N_{\text{b}} E^2}$.[2] Typical values of neutrino energies in supernovae is $E \sim \mathcal{O}(100)$ MeV and densities can

---

[2]Recall that we are interested only in the diffusion of μ or τ flavours and therefore only neutral current processes contribute to the scattering of both neutrinos and anti-neutrinos.

reach $N_{\rm b} \sim 2 \times 10^{38}\,{\rm cm}^{-3}$ so diffusion time can be as low as $\mathcal{O}(10^{-2}\,{\rm sec})$ – much below the period of time over which we analyse the sterile neutrino production. Therefore diffusion cannot be neglected. To describe the evolution of the lepton asymmetry we use kinetic diffusion equation with diffusion coefficient $D(r, E)$ in the relaxation time-approximation:

$$D(r, E) = \frac{\lambda_{\rm mfp}(r, E)}{3} = \frac{\pi}{3 G_F^2 N_{\rm b}(r) E^2} \qquad (3.61)$$

The collisional production of sterile neutrinos can also affect the evolution of the chemical potential. Indeed, let $\Gamma^{\rm coll}_{\nu_x \to \nu_s}$ be the rate of collisional production of sterile neutrinos $\nu_x \to \nu_s$, while $\Gamma^{\rm coll}_{\bar\nu_x \to \nu_s}$ be a similar rate for anti-neutrino production (of course, ν_x and $\bar\nu_x$ produce sterile states of opposite helicity). Naively, one could argue that as there are more ν_x than $\bar\nu_x$ in the resonance region, the collisions will predominantly convert $\nu_x \to \nu_s$, thus decreasing the asymmetry. This is, however, not the case as the collision rates are not the same, $\Gamma^{\rm coll}_{\nu_x \to \nu_s} \ll \Gamma^{\rm coll}_{\bar\nu_x \to \nu_s}$ in the resonance region, see *e.g.* [7] where the resonance enhancement/suppression of the collisional production rate is discussed. Indeed, the collision rates are proportional to $\sin^2(2\theta)$. In the resonance region, angle for anti-neutrinos is $\theta^{\bar\nu_x}_{\rm res} \sim \mathcal{O}(1)$, while for neutrinos $\theta^{\nu_x}_{\rm res} \simeq \frac{1}{2}\theta_0$, as one can see by replacing $V_{\rm eff} \to -V_{\rm eff}$ in Eq. (3.49) and making use of the condition (3.28). As a result

$$\Gamma^{\rm coll}_{\nu_x \to \nu_s} \sim \theta_0^2 \Gamma^{\rm coll}_{\bar\nu_x \to \nu_s} \qquad (3.62)$$

With chemical potential reaching $\mu_x/T \sim 3$ (see Fig. 3.12) $n_{\bar\nu_x} \sim 10^{-2} n_{\nu_x}$ and therefore we conclude that collisions do not contribute significantly to the wash out of lepton asymmetry for mixing angles that we are considering. In order to get the equation for the evolution of asymmetry parameter Y_τ we start from radial diffusion equation for distribution function with a source

$$\frac{\partial f_x(r, E, t)}{\partial t} = \frac{1}{r^2} \frac{\partial}{\partial r} \left(r^2 D(r, E) \frac{\partial f_x(r, E, t)}{\partial r} \right) + I_x(r, E, t) \qquad (3.63)$$

where f_x - distribution function of ν_x $(\bar\nu_x)$, $D(E, r)$ – diffusion coefficient, $I_x(r, E, t)$ – source. By taking Eq. (3.63) for neutrinos and anti-neutrinos, integrating their difference over momentum, and dividing by $N_{\rm b}$ we find:

$$\frac{\partial Y_x(r, t)}{\partial t} = \frac{1}{N_{\rm b}(r)} \frac{1}{r^2} \int \frac{\partial}{\partial r} \left(r^2 D(r, E) \frac{\partial}{\partial r} (f_x(E, r, t) - \bar f_x(E, r, t)) \right) d^3p + S_x(r, t) \qquad (3.64)$$
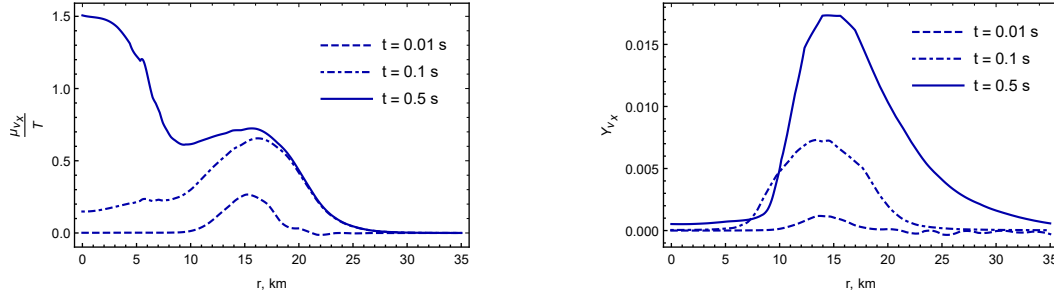
Figure 3.12: Evolution with time of the radial profiles of the lepton asymmetry Y_τ in the case of fiducial model. We have chosen the following parameters of sterile neutrino: $m_s = 7.1$ keV, the mixing angle $\sin^2 2\theta_\tau = 5 \times 10^{-11}$. We see, that production starts the most efficiently at radii $r = 10 - 15$ km right outside the stellar core, where the matter begin to decrease. With the growth of asymmetry it starts to diffuse to the inner and outer regions of the star. The core asymmetry is changing slowly as neutrinos there are trapped, while asymmetry at the large radius decrease rapidly. That is due to the increasing volume and that neutrinos efficiently escape the SN, hence it can not stack. It is seen, that equilibrium between diffusion and production is achieved in the outer layers within a fraction of a second and is maintained afterwards

here $S_x(r,t)$ is the integrated source of asymmetry

$$S_x(r,t) = \frac{\pi}{N_{\mathrm{b}}(r)} E^2_{\mathrm{res}}(r,t) f_x^{\overline{out}}(E_{\mathrm{res}}(r),r,t) P_{x\to s}(E_{\mathrm{res}}(r),r,t) \frac{dE_{\mathrm{res}}}{dr}(r,t)$$
(3.65)

Combining these results together, we arrive to the final equation describing the evolution of lepton number:

$$\frac{\partial Y_x(r,t)}{\partial t} = \frac{\pi}{6} G_F^2 r^2 N_{\mathrm{b}}(r) \frac{\partial}{\partial r}\left(\frac{r^2}{N_{\mathrm{b}}(r)} \frac{\partial \mu_x(r,t)}{\partial r}\right) +$$

$$+ \frac{\pi}{N_{\mathrm{b}}(r)} E^2_{\mathrm{res}}(r,t) \bar{f}_x(E_{\mathrm{res}}(r),r,t) P_{x\to s}(E_{\mathrm{res}}(r),r,t) \frac{dE_{\mathrm{res}}}{dr}(r,t) \quad (3.66)$$

Now, if we solve the system of equations (3.66) and 3.51 we can obtain the evolution of sterile neutrino spectra, produced resonantly.

3.6 Results: energy emission and the possibility of constraints

In our calculations, we have focused on the resonant production of sterile neutrinos, mixed solely with either ν_μ or ν_τ flavor. Following the approach

described in Sec. 3.5 we have calculated the emitted energy in the form of spectra of sterile neutrinos together with their spectra produced during the *first second* after the core bounce.[3] Besides the main "realistic" case, that accounts for every effect we mentioned, we have studied several regimes when diffusion is turned off as well as a regime with no back-reaction. Our results for the fiducial model are summarised in Fig. 3.13 (energy, carried out as a function of sterile neutrino parameters). We present the result for the $\nu_s - \nu_\tau$ mixing, the result for $\nu_s - \nu_\mu$ mixing does not differ. On the same plot, we add a modified fiducial model, where temperature in the central region $R \lesssim 20$ km is decreased by 20 %. It is for demonstration , on how contours may change under relatively small changes of internal parameters of the SN. We also

show, how the emitted energy depends on the temperature variation within our fiducial model as anther demonstration of how sensitive is the sterile neutrinos production to the exact temperature profile. To demonstrate the importance of the back reaction we have repeated the calculation procedure for two additional cases - *neglecting the back-reaction completely* and *neglecting the diffusion*. The comparison of the same-energy contours and comparison of neutrino spectra, produced for those three cases are given in Fig. 3.15 From our study, we see that the most important parameter, that defines the energy output is the maximal temperature in the SN interior in the area of conversion. Indeed, independently of the exact SN model, $Y_e \sim Y_{\nu_e} \sim 0.1$ therefore the resonance energy of the HNL production is

$$E_{\text{res}} \sim 9\,\text{MeV} \cdot \left(\frac{m_s}{10\,\text{keV}}\right)^2 \cdot \frac{\rho_B}{3 \cdot 10^{14}\,\text{g/cm}^3} \tag{3.67}$$

reaching $\mathcal{O}(100)$ MeV for $m_s \sim 30$ keV. With the decrease of SN media density or for neutrinos with larger masses, the resonance energy increases even more, significantly higher, than the temperature of the SN media. When $E_{\text{res}} \gg T_{\text{max}}$ the population of neutrinos is exponentially suppressed, effectively switching the sterile neutrino production off. Production with decrease of the mass below $m_s \lesssim 1$ keV is also suppressed in terms of energy emission. Although number density of neutrinos, available for conversion does not decrease as drastically as in the case of exponential suppression, but low-masses sterile neutrinos allow conversion for only low energy anti-neutrinos, that can not carry a lot of

---

[3]We neglected the production after the ~ 1 sec due to a decrease in temperature. Hence the production rate is essentially switched off.
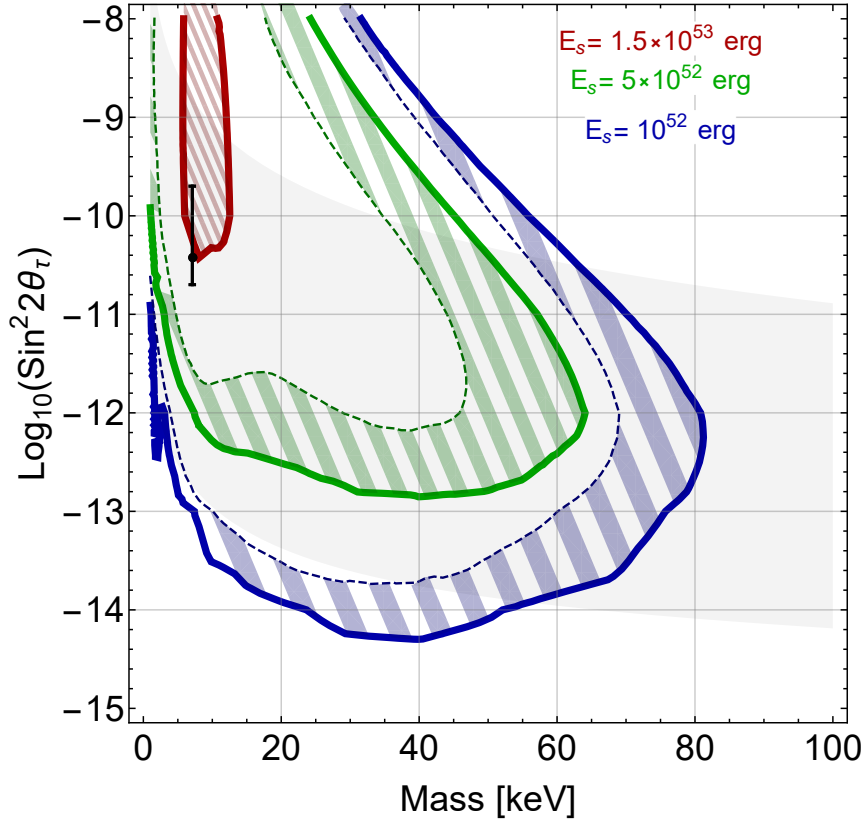
Figure 3.13: Main results: Energy, emitted in the form of sterile neutrinos mixed solely with ν_τ, produced in resonant conversion process during the first second after the core bounce. Thick solid lines correspond for contours of the same energy. A thinner dashed line of the same color corresponds to the same amount of energy as a thick line but in the SN model, where the temperature is artificially decreased by 20 % lower in the region close to SN core $R \lesssim 20$ km. And the shaded region is just an area, the contour passes if the temperature is modified. There is no dashed line for the central region since energy production is not sufficient to reach such values. As a reference value, we can use the total energy emitted in *all active neutrino species* which is $\approx 3 \times 10^{53}$ erg. We also add a light gray region which indicates, if the sterile neutrino can produce the correct dark matter density in the Early Universe in the *Neutrino Minimal Standard Model* (see Sec. 2). Though, it is not essential for SN production, if the sterile neutrino is a DM particle or not. Black dot with error bars corresponds to the 3.5 keV signal of [69, 76] interpreted in terms of decays of sterile neutrino dark matter.

energy so the energy output in this case is low. If we **ignore damping**, energy production rate for large mixing angles would be given by

$$\frac{d\mathcal{E}}{dt} \sim \int R^2 E_{\text{res}}^2 f_x(E_{\text{res}}, T) \frac{dE_{\text{res}}}{dR} dR \qquad (3.68)$$
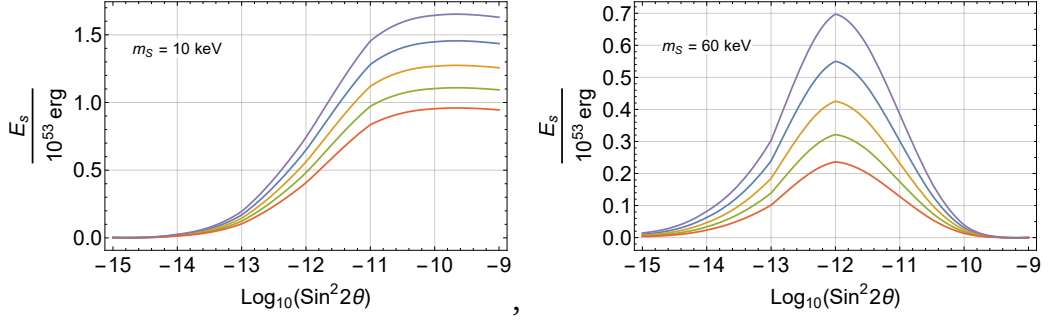
Figure 3.14: Energy, emitted in the form of sterile neutrinos for masses $m_s = 10$ keV (*top plot*) and 60 keV (*bottom plot*) depending on the mixing angle. Different contours correspond to temperature value modifier starting from 1 (base model) - the largest energy output, to the set of values 0.95, 0.9, 0.85, 0.8 as a sequence of contours with decreased production rate.
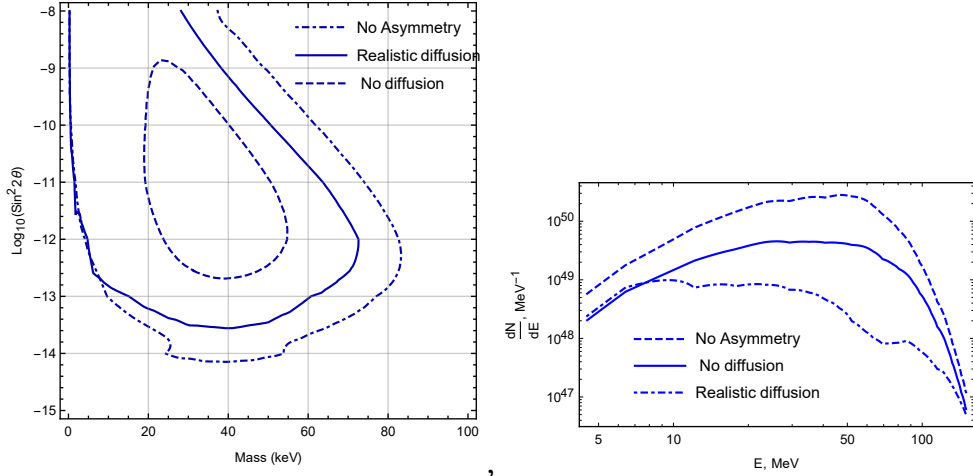
Figure 3.15: **Left panel:** Effects of the back-reaction of the sterile neutrino production. We have chosen the energy value $E_s = 0.25 \cdot 10^{53}$erg and found, which parameters of sterile neutrino are needed to emit this amount of energy during the resonance conversion in three cases of *realistic diffusion* (corresponding to our complete approach), *absence of diffusion* (where we take diffusion length to be infinitely small and hence, the depleted number of neutrinos is not affected by anything, then the resonance production) and *absence of back-reaction* which can be understood as an approximation of instant diffusion, when generated asymmetry is being washed out of the stars faster, that it is generated. **Right panel:** Spectra of sterile neutrinos with mass $m = 7.1$ keV and the mixing angle $\sin^2 2\theta_x = 5 \times 10^{-11}$ produced during the first second of explosion for three cases as was described for the left panel.

We can find, that the maximum (in terms of parameters of HNLs) of the production rate corresponds roughly to mass

$$\frac{d\mathcal{E}}{dm_s} = 0 \quad \rightarrow \quad m_s^{\mathrm{max}} = \sqrt{8 T_{\mathrm{max}} V_{\mathrm{eff}}}\big|_{r=r(T_{\mathrm{max}})} \tag{3.69}$$

This maximum mass production can be different at a different time due to varying temperatures and density profiles. There is no simple estimate for the emitted energy but one can assume that it also depends on the temperature at least as an energy density of active neutrinos $\sim T^4$ so the changes of this SN parameter is affecting the results quite significant and can depend on the explosion model a lot. Damping significantly distorts the picture as high energy/mass production becomes suppressed.

3.6.1 Supernovae toy model results, potential uncertainties

As a cross-check, that the values we obtained are not just accidental for a specific SN model we repeated all the machinery of calculations for our toy model described in Sec. 3.2.

The result is present at Fig. 3.16. Besides the toy model with parameters we introduced, we also calculated the result with slight variations of the - modified maximum temperature to values $T_{\max} = 25$ and 35 MeV and for another temperature profile (quadratic $T \sim r^{-2}$, compared to the linear one [4]). The influence of temperature modification in the toy model on the emitted energy is on a par with that in the fiducial model, such that that $10 - 20\%$ changes of temperature lead to modification of emitted energy via a factor of $\sim 2 - 3$.

Although we see a difference in the behavior of the emitted energy depending on the HNL parameter, which is absolutely expected due to the fact this toy model is very artificial of our model, some of the features remain the same in both fiducial and toy model results: *(i)* Maximum emitted energy in form of sterile neutrinos is always at the level $E_s \approx \mathcal{O}(1) \times 10^{53}$. It reflects that the back-reaction slows the conversion process efficiently in quite different conditions, such that it is hard to obtain the overproduction of sterile neutrinos over the production of active ones, *(i)* The influence of the potential uncertainty of temperature profile shape/ maximum values is relatively similar for both fiducial and toy model. Hence, this is not an accidental feature of a

---

[4] Assuming, that value of $T_{\max}$ in this profile as well as $T_{\min}$ is the same. As we have found out, energy emission at large radii is suppressed due to large resonant energy so the exact profile at $R \gtrsim 20 - 30$ km is not relevant.
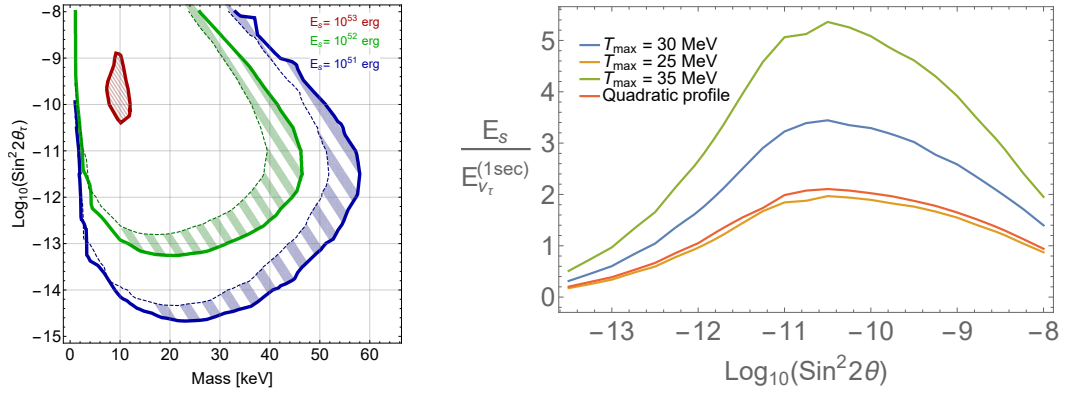
Figure 3.16: *Left panel:* Energy emitted by sterile neutrinos in a toy model (thick lines) and modified toy model (thin dashed lines) - when central temperature in the SN is decreased to 25 MeV, which correspond to scaling of temperature for $\approx 15\%$. Shaded region shows the corresponding "uncertainty" of production. Sterile neutrino are considered mixed solely with ν_τ. *Right panel:* Uncertainties related to the SN temperature models. Energy, emitted in the form of sterile neutrinos as a function of the mixing angle for the mass $m_s = 20$ keV. The curves show the effects of changing the maximal temperature $T_{\max}$ by ± 5 MeV as well as and different scaling of the temperature profile between $T_{\max}$ and $T_{\min}$ (quadratic rather than linear).

particularly chosen explosion simulation/particular snapshots. The production rate is indeed very sensitive to the exact values of the temperature inside the supernovae, information about which, unfortunately, we have nowhere to draw from. Since the inner part of the SW, close to the core, is non-transparent in relation to both neutrinos and photons. So we can only rely for now on the numeric simulations of star collapse and subsequent explosion, which, as we have shown in Fig. 3.5 can be very different. In order to qualify the uncertainties, we also repeat our calculations in the model with the same temperature profile, suppressed in amplitude by 20% – a highly conservative estimate The exact value of temperature modification we used does not have any well-defined origin. The main point here was to demonstrate, how much production of sterile neutrinos depends ont the assumed temperature. As the temperature difference (in the area of most intense production - around 10-20 km) may be much higher, than correction of $15 - 20$ %, see the comparison of temperature in two different simulations at Fig. (3.5). Hence, we only wish to demonstrate, that even smaller modification can lead to significant changes in sterile neutrino energy production. We stress that Fig. 3.13 *does not*

correspond to any constraints on sterile neutrino parameters. Given our current knowledge about SN explosions in general and about SN1987A in particular,

it is impossible to determine what energy loss would be incompatible with existing scarce observations (see Section 3.4 and **??** for discussion). Additionally, a pure resonant conversion without scattering production does not exceed the commonly used limit of $3 \cdot 10^{53}$ erg [181] so we avoid setting even order-of-magnitude constraints.

Cosmological constraints on HNLs

<div style="text-align: right">

4

</div>

4.1 BBN

One of the most important and accurate measurements referred to early Universe is the abundance of the light elements - D, He-3, He-4, Li-7. The Standard model scenario of production of such elements - primordial nucleosynthesis (BBN) can predict the corresponding abundances in the Universe with high accuracy. The corresponding cosmological observations can give those abundances relatively (compared to many others) high accuracy. As a consequence, the presence of feebly interacting particles that affect primordial nucleosynthesis may be significant enough to set constraints on their parameters.

4.1.1 Observation of primordial abundances

The abundance of the light elements does not remain unchanged after the BBN. After the star's formation started, nucleosynthesis inside them during thermonuclear burning reactions will transfer a fraction of light elements into heavier elements. Depending on the degree of star formation and burning, observed abundances of light elements would be shifted from the initial value while the presence of heavy - metal - elements would become noticeable. Hence, only low-metallicity regions become interesting for measurements.

Currently, Helium measurements are based on the relative strength of emission lines of H-I and He-I in metal-poor local galaxies. The observed value then can be extrapolated to zero metallicity. The same approach is used for other abundances, like deuterium $D/H \equiv \mathcal{N}(DI)/\mathcal{N}(HI)$ or other elements and isotopes.
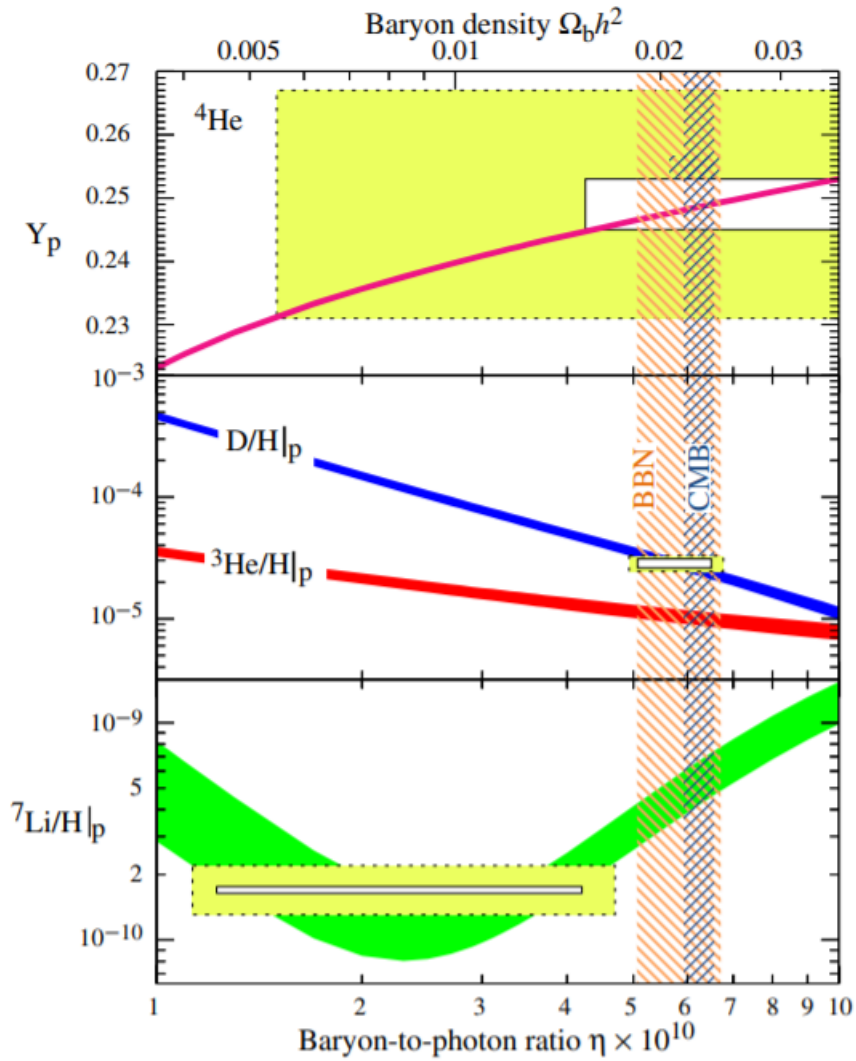
Figure 4.1: Light elements abundances observations (white boxes corresponding to statistical error, and the yellow - systematics) with 2σ confidence level data together with the SM predictions of their values for $D, {}^3He, {}^4He, Li$. Thickness of the lines correspond to theoretical uncertainty. Credits: [191]

According to PDG, the current most precise measurements provide around a one percent precision for deuterium:

$$D/H = (2.547 \pm 0.025) \cdot 10^{-6} \tag{4.1}$$

A different selection of observations may give a bit different result, which is still consistent with each other within $1\,\sigma$. The data is obtained from the regions with low metallicity $(0.001\text{-}0.03)\times$ Solar and since there are no more sources of deuterium, it will correspond to primordial value.

For the Helium-4 , PDG recommends the next value for mass fraction of Helium to total baryon mass:

$$Y_p = 0.245 \pm 0.003, \tag{4.2}$$

The uncertainty of a particular result may vary from $< 1\%$ ($Y_p = 0.2551\pm0.0022$ [135]) up to 2-2.5 % [**Fernandez:2018xx**, 40, 174, 222] at the level of 2σ. However, there is a discrepancy between those results which does not make them fully consistent. The possible reason could be different account of systematics [66]. Hence, while it is not completely stabilized, the error we consider would be the largest difference between the current results leading to the conservative bound

$$0.238 < Y_p < 0.257 \tag{4.3}$$

corresponding for $\approx 3.8\%$ error.

Another Helium isotope - $^3\mathrm{He}$ data comes only from Solar-metallicity regions in the Galaxy, hence could only roughly correspond to the primordial value. The observed abundance with no radial dependence in our galaxy was interpreted as upper limit for the primordial value [44]

$$^3\,\mathrm{He/H} < (1.1 \pm 0.2) \cdot 10^{-5} \tag{4.4}$$

In the case of Lithium-7, extrapolation for zero-metallicity is unavailable and observational data provides a lower bound for its abundance from low-metallicity stars ($\mathrm{Fe/H} \ll 10^{-3}(\,\mathrm{Fe/H})_{\text{solar}}$). The value may vary in differ-

ent star samples and can correspond to destruction of ^{7}Li in stars atmosphere.Therefore, available measurements (e.g. [196]) gives the next bound:

$$^7\text{Li/H} > (1.6 \pm 0.3) \cdot 10^{-10} \qquad (4.5)$$

There is no observation of primordial Tritium as it is unstable and decays, while the primordial abundances of Heavier stable elements would be extremely low. Therefore, the best accuracy of measurements is associated with deuterium and Helium-4. Illustration for abudances of light elements is shown at Fig. 4.1

4.2   SM BBN

The Standard model Big Bang Nucleosynthesis scenario is completely based on the neutron-to-proton ratio in the Universe at the moment of nuclei production. Free neutrons decay will not be observed since they decay fast $\tau_\text{n} \approx 880$s, so the relative abundance of all elements will be determined by neutrons and protons at the earliest stages of Universe evolution.

4.2.1   Instant freeze-out approximation

Let us start from the temperature, much higher, than the one, relevant to BBN. At the highest temperatures of $T > T_\text{QCD}$, there are no bound states of baryons or mesons and only free quarks are present at plasma. When the temperature drops below the QCD phase transition, quarks are getting bounded producing a huge variety of hadrons. Their population could be significantly higher, than allowed by thermal production since the $T_\text{QCD} \sim 10^2$ MeV is lower, than mass of most of hadrons while number density of quarks available for forming bound states before the transition was comparable to the one of photons due to low mass of first quark's generation. Hence, "excessive" hadrons would either decay fast or annihilate. Population of baryons, though, will not go to zero at low temperatures due to the presence of baryon asymmetry of the Universe resulting in a tiny fraction of baryons survive at the level of $n_b/n_\gamma \sim 10^{-10}$. At the temperature of few $\cdot$ MeV, only neutrons and protons are present at

plasma among all hadrons. Ratio of their densities is kept in equilibrium by weak reaction processes, converting $n \leftrightarrow p$:

$$n + \nu_e \leftrightarrow p + e^- \tag{4.6}$$

$$n + e^+ \leftrightarrow p + \bar{\nu}_e \tag{4.7}$$

$$n \leftrightarrow p + e^- + \bar{\nu}_e \tag{4.8}$$

Ratio of neutron to proton densities is given by Boltzman distribution:

$$\frac{n_n}{n_p} = Exp\left[-\frac{Q - \mu_e}{T}\right] \tag{4.9}$$

where μ_e - electron flavor asymmetry in leptons. This parameter in SM is very small, of the order of baryon asymmetry and hence, can be neglected. $Q = m_n - m_p. = 1.293$ MeV - mass difference between neutron and proton.

Weak processes decouple when their rate equal to Hubble rate

$$\Gamma_{\text{w}}(T) = H(T), \quad \Gamma_{\text{w}} \sim G_{\text{F}}^2 T^5, \quad H = \left(\frac{1.66\sqrt{g_*}T^2}{M_{\text{pl}}}\right) \tag{4.10}$$

where M_{pl} - Plank mass, g_* - effective number of relativistic species in plasma (see Plot 4.2), in the SM at temperatures $T \sim 1$ MeV plasma consist of photons, electrons, positrons and three neutino/anti-neutrino species each with either equilibrium or close to equilibrium distribution. Value of g_* in Standard model is:

$$g_* \approx 2 + \frac{7}{8}\left(2 \cdot 2 + 2 \cdot 3\right) = 10.75 \tag{4.11}$$

First-term corresponds for two photons polarisation, factor $\frac{7}{8}$ - for all fermions, for which $2 \cdot 2$ - two spin states for electrons and positrons and $2 \cdot 3$ - 1 spin state for each neutrino and anti-neutrino of each flavor. An accurate calculation of this parameter, that does not assume perfect equilibrium distribution of neutrinos will give a slightly different value. Due to electron-positron annihilation at lower temperatures, its value will decrease at $T < m_e$.

Such estimate gives a temperature of weak reaction decoupling $T \approx$ 2-3 MeV.
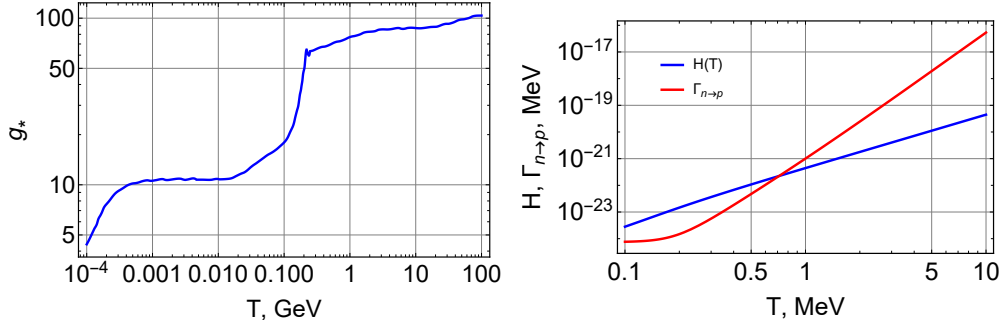
Figure 4.2: Left panel: evolution of effective number of relativistic species with temperature. Two rapid drops correspond to the electron-positron annihilation at $T \approx 0.1$ MeV and the QCD transition at $T \approx 150$ MeV. **Right panel**: Comparison of the SM Hubble and $n \to p$ weak conversion rate behaviour with temperature. At smaller temperature, $\Gamma_{n \to p}$ formally becomes higher, than Hubble rate. But only because it has a constant contribution from neutron decays. But at such temperatures, no more neutrons left.

More accurate calculation of $n \leftrightarrow p$ conversion rate is given by:

$$\Gamma_{\text{n} \to \text{p}} = \Gamma_{n\nu \to ep} + \Gamma_{ne^+ \to p\bar{\nu}} + \Gamma_{n \to pe\bar{\nu}} \tag{4.12}$$

With partial rates

$$\Gamma_{n\nu \to ep}(T) = \frac{(1 + 3g_1^2)G_F^2}{2\pi^3} \int\limits_0^\infty dk_\nu \sqrt{(Q + k_\nu)^2 - m_e^2}(Q + k_\nu)k_\nu^2 f_\nu(k_e)f_e(-Q - k_\nu), \tag{4.13}$$

$$\Gamma_{ne^+ \to p\bar{\nu}}(T) = n_e \sigma_{ne^+ \to p\bar{\nu}} \upsilon \approx \frac{(1 + 3g_1^2)G_F^2}{2\pi^3} \int\limits_0^\infty dk_e k_e^2 (Q + E_e)^2 f_e(E_e) f_\nu(-Q - E_e), \tag{4.14}$$

$$\Gamma_{n \to pe\bar{\nu}}(T) \approx \frac{(1 + 3g_1^2)G_F^2}{2\pi^3} \int\limits_0^{\sqrt{Q^2 - m_e^2}} dk_e k_e^2 (Q - E_e)^2 f_e(-E_e) f_\nu(-Q + E_e), \tag{4.15}$$

where $g_1 = 1.26$ - from axial current component. E_e energy of the electron, f_x - equilibrium distribution function of particle x. . Hubble and weak conversion rates become equal at temperature $T_n = 0.71$ MeV, see left panel of Fig. 4.2. We would refer to this temperature as *neutron freeze-out temperature*. Starting from this temperature, neutron abundance would change only due to decays of neutrons and Universe expansion.

When temperature drops below the electron mass, rate of EM reactions, that are in perfect equilibrium:

$$e^- + e^+ \leftrightarrow \gamma + \gamma \tag{4.16}$$

start to tend to the r.h.s. When the Universe cool down, energy of photons become not enough to produce electron -positron pair, while nothing stops the annihilation. As soon as temperature drops below $T \ll m_e$ the population of electrons and positrons almost completely disappear (up to the value of number density of protons, due to the electroneutrality). During this annihilation photons are being heated up with the annihilating electrons, but other decoupled species - nucleons and neutrinos do not recieve anything. As a result their relative (to photons) abundance decreases. For nucleons, the same as for neutrinos there appears additional factor for number density (and for energy, in the case of neutrinos). This factor can be found from entropy release. Due to relation of entropy conservation, we can find how would scaling factor change due to this rapid energy release at temperature of annihilation T_ann

$$s(T)a(T)^3 = \text{const}, \quad \frac{a(T > T_\text{ann})}{a(T < T_\text{ann})} = \frac{2}{2 + \frac{7}{8}4} = \frac{4}{11} \tag{4.17}$$

Hence number density of all decoupled particles would get a rapid decrease with factor $\left(\frac{4}{11}\right)$ and the energy of neutrinos would be changed with factor $\left(\frac{4}{11}\right)^{1/3}$.

Introducing neutron fraction at the moment of decoupling :

$$X_n^\text{eq}(T_n) \approx \frac{e^{-Q/T_n}}{1 + e^{-Q/T_n}}, \tag{4.18}$$

$$X_n^\text{eq}(T < T_n) = X_n^\text{eq}(T_n) \cdot Exp\left[-\frac{t(T)}{\tau_n}\right] \tag{4.19}$$

During the evolution of free neutrons, they can participate in nuclear reaction, forming deuterium $n + p \rightarrow d + \gamma$ since nuclear reactions have significantly higher rate, than weak processes. But in the same time, photo-disintegration by photons in plasma prevents deuterium to survive. It means, that there could not be a significant population of deuterium until photons can effectively destroy it. Such moment can be estimated as temperature, at which number

of photons with energy, higher, than deuteron binding energy $Q_d \approx 2.22$ MeV is equal to total number of baryons

$$n_\gamma^{E_\gamma > Q_d} = \int_{Q_d}^{\inf} f_\gamma(T, p_\gamma) d^3\mathbf{p}_\gamma \approx \frac{Exp[-T/Q_d]}{\pi^2} T \cdot (Q_d^2 + 2Q_d T + 2T^2) = \eta_B \cdot n_\gamma(T) \tag{4.20}$$

. Solution of this equation gives $T_d \approx 75$ keV and only weakly (logarythmic dependence)depends on the parameter of baryon-to-photon ratio. After this temperature, network of nuclear reactions start producing light nuclei. But going straight to the result, almost all neutrons that did not decay before $t_{BBN} \equiv T_d$ end up in Helium-4, so primordial mass abundance of ^4He can be estimated as

$$Y_p = 2X_n(t_{BBN}) = 2X_n^{eq}(T_n)e^{-t_{BBN}/\tau_n} \tag{4.21}$$

. It means, that accurate calculation of neutron-to-proton ratio at the moment of start of nuclear synthesis can be translated into Helium-4 abundance.

4.2.2 Exact evaluation of neutron abundance

The estimate, we shown before, can be refined using Boltzmann equation approach. The neutron abundance $X_n(t)$ is a solution of the following kinetic equation:

$$\frac{dX_n}{dt} = \Gamma_{p \to n}(t)(1 - X_n) - \Gamma_{n \to p}(t)X_n,$$

$$H^2(t) = \frac{8\pi G_N}{3}\rho(T), \tag{4.22}$$

To solve this equation we need the temperature (time) dependence of the $n \leftrightarrow$ p conversion rates - $\Gamma_{n \to p}(t)$, $\Gamma_{p \to n}(t)$ and $T(t)$, one can find the evolution of X_n. When those rates are much higher, than Hubble rate, solution of Boltzmann equation can be given by local equilibrium value obtained from setting r.h.s. of Eq.(4.22) to zero:

$$X_n^{eq}(T) \equiv \frac{\Gamma_{p \to n}}{\Gamma_{p \to n} + \Gamma_{n \to p}}, \quad \frac{n_n}{n_p} = \frac{\Gamma_{p \to n}}{\Gamma_{n \to p}}, \quad T > T_n \tag{4.23}$$

If all particle species participating the rates are in thermal equilibrium - with Fermi-Dirac distribution, n-to-p ratio from local equilibrium value can be calculated directly from conversion rates or from Boltzmann distribution. In the SM scenario, neutrinos decouple earlier, than the freeze-out of $n \leftrightarrow$

p conversions. But although neutrinos can not maintain their Fermi-Dirac distribution with weak reactions, there are no sources of significant distortions of their spectra.[1]

Let us compare the behaviour of $X_n(T)$ and final value $X_n(T_{BBN})$, obtained from Boltzmann equation and from estimate:
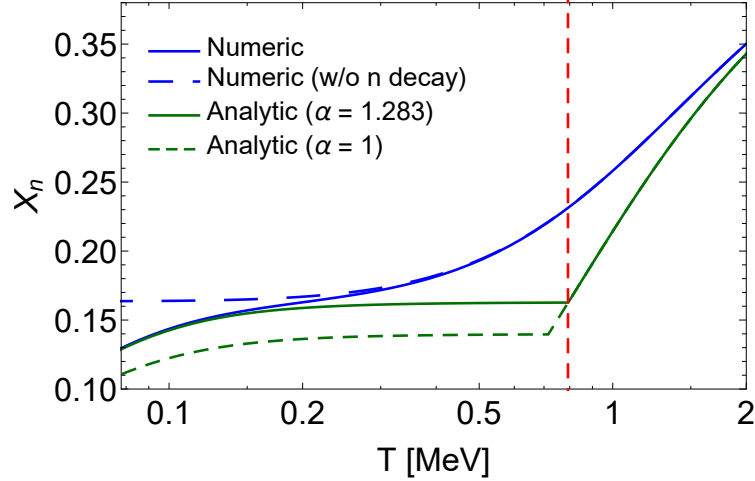
Figure 4.3: *Left panel*: a behavior of the neutron abundance X_n in SBBN. The blue lines denote the numeric solution of Eq. (4.22) with (solid line) and without (dashed line) neutron decays. The green lines correspond to the analytic estimate (4.21), according to which X_n is in dynamical equilibrium until the temperature T_n given by Eq. (4.24). The vertical red line denotes the value of $T_n \approx 0.793$ MeV for a choice $\alpha \approx 1.283$. *Right panel*: a behavior of X_n in presence of toy model $p \leftrightarrow n$ rates which are much larger than the SM rates, maintain $X_n = 1/2$ and rapidly switch off at $T = 1.2$ MeV. See text for details.

As expected, evolution of X_n at large temperatures completely coincides with the simple estimate. When temperature decreases, difference between numeric and analytic result increases and relative discrepancy can be as high as $(X_n^{\text{num}} - X_n^{\text{ana}})/X_n^{\text{num}} \approx 45\%$ at the estimated temperature of decoupling $T = T_n$ (so despite this estimate gives relatively good correspondence with the numeric result at higher and lower temperatures, at the decoupling, difference may be quite significant). With the further temperature decrease, the discrepancy is getting smaller finally became almost constant at the level of $X_n^{\text{analytic}}/X_n^{\text{numeric}}$ at $T \ll T_n$ once numeric solution shows freeze-out of neutrons. This relates for the final $X_n(T_{BBN})$ value as well.

---

[1]There are minor distortions occurring during electron-positron annihilation at $T \lesssim m_e$ due to annihilation channel $e + \bar{e} \to \nu + \bar{\nu}$, but it happens at temperatures, lower, than neutron freeze-out

Note, that analytic T_n behavior at temperatures $T_{n,\,\mathrm{dec}}$ does not have much in common with "true" freeze-out behavior of neutrons. It is seen from the Fig. 4.3, that only at the temperature of $T \approx 200 - 300$ keV neutron abundance start to evolve only due to decays, meaning, that all $n \leftrightarrow p$ conversion $2 \leftrightarrow 2$ reactions already decoupled (as we have mentioned, formal rate of neutron decay will become higher, than Hubble rate at some moment, but that does not mean anything, as all neutrons would be either bounded or decayed up to than moment). Such smooth decoupling is a result of the power law of interaction rates, that is partially canceled with Hubble rate temperature behavior.

Yet, at smaller temperatures, discrepancy is smaller so such estimate represent the final result relatively good. For the further estimates we can impose a bit "modified" estimate of the neutron decoupling temperature, that reproduces the numeric result:

$$\Gamma_{n \to p}(T_n) = \alpha \cdot H(T_n), \quad \text{where} \quad \alpha \approx 1.283, \tag{4.24}$$

It is seen in Fig. 4.3, that not only the final result for neutron abundance coincide, but temperature-dependent behavior at intermediate temperatures is closer to the numeric result.

4.2.3 Corrections

Now, let us look, how new physics can affect the BBN at the stages before start of light nuclei synthesis, (let us call it *pre-BBN phase*) or in other words, how neutron abundance can be affected. Let us consider the estimate (4.21) to classify, which quantities can be affected

- Neutron decoupling temperature T_n - defines the neutron-to-proton ratio at decoupling. This parameter can be affected by changing both the expansion rate of the Universe and the interaction rates.

- Neutron-to-proton ratio temperature dependence $X_n(T)$. In the SM case, n/p value is given by Boltzmann exponent so this value is fixed at decoupling but in the BSM case, non-equilibrium corrections for the conversion rates might change it due to (4.23).

- Neutron free decay time t_{BBN} - this parameter can be affected if the Hubble rate changes or the temperature of the deuterium bottleneck T_d is shifted. The latter case is highly unlikely as it depends on the highly-equilibrium photon distribution and baryon-to-photon ratio parameter η_B. In what follows we will see, that this value can be affected with decays of non-equilibrium particles.

Physically, change of those values is a result of the change of Hubble rate $\equiv$ change of effective number of relativistic degrees of freedom g_* or change of weak conversion rates that are separated into either modification of active neutrino spectra or rates, associated with particles, that are absent in the SM scenario.

For a simple beginner estimate, let us consider a case, when additional decoupled particle species are present in plasma at the moment of neutrino decoupling, hence not changing $n \leftrightarrow p$ conversion rates (for example, dark matter particles or HNLs with small mixing angle that did not decay yet). This would result in additional energy density compared to the SM case that can be expressed in a correction to the effective number of neutrino species:

$$\delta g_* \equiv \frac{\rho_{\,\mathrm{bsm}}}{\pi^2/30T_n^4} \tag{4.25}$$

Increase of the energy density leads to faster Universe expansion and hence - for an earlier decoupling of neutrons. Assuming δg_* is small compared to $g_{\mathrm{SM}}(T \sim \mathrm{MeV}) \approx 10.75$ in the SM case:

$$H(T) = \frac{1.66}{M_{pl}}\sqrt{g_*} = \left(1 + \frac{\delta g_*}{2g_{\,\mathrm{SM}}}\right) H_{\mathrm{SM}}(T) \tag{4.26}$$

Taking our modified estimate (4.24) and assuming for the rough estimate $\Gamma_{n \to p} \sim T^5$ we find correction for the decoupling temperature

$$T_n \approx T_n^{\mathrm{SM}} \left(1 + \frac{\delta g_*}{6g_{\,\mathrm{SM}}}\right) \tag{4.27}$$

leading to the change of neutron-to-proton ratio

$$\frac{n_n}{n_p} = \left(1 + \frac{Q}{T_n}\frac{\delta g_*}{6g\text{ SM}}\right)\frac{n_n}{n_p}\Big|\text{ SM} \tag{4.28}$$

Effect of correction to energy density is not limited to the change of neutron-to-proton ratio at decoupling. Larger value of the Hubble parameter leads to faster Universe cooling so it reaches the temperature of T_d faster and there is less time for neutrons to decay.

Strictly speaking, time-to-temperature relation depends on the dynamics of the g_* which is non-trivial even in the SM scenario due to electron-positron annihilation. But since most of time passes, when temperature is low and effective number of species is established we still can use simple estimate:

$$t(T_d) = \frac{M_{\text{pl}}}{2 \cdot 1.66\sqrt{g_{eff}}T_d^2} \approx t_{\text{ BBN}}\left(1 - \frac{\delta g_*}{2g\text{ SM}(T_d)}\left(\frac{4}{11}\right)^{4/3}\right) \tag{4.29}$$

here $t(T_d)|_{\text{ SM}} \approx 200$ s, factor $\left(\frac{4}{11}\right)^{4/3}$ appears since $e - e^+$ annihilation affects all decoupled species, diluting them. Note, that this estimate will work only in case if correction to energy density is generated by relativistic particles, otherwise their energy density contribution will not scale as T^4 but as T^3, only with number density. So in case of non-relativistic contribution, correction δg will be increasing with temperature.

Together with (4.28), final estimate for the change of neutron to proton ratio at $T = T_d \equiv$ estimate for Helium abundance change is

$$Y_p \approx Y_p^{\text{ SM}}\left(1 + \frac{Q}{T_n}\frac{\delta g_*}{6g\text{ SM}(T_n)} + \frac{t_{\text{ BBN}}}{\tau_n}\frac{\delta g_*}{2g\text{ SM}(T_d)}\left(\frac{4}{11}\right)^{4/3}\right) \approx Y_p^{\text{ SM}}(1 + 0.04 \cdot \delta g_*) \tag{4.30}$$

Increase of the energy density leads to increase of Helium outcome. Such estimate is the simplest constraint one can set for novel particles, that might be present before T_d. Note, that this estimate accounts only effect of decoupled species without considering their decays, energy injections, distortions of particles spectra etc. We will see in what follows, that this effect is only minor one compared to others. Moreover, it becomes completely negligible for a certain region of HNL parameters. We will not consider other minor changes, that might appear like change of neutron life-time due to Fermi-blocking in

case of presence of non-equilibrium corrections to neutrino spectra. Also, we will discuss *post-BBN* effect later.

4.2.4 Synthesis of lightest nuclei:Deuterium production

Besides weak reactions, there are also strong nuclear reactions between neutrons and protons. Although their rate is suppressed via low density of baryons governed by baryon-to-photon ratio $\eta_B \sim 10^{-10}$, cross-section of strong reactions is much higher, than of the weak. One can expect, that it should lead to effective production of deuterium in

$$p + n \to d + \gamma, \quad \langle \sigma v \rangle_{pn}^d \sim \alpha/m_\pi^2 \tag{4.31}$$

Let us estimate, when such reactions would go out of equilibrium:

$$\Gamma_{pn \to d} = H(T), \qquad \Gamma_{pn \to d} = \langle \sigma v \rangle_{pn}^d \cdot n_B \sim \frac{\alpha}{m_\pi^2} \eta_B T^3 \tag{4.32}$$

$$T_{s,\,\mathrm{dec}} = \frac{\sqrt{g_*(T_{s,\,\mathrm{dec}}) m_p^2}}{M_p l^* \eta_B} \sim 10^{-7}\ \mathrm{MeV} \tag{4.33}$$

Here we used geometrical cross-section estimate. Such rough estimate tells, that nuclear reactions will be in equilibrium until $\sim$ eV temperature, long after decoupling of weak reactions. But together with this process, photo-dissociation of deuterium proceed

$$d + \gamma \to p + n, \quad Q_{d,\,\mathrm{diss}} \approx -2.224\ \mathrm{MeV} \tag{4.34}$$

This reaction has a threshold defined with binding energy of deuterium. Cross-section of this process depends on energy. Analytic fit for it is given by [89] :

$$\sigma_{d,\,\mathrm{diss}}(E_\gamma) \approx 18.7\ \mathrm{mb} \left[\left(\frac{\sqrt{|Q|(E_\gamma - |Q|)}}{E_\gamma} \right)^3 + 0.008 \left(\frac{\sqrt{|Q|(E_\gamma - |Q|)}}{E_\gamma} \right)^2 \frac{1.3\ \mathrm{MeV}}{E_\gamma - 2.18\ \mathrm{MeV}} \right]$$
$$\tag{4.35}$$
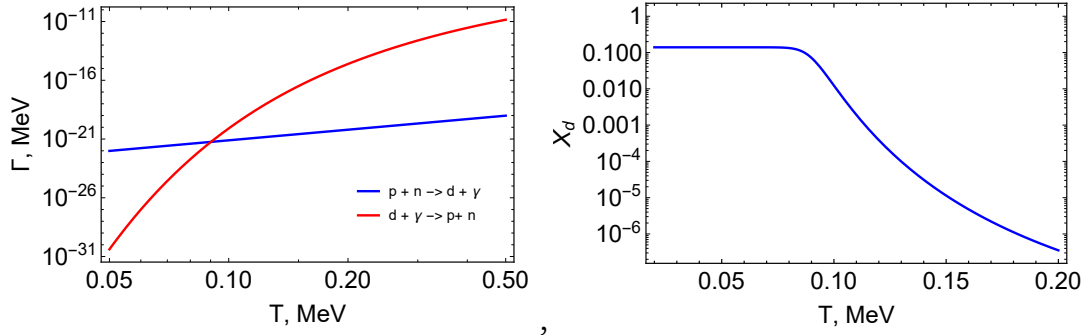
Figure 4.4: *Left panel:* Comparison of deuterium synthesis and photo-dissociation rates for different temperatures. Baryons species in the synthesis rate is not specified and taken as $n_B = \eta_B \cdot n_\gamma$ - total number density of baryons. This value can be lower if one take number density of neutrons. This does not change the result of the estimate significantly. *Right panel:* Evolution of number fraction of deuterium $X_d \equiv n_d/n_B$ if it can only be synthesised or dissociated without participating in other nuclear reactions. It perfectly corresponds to dynamic equilibrium values.

If there would be no more processes which involve deuterium, equation for its abundance would be:

$$\frac{dX_d}{dt} = \langle \sigma v \rangle_{pn}^d X_n n_p - \Gamma_{d,\text{ diss}} X_d \qquad (4.36)$$

At high temperature, photo-dissociation rate is several orders of magnitude larger, than synthesis rate. So the number density of deuterium n_d is negligible. But when temperature drops below $T \sim 0.1 \cdot Q_d$, number of photons, that can participate in conversions becomes exponentially suppressed and at temperature $T \sim 0.09$ MeV condition $\Gamma_{pn \to d} = \Gamma_{d,\text{ diss}}$ is satisfied, so $n_d \sim n_p \sim n_n$. With further decrease of temperature, photo-dissociation is turned-off and since nuclear reactions are still in a good equilibrium, all available pairs of neutrons and protons become bounded in deuterium nuclei.

Once production of deuterium is not suppressed via photo-dissociation, production of heavier nuclei starts.

4.2.5 Synthesis of elements, heavier, than deuterium

Values of binding energy for heavier elements nuclei are larger than in the case of deuterium, so photo-dissociation would have larger threshold energies. For example, for reactions with minimal threshold energies we would have $Q_t^{\gamma,th} \approx 6.25$ MeV for tritium, $Q_{^3\text{He}}^{\gamma,th} \approx 5.49$ MeV for Helium-3 and $Q_{^4\text{He}}^{\gamma,th} \approx 19.81$ MeV for Helium-4. It means, that we would lack photons with enough energy before deuterium started producing, so photo-dissociation would not affect the synthesis of such nuclei. Note, that some of the heavier nuclei might have relatively low threshold energy, as (see [89]) $Q_{^7\text{Li}}^{\gamma,th} \approx 2.46$ MeV or $Q_{^7\text{Be}}^{\gamma,th} \approx 1.58$ MeV. But production of those nuclei is possible only after previous - lighter, are already formed, so photo-dissociation would also not affect anything earlier. Also, no need to consider reactions with three nucleons as initial reactants as it will be significantly suppressed due to additional baryon-to-photon ratio factor.
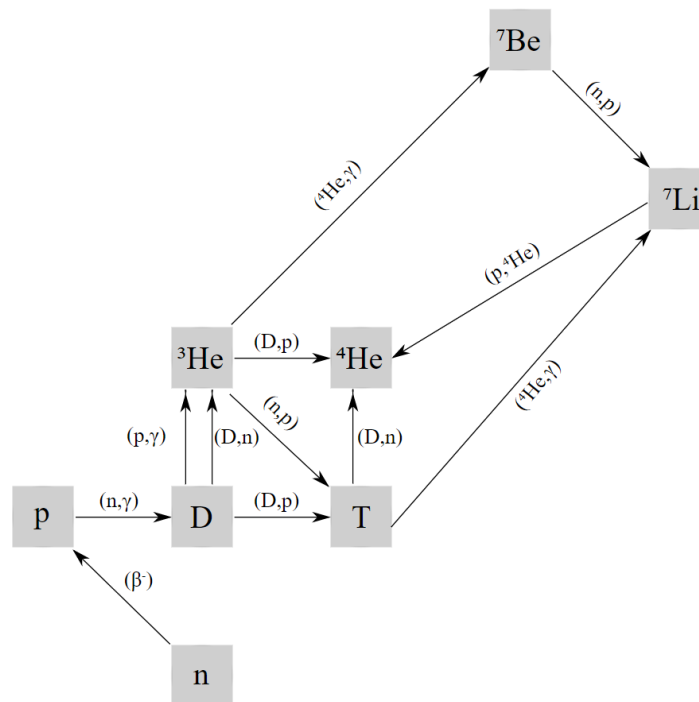
Figure 4.5: Nuclear reaction network in order, they proceed in the SBBN scenario
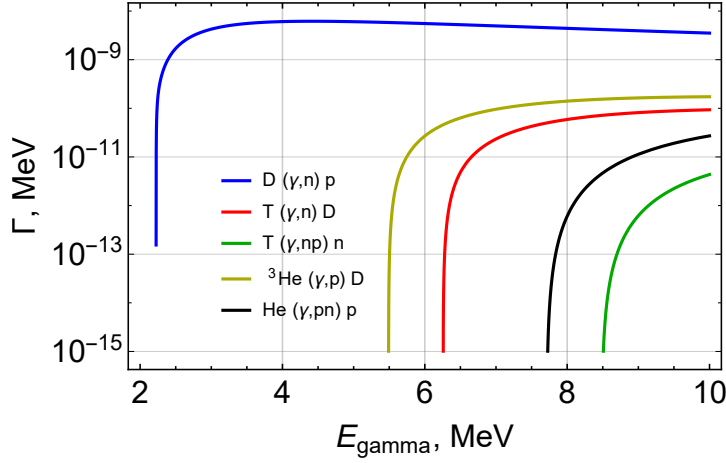
Figure 4.6: Comparison of photo-dissociation cross-sections of different nucleus - $D, T, {}^3He$. ${}^4He$ is not included as the threshold of the photo-dissociation is $Q_{{}^4He} \approx 20$ MeV, with negligibly small change to find a photon with such temperature. We see, dissociation of deuterium has in the same time smallest threshold and largest cross-section. It means, that at the moment, photo-dissociation became irrelevant for Deuterium, it became irrelevant for all particle species.

The next stage of nuclear reaction network is a production of Helium-3 and Tritium in reactions

$$D + D \to n + {}^3\text{He}, \quad D + p \to \gamma + {}^3\text{He}$$
$$D + D \to p + T, \quad D + n \to \gamma + T \tag{4.37}$$
$${}^3\text{He} + n \to p + T$$
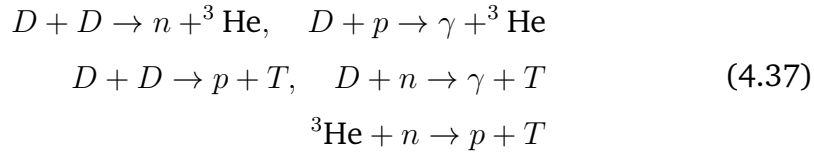
Unlike the previous case with deuterium, initial reactants in those processes are same-charged. Therefore, their cross-section has a contribution from Coulomb repulsion. For such reactions to proceed, nucleons must pass the Coulomb barrier with tunnelling, as the energy of nucleons is not enough to approach them at effective distance of strong force $r \sim m_\pi^{-1}$. Hence, the cross-sections would have form

$$\sigma v = \sigma_0(E) \cdot S_c(v, Z_1, Z_2, M) \tag{4.38}$$

where $\sigma_0(E)$ - strong cross-section in the absence of Coulomb contribution and $S_c(v, Z_1, Z_2, M)$ - tunnelling probability factor, that depends on velocity of nuclei v, charge of both reactants Z_1, Z_2 and their reduced mass $M = M_1 M_2/(M_1 + M_2)$. Value of $\sigma_0(E)$, in the range of energies $E \sim 10 - 100$ keV is varying a little ([128]) and for an estimate can be taken as constant. In reactions, where photons are not present $\sigma_0 \sim m_\pi^{-2}$, while if they are,

additional factor appears $\sigma_0 \sim \alpha \cdot m_\pi^{-2}$ so the processes with photons are additionally suppressed. The tunnelling amplitude is given by (see [191])

$$S_c = \frac{2\pi\alpha Z_1 Z_2}{v} \cdot e^{-2\pi\alpha Z_1 Z_2/v} \tag{4.39}$$

Then after averaging the cross-section over the Maxwell-Boltzmann distribution we have

$$\langle \sigma v \rangle \approx \sigma_0 \cdot \frac{2}{\sqrt{3}}(2\pi\alpha Z_1 Z_2)^{4/3}\left(\frac{M}{T}\right)^{2/3} e^{-\frac{3}{2}(2\pi\alpha Z_1 Z_2)^{2/3}\left(\frac{M}{T}\right)^{1/3}} \tag{4.40}$$

Values of averaged tunneling factor are given at Fig. 4.7.
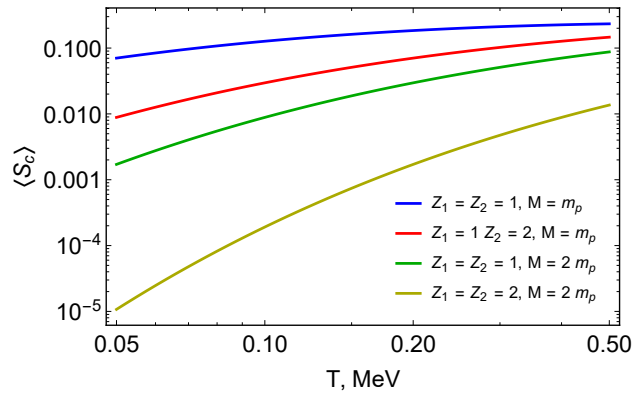
Figure 4.7: Coulomb tunnelling suppression factor for different reduced masses and charges of nuclei. With increase of mass and charge, this suppression factor might decrease up to several orders of magnitude. It is one of the reasons, that will prevent heavy nuclei to form in primordial nucleosynthesis.

Coulomb suppression is not significant for production of T and ^{3}He. Hence, nuclear reactions do not stop on production of deuterium. Consider the processes $D + D \rightarrow^3 \text{He}/T + p$. An estimate for their cross-section is the same. For both of them, the rate of deuterium burning depends on its own number density. Once n_d is large enough, such that burning rate is larger, than Hubble rate, the deuterium is getting converted to either ^{3}He or T.

$$\Gamma_{T,\text{Heprod}} = \langle \sigma v \rangle_{DD} n_d > H(T) \tag{4.41}$$

where $\langle \sigma v \rangle_{DD}$ is averaged cross-section (4.40) with $(M = m_p, Z_1 = Z_2 = 1)$. At temperature $T = T_{\text{BBN}}$, it is enough to have $n_D/n_p \sim 10^{-5}$ to satisfy the above condition. It can also serve as a very rough estimate, on the abundance

of deuterium, frozed-out at the end of BBN. More accurate estimate on this number, obtained from approximate solution of kinetic equation

$$\frac{dn_{Dn}}{dt} + 3Hn_{Dn} = -\langle\sigma v\rangle_{DD}n_D^2, \qquad n_{Dn} = n_n + n_D \qquad (4.42)$$

gives (see [191]) $\frac{n_D}{n_p} \approx 2\cdot 10^{-5}$.

We can also consider other processes, like $p + D \to^3 \text{He} + \gamma$. On the one hand, it's buring rate depends on density of protons, but this is a photon-involving process. Measurements of cross-section [92], [158] gives a value significantly lower, than in $D + D \to ...$ reaction $\langle\sigma v\rangle_{Dp} \sim 0.5 - 1\mu b$. It makes the process not relevant for definition of D/H freeze-out value.

Following the previous logic, if the were no other reactions with T and ^{3}He, almost all neutrons will end up bounded in those nuclei, since reactions freeze out only for low abundances of both neutrons (in D production) and deuterium (in its burning).

The next stage of nuclear network is a production of Helium-4. Corresponding processes would be

$$T + D \to n +^4 \text{He}, \qquad T + p \to \gamma +^4 \text{He}$$
$$^3\text{He} + D \to p +^4 \text{He}, \qquad ^3\text{He} + n \to \gamma +^4 \text{He} \qquad (4.43)$$
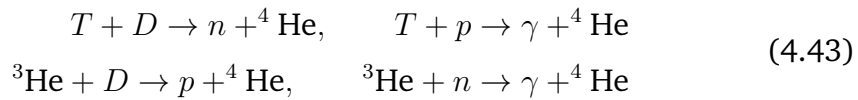
Similar to the (4.37), those reactions can be separated into one involving photons and without them. Reactions with γ would have additional suppression in cross-sections from EM-interaction. Note, that Helium-3 burning reaction $D +^3 \text{He} \to^4 He + p$ proceed through resonance and a simple geometrical estimate is not viable here ([88]).

Instead, cross section can be estimated as ([191])

$$\langle\sigma v\rangle_{^3\text{He}D} \approx 0.03\text{barn} \cdot \left(\frac{T}{0.086\text{ MeV}}\right)^{-1/2} e^{-1.8\cdot(0.086\text{ MeV})/T} \qquad (4.44)$$

Somewhat similar estimate also present for cross section of Tritium burning $T + D \to^4 \text{He} + n$

$$\langle\sigma v\rangle_{TD} \approx 0.03\text{barn} \cdot \left(\frac{T}{0.086\text{ MeV}}\right)^{-2/3} e^{-0.5\cdot(0.086\text{ MeV})/T} \qquad (4.45)$$

Both of these cross-sections are higher, than those of deuterium production and burning, although Coulomb correction is stronger in the latter case at low temperatures $T \sim 10$ keV. Following the same logic as before, residual abundances of ^{3}He and T right after BBN would be small, transferring neutrons into being bounded in Helium-4 nuclei. Note, that T primordial abundance can not be measured as it is unstable so we would be interested only in

It is, although, not a completely trivial statement. The processes we mentioned above are all dependent on the abundance of deuterium. If its burning rate was significantly higher, than the burning rate of ^{3}He to T, at some moment all deuterium would be transferred into either Helium-3 or tritium and in this case those processes (4.43) with D would be terminated. Production of Helium-4 would be still available but with the considerably lower rate, leading to completely different abundances of light elements. Though, it is not the real scenario, as the burning rate of ^{3}He is actually significantly higher, than the one of deuterium. It allows all neutrons to gradually be "transferred" first to deuterium, than to Helium-3 and Tritium and afterwards - to Helium-4 without "staggering" anywhere.

In principle, we could expect continuation of this scenario and production of more and more heavy nuclei. But Coulomb barrier suppression becomes too significant, together with fact, that reactions of production of next elements - lithium-7/6 and berilium-7 all proceeds with emission of a photon, hence with additional EM constant suppression.

$$T +^4 \mathrm{He} \to \gamma +^7 \mathrm{Li}, \quad ^3\mathrm{He} +^4 \mathrm{He} \to \gamma^7\mathrm{Li}, \quad ^4\mathrm{He} + D \to \gamma +^6 \mathrm{Li} \qquad (4.46)$$
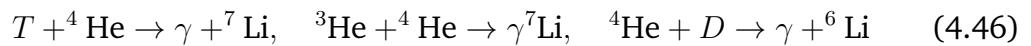
Numerical value of T burning cross-section can be estimated from

$$\langle \sigma v \rangle_{^3\mathrm{He}D} \sim 33\mu\mathrm{barn} \cdot \left(\frac{T}{0.086 \ \mathrm{MeV}} \right)^{-2/3} e^{-8\cdot(0.086 \ \mathrm{MeV})/T} \qquad (4.47)$$

the corresponding rate at T_{BBN} is already smaller, than expansion rate

$$\frac{\langle \sigma v \rangle_{^3\mathrm{He}D} \cdot n_{^4\mathrm{He}}}{H(T)} \sim 0.1 \quad \text{at T} = T_{\mathrm{BBN}} \qquad (4.48)$$

. Moreover, Lithium burning $^7\text{Li} + p \to\ ^4\text{He} +\ ^4\text{He}$ cross section does not involve photon and has the similar Coulomb suppression, so it is significantly higher, than Lithium production rate.

$$\langle \sigma v \rangle_{^3\text{He}D} \sim 33 \cdot 10^3 \mu\text{barn} \cdot \left(\frac{T}{0.086 \text{ MeV}} \right)^{-2/3} e^{-8.5 \cdot (0.086 \text{ MeV})/T} \qquad (4.49)$$

This prevents the effective production of heavier nuclei in primordial nucleosynthesis.

Summarising the story we see, that nuclear reaction dynamics lead to such a redistribution between different, that abundances of D, T, ^{3}He, ^{6,7}Li, ^{7}Be are much less than one, for the lightest nuclei it is supported by fast burning rates, while for heavier - on the contrary, with production rate that is too slow. The only abundance values, that are relatively large correspond to Helium-4, where almost all neutrons, available as free particles at $T \gg T_{\text{BBN}}$ are stored.

4.3 HNLs before BBN epoch

The impact of the HNLs on the BBN depend on their number and energy density. And since the decoupling process of neutrons is not instant, we will require not only instantaneous value at $T = T_n$ but evolution of corresponding parameters. This evolution can be separated into several periods -*(i)* before HNLs final decoupling from the SM plasma $T < T_{\text{dec}}$ (strictly speaking, due to matter effects HNLs will be decoupled from the SM plasma at the highest temperature, then they might enter the stage of equilibrium with other species and with temperature decrease and only after that would be completely decoupled from plasma); *(ii)* free HNLs evolution before their decays $t \lesssim \tau_N$; *(iii)* Evolution of HNls during their decays until the negligible population reached.

4.3.1 $T < T_{\text{dec}}$ Production and decoupling of HNLs

Heavy neutral leptons can interact in νMSM with other particles only via mixing to active neutrinos. Hence, they can participate in any SM reaction of the form

$$\sum_i A_i \to \sum_j B_j + \nu, \quad \sum_i C_i + \nu \to \sum_j D_j \qquad (4.50)$$

instead of active neutrino if such reaction would be allowed by energy-momentum conservation, since HNLs compared to active neutrinos might me significantly heavier. Any matrix elements, cross-sections or rates of such reaction will be suppressed via mixing parameter U with corresponding power. Due to this suppression, production of HNLs can be significant only at high temperatures, higher, than active neutrino decoupling $T > T_{\nu,\,\text{dec}}$ and in reactions . We have used matrix elements from [194] (Appendix D.) Roughly, one can expect, that the interaction rate of sterile neutrinos will be $\Gamma_N^{\text{int}} \propto U^2 G_F^2 T^5$ and hence there will always be a temperature, when the interaction rate is significantly higher, than the Hubble rate as it scales with T as: $H \sim T^2$. But due to matter effects, that are present in hot and dense SM plasma, mixing parameter will obtain an effective value. In the case of absence of lepton asymmetry, at temperatures $T \gtrsim 1$ GeV its effective value becomes (see *e.g.* [168, 98]):

$$U_{\text{m}}^2(T) \approx \frac{U^2}{\left[1 + 9.6 \cdot 10^{-24} \left(\frac{T}{1\text{ MeV}} \right)^6 \left(\frac{m_N}{150\text{ MeV}} \right)^{-2} \right]^2} \qquad (4.51)$$

Numeric coefficients may vary at some level, due to different species population available in plasma, but the general conclusion is that interaction rate $\Gamma_N^{\text{int}} \propto G_F^2 T^5 U_{\text{m}}^2$ is suppressed both at low (as T^5) and high (as T^{-7}) temperatures. Now , this interaction rate can be compared with Hubble rate. Two cases are possible:

- There was a period, when interaction rate was higher, than of expansion $\Gamma_N^{\text{int}} \gtrsim H(T)$. Then we can expect, that HNL's population achieved equilibrium value. In this case, their number and density is totally

defined via temperature of plasma and mass of neutrino and while neutrinos are coupled to SM plasma, they have Fermi-Dirac distribution

$$f_N = \frac{1}{Exp\left(\frac{\sqrt{p^2+m_N^2}}{T}\right) + 1} \qquad (4.52)$$

- Interaction rate was always lower, than of expansion $\Gamma_N^{\text{int}} \lesssim H(T)$. In this case, number density of HNLs is defined by whole evolution period and can be obtained by solving Boltzmann equation

$$\frac{\partial n_N}{\partial t} + 3H \cdot n_N = \Gamma_N^{\text{int}} \cdot n_N \qquad (4.53)$$

From (4.53) we can set a condition, when HNLs may enter equilibrium. From (4.51) and $\Gamma_N^{\text{int}} \propto G_F^2 T^5 U_{\text{m}}^2$, temperature, where interaction rate reaches its highest value T_{max} is roughly (see Fig. 4.13).

$$T_{\text{max}} \approx 10 \text{ GeV} \cdot \left(\frac{m_N}{1 \text{ GeV}}\right)^{1/3} \qquad (4.54)$$

We imply condition $\Gamma_N^{\text{int}}(T_{\text{max}}) = 3H(T_{\text{max}})$ to find the smallest mixing angle values dependence on mass for HNLs that might enter equilibrium:

$$U_{\text{min}}^2 \gtrsim 6 \cdot 10^{-12} \cdot \frac{1 \text{ GeV}}{m_N} \qquad (4.55)$$

In this work, we will only consider HNLs with mixing angles above U_{min}. Eq. (4.55) thus provides the lower bound below which our studies are not valid.[2] Notice that if HNLs are responsible for the generation of neutrino masses, there exists another lower bound on the mixing angle – the seesaw bound. At least one HNL with mass m_n should have a mixing angle above this bound to be responsible for the generation of the atmospheric neutrino mass difference, *c.f.* [25]. The bound depends on details of the given HNL model – mixing pattern and neutrino mass hierarchy (see, e.g., [104, 192]).

---

[2]Our results can be readily extended for non-equilibrium and non-resonantly produced HNLs [94, 36]. See *e.g.* [120].

For simplicity, as the scale of the see-saw bound we will use the toy-model estimate

$$U^2 \gtrsim U_{\text{see-saw}}^2 \simeq 5 \cdot 10^{-11} \left(\frac{1\,\text{GeV}}{m_n} \right) \tag{4.56}$$

The true see-saw bound may differ from the toy model estimate by within an order of magnitude.

In the second case of never-enter-equilibrium HNLs, there is no decoupling temperature but in the first case, we can introduce two temperatures T_+ and T_- of entering the equilibrium and decoupling correspondingly. While the first value T_+ does not represent much interest since subsequent ($T < T_+$) evolution will only lead to equilibrium, the second value T_- will define the final distribution/number densities of HNLs. They will be frozen-out at T_- and will serve as the initial condition for the period of free evolution before decays.

Let us roughly define the freeze-out condition for T_- as smaller solution of equation

$$\Gamma_N^{\text{int}}(T) = 3H(T), \tag{4.57}$$

see Fig. 4.13. An estimate for the decoupling temperature can be done:

$$T_- \simeq T_{\nu,\,\text{dec}} \times \begin{cases} \dfrac{1}{U^{2/3}} \dfrac{1}{n_{\text{int}}^{1/3}} \left(\dfrac{g_*(T_-)}{10.75} \right)^{1/6}, & \text{UR regime} \\[4mm] \dfrac{1}{U^2} \dfrac{1}{n_{\text{int}}} \left(\dfrac{100\,\text{MeV}}{m_N} \right)^2 \left(\dfrac{g_*(T_-)}{10.75} \right)^{1/2} & \text{NR regime,} \end{cases} \tag{4.58}$$

here UR and NR regime stands for cases, when $T_- \gg m_N$ and $T_- \ll m_N$ correspondingly, $T_{\nu,\,\text{dec}} \approx 1.4$ MeV is the decoupling temperature of active neutrinos, $n_{\text{int}} = \Gamma_{N,\,\text{int}}/G_F^2 T^5/96\pi^3$ - parameter, that varies from 1 at $T \simeq \mathcal{O}(1\,\text{MeV})$ to $\simeq 3$ at GeV temperatures. It depends on the constituents of plasma and particle species, HNLs are interacting with.

Such difference appears since the rough estimate of interaction rate $\Gamma_N^{\text{int}} \propto G_F^2 T^5 U_{\text{m}}^2$ is not fully correct. In the case of massive HNLs we would have

$$\Gamma_N^{\text{int}} = U^2 G_F^2 s \cdot n_i(T) \propto \begin{cases} U^2 G_F^2 T^5 & \text{UR regime} \\ U^2 G_F^2 m_N^2 T^3 & \text{NR regime,} \end{cases} \tag{4.59}$$

as the center of mass energy begins to depend on mass of HNL in non-relativistic regime. These different rates lead to the different behavior of decoupling temperature with HNL parameters. The values of T_- for different masses are shown in Fig. 4.12 (left). It is important, that HNLs can decouple non-relativistic. It means, that even the equilibrium population can be very low if it is being suppressed via Boltzmann factors. Due to different dependence on the mass of HNL and another (compared to active neutrinos) temperature behavior of interaction rate, HNLs might decouple even later, than active neutrinos but in this case population of $m_N \gtrsim$ MeV particles will be completely suppressed.

Finally let us estimate the number densities of HNLs at the moment of decoupling in these 2 regimes. It is convenient for the following to parametrize the population of HNLs in terms of the abundance, defined by

$$Y_N = \left(\frac{n_N}{s}\right)_{T=T_-}, \tag{4.60}$$

where n_N is the number density of HNLs and $s = g_* \frac{2\pi^2}{45} T^3$ is the entropy density of the Universe. We use SM value of g_* here. Contribution for entropy density from HNLs is small as it can give no more than $2 \cdot 7/8$ effective species to g_*, while SM values of relativistic degrees of freedom at high temperatures is $g_* \sim 10^2$. Since entropy density scales with the expansion of Universe in the same way as number density due to relation $sa^3 =$ const, this parameter will remain constant until decays of HNL start. Depending on the decoupling regime - UR or NR, abundance may significantly vary. Note, that abundance also depends on the effective number of relativistic species in SM plasma at moment of decoupling.

Using $n_N = \frac{3}{4} 2 \frac{\zeta(3)}{\pi^2} T^2$ for the UR regime and $n_N \sim \left(\frac{m_n}{T_-}\right)^{3/2} e^{-m_n/T_-}$ for the NR regime, we can get the abundance in these two limit cases:

$$Y_N \simeq \begin{cases} \dfrac{0.6}{g_*(T_-)}, & \text{UR regime} \\[2ex] \alpha(m_N, \tau_N) \left(\dfrac{m_n}{T_-}\right)^{3/2} e^{-m_n/T_-}, & \text{NR regime} \end{cases} \tag{4.61}$$

Here we introduced numeric coefficient $\alpha(m_N, \tau_N)$, since on the one hand Boltzmann distribution can be very sensitive to temperature due to suppression

exponent and on the other hand, the decoupling process is not instantaneous. Absolutely similar to the case of neutron decoupling, estimated decoupling temperature does not necessarily correspond to the obtained freezed-out number density of particles. And the more sensitive exponent is, the more inaccuracy might appear. This factor can vary as much as $\mathcal{O}(10)$. For the exact value, we need to solve the Boltzmann equation as in the case of never under-equilibrium HNLs (see Appendix A.4.) There is no such problem in the UR regime. In this case, no mass-dependence for number density appears (up to change of $g_*(T_-)$) and although decoupling is still a continuous process it proceeds faster due to another power law of rates ($\sim T^5$ in UR regime compared to $\sim m_N^2 T^3$ in NR) giving us a chance of simple estimate.

The values of calculated abundances for a range of HNL parameters (10^{-2} GeV $\lesssim m_n \lesssim 2$ GeV and $\tau_N > 10^{-3}$ sec) are presented at Fig. 4.12. For masses $m_N > 0.2$ GeV, decoupling is UR and occurs at temperature higher, than QCD transition. While for lower masses, decoupling may occur after QCD transition. Since there is a significant jump in the number of effective species (see 4.2) at QCD transition, there will also be a rapid increase of abundances value.

After the decoupling, the frozen-out population of HNLs continues to evolve as separate speciment affecting only total energy density of the Universe.

4.3.2 Evolution after decoupling $T < T_{\mathsf{dec}}$ and before start of decays

After decoupling, distribution function of HNLs is changed according to redshift affecting neutrino momentum $p \to p\frac{a(T_{\mathsf{dec}})}{a(T)}$ where $\frac{a(T_{\mathsf{dec}})}{a(T)}$ is the ratio of Universe scale factors at the moment of decoupling and at some later moment defined by temperature T. The corresponding number density of HNLs is being scaled as

$$n_N(T) = n_N(T_{\mathsf{dec}}) \left(\frac{a(T_{\mathsf{dec}})}{a(T)} \right)^3 \tag{4.62}$$

Scaling of energy density depends on the mass, temperature, and decoupling regime. In the case of the NR regime, $E \approx m_N$ and hence energy density

changes as number density. In the case of UR - at $T \gg m_N$ scaling would correspond to radiation

$$\rho_N(T) = \rho_N(T_{\text{dec}}) \left(\frac{a(T_{\text{dec}})}{a(T)} \right)^4 \qquad (4.63)$$

, at lower temperatures scaling would transit to similar to the NR regime. According to the mass and lifetime range of HNLs we are interested in, at the temperatures of neutron decoupling $T \sim 1$ MeV, HNLs will be completely non-relativistic. That leads to the potential outcome, that long-living, massive HNLs might achieve a larger contribution to energy density, than SM plasma which continues to scale as radiation up to very late times, so the ratio $\rho \, \text{HNL}/\rho \, _{\text{SM}} \propto Y_N \frac{m_N}{T}$ might become larger, than 1. But we will see, that neutrinos, surviving for so long would be already excluded so we do not need to consider any transition to matter-dominated expansion.

Number density of HNLs before decays is defined from abundance and entropy density values

$$n_N(T) = Y_N \cdot s(T) = Y_N \cdot g_*(T) \frac{2\pi^2}{45} T^3 \qquad (4.64)$$

In the SM parameter g_* undergoes significant change at $T \sim 200$ MeV (see Fig. 4.2) when quarks are harmonized. This leads to rapid change in the number density of HNLs. It can be understood in a next way.

Recall the process of electron-positron annihilation in the early Universe in the SM scenario. At temperatures below electron mass, such annihilation heats up photons but does not change the temperature of neutrinos as they are already decoupled. The number of photons and their temperature increase after annihilation. Which can be understood as the dilution of neutrinos compared to photons. Let us generalize this statement:

Assume there are two types of particles in plasma - decoupled and equilibrium species. And some of equilibrium species begin to decay or annihilate through channels into others equilibrium species but do without restoring their population, due to the mass-temperature ratio. In this case, all decoupled species can be thought of as effectively diluted compared to equilibrium ones.

This scenario occurs for HNLs as they are decoupled from the SM plasma. At the temperatures of $T = T_{\text{QCD}}$ there is only a small change due to details

of this transition. At $T > T_{QCD}$ there are free quarks and gluons in plasma, and they are not hadronized. Their mass is enough to exist up to relatively low temperatures (especially for u- and d-quarks) but once T drops below T_{QCD}, hadronization occurs, leaving no free quarks and hence, gluons. They form another effective degree of freedom in form of mesons and baryons. But even the lightest of hadrons - π^0 and $\pi^\pm$ mesons with $m_{\pi^0} = 134.9$ MeV and $m_{\pi^\pm} = 139.57$ MeV are already close to $T_{QCD} \sim 150$ MeV so their population can not be restored effectively. On the other hand, only protons and neutrons have long lifetimes compared to other hadrons ($\tau_b \lesssim 10^{-10}$ sec among other baryons and $\tau_m \lesssim 10^{-8}$ among mesons). Hence, when temperature decreases further, most of the mesons and baryons either decay or annihilates into remaining longer-living or stable SM particles, leaving only a tiny fraction of baryons due to initial symmetry. During that decay/annihilation process all remaining SM sector that is in equilibrium is being heated while HNLs are untouched.

It results in an additional dilution of HNLs, decoupled at $T \gg T_{QCD}$ and no such dilution if $T_{dec} \ll T_{QCD}$. Roughly, that leads to the change of population by the factor of 10. Hence, early decoupled HNLs would be significantly less abundant, than those, decoupled later. This is not the final relation, because later-decoupled HNLs may be produced in an NR regime with significant Boltzmann suppression. Finally, we need to study, how the decays of HNLs can affect the Universe's evolution.

4.3.3 Decays of HNLs, $t \gtrsim \tau_N$

Before considering decays, let us estimate the ratio of the HNL energy density compared to the SM particles energy density:

$$
\begin{aligned}
\frac{\rho_N}{\rho_{SM}} &= \left(\frac{a(T_-)}{a(T)}\right)^3 \frac{n_N(T_-) \cdot m_N}{\frac{\pi^2}{30} g_{*,\,sm} T^4} = \frac{Y_N \cdot m_N \cdot s(T)}{\frac{\pi^2}{30} g_{*,\,sm} T^4} \simeq \\
&\simeq 5 \left(\frac{g_*}{g_{*,\,sm}}\right) \left(\frac{Y_N}{10^{-2}}\right) \left(\frac{3 \text{ MeV}}{T}\right) \left(\frac{m_N}{1 \text{ GeV}}\right)\Bigg|_{t(T) \ll \tau_N}
\end{aligned}
\tag{4.65}
$$

Here we neglect the HNL decays and assume that there are no other non-SM particles apart from HNLs in question; $a(T)$ is the scale factor at temperature T, $g_{*,\,\mathrm{SM}} \approx 10.75$ is the number of relativistic degrees of freedom in SM at $\mathcal{O}(\,\mathrm{MeV})$ temperatures, whereas g_* is the total effective number of relativistic species, including the effective contribution of HNLs; and we used Eq. (4.60).

According to expectations, since the energy density of NR HNLs is scaled as number density it can become a considerable fraction of the energy density of the Universe at temperature $T \sim \mathrm{MeV}$. This would significantly affect weak reaction decoupling processes as the Hubble rate will be changed. But when decays start, such large HNL energy will be injected into the SM sector. This would head SM plasma in the same way it was heated during electron-positron annihilation or meson/baryon annihilation and decays after QCD phase transition. As was explained before, this energy injection can be treated as dilution of decoupled species - while this happens at $T \gg T_{\nu,\,\mathrm{dec}}$, only HNLs will be diluted, but if this injection occurs at $T \ll T_{\nu,\,\mathrm{dec}}$ neutrinos, that are already decoupled will be also diluted. Impact of decays on other particle species we postpone for the further sections and concentrate only on effect on HNLs themselves.

Similar to the factor $\left(\frac{4}{11}\right)^{4/3}$ in case of dilution of active neutrinos, we can estimate the value of similar dilution factor for HNLs. Starting from Eqn. 4.64 with g_* as in SM, HNL's contribution to effective number of relativistic species:

$$\Delta g_{*,\,\mathrm{HNLs}}(T) \approx \frac{m_N n_N(T)}{\pi^2 T^4/30} \approx 150 \frac{g_*}{10.75} \frac{m_N}{1\,\mathrm{GeV}} \frac{Y_N}{10^{-2}} \frac{1\,\mathrm{MeV}}{T} e^{-t(T)/\tau_N} \qquad (4.66)$$

Contrary to the active neutrino case, when effective g_* has it's maximum value at largest temperatures, $\Delta g_{*,\,\mathrm{HNLs}}$ from HNLs is small at the moment of decoupling and begin to increase when they become non-relativistic. Reaching its maximum value at temperature T_{max}, it starts decreasing due to decays. Estimate for T_{max} and corresponding $\Delta g_{*,\,\mathrm{HNLs}}(T_{\mathrm{max}}) \equiv \Delta g_{*,\,\mathrm{HNLs,max}}$ assuming SM time-to-temperature relation yields:

$$\Delta g_{*,\,\mathrm{HNLs,max}} \approx 22.5 \frac{g_*}{10.75} \frac{Y_N}{10^{-2}} \sqrt{\frac{\tau_N}{0.1\,\mathrm{s}} \frac{m_N}{1\,\mathrm{GeV}}}, \qquad T_{\mathrm{max}} \approx 3.86\,\mathrm{MeV}\sqrt{0.1\,\mathrm{s}/\tau_N} \qquad (4.67)$$

Now we can use this value to estimate the dilution factor.

$$\zeta(\Delta g_{*,\,\mathrm{HNLs,max}}) = \frac{g_*(T_{\mathrm{max}})}{\Delta g_{*,\,\mathrm{HNLs,max}}(T_{\mathrm{max}}) + g_*(T_{\mathrm{max}})}, \qquad (4.68)$$
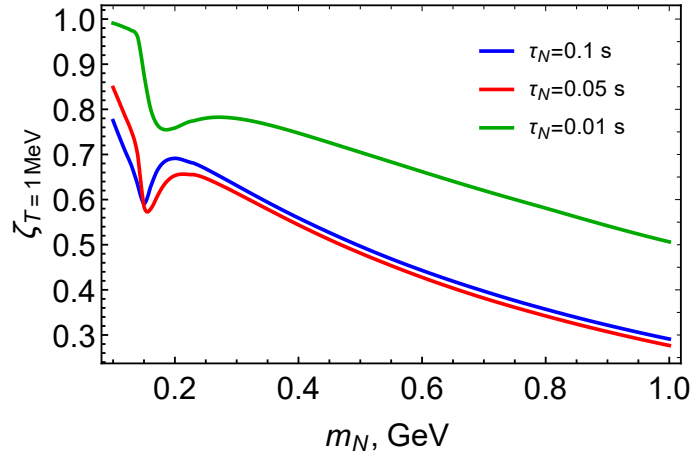
Figure 4.8: Dependence of analytic estimate of the dilution factor on the mass of HNL for different lifetimes. The dilution becomes the largest for HNLs with large masses since their abundance differs only slightly (until the decoupling temperature crosses the temperature of the QCD transition). The "bump" on lower masses corresponds to the rapid change of abundance of HNLs, decoupled before and after the QCD transition

For this estimate we used simplified scenario, when entropy was considered as in SM. It can be specified if we substitute $g_{*,\text{HNLs,max}}(T_{\max})$ with scaled parameter $\bar{g}_{*,\text{HNLs,max}}(T_{\max})$:

$$\Delta \bar{g}_{*,\text{ HNLs,max}} = \Delta g_{*,\text{ HNLs,max}} \left(\frac{g_*(T_{\max}) + \Delta g_{*,\text{ HNLs,max}}}{g_*(T_{\max})} \right) \qquad (4.69)$$

Values of estimate of dilution parameter are presented at Fig.4.8 With this, to find number density of remaining HNLs after their major part already decayed we can use the following expression:

$$n_N(T) = \zeta(T) \cdot Y_N \cdot s(T) \cdot e^{-\frac{t(T)}{\tau_N}}, \qquad (4.70)$$

Such estimate is a useful demonstration, that HNLs can significantly affect their own evolution, effectively diluting their number density compared to SM particles that can easily lead to factor $\zeta \sim 0.1$. Checking this estimate requires solving system of Friedman equations. For the case of $\tau \ll 1$ sec, we do not have to think about decoupling of active neutrinos, so their energy density and temeperature can be taken the same as for EM sector. This would be a

particular case of interest for BBN-constraining HNLs. Resulting system of equations will be:

$$\frac{dT}{dt} = \frac{-4H(\rho_\gamma + \rho_\nu) - 3H(\rho_e + p_e) + \rho_N/\tau_N}{\partial(\rho_\gamma + \rho_\nu)/\partial T_\gamma + \partial \rho_e/\partial T_\gamma}, \qquad (4.71)$$

$$\frac{\dot{a}(t)}{a(t)} = H(t) = \frac{1}{m_{\text{Pl}}}\sqrt{\frac{8\pi}{3}\left(\sum_\alpha \rho_{\nu_\alpha} + \rho_\gamma + \rho_e + \rho_N\right)} \qquad (4.72)$$

Here:

$$\rho_e = 2 \cdot \int \frac{d^3\mathbf{p}}{(2\pi)^3}\sqrt{p^2 + m_e^2}f_{\text{FD}}(p,T), \quad \rho_\gamma = \frac{\pi^2}{15}T^4, \quad \rho_\nu = 3\cdot\frac{7\pi^2}{120}T^4 \quad (4.73)$$

and f_{FD} - Fermi-Dirac distribution function of electrons. Numeric solution of this system of equaitons will give us evolution of time-to-temperature relation $T(t)$ together with evolution of scale parameter $a(t)$. Comparison of such evolution in the SM case and in presence of HNLs are presented at Fig. **??**. As both of this parameters affect evolution of HNLs number density, analogue for analytic ζ (eqn. (4.68)) would be value

$$\zeta_{\text{num}}(T) = \left(\frac{a_{\text{SM}}(T)}{a_{\text{SM+HNLs}}(T)}\right)^3 Exp\left[\frac{t_{\text{SM}}(T) - t_{\text{SM+HNLs}}(T)}{\tau_N}\right] \qquad (4.74)$$

Comparison of numeric results and analytic estimates of dilution parameter are presented at Fig. 4.9. The described picture means, that while considering the effect of HNLs on BBN, there are two more factors needed to be accounted for, arising from details of HNLs evolution in the early Universe. Both of them suppressing the number density of HNLs besides regular decays. These are dilution due to QCD phase transition (for early-decoupled HNLs) and dilution due to their own energy injection to SM plasma. Together, these two factors can introduce additional suppression of the order $\sim 10^{-2}$. Now, we can obtain HNLs population characteristics at the moment of weak reaction decoupling and proceed to estimate their effect on BBN itself.

Finally, let us provide a branching ratios of HNLs decays into hadrons, leptons and neutrinos [59], which are shown at Fig. 4.10. We also add a contribution of secondary neutrinos, that appear after muons and hardons decays.
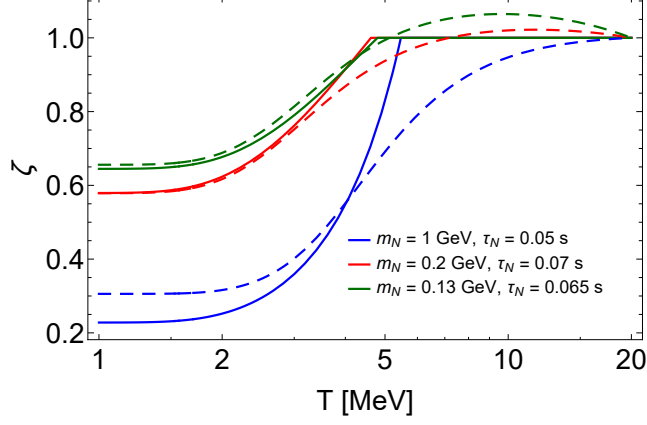
Figure 4.9: Comparison of the evolution dilution factor according to numeric computation and according to our estimate (4.68). We see a good correspondence between the exact solution and analytic approximation in terms of final (at $t \gg \tau_N$) value of the dilution factor. Although, at intermediate temperatures, the discrepancy might be significant.
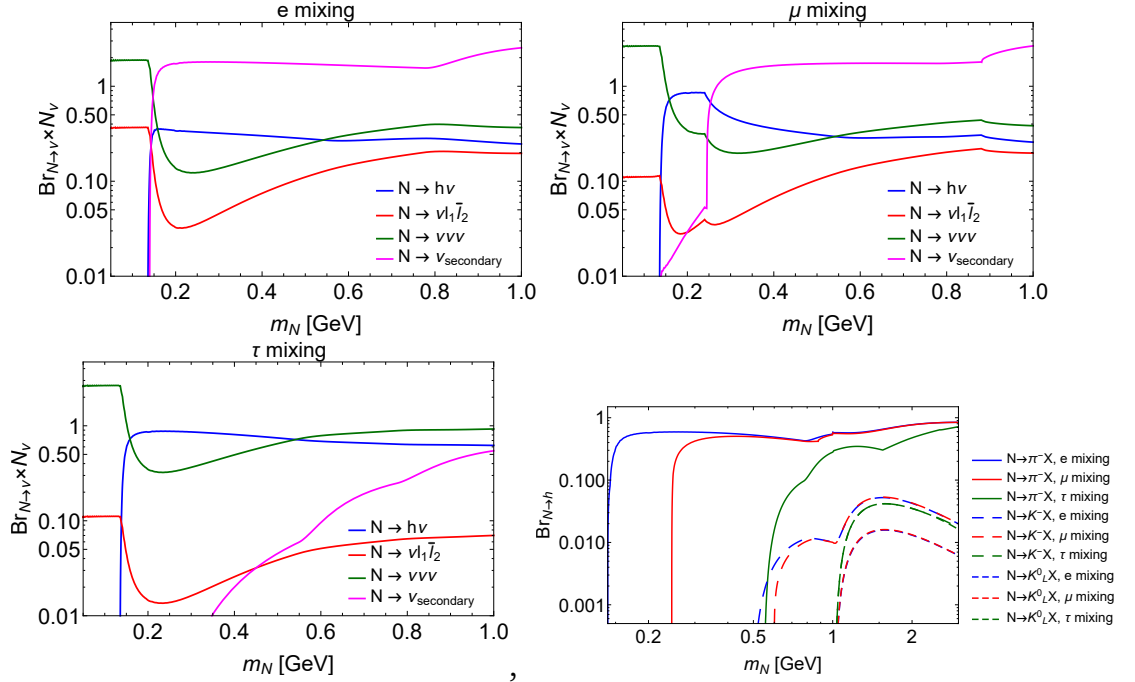
Figure 4.10: **Top panels and bottom left**:Branching ratios of HNLs into neutrinos/antineutrinos together with branching into secondary neutrinos and hadrons, multiplied by the number of neutrinos in each channel. **Bottom tight panel**: Branching of HNL decay into specific mesons

Eq. (4.61) means that for UR regime later decoupling (*i.e.* larger mixing angles) leads to larger HNL abundance. In Fig. 4.13 (right panel) we summarize the HNL parameter space explored by the current study. It shows the domain in which HNLs never entered thermal equilibrium as well as the regime in which
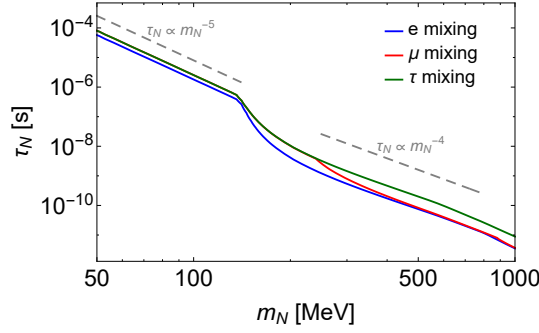
Figure 4.11: HNL lifetime as a function of mass for mixing with different flavors. The dashed gray lines show the scaling of the lifetime with mass. The lifetimes is shown for $U^2 = 1$ and scales as U^{-2}.
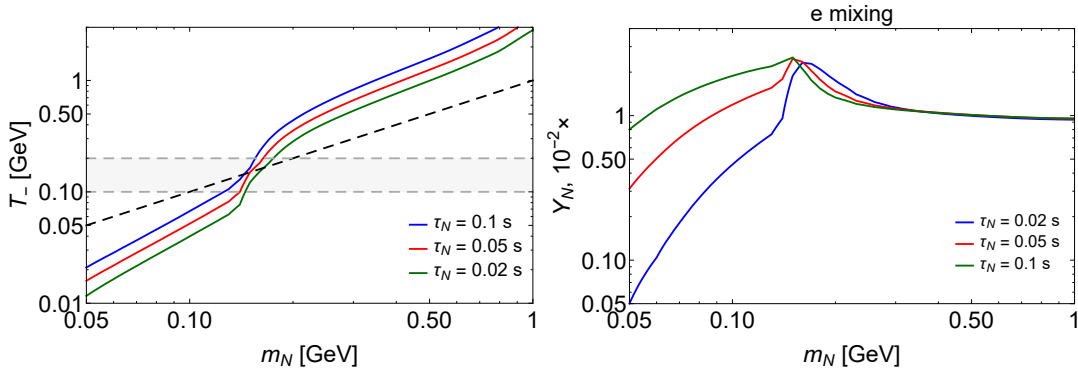
Figure 4.12: *Left panel*: the behavior of the decoupling temperature T_- versus the HNL mass for particular lifetimes. The Black dashed line is $T_- = m_n$ which roughly indicates the transition from a relativistic to the non-relativistic decoupling regime. The Gray horizontal band shows the temperature when the hadronization of quarks takes place and therefore the effective number of relativistic degrees of freedom drops sharply. *Right panel*: HNL abundances versus the HNL mass for particular values of the lifetime. Details of the calculation of the abundances are given in Appendix A.4

HNLs decouple while being non-relativistic. We see that these two regimes are separated by the broad parameter space for which HNLs enter thermal equilibrium and decouple while being UR. A dashed line in the middle of this region is the seesaw bound (4.56).

4.3.4 HNLs effect on the expansion of Universe during the BBN

The contribution of HNL energy density to the effective number of degrees of freedom varies with temperature. We have already mentioned, that HNLs may
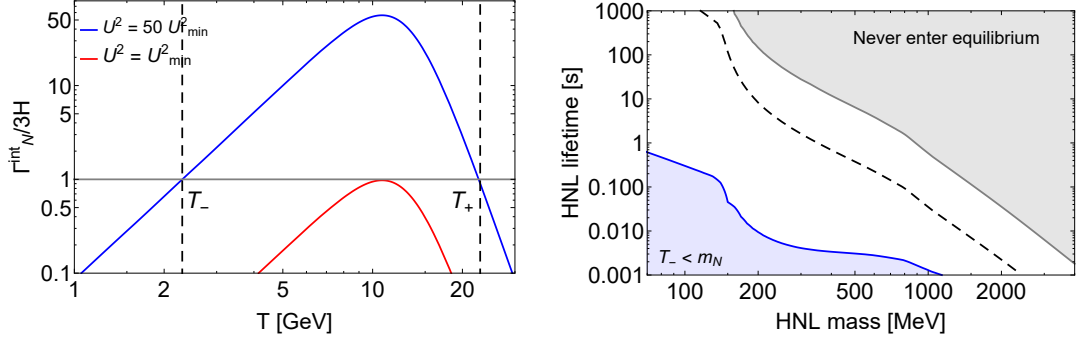
Figure 4.13: *Left panel*: The reaction rate of the HNL with SM particles, Γ_N^{int}, compared to the Hubble rate, $H(T)$. T_+ and T_- are the temperatures at which HNLs enter and exit the thermal equilibrium. For illustration, we used HNL mass $m_N = 1$ GeV, and mixing angles $U^2 = U_{\min}^2$ and $U^2 = 50U_{\min}^2$, see Eq. (4.55). *Right panel*: For lifetimes in the gray solid gray shaded region HNLs never enter thermal equilibrium (we do not consider this case below, but see [120]). White region corresponds to HNLs that were in equilibrium and decoupled (mostly) relativistic. The blue shaded domain represents HNLs that were in equilibrium and decoupled already being non-relativistic ($T_- < m_N$). The dashed line corresponds to the seesaw bound (4.56). For details, see Appendix A.4

give a significant contribution to the effective number of relativistic degrees of freedom as follows from rough estimate - Eqn. (4.66) at low temperatures. This contribution will differ significantly at different temperatures. Before decoupling $T > T_-$, it can not be larger, than $g_*^{\text{HNL}} \lesssim 2 \cdot \frac{7}{8}$, which corresponds to ultra-relativistic HNLs in equilibrium. If they have never undergone equilibrium or the temperature decreases, such that they become non-relativistic before decoupling, the value of g_*^{HNL} would be even smaller. Since the SM value of $g_* \gtrsim 10$ for temperatures $T \gtrsim 1$ MeV, such contribution is quite negligible and its effect may not be considered before the decoupling T_-. While HNLs remain ultra-relativistic, their contribution to g_* is scaled with temperature as $(g_*(T)/g(T_-))^{4/3}$ so it can only decrease if, for example, some particles disappear from plasma. When temperature drops below HNL mass (which is always much higher, than our temperature of interest $T \lesssim 1$ MeV for the considered HNL mass range 50 MeV $\lesssim m_N \lesssim 1$ GeV), their energy density start to scale as

$$\rho_N \sim \left(\frac{g_*(T)T^3}{g_*(T_-)T_-^3} \right) \tag{4.75}$$

, corresponding to matter contribution to g_* , while other particle species are still ultra-relativistic, hence scaling as $\rho^{\text{SM}} \sim T^4$. Starting from this moment, the effective number of degrees of freedom increases which continues

until HNLs start to decay. Taking into account entropy dilution, encoded in parameter ζ - Eqn.(4.74) we got

$$
\begin{aligned}
g_*^{\text{HNL}} &= \zeta(T) \cdot m_N \cdot \frac{Y_N \cdot s_{\text{SM}}(T)}{\frac{\pi^2}{30} T^4} \cdot Exp\left(\frac{-t_{\text{SM}}(T)}{\tau_N}\right) = \\
&= 5\zeta(T) \cdot \left(\frac{Y_N}{10^{-2}}\right)\left(\frac{3\ \text{MeV}}{T}\right)\left(\frac{m_N}{1\ \text{GeV}}\right) Exp\left[-\left(\frac{0.74\ \text{s}}{\tau_N}\right)\left(\frac{1\ \text{MeV}}{T^2}\right)^2\left(\frac{10.75}{g_{\text{eff, SM}}(T)}\right)\right]
\end{aligned} \tag{4.76}
$$

Here, all parameters, marked with subscript "SM" refers to their standard model versions, unaffected by HNLs. Y_N - is the abundance of HNLs, $s(T)$ - entropy density. Value of $g_{\text{eff, HNL}}$ for a range of masses , lifetimes and for different temperatures is presented at Fig.4.14
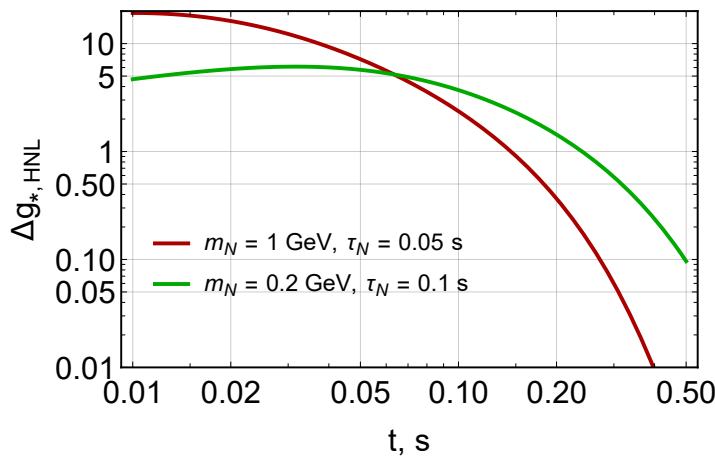
Figure 4.14: Contribution of HNLs to the effective number of relativistic species for two sets of HNL parameters. We see, that at high temperatures, corresponding to small-time, HNLs can contribute to the energy density of the Universe even more, than SM particles. But as soon, as temperature drops, their contribution vanishes due to small lifetimes, such that at the time $t \sim 1$ s, when X decoupling of neutrons is estimated, they do not affect the energy density at all.

Due to the smallness of abundance and presence of dilution factor, even for long-living HNLs it is unlikely to contribute to energy density stronger, than the SM part of g_* at $T \sim T_n$. In the most interesting domain of lifetimes $\tau \sim 0.1$ sec, that may be relevant for BBN, the contribution of HNLs is either low or completely negligible during the process of neutron decoupling and hence, not relevant for us. HNLs with smaller lifetimes $\tau_N \lesssim$ may give a noticeable contribution at higher temperatures $T \gtrsim T_n$ and although it is not relevant for direct impact on neutron abundance, it can still affect the factor $\zeta(T)$. At large lifetimes, there could be a temperature, when the contribution

of g_*^{HNL} becomes the major part of total g_*. It will turn the Universe into a matter-dominated expansion stage of evolution which will continue up to the decays of HNLs.

4.4 HNLs effect on BBN: meson-driven constraints

4.4.1 Mesons from HNL decays

HNLs, heavy enough, can decay into π, K, *etc* - mesons (see [126, 59] or g C in [**SOM**]). For HNLs, up to ≈ 1 GeV mass we might obtain mesons with following masses and lifetimes ([**PDG**]).

$$m_{\pi^\pm} = 139.57 \text{ MeV}, \quad \tau_{\pi^\pm} = 2.6 \cdot 10^{-8} \text{ sec} \quad (4.77)$$

$$m_{\pi^0} = 134.97 \text{ MeV}, \quad \tau_{\pi^0} = 8.4 \cdot 10^{-17} \text{ sec} \quad (4.78)$$

$$m_{K^\pm} = 493.67 \text{ MeV}, \quad \tau_{K^\pm} = 1.2 \cdot 10^{-8} \text{ sec} \quad (4.79)$$

$$m_{K^0/\bar{K}^0} = 497.61 \text{ MeV}, \quad \tau_{K_L^0} = 5.1 \cdot 10^{-8}, \quad \tau_{K_S^0} = 8.9 \cdot 10^{-11} \text{ sec} \quad (4.80)$$

$$m_\eta = 547.86 \text{ MeV}, \quad \tau_\eta = 5 \cdot 10^{-19} \text{ sec} \quad (4.81)$$

$$m_{\rho^\pm/\rho^0} \approx 775.4 \text{ MeV}, \quad \tau_{\rho^\pm/\rho^0} \sim 4.5 \cdot 10^{-24} \text{ sec} \quad (4.82)$$

here we did not used uncertainties in lifetime for several meson species, although they can be relatively large, since it would be irrelevant for future analysis.

The main feature of such mesons is that they participate in $n \leftrightarrow p$ conversion rates through strong interactions. A reasonable estimate for nuclear cross sections is a geometrical estimate $\langle \sigma_{p\leftrightarrow n}^\pi v \rangle \sim m_p^{-2}$ leading to very large ratio of strong to weak cross section at MeV temperatures:

$$\frac{\langle \sigma_{p\leftrightarrow n}^\pi v \rangle}{\langle \sigma_{p\leftrightarrow n}^{\text{Weak}} v \rangle} \simeq \frac{1}{G_F^2 m_p^2 T^2} \sim 10^{16} \left(\frac{1 \text{ MeV}}{T} \right)^2, \quad (4.83)$$

Such estimate holds for all mesons, separating their effect from weak conversion rates effect and change of g_*.

Let us compare the charged pion decay rates and meson-driven conversion rate from the estimate of cross-section:

$$\frac{\Gamma_{m,\,\text{dec}}}{\Gamma^h_{n \Leftrightarrow p}} = \frac{1}{\tau_{\pi^\pm} \langle \sigma^\pi_{p \leftrightarrow n} \, v \rangle \cdot \eta_B \cdot n_\gamma(T)} \simeq 150 \cdot \left(\frac{T}{1 \text{ MeV}} \right)^{-3} \cdot \left(\frac{\eta_B}{6.01 \cdot 10^{-10}} \right)^{-1}$$

$$(4.84)$$

At temperatures, close to $\sim$ MeV scale, mesons decay rate dominates over the rate of conversion for charged pions, so we expect that only fraction of pions will participate in conversions. Since lifetimes of other mesons are either of the same order or smaller, this is true for them too. Moreover, mean lifetime of $\eta, K^0_S, \pi^0, \rho^\pm, \rho_0$ is so much smaller, than of $\pi^\pm, K^\pm, K^0_L$, that independently on if there are any conversion reaction available for them, they will be completely subdominant compared to either pions or kaons.

But those mesons can decay into lighter and more long-living, doing effective contribution. For example,

$$\eta \to \pi^+ + \pi^0 + \pi^-, \quad K^0_S \to \pi^+ + \pi^-, \quad \rho^\pm \to \pi^\pm + \pi^0 \qquad (4.85)$$

Since the decay rate is high, we might simply consider, that HNL decay into $\pi^\pm$ or $K^\pm, K^0_L$ with effective branching ratio

$$Br^{\text{eff}}_{N \to \pi^\pm} = Br_{N \to \pi^\pm} + \sum_A Br_{N \to A} Br_{A \to \pi^\pm} + \sum_{K^{\pm,0}} Br_{N \to K^{\pm,0}} Br_{K^{\pm,0} \to \pi^\pm} \quad (4.86)$$

$$Br^{\text{eff}}_{N \to K^{\pm,0}} = Br_{N \to K^{\pm,0}} + \sum_A Br_{N \to A} Br_{A \to K^{\pm,0}} \qquad (4.87)$$

In the first equation we included term with kaons decay into pions separately. Although we will see, that it will not give a noticeable contribution, due to dominance of pion branching ratio among kaon, this term is not completely correct. kaons, participating in conversions might not survive to be able to decay into pions. So that last term might be suppressed. This is not the case for heavier mesons, as they decay too fast to react with nucleons. The only one remaining detail is that if decaying HNL is massive enough, resulting mesons might be relativistic right after decay. This is mostly important for pions, as other mesons are too heavy, so that in 2 or 3-body decays of HNL with $m_N \lesssim 1$ GeV, they could not achieve significant kinetic energy. But charged or neutral

pion might be the case and this would lead to decrease of their decay rate due to Lorentz factor

$$\Gamma^A_{\text{decay}}(E_A) = \frac{m_A}{\langle E_A \rangle} \frac{1}{\tau_A} \qquad (4.88)$$

where index A stands for a particular meson and τ_A - lifetime of a meson A. Since maximum energy of decay is given by mass of HNL, this can give a correction up to factor of few for charged and neutral pion.

This would not be enough to increase the lifetime of neutral pion to make it worth considering. In the same time, charged pions appear in surrounding of EM plasma with mean energy $3.15 \cdot T \ll m_\pi$. In this plasma, Coloumb scattering of electrons and positrons and inverse Compton scatterings of photons would lead to thermalization of mesons and decrease of their energy.

Estimate of pions thermalization rate gives:

$$\Gamma^\pi_{th} \sim \frac{\alpha^2_{EM}}{E^2_\pi} n_\gamma(T) \sim 3 \cdot 10^{-9} MeV = 4 \cdot 10^{12} \text{ sec}^{-1} \gg \Gamma^\pi_{\text{decay}} \qquad (4.89)$$

We therefore have the following separation of rates and corresponding time scales:

$$\Gamma^\pi_{th} \gg \Gamma^\pi_{\text{decay}} \gg \Gamma^\pi_{p \leftrightarrow n} \qquad (4.90)$$

which means, that right after HNL decay at MeV temperatures mesons will thermalize, losing their initial kinetic energy in EM plasma. After that, decays of mesons will start and only a fraction of them might participate in $p \leftrightarrow n$ conversion processes.

4.4.2 Pion-driven reactions

Charged pions and kaons participate in neutron-proton conversions with reactions (see [180]):

$$\pi^- + p \to n + \gamma, \quad \langle \sigma^{\pi^-}_{p \to n} v \rangle^{\text{th}} \approx 0.57 \text{ mb}, \quad Q = 138.3 \text{ MeV} \qquad (4.91)$$

$$\pi^- + p \to n + \pi^0, \quad \langle \sigma^{\pi^-}_{p \to n} v \rangle^{\text{th}} \approx 0.88 \text{ mb}, \quad Q = 3.3 \text{ MeV} \qquad (4.92)$$

$$\pi^+ + n \to p + \pi^0, \quad \langle \sigma^{\pi^+}_{n \to p} v \rangle^{\text{th}} \approx 1.7 \text{ mb}, \quad Q = 5.9 \text{ MeV} \qquad (4.93)$$
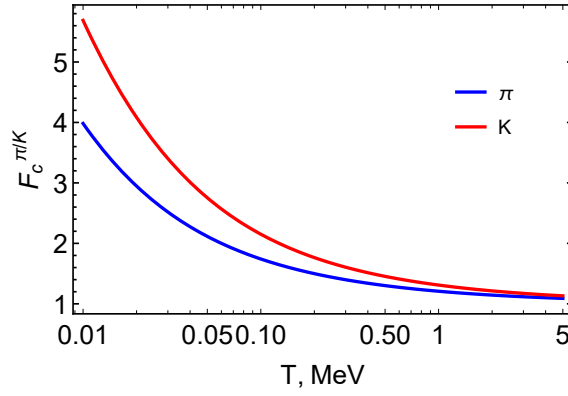
Figure 4.15: Sommerfeld enhancement factor for charged pions and kaons. At large temperatures, when kinetic energy of all particles is large it does not play any role, starting from $T \sim 0.1$ MeV it starts to increase, obtaining values significantly higher, that 1 at $T \sim 0.05$ MeV which can be important for the nucleosynthesis process.

All these reactions proceeds with energy release, so they can proceed for different temperatures without stopping. These cross-sections, given at thermal threshold are not final as $\pi^- - p$ interaction is a subject for Coloumb correction for a process that leads to Sommerfeld enhancement of a corresponding cross-sections. With this, cross-sections can be rewritten as

$$\langle \sigma^{\pi^-}_{p \to n} v \rangle = \langle \sigma^{\pi^-}_{p \to n} v \rangle^{\text{th}} \cdot F_c^\pi(T) \approx 4.3 \cdot 10^{-23} F_c^\pi(T) \text{ m}^3/s, \quad \frac{\langle \sigma^{\pi^-}_{p \to n} v \rangle}{\langle \sigma^{\pi^+}_{n \to p} v \rangle} \approx 0.9 \, F_c^\pi(T),$$
(4.94)

where $F_c^\pi(T)$ is an enhancement factor, that depends on the relative velocity of pion and proton.

$$F_c^\pi = \frac{x}{1 + e^{-x}}, \quad \text{where} \quad x = \frac{2\pi \alpha_{\text{EM}}}{v_e},$$
(4.95)

Since both pions and protons are already thremalized and $m_p \gg m_\pi$ velocity can be estimated as $v_e \simeq \sqrt{\frac{2 \cdot T}{m_\pi}}$. Now we can find the probability for a pion to participate in $p \leftrightarrow n$ conversion before decay. Assuming the separation of scales $\Gamma^\pi_{p \leftrightarrow n} \ll \Gamma^\pi_{\text{decay}}$, define it with

$$P^\pi_{\text{conv}} \approx \frac{\langle \sigma^\pi_{p \leftrightarrow n} v \rangle n_B}{\Gamma^\pi_{\text{decay}}},$$
(4.96)

Taking the cross-sections above and decay widths of pion [217]

$$\Gamma^{\pi^\pm}_{\text{decay}} \approx 3.8 \cdot 10^7 \text{ s}^{-1},$$
(4.97)

for the $p \to n$ conversion probability we got

$$P_{\text{conv}}^{\pi^-}(T) \approx 2.5 \cdot 10^{-2} \cdot F_c^{\pi} \left(\frac{T}{1 \text{ MeV}} \right)^3 \tag{4.98}$$

Sommerfeld enhancement factor is of the order of 1 (see Fig. 4.15), so such probability remains < 1, as it should be, at temepratures $T \lesssim 3.3$ MeV. At higher temperatures, density of nucleons is sufficient, such that conversion rate become faster, than decay rate. In this regime, mesons disappear from plasma mostly due to conversions and not decays. The expression 4.98 can not be used in such case and instead we have to consider the unsimplified probability

$$P_{\text{conv}}^{\pi^-}(T) = 1 - Exp \left[-\Gamma_{p \leftrightarrow n}^{\pi} / \Gamma_{\text{decay}}^{\pi} \right] \tag{4.99}$$

Note, that here we used SM value of baryon-to-photon ratio. But we described in 4.3, entropy release from HNLs decays can affect it significantly. So before HNL's decayed we could have had larger number density of baryons. It would change the conversion probability on the corresponding factor $\zeta(T)^{-1}$.

Although mesons decay rate is large, it proceeds through weak interactions, while conversions - through strong force. This is the reason, why the similar scenario can not be efficient for another quickly decaying HNL product - $\mu^{\pm}$. Although muons can participate in conversions, they would be driven by weak force, leading to significantly smaller conversion probability before decay.

4.4.3 Kaon-driven reactions

Lifetime argument, we mentioned before, tells that we might be interested in reactions, involving both charged kaons $K^{\pm}$ and long-living neutral kaon K_L^0. But it becomes a bit more complicated. In analogy to processes 4.93, there are "direct" charge-exchange reactions like

$$K^- + p \to \bar{K}^0 + n, \qquad Q = -5.2 \text{ MeV} \tag{4.100}$$

$$n + K^+ \to p + X, \qquad Q = -2.8 \text{ MeV} \tag{4.101}$$

but such reactions have a threshold. That will be a reason for significant their suppression at low temperatures we consider. Instead, there are processes with short-living baryons as final states - $\Sigma^{\pm}$, Σ^0 and Λ - hyperons are the lightest

ones. After this, hyperons will rapidly decay into protons, neutrons and pions giving the following chains of reactions that are all threshold-less:

$$
\begin{aligned}
K^- + p &\to \Sigma^{\pm/0}/\Lambda + \pi^{\mp/0}/\pi^0 \to n + 2\pi, \\
K^- + n &\to \Sigma^{-/0}/\Lambda + \pi^{0/-}/\pi^- \to n + 2\pi, \\
\bar{K}_L^0 + p &\to \Sigma^{0/+}/\Lambda + \pi^{+/0}/\pi^+ \to n + 2\pi, \\
\bar{K}_L^0 + n &\to \Sigma^{\pm/0}/\Lambda + \pi^{\mp/0}/\pi^0 \to p + 2\pi,
\end{aligned}
\tag{4.102}
$$

Note, that there is no process $K^+ \to n \to ....$ All reactions above goes through the exchange of strange quark. The similar process with K^+ would require existence of a hyperon with strangeness S=-1 and baryon number B=+1. Though, such particle do not exist. Similar to the pion case, cross-sections of (4.102) can depend on the energy of the meson and the first reaction would also be affected by Coloumb attraction.

While the estimate on the thermalization process of charged kaons gives the same consequence as in pions case - lose of energy before interaction or decay, neutral kaons are not stopped by EM interactions. But since as we already mentioned, for the mass range of HNLs we consider it is reasonable to follow [179] and assume kaons are injected with energy close to thermal threshold. So only Coloumb contribution remains. Resulting cross-sections are

$$
\langle \sigma_{p \to n}^{K^-} v \rangle \approx 9.6 \cdot 10^{-22} F_c^K(T) \text{ m}^3/s, \quad \frac{\langle \sigma_{p \to n}^{K^-} v \rangle}{\langle \sigma_{n \to p}^{K^-} v \rangle} \approx 2.46 \; F_c^K(T),
\tag{4.103}
$$

$$
\langle \sigma_{p \to n}^{K^0} v \rangle \approx 1.95 \cdot 10^{-22} \text{ m}^3/\text{ s}, \quad \frac{\langle \sigma_{p \to n}^{K_L^0} v \rangle}{\langle \sigma_{n \to p}^{K_L^0} v \rangle} \approx 0.41.
\tag{4.104}
$$

with $F_c^K(T)$ similar to (5.13) up to change of $m_\pi \to m_K$ in velocity of meson. Similar to the case of pions, we can define conversion probabilities for kaons. Using decay rates:

$$
\Gamma_{\text{decay}}^{K^-} \approx 8.3 \cdot 10^7 \text{ s}^{-1}, \quad \Gamma_{\text{decay}}^{K_L^0} \approx 2 \cdot 10^7 \text{ s}^{-1}
\tag{4.105}
$$

we got for a threshold cross-sections:

$$
P_{\text{conv}}^{K^-}(T) \approx 2.8 \cdot 10^{-1} \left(\frac{T}{1 \text{ MeV}} \right)^3, \quad P_{\text{conv}}^{K_L^0}(T) \approx 1.6 \cdot 10^{-1} \left(\frac{T}{1 \text{ MeV}} \right)^3
\tag{4.106}
$$

Obtained conversion probabilities are higher, than in the case with pions. Hence, conversions start dominating decays at temperature $T \gtrsim 2$ MeV.

4.4.4 Meson-driven n/p ratio

In the SM scenario, n/p-ratio before neutron freeze-out is governed by local thermal equilibrium in which ratio of number densities equals to ratio of corresponding conversions processes (Eqn. (4.23)) driven by electrons and neutrinos. If we add mesons, we get additional terms in conversion rates. If they are large enough, they might dominate in determining n/p ratio. Let us compare weak and meson-driven conversion rates. We have already estimated, that strong force meson-driven reactions have cross section with several orders of magnitude larger, than thermally given weak rates. They might be balanced via significantly lower number density of mesons in plasma. For this we need to estimate, how much mesons will be present. Consider the regime, when mesons decay faster, than participate in $p \leftrightarrow n$ conversions which is completely true at MeV temperatures. In this case, the instantaneous number density of mesons is a result of balance between their production rate (rate of HNls decays) and their decays rate

$$n_{\pi/K}^{\text{inst}} = n_N(T) \cdot \text{Br}_{N \to \pi/K} \frac{\Gamma_{N,\,\text{dec}}}{\Gamma_{\pi/K,\,\text{dec}}} = n_N(T) \cdot \text{Br}_{N \to \pi/K} \frac{\tau_\pi/K}{\tau_N}. \qquad (4.107)$$

Here, $\text{Br}_{N \to \pi/K}$ are the branchings of HNLs into mesons, including effective contribution from decays to other mesons (Eqns. (4.87),(4.86)) and $n_N(T)$ - number density of HNLs ((4.70)). It follows, that instantaneous number density of mesons can be suppressed via several factors: *(i)* ratio of meson and HNL lifetimes $\frac{\tau_\pi/K}{\tau_N} \sim 10^{-9} - 10^{-10}$, *(ii)* abundance and dilution factor $Y_N \cdot \zeta(T) \sim 10^{-2}$ and *(iii)* HNLs decays. Now, comparing the weak and strong rates

$$\frac{\Gamma_{p \leftrightarrow n}^{\pi,K}}{\Gamma_{p \leftrightarrow n}^{\text{Weak}}} \sim \frac{\langle \sigma_{p \leftrightarrow n}^{\pi/K} v \rangle \cdot n_{\pi/K}^{\text{inst}}}{G_F^2 T^5} \sim 10^4 \cdot \left(\frac{Y_N \cdot \zeta(T)}{10^{-2}} \right) \left(\frac{\tau_{\pi/K}}{10^{-8}} \right) \left(\frac{\tau_N}{10^{-2}} \right)^{-1} \cdot \qquad (4.108)$$

we see, that meson-driven conversions completely dominate over the weak reactions unless HNLs almost decayed. So at times $t \gtrsim \tau_N$ we can neglect weak contribution to local-equilibrium value of n/p ration and define it only from

meson rates. Let us consider HNL, that can decay only into pions. Neutron-to-proton ratio will be given by

$$\left(\frac{n_n}{n_p}\right)^\pi = \frac{\Gamma^{\pi^-}_{p\to n}}{\Gamma^{\pi^+}_{n\to p}} = \frac{\langle \sigma^{\pi^-}_{p\to n} v\rangle}{\langle \sigma^{\pi^+}_{n\to p} v\rangle} \approx 0.9\ F_c^\pi(T), \qquad (4.109)$$

So if present in plasma, pions will maintain ratio of densities close to 1. Notice, that although we have a system in a good equilibrium, as interaction rates are significantly higher, than Hubble rate, number densities ratio is far from thermal Boltzmann exponent as in the SM scenario. There are several reasons for this: *(i)* population of pions is not given by thermal value, *(ii)* there are no backwards reaction in (4.93) - neutral pions decay too fast and photons lose their energy below threshold (iii) isotopic symmetry for pions and closeness of cross-sections. Only when HNLs population will reduce significantly, at $t \gg \tau_N$, the ratio will move away from unity. It is also true at large temperatures when weak rates are high, but this is irrelevant for us. After HNLs has decayed,

weak processes will try to change n/p ratio, shifting it to thermal equilibrium value. If disappearance of mesons occur at large temperatures, SM rates can successfully erase any traces of unusually large n/p ratio. But closer to neutron freeze-out it might not be true and corresponding ratio will never return to its SM value. The similar picture is present for heavier HNLs that can decay into kaons. But in this case we have to include all contributions from both pions and kaons, if they are present. Modified neutron-to-proton ratio will have form

$$\left(\frac{n_n}{n_p}\right)^{\pi+K} = \frac{\langle \sigma^{\pi^-}_{p\to n} v\rangle \mathrm{Br}_{N\to\pi^-} + \langle \sigma^{K^-}_{p\to n} v\rangle \mathrm{Br}_{N\to K^-} + \langle \sigma^{K^0}_{p\to n} v\rangle \mathrm{Br}_{N\to K^0}}{\langle \sigma^{\pi^+}_{n\to p} v\rangle \mathrm{Br}_{N\to\pi^+} + \langle \sigma^{K^-}_{n\to p} v\rangle \mathrm{Br}_{N\to K^-} + \langle \sigma^{K^0}_{n\to p} v\rangle \mathrm{Br}_{N\to K^0}} \quad (4.110)$$

Resulting value depends on the mass and mixing of HNLs leading to a bit different n/p ratio than in the case of pure pions. But presence of kaons does bring any qualitative changes.

4.4.5 Estimate of BBN based constraint

Presence of mesons can only increase the number density of neutrons, hence always leading for the positive correction for helium abundance.
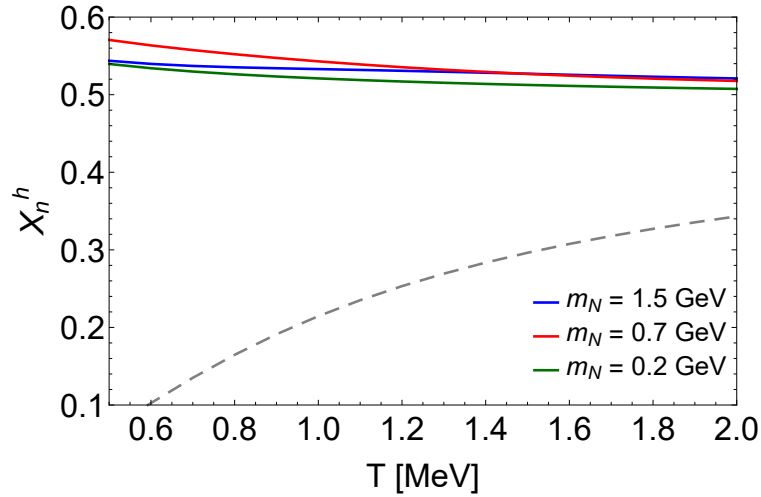
Figure 4.16: Evolution of the neutron mass fraction with temperature in presence of mesons from HNL decays for three different masses of HNLs. Grey dashed line corresponds to SBBN-driven equilibtium value of neutron abundance. We consider HNLs mixing with e flavor and different masses: $m_N = 200$ MeV (only pions are present), $m_n = 700$ MeV (pions and charged kaons are present), $m_n = 1.5$ GeV (pions, charged and neutral kaons are present).

We set the following condition for the estimate according to picture above. Heavy neutral lepton, that can decay into mesons would have constrained mass and lifetime if Standard Model weak conversion rates would not be able to reduce discrepancy between meson-dominated neutron-to-proton ratio and SM value below measurable limit starting from the temperature, when meson contribution is turned-off.

We can separate this question into two parts:

- Find a temperature T_0, such that if $n_n/n_p(T_0) = 1$, evolution at $T < T_0$ with SM rates only would lead to $(X_n - X_n^{\text{SM}})|_{T=T_{\text{BBN}}} < \delta\%$, where δ - desired accuracy

- Find the maximum lifetime of HNL with given mass, such that at $T > T_0$, mesons from its decays could not dominate the $p \leftrightarrow n$ conversions

Starting from the first step, we solve Boltzmann equation (4.22) with initial condition $X_n(T_0) = 0.5$ (exact value, given by meson-driven n/p ratio, affects feebly on the result). The relation between T_0 and resulting correction as well as example of X_n behaviour under such condition are presented at Fig.4.17

Proceeding to second step we impose the following condition. The number of $p \leftrightarrow n$ conversions, that can occur due to mesons starting from temperature T is

$$N_{p \leftrightarrow n}^h (T) = \sum_h \int_{t(T)}^{\infty} dt \, n_h^{\text{inst}}(T) \cdot \langle \sigma_{p \leftrightarrow n}^h v \rangle \approx$$

$$\approx \frac{n_N(T)}{n_B} \cdot e^{-\frac{t(T)}{\tau_N}} \cdot \text{Br}_{N \to h} \cdot P_{\text{conv}}, \quad (4.111)$$

here sum $\sum_h$ goes over all mesons with corresponding probabilities of conversions P_{conv} ((4.106),(4.98)). Mesons can no more dominate the conversion process if this number of conversions becomes less than one. Therefore, after condition

$$N_{p \leftrightarrow n}^h (T_0) = 1 \quad (4.112)$$

is satisfied, weak SBBN reactions are trying to relax the neutron-to-proton ratio to its SBBN value. Having the lower bound on the meson turn-off temperature $T_0 = T_0^{\text{min}}$, we can solve (4.112) with respect to lifetime and find an upper limit on the HNL lifetime with given mass

$$\tau_N \lesssim \frac{t(T_0^{\text{min}})}{\ln \left[\sum_h \frac{n_N(T_0) P_{\text{conv}} \, \text{Br}_{N \to h}}{n_\gamma(T_0^{\text{min}}) \eta_B} \right]}. \quad (4.113)$$

here time-to-temperature relation $t(T)$ can be taken as in SBBN, since HNLs already decayed a lot. $t(T) = \frac{M_*}{2T^2}$, $M_* = \frac{M_{\text{Pl}}}{1.66\sqrt{g_*}}$ the reduced Planck mass, where $g_*(T) \simeq 10.6$ for $T \simeq 1 - 2$ MeV. The same reason allow to use the SBBN value of η_B at temperatures above electron-positron annihilation:

$$\eta_B \approx \frac{10.75}{3.36} \cdot 6.09 \cdot 10^{-10}, \quad (4.114)$$

The constraint on the lifetime can be rewritten in more convenient form:

$$\boxed{\tau_N \lesssim \frac{0.019 \left(\frac{1.5 \text{ MeV}}{T_{0,\text{min}}} \right)^2 \text{ s}}{1 + 0.06 \ln \left[\frac{P_{\text{conv}}}{0.1} \frac{\text{Br}_{N \to h}}{0.4} \frac{Y_N \cdot \zeta(T_0)}{10^{-2}} \right]}} \quad (4.115)$$

Using the values of branching ratios $\text{Br}_{N \to h}$, conversion probability P_{conv} and entropy dilution factor $\zeta(T)$ (Figs. 4.8, 4.10 and Eqns. (4.106),(4.98)) we see,
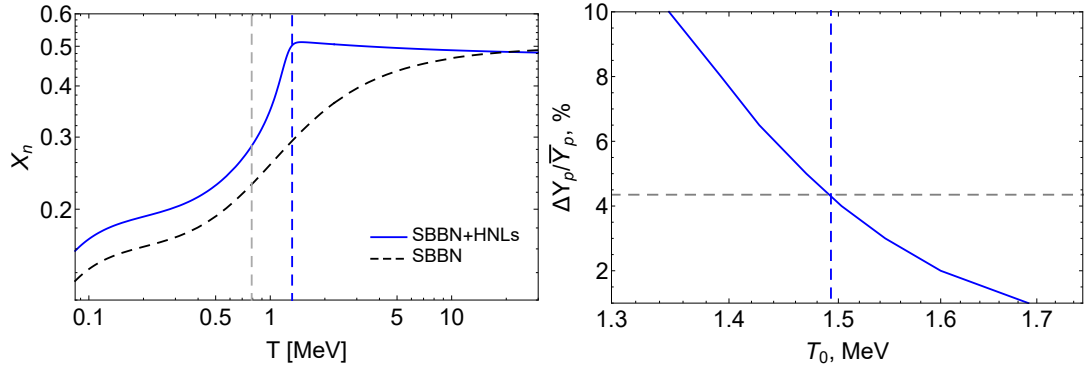
Figure 4.17: *Left panel*: The evolution of neutron fraction in presence of pions of HNL decays. We used $m_N = 400$ MeV and lifetime $\tau_N = 0.03$ s. Pions drive the neutron fraction until number of HNLs becomes suppressed with decays so much, that there is not enough pions to convert each baryon. In this case, the temperature is approximately $T_0 \approx 1.3$ MeV. At smaller temperatures, since the remaining HNL population decays and no pions left, SM rates of $p \leftrightarrow n$ conversion are trying to get the X_n value to equilibrium, but since the "decoupling" of pions occured too late, the resulting correction to neutron abundance at T_{BBN} will be large. *Right panel*: a relation between the temperature T_0 (defined by Eq. (4.112))and corresponding relative correction to expected helium abundance Y_p. The gray dashed line corresponds to maximum correction $\Delta Y_p/\bar{Y}_p = 4.35\%$ we adopted to get a robust constraint. Blue dashed line shows the intersection of grey line and corresponds to T_0^{min} we will use

that almost independently on mass, once meson decays become kinematically allowed, constraint on the lifetime remains at the level of $\tau_N^{max} \simeq 2 \cdot 10^{-2}$ s. Also notice, that even significant modifications of HNL parameters will not affect the result as it depends on logarythm that is additionaly suppressed with factor 0.06. Therefore, the only important parameter, defining the constraint is the minimum temperature for relaxation T_0. Even if we ask for a much higher accuracy, though it is not the case for current observations, $T_0^{\min}$ will not change much as well as corresponding upper limit on τ_N. That is so, because we are already at the tail of the decaying exponent and further decrease of HNL lifetime will completely vanish their effect very fast.

In this estimate we assumed, that at some moment, mesons contribution is turned-off instantaneously. In real situation, it happens gradually which can affect the conversions, changing the number of $p \leftrightarrow n$ reactions from estimate (4.111) and hence, the resulting constraint. We also neglected other effects of HNLs decays on the neutron-to-proton ratio. It is well justified by the strength of meson-driven effect. Note, that this constraint *can not* be extended to arbitrary long lifetimes. It is applicable only if mesons do not survive untill the onset of nuclear reaction network T_{BBN}. Otherwise they can potentially disintegrate the light nuclei, decreasing their mass fraction back to the SBBN values. We will use this condition to limit our constrained parameters range from above.

4.4.6 Numerical calculation of meson-driven constraint

To improve the analytic estimate (4.115) we have to solve a system of Boltzmann equations on the number densities of $\pi^{\pm}, K^-, K_L^0$ mesons, together with X_n equation. Using the processes (4.102),(4.93), decay rates (4.97), (4.105) and conversions cross section (4.94), (4.103), (4.104) we have:

$$\begin{cases} \frac{X_n}{dt} = \left(\frac{dX_n}{dt}\right)_{\text{SM}} + \left(\frac{dX_n}{dt}\right)_\pi + \left(\frac{dX_n}{dt}\right)_{K^-} + \left(\frac{dX_n}{dt}\right)_{K_L^0}, \\[2mm] \frac{dn_{\pi^-}}{dt} = n_N \frac{\text{Br}_{N\to\pi^-}}{\tau_N} - \Gamma^{\pi^-}_{\text{decay}} n_{\pi^-} - \langle\sigma^{\pi^-}_{p\to n}v\rangle(1-X_n)n_B n_{\pi^-}, \\[2mm] \frac{dn_{\pi^+}}{dt} = n_N \frac{\text{Br}_{N\to\pi^+}}{\tau_N} - \Gamma^{\pi^+}_{\text{decay}} n_{\pi^+} - \langle\sigma^{\pi^+}_{n\to p}v\rangle X_n n_B n_{\pi^+}, \\[2mm] \frac{dn_{K^-}}{dt} = n_N \frac{\text{Br}_{N\to K^-}}{\tau_N} - \Gamma^{K^-}_{\text{decay}} n_{K^-} - \langle\sigma^{K^-}_{p\to n}v\rangle(1-X_n)n_B n_{K^-} - \langle\sigma^{K^-}_{n\to p}v\rangle X_n n_B n_{K^-}, \\[2mm] \frac{dn_{K_L^0}}{dt} = n_N \frac{\text{Br}_{N\to K_L^0}}{\tau_N} - \Gamma^{K_L^0}_{\text{decay}} n_{K_L^0} - \langle\sigma^{K_L^0}_{p\to n}v\rangle(1-X_n)n_B n_{K_L^0} - \langle\sigma^{K_L^0}_{n\to p}v\rangle X_n n_B n_{K_L^0} \end{cases}$$
(4.116)

Here,

$$\left(\frac{dX_n}{dt}\right)_\pi = (1-X_n)n_{\pi^-}\langle\sigma^{\pi^-}_{p\to n}v\rangle - X_n n_{\pi^+}\langle\sigma^{\pi^+}_{n\to p}v\rangle, \qquad (4.117)$$

$$\left(\frac{dX_n}{dt}\right)_K = (1-X_n)(n_{K^-}\langle\sigma^{K^-}_{p\to n}v\rangle + n_{K_L^0}\langle\sigma^{K_L^0}_{p\to n}v\rangle) - X_n(n_{K^-}\langle\sigma^{K^-}_{n\to p}v\rangle + n_{K_L^0}\langle\sigma^{K_L^0}_{n\to p}v\rangle)$$
(4.118)

Last four equations in the system define the instantaneous number densities of different mesons. But since both their decay rate and interaction rates are much higher, than Hubble rate we can instead use LTE values for their number densities

$$n_{\pi^-} = \frac{n_N \cdot \text{Br}_{N\to\pi^-}}{\tau_N(\Gamma^{\pi^-}_{\text{decay}} + \langle\sigma^{\pi^-}_{p\to n}v\rangle(1-X_n)n_B)}, \quad n_{\pi^+} = \frac{n_N \cdot \text{Br}_{N\to\pi^+}}{\tau_N(\Gamma^{\pi^+}_{\text{decay}} + \langle\sigma^{\pi^+}_{n\to p}v\rangle(1-X_n)n_B)},$$
(4.119)

$$n_{K^-/K_L^0} = \frac{n_N \cdot \text{Br}_{N\to K}}{\tau_N(\Gamma^{K^-/K_L^0}_{\text{decay}} + \langle\sigma^{K^-/K_L^0}_{p\to n}v\rangle(1-X_n)n_B + \langle\sigma^{K^-/K_L^0}_{n\to p}v\rangle X_n n_B)}, \quad (4.120)$$

So we only need to solve the first equation in system (4.116), where we plug LTE number densities in terms (4.118). We solve those equations until temperature T_{BBN} and translate obtained deviation from SM value $\delta X_n(T_{\text{BBN}})/X_n(T_{\text{BBN}}) \approx 4.3\%$ onto constraint.

4.4.7 Upper limit for applicability of constraint

At lifetimes, higher, than allowed by our constraint, neutron-to-proton abundance monotonically increase and so the helium abundance. But if lifetime of HNLs is large enough, pions may be present in plasma, when He-4 appears, it can dissintegrate it. Such threshold reactions would be:

$$\pi^- +^4\text{He} \to T + n, \quad \langle\sigma v\rangle^{\pi^-}_{Tn} \approx 1.1\text{mb}, \quad Q = 118.5 \text{ MeV} \quad (4.121)$$

$$\pi^- + He^4 \to D + 2n, \quad \langle\sigma v\rangle^{\pi^-}_{Dnn} \approx 4.1\text{mb}, \quad Q = 112.2 \text{ MeV} \quad (4.122)$$

$$\pi^- + He^4 \to p + 3n, \quad \langle\sigma v\rangle^{\pi^-}_{pnnn} \approx 1.3\text{mb}, \quad Q = 110 \text{ MeV} \quad (4.123)$$

as a threshold values with total dissintegration cross-section $\langle\sigma v\rangle^{\pi^-}_{^4\text{He, diss}} = 6.5\text{mb}$. These reactions are also affected by Coloumb correction resulting in Sommerfeld enhancement factor similar to (5.13). At the temperature around T_{BBN} it will give a factor $F_c^{\pi^{4\text{He}}} \approx 3.5$.

Pions can also participating in processes, dissintegrating other nuclei - ^{3}He, T, D or heavier one. But for now let us consider only He-4, since nuclear reaction network would transfer almost all available free neutrons into this isotope of helium. The situation would be same as in SBBN scenario even with significantly higher neutron abundance, because the only reason reaction stops is that the number density of reactant drops too much. Hence, initially large value can not prevent neutrons to settle down in form of He-4.

We can introduce number of disintegrations in the same way as 4.111:

$$N^h_{^4He,\text{ diss}}(T) = \int\limits_{t(T)}^{\infty} dt\, n_{\pi^-}^{\text{inst}}(T) \cdot \langle\sigma v\rangle^{\pi^-}_{^4\text{He, diss}} \approx$$

$$\approx \frac{n_N(T)}{n_B} \cdot e^{-\frac{t(T)}{\tau_N}} \cdot \text{Br}_{N\to\pi} \cdot P_{\text{He diss}}, \quad (4.124)$$

here $P_{\text{He diss}}$ - disintegration probability:

$$P_{\text{He diss}} = \frac{\langle \sigma v \rangle^{\pi^-}_{^4\text{He, diss}} n_{\text{He}}}{\Gamma^{\pi}_{\text{decay}}} \simeq 8.3 \cdot 10^{-2} \cdot \frac{4 \cdot n_{\text{He}}}{n_B} \left(\frac{T}{1 \text{ MeV}}\right)^3, \qquad (4.125)$$

Now, if number of disintegrations $N^h_{^4He, \text{ diss}}(T)$ starting from T_{BBN} would be smaller, than differnce between number of Helium nuclei in the SM+HNL and SBBN scenario, than pions from HNL decays would not be able to restore the SBBN value of $Y_{^4\text{He}}$ as we can neglect any SM-driven dissociation process due to low temperature of photons.

This condition is formulated as

$$n_N \cdot \text{Br}_{N \to \pi^-} \cdot P_{\text{He diss}} = n_{\text{He}}(T_{\text{BBN}}), \qquad (4.126)$$

c.f. Eq. 4.115.

To find the number density of HNLs at temperature T_{BBN} we have to solve the system of Friedmann equations. Note, that we can not use system with Eqns. (4.71) since neutrino and EM plasma becomes decoupled at $T \lesssim 1$ MeV, and in general we have to write a separate equation of type (4.71) for each component together with account of energy transition between components of plasma. This prevents us making a meaningful simple analytic estimate on the parameter ζ which affects both baryon and HNL number densities. We will discuss this question in the next section in more details.

For now we can just say, that using $T_{\text{BBN}} \approx 84$ keV for more robust estimate, and assuming all neutrons become bounded at that temperature, we obtain $\tau_N \lesssim 40$ s as a limit, when our analysis is applicable.

Comparing the see-saw limit with this number, we see that only in the case of e-mixing there exist a window for HNL masses $m_N \lesssim 200$ MeV when HNL lifetimes are not constraint from this 40 s limit. For higher masses, see-saw line is below this robust estimate. It justifies, that we do not need to consider other heavier mesons.

This estimate is very rough, it does not take either disintegrations of lighter nuclei, which number will increase after disintegration of ^{4}He. Also we do not

consider the following re-synthesis of nuclei. It means, that "real" limit of our BBN analysis constraints may be at significantly higher lifetimes.

4.4.8 Results

Obtained constraints in the terms of lifetime for electron mixing are presented at Fig. 4.18. We see, that numeric calculation has levelled down the upper limit for allowed lifetime to the $\tau_N \lesssim 0.019 - 0.021$ s.
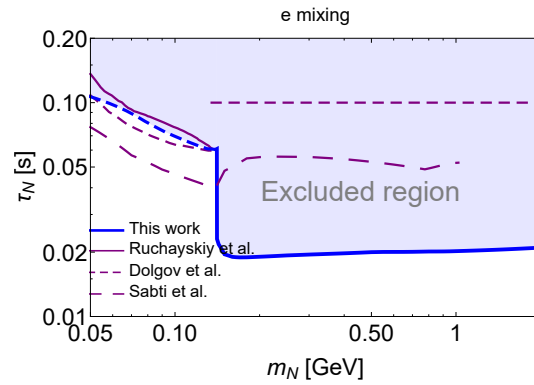
Figure 4.18: *Left panel*: comparison of the meson-driven constraint we obtained with the results of the previous works [193, 99, 194]. The meson-driven constraint can only work for masses $m_N > m_\pi$ but we also added (with a dashed line), the results for non-meson driven constraint for lower masses. It should be noted, that we are comparing the constraints that were stated in those works, although our maximum available correction is larger to take care about all available data.

Comparison of our bound with different experimental searches are presented at Fig. 4.19

Our constraint correspond to lower lifetimes as compared to the result $\tau_N \lesssim 0.1$ s of [99], that was commonly used in the literature for HNLs in this mass range. Which makes them a better complementary constraint compared to the parameters region, covered by SHiP.

Also, our approach can be used not only for heavy neutral leptons. It requires only parameters of branching ratios into charged pions or kaons, mass and lifetime. With this, we can completely repeat the approach for other hypotetical particles to obtain meson-driven constraints from BBN.
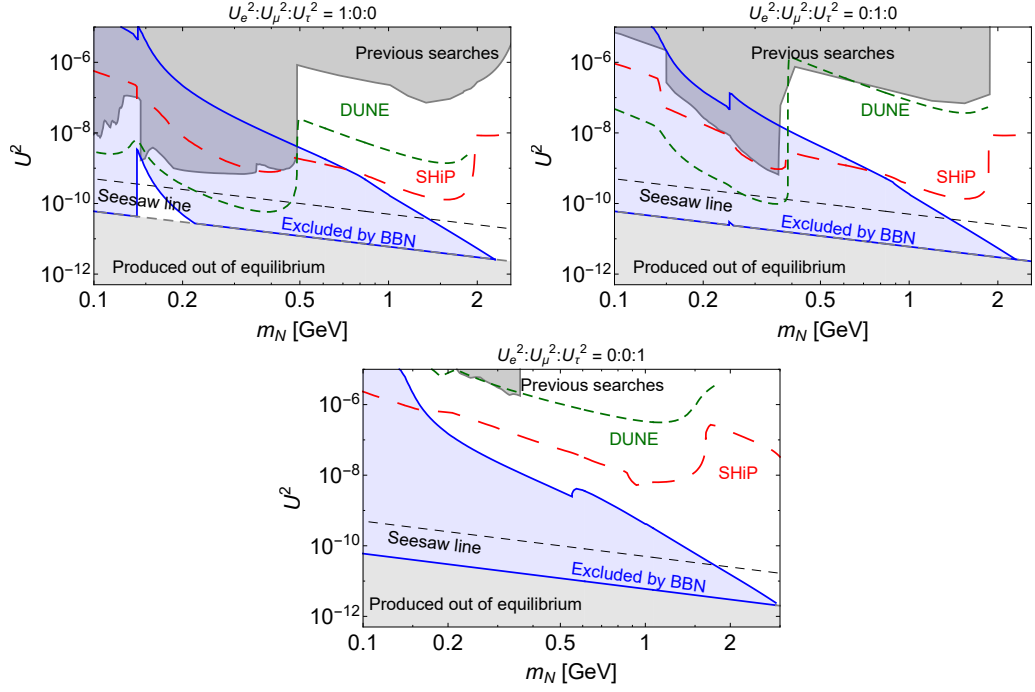
Figure 4.19: Final bounds for HNLs mixed solely with one particular flavour (e, μ ot τ). For comparison, darker grey area is excluded by previous searches ([25], [87]), while the light grey area correspond to out-of-equilibrium production that we did not study. Dashed lines represent the expected area, that future experiments would be sensitive to (SHiP [20, 124] and DUNE [42, 11, 86] (see [47])). Black dashed line corresponds to a see-saw limit and can be taken into consideration if HNLs are to be responsible for neutrino oscillations ([192, 25]).

4.4.9 Long-living HNLs

Let us now briefly discuss effect of HNLs with larger lifetimes on abundances of light elements in case, if they survive until the onset of nuclear reaction network. We have already mentioned such lifetimes when considering robust limit on applicability of our meson-driven constraint. According to that limit and see-saw constraint, there exist an unconstrained region in the range of masses $m_N \lesssim 200$ MeV and lifetimes $\sim 10^4$ s $\lesssim \tau_N \lesssim 40$ s. Decay products of such neutrinos would affect not only neutron abundances at $T > T_{\text{BBN}}$ but also light nuclei at $T < T_{\text{BBN}}$.

For neutrinos with allowed pion decay channel, neutron-to-proton ratio at T_{BBN} is given by Eqn. (4.109) since pions dominate this ratio long after the freeze-out of weak reactions. Since Sommerfeld enhancement is not large at that temperatures, it still has a value of the order of unity $F_c^{\pi^-}(T_{\text{BBN}}) \approx 1.8$,

the resulting dynamic equilibrium value of neutron bundance is not $X_n = 0.5$ as at high temperatures. If mass of HNL is lower than the pion threshold, than change of n/p ratio would be given primarily by the change of g_* instead of decoupled weak reactions. It would lead to less drastic change of n/p ratio than in the meson case so potential restoration process would require less disintegrations. But in the same time, hadron channel is closed for HNLs and only neutrons and photons might be reliable for this.

Initial conditions at T_{BBN}

Let us collect the initial conditions at the start of nuclear reactions.

- As we described before, depending on the mass, n_n/n_p is shifted from SBBN value with either meson-driven ratio or change of g_*. The first option can be easily estimated via Eqn. (4.109) while for the second, system of equations (4.144) -(4.146) and (4.22) with account of g_* correction have to be solved.

- Number density of HNLs are obtained by solving the same system of equations

- Temperature of start of nuclear reaction network: decaying HNLs affect baryon to photon ratio, decreasing it. Since we assume commonly used value in SBBN scenario $\eta_B^{\text{SM}} = 6.09 \cdot 10^{-10}$ is the one, obtained at T_{CMB}, it will have higher value before HNL decays.

$$\eta_B(T_{\text{BBN}}) = \eta_B^{\text{SM}} \cdot \frac{\zeta(T_{\text{CMB}})}{\zeta(T_{\text{BBN}})} \tag{4.127}$$

This higher baryon-to photon ratio would shift the start of nuclear reactions defined by (4.20). Larger η_B would increase T_{BBN}. But since the dependence on this parameter is logarythmic:

$$T_{\text{BBN}} \approx -Q_d \cdot \text{Log}\left[2\zeta(3)\eta_B \frac{T_{\text{BBN, SM}}^2}{Q_d^2}\right] \tag{4.128}$$

here ζ - Riemann zeta function, $T_{\text{BBN, SM}}$ - SBBN value of temperature of start of nuclear reactions, $Q_d = 2.2$ MeV - deuterium photo-dissociation energy threshold. Even order of magnitude changes of η_B change T_{BBN}

only to a few keV. High energy-photons, appearing from secondary decays or annihilations of decay products would also not shift the start as EM reactions are still in good equilibrium. We would also study, if pions can delay this temperature.

- Hubble rate can be significantly higher, than the one given by SBBN value due to HNLs contribution, that increase with temperature before decays have started (Eqn. (4.76)). But nuclear reactions are proceeding very fast, so they are in a good LTE. Hence, change of expansion rate would not affect start of nuclear network but it can affect remaining abundances of light elements. Recall, that abundances of deuterium and Helium-3 as well as tritium (right after the complete stop of BBN) are defined by decoupling of nuclear reactions due to decrease of reactant abundance. Faster expansion would result in larger freeze-out abundances of those light nucleus.

- Change of $N_{\rm eff}$ and corresponding change of neutrino temperature is relevant only for change of Hubble rate as decoupled neutrinos do not play any any role in nuclear reactions.

Let us now focus on the region of HNL parameters, that is remaining as opened window below the see-saw line. **Lifetimes** $t_{\rm BBN} \lesssim \tau_N \lesssim 10^4$ **s** Once

lifetime τ_N reaches $\simeq t_{\rm BBN}$, HNLs start affecting the nuclear dynamics directly – via the meson-driven and photon-driven dissociation, modification of time-temperature relation and η_B. In this section, we will consider HNLs with lifetimes $\tau_N \lesssim 10^4$ s. For such HNLs, photodissociation is a sub-dominant effect in comparison to the meson-driven dissociation, and we may neglect it. For these lifetimes the abundances of light elements ($d, {}^3{\rm He}, {\rm He}$) increase.

Two possibilities may appear: either the meson abundance X_π is enough for keeping all the nucleons unbounded, disintegrating the nuclei or it is suppressed and does not prevent BBN from starting. However, in any case after the disappearing of mesons we are left with an excess of free neutrons in comparison to SBBN. If mesons disappear before the freeze-out of BBN reactions, this excess leads to the overabundance of the primordial helium – more protons may be bounded in He. Roughly, we have $Y_p = m_{\rm He} X_{\rm He}/m_p \approx 4 X_n X_p \approx 1$, where we used $X_n \approx X_p \approx 1/2$.

BBN dynamics in presence of HNLs To make quantitative predictions on the abundances of other light nuclei and estimate whether the He abundance is suppressed as far as mesons from HNLs are present in the plasma, we need to consider their full dynamics. It is an interplay between the SBBN synthesis processes and the meson-driven dissociation processes:

$$\frac{dX_i}{dt} \propto X_j X_k n_B \langle \sigma_{jk \to i} v \rangle - X_i X_m n_B \langle \sigma_{im \to \dots} v \rangle, \qquad (4.129)$$

where $X_i \equiv n_i / n_B$.

Given the SBBN synthesis $D + C \to A + X$ and the meson-driven dissociation processes $\pi + A \to X'$, the abundance X_A is given by the quasi-static equilibrium:

$$X_A^{\text{eq}} \sim \frac{X_D X_C}{X_\pi} \frac{\langle \sigma_{DC \to AX} v \rangle}{\langle \sigma_{A\pi \to X'} v \rangle} \qquad (4.130)$$

In this regime, the values of the abundances X_d, $X_{^3\text{He}}$ are larger than in SBBN, which leads to the overabundance of these nuclei.

Let us first estimate the pion abundance:

$$X_\pi = \frac{n_\pi^{\text{inst}}}{n_B} \approx 2 \cdot 10^{-3} e^{-t/\tau_N} \frac{n_N(T_{\text{dec}})}{n_\gamma(T_{\text{dec}})} \frac{\zeta(T_{\text{CMB}})}{4 \cdot 10^{-4}} \frac{1000 \text{ s}}{\tau_N} \text{Br}_{N \to \pi}, \qquad (4.131)$$

Here, T_{dec} is a temperature at which the population of HNLs completely decoupled from the plasma. The suppression of X_π comes from ζ and the instant meson population factor, $n_\pi^{\text{inst}} \propto \tau_\pi / \tau_N \sim 2.5 \cdot 10^{-11} \cdot (1000 \text{ s}/\tau_N)$, which is only partially compensated by η_B.

Let us now apply Eq. (4.130) to the case of the deuterium synthesis. The synthesis is driven by $p + n \to d + \gamma$. Its cross-section is suppressed in comparison to the one of the pion-driven dissociation by $\sim 0.1 \alpha_{\text{EM}} \simeq 10^{-3}$ [89]. This suppression cannot compensate the suppression coming from the baryon-to-pion ratio (4.131), and for the right hand-side of Eq. (4.130) we get

$$X_n \cdot X_p \cdot 40 \frac{\tau_N}{1000 \text{ s}} \cdot \frac{n_\gamma(T_{\text{dec}})}{n_N(T_{\text{dec}})} \cdot \text{Br}_{N \to \pi}^{-1} \cdot e^{t/\tau_N} \cdot \frac{4 \cdot 10^{-4}}{\zeta(T_{\text{CMB}})} \gg 1, \qquad (4.132)$$

which means that BBN successfully starts even in presence of mesons from HNLs. It means, that the major fraction of neutrons would become bounded anyways. It means, that for such lifetimes, the bounded fraction of baryons will still be larger, than in the SM scenario. So our naive estimate of $\tau_N \lesssim 40$ s is actually can be extended to a much higher values. The first possibility to have the window for HNLs parameters opened would appear only for lifetimes, that correspond to decoupling of strong reactions. As it is the only chance for pions to destroy the already formed light nuclei so that they are not synthesized again.

4.5 HNLs and BBN: non-meson driven effects

We have stated in the previous section, that the meson effect on primordial abundances is dominating for HNLs if those mesons are allowed to appear in decays. Mostly, this statement was based on the comparison of weak and strong interaction rates. In this section we will estimate the effect of HNLs decays on the weak reaction rates and g_* as two main components, defining neutron-to-proton ratio and hence, Helium abundance. Contrary to the meson-driven effects, we can not separate them from each other. It is already clear from SM scenario, that expansion rate, as well as interaction rates, play the role of the same order, as in estimate 4.24 we actually find when those rates are equal. There is another, less obvious reason, why those effects can not be accounted independently.

Change of weak reaction rates can be associated with: *(i)* Change of temperature of neutrino spectrum T_{ν_α} (compared to EM-interacting particles temperature T_γ), *(ii)* distortions of spectrum of neutrinos from their equilibrium Fermi-Dirac shape for given temperature and *(iii)* appearance of particle, species, absent in the SM scenario at $T \sim 1$ MeV.

Formally, expansion rate depends only on the energy density of the universe, so we are interested in the contributions of neutrinos, EM particles, and HNLs themselves without considering detailed shape of spectrum. But let us recall, that we are interested in temperatures around neutrinos decoupling $T_{\nu,\,\mathrm{dec}}$. In this case, any created spectral distortions in neutrino spectra (whether it is

considered as the change of temperature of neutrino or the change of Fermi-Dirac shape) will affect the processes of energy transition between neutrino and EM sector. So both of above mentioned distortions *(i)* and *(ii)* do affect g_* through changing its evolution.

Hence we need to estimate, how HNL's decay products evolve and how they can affect neutrino spetra during this evolution.

4.5.1 HNLs decay products' evolution

At first, let us consider the case of a single neutrino of flavor α, injected at temperature $T_{\rm inj}$ with energy $E_{\rm inj} \gg T_{\rm inj}$. It would correspond to neutrino, that appear after in decay of massive HNL at temperatures $T \sim$ MeV. Such neutrino participate in interactions with SM plasma, that proceed with rates, significantly higher, than for thermal neutrinos.

It is convenient to classify different weak reactions for such highly non-equilibrium neutrino ($\nu_{\rm non\text{-}eq}$), neglecting interactions with nucleons. Depending, on how it may affect non-equilibrium part of spectra we have: It is convenient to classify different interactions of a non-equilibrium neutrinos $\nu_{\rm non\text{-}eq}$ with SM particles in the following way:[3]

1. Processes that do not change the number of neutrinos of α flavor:

$$\nu_\alpha^{\rm non\text{-}eq}/\bar\nu_\alpha^{\rm non\text{-}eq} + e^\pm \rightarrow \nu_\alpha^{\rm non\text{-}eq}/\bar\nu_\alpha^{\rm non\text{-}eq} + e^\pm \qquad (4.133)$$

2. Processes that do not change the number of α flavor but increase the total $\nu^{\rm non\text{-}eq}$ number:

$$\nu_\alpha^{\rm non\text{-}eq}/\bar\nu_\alpha^{\rm non\text{-}eq} + \nu_\beta/\bar\nu_\beta \rightarrow \nu_\alpha^{\rm non\text{-}eq}/\bar\nu_\alpha^{\rm non\text{-}eq} + \nu_\beta^{\rm non\text{-}eq}/\bar\nu_\beta^{\rm non\text{-}eq}, \quad \beta \neq \alpha \quad (4.134)$$

3. Processes decreasing the total number of neutrinos:

$$\nu_\alpha^{\rm non\text{-}eq} + \bar\nu_\alpha^{\rm non\text{-}eq} \rightarrow e^+ + e^- \qquad (4.135)$$

---

[3]Below all changes about increasing or decreasing number is referred only to **non-equilibrium** part of spectra.

4. Processes decreasing the number of α flavor but increasing the total $\nu^{\text{non-eq}}$ number by annihilation to another flavor:

$$\nu_\alpha^{\text{non-eq}} + \bar{\nu}_\alpha \to \nu_\beta^{\text{non-eq}} + \bar{\nu}_\beta^{\text{non-eq}}, \quad \beta \neq \alpha \qquad (4.136)$$

5. Processes increasing both the numbers of α flavor and all neutrinos:

$$\nu_\alpha^{\text{non-eq}} + \nu_\alpha/\bar{\nu}_\alpha^{\text{non-eq}} \to \nu_\alpha^{\text{non-eq}} + \nu_\alpha^{\text{non-eq}}/\bar{\nu}_\alpha^{\text{non-eq}} \qquad (4.137)$$

We have put index "non-eq" for neutrinos in the r.h.s. since we assume, that reaction products will be also highly non-equilibrium. According to high injection energy, that is a reasonable approximation. We do not use any index for EM particles, as their equilibration rates are significantly higher, than weak rates. Hence, for every reaction with EM particles in products, we can assume, that all energy of that EM particle was injected to EM plasma, heating it.

With this we can give a simplified picture of the evolution of injected neutrino.

1. HNL decays, producing high energy non-equilibrium neutrino

2. While participating in weak reactions, this neutrino can either knock-out of equilibrium another neutrino or produce an EM particle, injecting part of its energy to EM plasma.

3. If there was at least one neutrino in decay products, its energy decreases compared to injected one and it acts the same, as the initial neutrino

4. Due to reactions, when the number of non-eq neutrinos increases, one injected neutrino can lead to cascade production of non-equilibrium neutrinos, but with lower energy.

5. When the energy of non-equilibrium neutrinos from r.h.s. of reactions becomes close to thermal, this simple picture can be used only for rough estimate

With this simplified overview of the evolution of HNL decay products after their injection into SM particles plasma we can proceed to estimate of the contributions, those decay products do with respect to BBN-related quantities. We will start with estimate of how HNL's decay products affect the number of relativistic degrees of freedom and the effective number of neutrino species in particular.

4.5.2 How HNLs change N_{eff} and relativistic numbers of degrees of freedom

Change of g_* by HNLs decays product

In this section we will refer to parameter of N_{eff} - effective number of neutrino species. It is defined by

$$N_{\text{eff}} \equiv \frac{8}{7}\left(\frac{11}{4}\right)^{4/3}\left(\frac{\rho_{\text{rad}} - \rho_\gamma}{\rho_\gamma}\right) , \qquad (4.138)$$

where ρ_{rad} - energy density of radiation (photons and neutrinos after electron-positron annihilation) and ρ_γ - energy density of photons. It corresponds to the number of neutrino flavors, that will produce a similar contribution to energy density as massless particles with perfect Fermi-Dirac distribution. Or in terms of neutrino T_{ν_α} and photon T_γ temperatures:

$$N_{\text{eff}} = \left(\frac{11}{4}\right)^{\frac{4}{3}} \sum_{\alpha=e,\mu,\tau} \left(\frac{T_{\nu_\alpha}}{T_\gamma}\right)^4 \Bigg|_{T \ll m_e} \qquad (4.139)$$

Note, that factor $(11/4)^{4/3}$ has to be applied only after rhe electron-positron annihilation. Its SM value can be calculated with high accuracy $N_{\text{eff}}^{\text{SM}} = 3.043 - 3.045$ [50, 109, 51]. The deviation from $N_{\text{eff}} = 3$ comes from details of neutrino decoupling process and contribution of high-order QED corrections. This quantity is a convenient parameter that shows the contribution of neutrinos to the total energy density of plasma. Decaying HNLs affect g_* and N_{eff} in the following way:

- **Injections into EM plasma** Decaying HNL can produce EM-interacting particle. It could be either stable particles like electron/positron and photons or unstable particles - muons, charged mesons ($\pi^{\pm}, K^{\pm}$). Large rate of the EM-interactions leads to almost instant thermalization of those decay products, while $e^{\pm}, \gamma$ become a part of a thermal spectra, transferring their whole energy into it, non-stable fraction of decay products would first lose all their kinetic energy (again, by transferring it into EM-spectra) and decay afterwards. In this secondary (with respect to HNL) decay, the similar situation occurs and we can apply the same argument until final decay products would become either EM-interacting stable particles or neutrinos. An example of the discussed matter could be an HNL decaying into charged pion and electron at low relatively tempratures ($m_e < T \ll m_\pi$):

$$N \to \pi^+ + e^-, \quad E_\pi \approx \frac{m_N^2 + m_\pi^2}{m_N}, \qquad E_e \approx \frac{m_N^2 - m_\pi^2}{m_N} \qquad (4.140)$$

  The energy of the electron E_e and kinetic energy of pion $E_\pi - m_\pi$ are directly injected into EM plasma. After this, decay of the pion occurs. With large Br ≈ 1 ([242]) it decays into muon and neutrino

$$\pi^{\pm} \to \mu^{\pm} + \nu_\mu / \bar{\nu}_\mu \qquad (4.141)$$

  And the story repeats. Muon in this decay first lose his (small) kinetic energy in thermal plasma and afterward - decays into neutrinos/antineutrinos and electrons/positrons which transfer another fraction of initial decaying HNL mass into the EM plasma.

- **Injections into neutrino plasma**. HNLs decay products, as well as secondary decays of latter, might produce a population of non-equilibrium neutrinos of different energies. On the one hand, this is a bit similar to the EM injections story in terms of the decay cascade. But on the other hand, neutrinos do not thermalize instantly and they can BE dangerous. Moreover, neutrinos interact with both neutrino and EM ($e^{\pm}$ sector), allowing the transition of energy between neutrino and EM sector during neutrino thermalization.

- **Post-thermalization effect**. After High-energy neutrinos has almost thermalized and its energy has already been distributed between neutrino

and EM sector, if it happens on temperatures $T \gtrsim 0.1-0.3$ MeV we should take into account energy exchanges between EM and neutrino sector.

according to the picture we presented in the beginning of Sec. 4.5.1, it is natural to separate the calculation of g_* into the following steps:

- Evaluate the total energy, that will be injected into the EM sector via HNL decay products, not including the neutrinos (only EM-interacting particles injections) - taking the lifetimes of decaying particles and EM interaction rate, can be treated as instantaneous.

- Estimate the energy, that will be transferred from the neutrino sector to EM during the thermalization of high-energy neutrino. We would consider this process also as instant due to high neutrino energy, relevant for it.

- Calculation of evolution of the total system of HNLs, neutrinos and EM plasma in terms of their energy densities taking into account exchanges of energy. This slower process requires would require solving a system of equations for the temperature of each spectra component.

Although there is no physical difference between energy transition between EM and neutrino sectors for either low- or high-energy neutrinos, we still want to separate those processes due to very different time scales. They allow us for applying a simplified treatment of a high-energy neutrino thermalization.

In the SM plasma before neutrino decoupling largest relevant rate scale (after the EM interaction rate) is a rate of weak processes with thermal particles, which is also related to energy transition rates. But interaction rate of high-energy neutrinos, injected into plasma after HNL decay may be significantly higher at $T \sim$ MeV.

$$\frac{\Gamma_{\text{non-eq}}}{\Gamma_{\text{therm}}} \sim \frac{G_F^2 T^4 E_\nu^{\text{inj}}}{G_F^2 T^5} = \frac{E_\nu^{\text{inj}}}{T} \gg 1 \,, \qquad (4.142)$$

as energy of injected non-equilibrium neutrinos $E_\nu^{\text{inj}} \sim m_N \gg$ MeV.

Calculation of energy injection
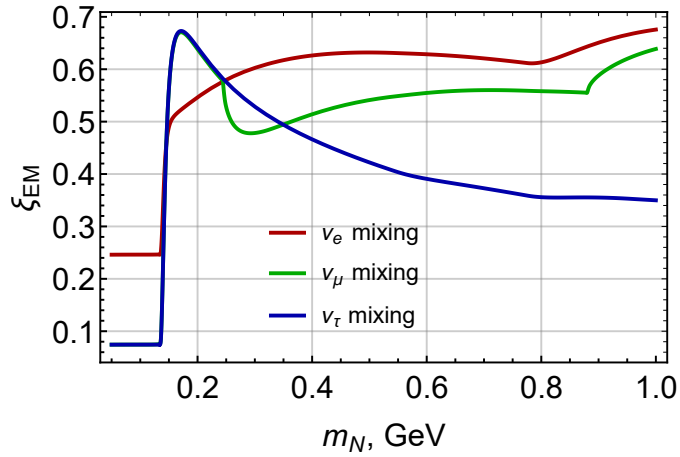
Figure 4.20: Fraction of HNL mass, that will be transferred directly into EM plasma component in EM interactions, neglecting the contribution from thermalizing neutrinos. This quantity already includes the contribution from secondary decays.

Let us introduce the quantity ξ_{EM}, that will correspond to a fraction of energy of initial HNL mass, injected into EM-sector directly (without neutrinos thermalization) and corresponding $\xi_\nu = 1 - \xi_{\text{EM}}$ is the energy fraction that HNL directly injects into the neutrino sector. The value of ξ_{EM} parameters for three mixing cases are shown at Fig.4.20. If, by some reason, the interaction between neutrino and EM sector would be switched off, this quantity would completely parametrize the resulting g_* as it would not depend on anything else. This could be the case, if we consider very late injections $T_{\text{inj}} \ll m_e, T_{\nu, \text{dec}}$ for a very long-living HNLs. Now we have to account for the neutrino thermalization contribution. Besides the pure thermalization, as we have stated in the beginning of Sec. 4.5.1, there could be a non-trivial contribution from the energy transfer due to dragging of neutrinos out of equilibrium by high-energy particles during the thermalization (reactions (4.134), (4.136) and (4.135)).

Some extra explanation might be useful here. Consider the case of low temperature, at which interactions between thermal neutrinos and EM thermal bath are almost switched off, such that small heating of either neutrinos or EM part does not change this. Consider an HNL with such mass m_N, that the high-energy neutrino thermalization rate $\Gamma \sim G_F^2 m_N T^4$ is still higher, than Hubble rate. If the dragging of thermal neutrinos is neglected, than the total energy deposit available for redistribution between ν/EM sectors is given by initial HNL mass. But, if we take it into account, each neutrino, that had thermal energy $E_{\text{therm}} = 3.15 \cdot T$ after being dragged out of equilibrium, add

its energy to the redistributable deposit. Although the contribution of a single neutrino seems irrelevant $3.15 \cdot T/m_N \ll 1$, but as we stated in the beginning processes (4.137), and (4.136) could eventually lead for the cascade, and the number of those neutrinos could become significantly higher, than one. This might produce a correction, important for account in calculation of energy transitions and thermalizations.

Now, let us introduce quantity $\xi_{\text{EM, eff}}$:

$$\xi_{\text{EM, eff}}(E_\nu^{\text{inj}}, T) = \xi_{\text{EM}} + \xi_\nu \times \epsilon(E_\nu^{\text{inj}}, T) , \qquad (4.143)$$

which takes into account, that some fraction (parametrized by $\epsilon(E_\nu^{\text{inj}}, T)$) of the energy, injected initially in the form of neutrinos (with a fraction ξ_ν of the HNL mass) would transit to EM plasma. Factor ϵ consist of two contributions - $\epsilon = \epsilon_{\text{non-eq}} + \epsilon_{\text{thermal}}$ where $\epsilon_{\text{non-eq}}$ - fraction of non-equilibrium neutrinos energy "lost" in the EM plasma ($\epsilon_{\text{non-eq}} = E_\nu^{\text{non-eq}\to\text{EM}}/E_\nu^{\text{inj}}$) and $\epsilon_{\text{thermal}}$ is not a fraction in a full sense, but an *effective* contribution, that defines the ratio of the dragged thermal energy, that was transferred to EM part to injected energy ($\epsilon_{\text{thermal}} = E_\nu^{\text{thermal}\to\text{EM}}/E_\nu^{\text{inj}}$). Due to latter contribution, the value of ϵ does not have to be limited by unity.

Naively, Eq. (4.143) tells, that if $\epsilon > 1/2$, then energy, stored in the EM sector would increase more, than in the neutrino sector so the ratio of ρ_ν/ρ_γ would decrease and g_* and N_{eff} would effectively decrease (remember, that parameters of effective number of particles is given with respect to photon temperature, hence the "unexpected" decrease of N_eff after the injections of neutrinos may occur, if there is also injections into EM plasma). This is the situation when more than a half of HNLs mass has left in the EM sector. But this naive guess does not take into account the subsequent energy redistribution between the neutrino and EM sector. If there was a mechanism, keeping the distribution functions of neutrinos in a perfect equilibrium shape and in the same time leaving the the interactions between neutrinos and EM sector untouched, then the relation between the value of ϵ and significant change in Δg_* or ΔN_{eff} we had from a naive point of view, would be correct. But in realistic scenario, the neutrino spectrum would have a spectral distortion at high energies as a trace of incomplete neutrino thermalization. Hence, the average energy of neutrinos might be *higher,* than the thermal one. And since the highest-energy neutrinos are the most important for energy exchange (due to their higher

interaction rate), it might have consequences for the interaction of neutrinos and electrons, changing the result of energy redistribution between them. In detail, this effect can be captured only by solving the system of Boltzmann equations for neutrinos spectra.

Here we are interested in an approximate treatment, that will capture the main effect so we will not discuss the distortions of neutrino spectra for now.

Energy transition and system evolution

For the calculation of resulting N_{eff} we will use a system of Friedman equations, taking into account, that contrary to the approximation we had in the preliminary study of HNLs evolution, each component of plasma - three neutrino flavors and EM-sector, containing electrons, positrons and photons may have different temperature. In this case, we have a system of 5 equations to solve: The resulting system of equations we need is

$$\frac{dT_\gamma}{dt} = \frac{-4H\rho_\gamma - 3H(\rho_e + p_e) + \rho_N/\tau_N \cdot \epsilon_{\text{EM, eff}} - \sum_\alpha \delta\rho_{\nu_\alpha}/\delta t}{\partial\rho_\gamma/\partial T_\gamma + \partial\rho_e/\partial T_\gamma}, \qquad (4.144)$$

$$\frac{dT_{\nu_\alpha}}{dt} + HT_{\nu_\alpha} = \frac{\delta\rho_{\nu_\alpha}/\delta t + \rho_N/\tau_N \cdot (1 - \epsilon_{\text{EM, eff}})/3}{\partial\rho_{\nu_\alpha}/\partial T_\nu}, \qquad (4.145)$$

and the last equation is not changed as it is just a definition of Hubble rate

$$\frac{\dot{a}(t)}{a(t)} = H(t) = \frac{1}{m_{\text{Pl}}}\sqrt{\frac{8\pi}{3}\left(\sum_\alpha \rho_{\nu_\alpha} + \rho_\gamma + \rho_e + \rho_N\right)} \qquad (4.146)$$

Here: T_γ, T_{ν_α} are temperatures of the EM plasma and neutrinos of the flavor α correspondingly;

$$\rho_e = 2 \cdot \int \frac{d^3\mathbf{p}}{(2\pi)^3}\sqrt{p^2 + m_e^2}f_{\text{FD}}(p, T_\gamma), \quad \rho_\gamma = \frac{\pi^2}{15}T_\gamma^4, \quad \rho_{\nu_\alpha} = \frac{7\pi^2}{120}T_{\nu_\alpha}^4 \quad (4.147)$$

are the energy densities of $e^\pm$, photons and neutrinos of the flavor α correspondingly, while p_e is the pressure of $e^\pm$; ρ_N is the energy density of the FIP. Factor $1/3$ in front of $(1 - \epsilon_{\text{EM, eff}})$ appears, since we average the neutrinos over flavours during the thermalization of high-energy neutrino. Finally, $\delta\rho_{\nu_\alpha}/\delta t$ is the rate of the change of the energy density of $\nu_\alpha, \alpha = e/\mu/\tau$ due to $\nu - \nu$

and $\nu - e$ interactions, averaged over neutrino flavors with the temperature oscillation probabilities $P_{\alpha\beta}$ (see [209, 194]):

$$\frac{\delta\rho_{\nu_\alpha}}{\delta t} = \sum_\beta P_{\alpha\beta}(T, E_\nu = 3.15T_\nu) \cdot \frac{\delta\rho_{\nu_\beta}^{\text{pure}}}{\delta t}, \qquad (4.148)$$

where $\delta\rho_{\nu_\beta}^{\text{pure}}/\delta t$ is the pure rate without neutrino oscillations,

$$\frac{\delta\rho_{\nu_\beta}^{\text{pure}}}{\delta t} = \frac{G_F^2}{\pi^5}(1 \pm 4s_W^2 + 8s_W^4)\mathcal{F}(T_\gamma, T_{\nu_\beta}) - \frac{G_F^2}{\pi^5}\sum_{\beta'\neq\beta}\mathcal{F}(T_\beta, T_{\beta'}) \qquad (4.149)$$

with "+" corresponding to ν_e and "-" belonging to $\nu_{\mu/\tau}$.

$$\mathcal{F}(T_1, T_2) = 32 \cdot 0.859 \cdot (T_1^9 - T_2^9) + 56 \cdot 0.824 \cdot T_1^4 T_2^4(T_1 - T_2) \qquad (4.150)$$

In the system above, energy transition rates are obtained in the assumption of equilibrium shape of neturinos spectrum, given by corresponding temperature. The factor ϵ is yet to be calculated. Note, that we have found, that if we include additional fitting factor $x = 0.8$ in the energy transition rate (4.148) such that it becomes

$$\frac{\delta\rho_{\nu_\alpha}}{\delta t} = \sum_\beta P_{\alpha\beta}(T, E_\nu = 3.15T_\nu) \cdot x \cdot \frac{\delta\rho_{\nu_\beta}^{\text{pure}}}{\delta t}, \qquad (4.151)$$

than the system begin to describe the evolution of N_{eff} way better *independently* on the injected energy. This factor physically should correspond to spectral distortions, that make neutrino plasma hotter, which decreases energy exchange rate with EM plasma, as we saw when comparing the result with the publicly available code pyBBN[4] [194]. The only remaining detail in this model is the value of parameter ϵ which we will estimate in the following manner:
Value of parameter ϵ

We follow our illustrative picture of the evolution of high-energy neutrinos when they get injected into SM plasma. Let us start from a description of energy redistribution caused by a single high-energy neutrino, injected at temperature T_{inj} with energy E_ν^{inj}, that appeared from either 2- or 3- body decay. We expect such neutrino to create a cascade of secondary neutrinos during its thermalization process in reactions (4.133)−(4.137). Every time a neutrino participates in a reaction with thermal neutrino it drags it out of equilibrium or annihilates into electron-positron pair and while interacting

---

[4]https://github.com/ckald/pyBBN

with electron/positron, it leaves half of its energy in the EM plasma. To evaluate the energy, that will remain in the neutrino plasma we have to know the number of reactions in a cascade. Roughly, since we expect the high-energy neutrino to lose half of its energy in every reaction, thermalization should occur during

$$N_{\text{therm}} \simeq \log_2(E_\nu^{\text{inj}}/3.15T) \qquad (4.152)$$

energy-loss interaction processes (we add "energy-loss" here, since neutrino can lose all it's energy by annihilating into $e - e^+$ pair). Every process of $(4.133) - (4.137)$ can decrease the number of non-equilibrium neutrinos by one (annihilation), do not change it (scattering ob the EM plasma components) or double the neutrino number (scattering with thermal neutrino and dragging it out of equilibrium). Thus, average number of neutrinos on "k"-th and "k-1" - th step of thermalization would be related as

$$N_\nu^{(k)} = N_\nu^{(k-1)} \left(2P_{\nu\nu\to\nu\nu} + P_{\nu e\to\nu e}\right) = N_\nu^{(0)} \left(2P_{\nu\nu\to\nu\nu} + P_{\nu e\to\nu e}\right)^k , \qquad (4.153)$$

While at the first step we take $N_\nu^{(0)} = 1$. Here we introduced probabilities of the processes of doubling the neutrino numbers $P_{\nu\nu\to\nu\nu}$ and process of scattering on EM plasma without change of neutrino numbers $P_{\nu e\to\nu e}$. These probabilities are defined as as $P_i = \Gamma_i/\Gamma_\nu^{\text{tot}}$, where Γ_i is the interaction rate of each process and Γ_ν^{tot} is the total neutrino interaction rate.

$$P_{\nu\nu\to\nu\nu} \approx 0.78, \quad P_{\nu\nu\to ee} \approx 0.041, \quad P_{\nu e\to\nu e} \approx 0.166 . \qquad (4.154)$$

These values are obtained in the assumption of Fermi-Dirac distribution of neutrinos with temperature, equal to the photon temperature. The corresponding rates are presented at 4.1. Note, that these probabilities are obtained without any consideration if the interaction rate of neutrinos and EM plasma is decoupled or not. We know, that at low temperatures any transition between EM and neutrino components has to be switched off. To incorporate this switching-off we manually introduce additional factor $\min[\Gamma_i/H, 1]$, where $\Gamma_i = \Gamma_i(E_\nu^{\text{inj}}/2^k)$ is the interaction rate corresponding process. As we have found, this does not affect the results noticeably. Taking into account, that the energy of those individual neutrinos decreases as $E_\nu^{(k)} = E_\nu^{\text{inj}}/2^k$, the remaining energy in the neutrino sector will be

$$E_\nu^{(k)} = E_\nu^{(k-1)} \left(P_{\nu\nu\to\nu\nu} + \frac{1}{2}P_{\nu e\to\nu e}\right) = E_\nu^{\text{inj}} \left(P_{\nu\nu\to\nu\nu} + \frac{1}{2}P_{\nu e\to\nu e}\right)^k , \qquad (4.155)$$
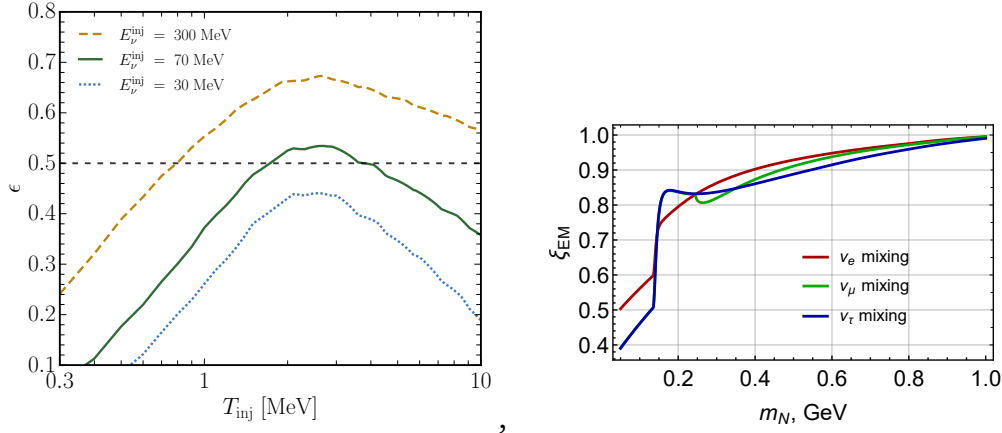
Figure 4.21: Left panel: values of $\epsilon_{\text{thermal}}, \epsilon_{\text{non-eq}}$ and their total value for different masses of HNLs assuming injection occurs at $T = 1$ MeV. Thermal contribution is subdominant everywhere but still can give a contribution with an order of $5 - 10\%$. **Right panel:** Estimate of a resulting fraction of HNL energy injected into EM plasma for three different flavous. The value is calculated at temperature $T = 1$ MeV for the case of 2-body decay as an example.

Now we can get the final value of the $\epsilon_{\text{non-eq}}$ that accounts for the energy transfer from non-equilibrium neutrinos to the EM plasma:

$$\epsilon_{\text{non-eq}} = \frac{1}{E_\nu^{\text{inj}}} \sum_{k=0}^{N_{\text{therm}}} \left(\frac{P_{\nu e \to \nu e}}{2} + P_{\nu\nu \to ee} \right) E_\nu^{(k)} . \tag{4.156}$$

But as we have mentioned, together with redistribution of energy of injected neutrino we have a catalysing of thermal energy when equilibrium neutrino is being dragged out. The effective contribution coming from this transfer is therefore:

$$\epsilon_{\text{thermal}} = \frac{3.15T}{E_\nu^{\text{inj}}} N_\nu^{\text{therm} \to \text{EM}} = \frac{3.15T}{E_\nu^{\text{inj}}} P_{\nu\nu \to ee} \left(\sum_{k=0}^{N_{\text{therm}}} N_\nu^{(k)} + \left[P_{\nu\nu \to \nu\nu} + \sum_{k=1}^{N_{\text{therm}}} (2P_{\nu\nu \to \nu\nu})^{(k)} \right] \right), \tag{4.157}$$

here the first term comes from the annihilation to $e - e^+$ pair (as it also directly injects thermal energy into EM plasma), and the term in the square brackets corresponds to contribution from process of neutrino-neutrino scattering. The value of the thermal dragging contribution, non-equilibrium part and is presented at Fig. 4.21 Now, with the value of ϵ we can solve the system of equations for the evolution of temperature and scale factor to obtain the correction to N_{eff} as a function of HNL parameters.

Results

Our main result for the analytic estimate of the change of N_{eff} is presented at Fig. 4.22 for a wide variety of HNL parameters. We did not limit ourselves to small BBN-related lifetimes but expanded the study for $\tau_N \gg t_{\text{BBN}}$. Out estimate is not limited to small lifetimes because we treat the change of N_{eff} primarily through using the integral values like total injected energy instead of dealing with the spectra of neutrinos, which detailed study at large time intervals can be insanely time-consuming in the case of numeric computation. At a high lifetime with very late injections, the change of N_{eff} if not related
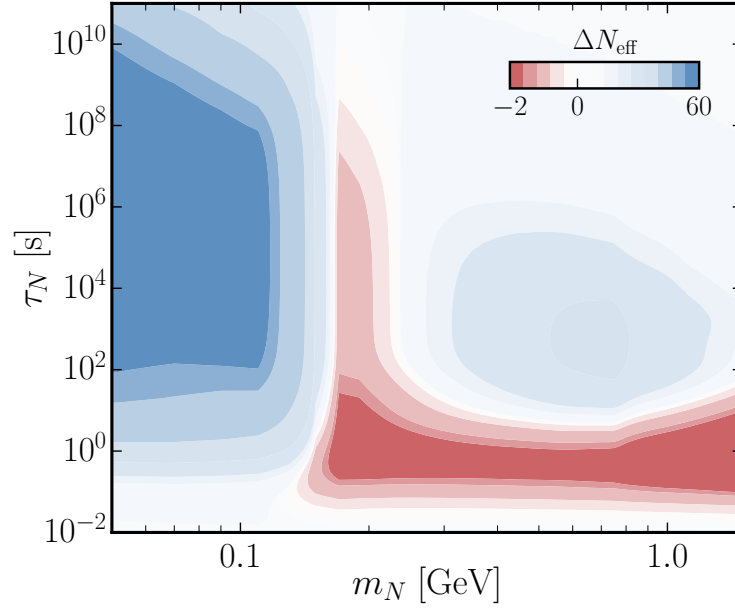
Figure 4.22: Value of ΔN_{eff} as it follows from semi-analytic estimate we described above for the case of τ mixing. Although for low-mass and short lifetime HNLs $\tau_N \lesssim 10^{-1} - 10^{-2}$, that lead to small changes of N_{eff} accuracy compared to the results of pyBBN code is only up to a factor of few, for high masses and higher lifetimes we have found a good correspondence. Independent on mass and lifetime we get, that our semi-analytic approach provides a good qualitative understanding of the behavior of N_{eff}. We see, that the strongest effect on the N_{eff} comes from HNLs with large lifetimes and small masses. It is so because such HNLs produce a lot of neutrinos that are already decoupled, but do not inject much energy into EM plasma. High mass and large lifetimes HNLs affect N_{eff} weakly as their abundance become non-thermal at some moment and afterward - decreases with the increase of lifetime

to any energy transitions between plasma components or thermalizations of neutrinos since all those processes are decoupled a long time ago. In this case, the resulting value begins to depend solely on the ξ EM as its effective value is the same with $\epsilon \to 0$.

The example of the temperature of all plasma components evolution for 2 sets of HNL parameters are presented at Fig. 4.23. We will use our approach and

,
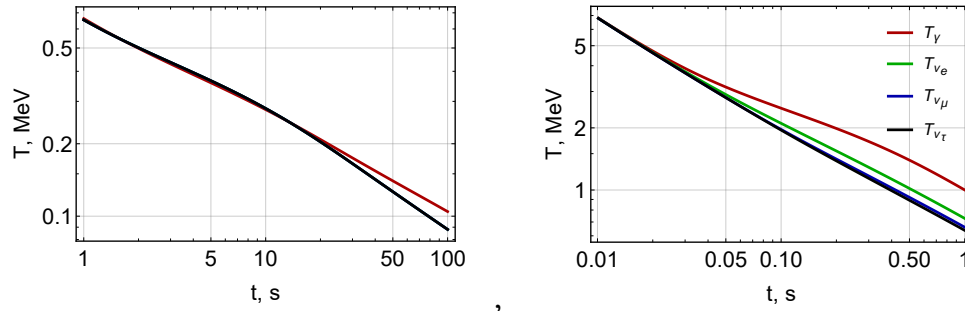
Figure 4.23: Evolution of temperature of photons T_γ and neutrinos of all flavours T_{ν_α}, $\alpha = e, \mu, \tau$ with time in presence of decaying HNLs with the following parameters: $m_N = 1$ GeV, $\tau_N = 0.2$ s (**right panel**) and $m_N = 0.1$ GeV, $\tau_N = 5$ s (**left panel**). For the case of large mass HNL with a small lifetime, it is seen, that due to the large injection of its energy into the EM component, temperature T_γ increases significantly compared to three other temperatures as soon as HNLs start decaying. The temperature of electron neutrinos in its turn is higher than of two other flavors, as their interaction with electrons/positrons heats them a little. For the case of a low mass HNL with a higher lifetime, an interesting feature can be noticed, that at first, the temperature of neutrinos become higher, than of the photons, but with time, when electron-positron annihilation proceeds, its effect becomes stronger than the change of N_{eff} by HNLS and photons become hotter.

described machinery to calculate the total effect of HNLs on the BBN.

4.5.3 Distortions of neutrino spectrum

At the beginning of Sec. 4.5.1 we have given an illustrative picture of the evolution of HNL decay products and in particular - of high-energy neutrinos. To find the corrections for neutrino-driven conversion rates $\Gamma^{\nu}_{p\leftrightarrow n}$ we need to know the form of spectral distortions. Formally, for this we need to solve the Boltzmann equation for each neutrino flavor:

$$\frac{\mathrm{d}f_\alpha}{\mathrm{d}t} = \frac{\partial f_\alpha}{\partial t} - Hp\frac{\partial f_\alpha}{\partial p} = I_\alpha, \qquad (4.158)$$

here I_α - collision integral, that accounts all interactions, which particle α participates, in our case, it is one of neutrino flavors. In its general form, a collision term for reaction involving n particle species one of which is a neutrino:

$$\alpha + 2 + 3 + ... + k \leftrightarrow (k+1) + (k+2) + ... + n \qquad (4.159)$$

can be written as ([145])

$$I_\alpha = \sum_{i=\alpha}^{n} \int \frac{1}{2E_\alpha g_\alpha} \prod_{i=2}^{n} \frac{\mathrm{d}^3 p_i}{(2\pi)^3 2E_i} S|\mathcal{M}|^2 F[f](2\pi)^4 \delta^4(P_{\mathrm{in}} - P_{\mathrm{out}}) , \qquad (4.160)$$

here g_α - number of degrees of freedom for particle α, P_{in} and P_{out}) - total 4-momentum of particles in initial and final state of process (4.159), S is the symmetry factor, not included in the non-averaged squared matrix element $|\mathcal{M}|^2$. Summation goes over all initial and final states' degrees of freedom of all particles. Factor $F[f]$ responsible for phase space distributions of initial state- and Pauli blocking (for fermions) or Bose enhancing (for bosons) for final state- particles:

$$F[f] = (1 \pm f_\alpha)\dots(1 \pm f_k)f_{k+1}\dots f_n - f_\alpha \dots f_k(1 \pm f_{k+1})\dots(1 \pm f_n) \quad (4.161)$$

It consists of two terms, as it accounts for both directions of process (4.159) - direct, corresponding to "disappearance" of α and reverse - relevant for production. If the interaction rate Γ_{int} is significantly larger, than expansion

rate, all particles distribution functions takes the shape of Fermi-Dirac or Bose-Einstein shape during some characteristic time $\tau_{\text{therm}} = \Gamma_{\text{int}}^{-1}$ if they were disturbed which drives the value of $F[f]$ to zero making the collision integral also effectively zero - local thermal equilibrium. In the SM scenario, thermal equilibrium is supported with high accuracy, such that the distribution function of neutrinos is always almost with equilibrium shape.

In the case of HNL presence, they are distorted by injection of high-energy neutrinos and their subsequent thermalization, which makes the collision term differ from zero equilibrium value. It is enough to consider only processes of 2- and 3-body decays of HNLs and $2 \to 2$ scattering reactions to calculate the distribution function of neutrinos with great accuracy. The standard procedure (see, for example, [194]) can reduce the dimension of integration to only two. But even with such simplification, it is still a challenging task to compute the evolution of the distribution function of neutrinos and it requires a numeric solution of the system of Boltzmann equations. After calculating the distribution function evolution, one can solve the Boltzmann equation for neutron abundance (4.22). This a method, typically used to set BBN-based constraints on the HNL's parameters ([193, 95, 194]). Although all those numeric codes may undergo different tests and provide extremely high accuracy of computation, they still remain a very complicated "black-box" instrument, hence we believe, that is important to see, if it is possible to capture the computable effects via some analytic or semi-analytic (without the requirement of solving Boltzmann equation) approximations. For this, we try to find a reasonable model to account the distortions of the neutrino spectrum.
One step thermalization

The simplest estimate one can make is to consider a "one-step" thermalization. Namely, a neutrino, after being injected in the SM plasma will have large interaction rate $\Gamma_{\nu,\text{therm}}(E_{\text{inj}}) \sim G_F^2 T^4 E_{\text{inj}}$ (compared to Hubble or thermal neutrinos interaction rates) even at temperature close to decoupling of neutrinos $T_{\nu,\text{dec}} \sim 2 - 3$ MeV ([95]). We can assume, that due to this large interaction rate, neutrinos thermalize very fast in one interaction. In this case, a distorted spectrum would be given by dynamic equilibrium between decaying of HNLs and thermalization of high-energy injected neutrinos.

$$f_{\nu,\text{inj}}(p, T) = n_N(T)\, \text{Br}_{N \to \nu} \frac{\Gamma_{\nu,\text{therm}}(p)^{-1}}{\tau_N} F_\nu(p) \qquad (4.162)$$

where $\mathrm{Br}_{N \to \nu}$ branching ratio of HNL decay into neutrino, $F_\nu(p)$ - decay spectra of neutrinos from HNL. Moreover, one can expect, that since weak conversion rate scales with energy of neutrino as $\sim E_\nu^2$, only the highest energy neutrinos would matter. Such approach is identical to the approach of meson-driven conversions - before neutrino "decays", it can participate in the $p \leftrightarrow n$ conversion with probability similar to meson conversion probabilities (4.98), (4.106):

$$P_{\mathrm{conv}}^\nu = \frac{n_B \langle \sigma_{p \leftrightarrow n}^\nu v \rangle}{\Gamma_{\nu,\mathrm{therm}}} \qquad (4.163)$$

Thermalization rate for neutrinos with energy $E_{\mathrm{inj}} \sim 10^2$ MeV at temperature $T = 1$ MeV is $\Gamma_{\nu,\mathrm{therm}} \sim 10^{-7} \tau_\pi^{-1}$ while the weak conversion rate is $n_B \langle \sigma_{p \leftrightarrow n}^\nu v \rangle \sim 10^{-16} \left(\frac{1\,\mathrm{MeV}}{E_{\mathrm{inj}}} \right)^2$. So the probability of conversion is 6-8 orders of magnitude smaller, than in the case of mesons. Direct use of constraint (4.115) with the change of conversion probability would give a limit at the level of $\tau_N \gtrsim 0.1 - 0.2$ s for large mass HNLs which is already order of magnitude weaker, than meson constraints. For HNLs with smaller masses, that injects neutrinos with even smaller energy, such constraint would be significantly higher.

Note, it is not correct to use the meson constraint directly. The value of neutron abundance in dynamic equilibrium in the presence of high-energy neutrinos may differ from the case of mesons (which is the case, as will be shown later) and be closer to the SM-given value. This would lead to the decrease of $T_{0,\mathrm{min}}$ which would increase the constrained lifetime even more.

We can avoid further study of this approximation not only because it gives too high values for constrained HNL lifetimes. We have already shown, that account of the evolution of decay products after injection leads to dependence of N_{eff} not only on the pure branchings into neutrino or EM plasma, but on the additional quantity $\epsilon(E_{\mathrm{inj}}, T)$, that parametrize, how energy is additionally redistributed between EM and neutrino sector during the thermalization of decay products. Which gives non-trivial consequences on when N_{eff} might increase or decrease. Value of g_*, that includes N_{eff} is important for the calculation of neutron abundances and requires accounting not only the first step of neutrino thermalization. Hence we should improve our approximation to do the same for neutrino spectra.

Multiple steps thermalization

Now let us take into account, that high-energy neutrino does not thermalize in one reaction. Let us still consider the case, when neutrino distribution function can be separated into fully equilibrium part and non-equilibrium distortion

$$f_\nu = f_{\nu,\text{eq}} + f_{\nu,\text{non-eq}} \tag{4.164}$$

We would consider neutrinos as non-equilibrium if their energy is such that the thermalization rate is significantly higher than the Hubble rate. If we use distribution function in such form for kinetic equation 4.158, we would get a Boltzmann equation for $\partial f_{\nu,\text{non-eq}}/\partial t$ with collision term describing neutrino-neutrino interactions separated into two components. One - corresponding to interaction between non-equilibrium and equilibrium components, proportional to $f_{\nu,\text{eq}} \cdot f_{\nu,\text{non-eq}}$ and another one - for interactions within non-equilibrium component. The equilibrium-equilibrium part would be canceled as it vanishes the collision integral. It is a reasonable approximation to neglect the the interaction within non-eq component compared to interaction with equilibrium part as its population has to be significantly limited via thermalization process rate and HNLs decay rate. It corresponds to $f_{\nu,\text{non-eq}} \ll 1$, $n_{\nu,\text{non-eq}} \ll n_{\nu,\text{eq}}$.

In this case, the evolution of the non-eq part of the spectrum will be governed by interaction with the equilibrium component and by decays of HNLs. Contribution from decays is quite straight-forward, if we know the momentum distribution for a decay of a single HNLs, then the contribution to collision integral I_α is given by

$$I_\alpha^{\text{inj}} = \partial n_N(T) \partial t \, \text{Br}_{N \to \nu} F_\nu(p_\alpha) \tag{4.165}$$

For interaction terms, the argument about the smallness of $f_{\nu,\text{non-eq}}$ can be applied to Fermi blocking factors. Since we consider relatively large energies, blocking factors $1 - f_x$ can be neglected, such that $F[f]$ becomes

$$F[f] = f_{\nu,\text{non-eq}}(p_3) f_{\nu,\text{eq}}(p_4) + f_{\nu,\text{non-eq}}(p_4) f_{\nu,\text{eq}}(p_3) - f_\alpha(p_\alpha) f_{\nu,\text{eq}}(p_2) \tag{4.166}$$

Here the first two terms corresponding to process, when higher-energy non-equilibrium neutrinos are thermalizing are supplying lower energies (but still non-eq) population. The last term corresponds to depleting of non-eq

population due to energy loss and annihilation processes and can be integrated explicitly leading to contribution

$$I_\alpha^{\text{depl}} = -f_\alpha \Gamma_\nu(p_\alpha, T) \tag{4.167}$$

where $\Gamma_\nu(p_\alpha, T)$ - interaction rate of neutrinos of momentum p_α with surrounding SM plasma at temperature T. The first two terms can not be integrated directly without making about any assumptions about the shape of distribution function. In total evolution of non-equilibrium spectrum is affected by:

- HNL decays that populates mostly high-energy part of spectrum ($E_{\text{inj}} \sim m_N$) with the rate of HNL decay

- Energy-loss and annihilation processes, that depletes the population with the rate of interaction rate of neutrino of corresponding energy

- Energy loss processes also populates the lower-energy part of spectrum

For this assumption, we will use the following model, based on the Sec.4.5.1. Since the thermalization rate decreases with energy but still significantly higher than expansion or HNL decay rate (for lifetimes of interest) there will be local dynamic equilibrium for the above described repopulation and depletion processes. Now, for simplicity let us assume, that the HNLs decay spectrum is a narrow peak. Then, the population of neutrino spectrum at very high energies will be given by dynamic equilibrium between decays and depletion while at lower-energy part - by dynamic equilibrium between depletion and re-population with energy loss.

In this case, for highest energies:

$$n_\nu(E_\nu \sim m_N) = n_N(T) \, \text{Br}_{N \to \nu} \frac{\Gamma_{\nu,\text{therm}}(E_\nu)^{-1}}{\tau_N} \tag{4.168}$$

Now, consider neutrino energy $T \ll E_\nu < E_{\text{inj}} \sim m_N$ that appears due to one energy loss process (4.133). Dynamical equilibrium value of that population is given by

$$n_\nu(E_\nu) = n_\nu(E_{\text{inj}}) \frac{\Gamma_{\nu,\text{therm}}(E_{\text{inj}})}{\Gamma_{\nu,\text{therm}}(E_\nu)} = n_\nu(E_{\text{inj}}) \frac{E_{\text{inj}}}{E_\nu} \tag{4.169}$$

We can continue this chain for lower energies in the same way until we reach the limit energies for neutrino, that are non-thermal. So populations of non-equilibrium neutrinos at energies, separated via one process (4.133) are related as:

$$\frac{n_\nu(E_{\nu,a})}{n_\nu(E_{\nu,b})} = \frac{E_{\nu,b}}{E_{\nu,a}} \qquad (4.170)$$

The increase of number density with the decrease of energy can be understood as follows: the "lifetime" of neutrino on large energy determines the time, when neutrinos can "stack" on corresponding energy level. During the time of thermalization of neutrino, the number density of HNLs would not change significantly ($\tau_N \gg \Gamma_{\nu,\text{therm}}$), so the "refilling" rate is also constant during the dynamical equilibrium establishment. Hence, the population on different energies depends only on "stacking time".

Therefore, since we know population of injected neutrinos, we can restore the population on any lower energy. Take the energy intervals as $E_{\text{inj}}, E_{\text{inj}}/2, E_{\text{inj}}/4, E_{\text{inj}}/8, ...$ as it's a reasonable steps of how neutrinos lose their energy in average. We have:

$$n_\nu(E_{\text{inj}}/2) = 2n_\nu(E_{\text{inj}}), \quad n_\nu(E_{\text{inj}}/4) = 4n_\nu(E_{\text{inj}}), \quad ... \qquad (4.171)$$

in reality, we know that there are more processes affecting the distribution function of neutrinos (Eqns. (4.133)- (4.137)) and as we mentioned, they can also change the total number density of non-equilibrium neutrinos by dragging thermal neutrinos out of equilibrium. This will result in different relations of neutrino number densities on different energies.

Using matrix elements of the processes (4.134)-(4.137) from [194] (that updated [193]), we obtained the interactions rates $\Gamma_1 \ldots \Gamma_5$. Our results agree with those from [113, 108].[5] The rates of particular processes (4.133)-(4.137), which we denote as $\Gamma_{1,2,3,4,5}$, are given in Table 4.1 . We also provide there the values of the total interaction rate $\Gamma_{\text{int}}^{\text{non-eq}}$,

$$\Gamma_{\text{total}}^{\text{non-eq}} = \sum_i \Gamma_i \qquad (4.172)$$

---

[5]Note that temperatures in Γ_{1-5} in Table 4.1 are temperatures of low energy particle (electron or neutrino), so for different temperatures of EM and neutrino components of plasma, corresponding temperature ($T_{\gamma,\nu_{e,\mu,\tau}}$ depending on process) must be used.

and the energy loss rate $\Gamma^{\text{non-eq}}_{\text{E loss}}$, which we define as the sum over the rates of processes

$$\nu^{\text{non-eq}} + X \to \nu^{\text{non-eq}} + X \qquad (4.173)$$

Process	(4.133)	(4.134)	(4.135)	(4.136)	(4.137)	$\Gamma^{\text{non-eq}}_{\text{total}}$	$\Gamma^{\text{non-eq}}_{\text{E loss}}$
$\Gamma^{\text{e flavor}}/G_F^2 T^4 E_\nu$	0.37	0.33	0.09	0.08	0.4	1.28	1.1
$\Gamma^{\mu/\tau\ \text{flavor}}/G_F^2 T^4 E_\nu$	0.04	0.16	0.01	0.04	0.13	0.8	0.69

Table 4.1: Neutrino interaction rates: of the processes (4.133)-(4.137), total interaction and energy loss rates. The total rate is obtained under the assumption that $T_\gamma = T_\nu$, *i.e.* is valid for equal neutrino and photon temperatures. If this is not the case, one can use separate temperature for each rate. Electrons are assumed ultra-relativistic.

Let us introduce the probabilities of annihilation ((4.135)) and scattering ((4.135)):

$$P_{\text{ann}} = \frac{\Gamma_{\nu_{\text{non-eq}}\bar{\nu}\to e^+ e^-}}{\Gamma^{\text{non-eq}}_{\text{total}}}, \quad P_{\text{EM scat}} = \frac{\Gamma_{\nu_{\text{non-eq}}e^\pm \to \nu_{\text{non-eq}}e^\pm}}{\Gamma^{\text{non-eq}}_{\text{total}}} \qquad (4.174)$$

After averaging over neutrino flavors, their values are

$$P_{\text{ann}} \approx 0.041, \quad P_{\text{EM scat}} \approx 0.166 \qquad (4.175)$$

In each process (4.134), (4.136), (4.137) the number of non-equilibrium neutrinos grows by a factor of two, in each process (4.135) non-equilibrium neutrinos disappear, whereas in the process (4.135) their amount does not change. Therefore, number of non-equilibrium neutrino after one scattering is changed via factor

$$(1 - P_{\text{EM scat}} - P_{\text{ann}}) \cdot 2 + P_{\text{EM scat}} \cdot 1 + 0 \cdot P_{\text{ann}} = (2 - 2P_{\text{ann}} - P_{\text{EM scat}}) \approx 1.77, \quad (4.176)$$

fnd since its value is larger than one, so number of neutrino actually increase. Hence one injected high energy neutrino produce a cascade of reactions that increases total number of non-equilibrium neutrino. Then for one injected neturino, number of neutrinos on k-th step is given by factor

$$F_\nu^{(k)} = (2 - 2P_{\text{ann}} - P_{\text{EM scat}})^k, \qquad (4.177)$$

So we need to modify relations (4.169), (4.170) using this factor. Now, relation between number density of injected neutrinos and number density at step "k" is given by

$$n_\nu(E_{\text{inj}}/2^k) = F_\nu^{(k)} 2^k n_\nu(E_{\text{inj}}) \tag{4.178}$$

Finally, we can calculate the correction for the $p \leftrightarrow n$ conversion rate driven by high-energy neutrinos. for the total conversion rate due to HE neutrinos we get

$$\Gamma_{p \leftrightarrow n}^{\text{HE, tot}} \approx \Gamma_{n \leftrightarrow p}^{\text{HE}}(E_{\nu,\text{inj}}) \cdot f_{\text{corr}}^{n \leftrightarrow p}(E_{\nu,\text{inj}}), \tag{4.179}$$

where the **correction factor** f_{corr} is

$$
f_{\text{corr}}^{n \leftrightarrow p}(E_{\nu,\text{inj}}) = \sum_k \frac{n_{\nu_e}^{\text{HE}}(E_\nu^{(k)})}{n_{\nu_e}^{\text{HE}}(E_{\nu,\text{inj}})} \frac{\langle \sigma_{n \leftrightarrow p}^{\text{HE}} v \rangle(E_\nu^{(k)})}{\langle \sigma_{n \leftrightarrow p}^{\text{HE}} v \rangle(E_{\nu,\text{inj}})} =
$$

$$
= \sum_{k=0}^{k_{\max}(E_{\nu,\text{inj}})} (2(1 + \beta_{\nu_e}))^k \frac{\langle \sigma_{p \leftrightarrow n} v \rangle(E_\nu^{(k)})}{\langle \sigma_{p \leftrightarrow n} v \rangle(E_{\nu,\text{inj}})} \tag{4.180}
$$

Value of $k_{\max}(E_{\nu,\text{inj}})$ is defined from minimal non-equilibrium energy $E_{\min,\text{non-eq}}(T)$ as

$$k_{\max}(E_{\nu,\text{inj}}) = \log_2\left[\frac{E_{\nu,\text{inj}}}{E_{\min,\text{non-eq}}(T)}\right] \tag{4.181}$$

Naive dependence of the cross section on the neutrino energy $\langle \sigma_{p \leftrightarrow n} v \rangle \sim E_\nu^2$ would lead to estimate of the correction factor as

$$f_{\text{corr}}^{p \leftrightarrow n} = \sum_{k=0}^{k_{\max}(E_{\nu,\text{inj}})} \left(\frac{F_\nu}{2}\right)^k \tag{4.182}$$

For a neutrino injection energy $E_{\nu,\text{inj}} \lesssim 500$ MeV at temperature $T \sim$ MeV its value will be $f_{\text{corr}}^{p \leftrightarrow n} \sim 5$.

In reality, for such high-energy neutrinos, nucleon form factors have to be used in calculations of $p \leftrightarrow n$ conversion rates (see App.A.3). This would make the correction factor different for $p \to n$ and $n \to p$ rate. In the range $E_\nu \leqslant 0.5$ GeV we have $f_{\text{corr}}^{n \to p} \leqslant 3.5$, $f_{\text{corr}}^{p \to n} \leqslant 5.5$. The difference is caused by slower E_ν dependence of $\langle \sigma_{p \to n} v \rangle$. Hence high energy non-equilibrium neutrinos would not shift the neutron to proton ratio to unity even if there was large abundance of them. Instead, we have temperature dependent (since the minimum energy and hence - parameter $k_{\max}$ depends on it) local equilibrium value.
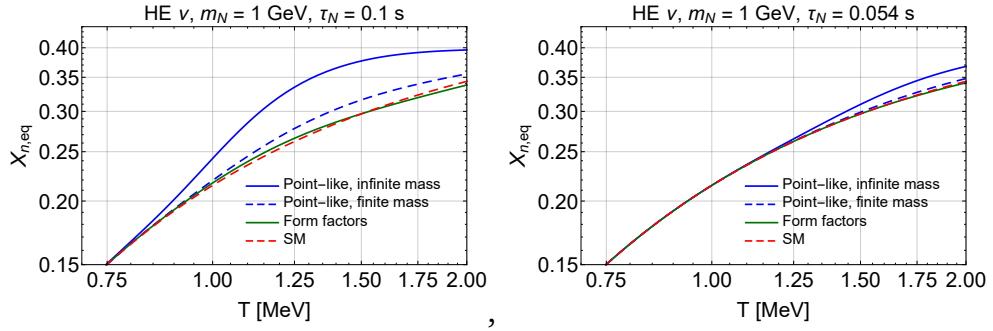
Figure 4.24: Evolution of equilibrium value of neutron abundance as given by the high-energy neturinos from HNL decays for two sets of paramters: $m_N = 1$ GeV, $\tau_n = 0.1$ s (**left panel**) and $m_N = 1$ GeV, $\tau_n = 0.054$ s (**right panel**) . If we would use the point-like approximation, the abundance of Helium would be affected significantly, but the occasional proximity of the SBBN value of X_n and the ratio of $p \leftrightarrow n$ weak reactions cross sections has led to a very small deviation of $X_n(T)$ from the SBBN value.

So as we see, taking into account several steps of neutrino thermalization indeed increases significantly their contribution to conversion rates compared to naive assumption. Although the contribution of a single neutrino indeed drops with energy significantly, but the number of neutrinos increases, hence compensating the cross-section drop. But local equilibrium value X_n^{eq} accidentally remains very close to the one, given by SBBN. It is a result of nucleon form factors which we didn't include in our simplest estimate 4.5.3. Such unexpected result shows, that contribution from high-energy non-equilibrium neutrinos is a counter-intuitively *subdominant* effect if we compare it with, for example, effect of g_* change.

There are two remaining effects we did not take into account yet, that are relevant :

- Spectral distortions due to change of temperature of neutrinos. When HNLs inject energy into EM and neutrino spectra, changing their temperature, and energy-redistribution processes start, they do not proceed with the same rate on each energy. While EM-particles ($e^\pm, \gamma$) spectra remain always with FD distribution, neutrinos don't have to. It distorts the spectrum of neutrinos.

- Distortions on low energies. Previously we avoided them since they were naively subdominant to high-energy neutrinos, but as we saw, the effect

of such neutrinos is accidentally suppressed. So we need to estimate the effect for lower $E_{\nu,\text{non-eq}}$ also.

Temperature-difference driven distortions

Previously we have separated the spectrum of neutrinos into equilibrium and non-equilibrium parts, assuming for simplicity, that the equilibrium component keeps perfect FD distribution. But as we saw in Sec.4.5.2, the temperature of neutrinos may differ from EM-plasma temperature already at neutrino decoupling. The neutrino decoupling process is not instant, hence even if lower-energy neutrinos can be considered as decoupled, a hotter part of the spectrum may still interact. If we introduce effective temperature of neutrinos, such that spectrum would be given by:

$$f_\nu = \frac{1}{1 + e^{p_\nu/\mathcal{T}_{\text{eff}}(p_\nu)}} \tag{4.183}$$

We can expect, that population of neutrinos at high energy would correspond to $\mathcal{T}_{\text{eff}} \approx T_\gamma$, while lower energies may have $\mathcal{T}_{\text{eff}}$ higher or lower, than photon temperature, depending on the injected energy to each component. In what follows we would refer to this distorted population as to quasi-equilibrium $f_{\text{quasi-eq}}$. For estimate of the level of the distortions we would follow approach of (see [96]) where the similar process was studied. Namely, authors has considered the change of neutrino spectrum after electron-positron annihilation that has also lead to difference between T_ν and T_γ. It was obtained, that correction for neutrino spectrum can be expressed as

$$\delta f_\nu(p,t) = \frac{8G_F^2(g_L^2 + g_R^2)}{3\pi^3}\frac{p}{T_\nu}\left[\frac{11}{4}\frac{p}{T_\nu} - 3\right] \cdot \int\limits_{t_0}^{t(T_\gamma)} dt T_\nu^5 \left(\frac{T_\gamma}{T_\nu} - 1\right), \tag{4.184}$$

where $g_L = 1/2 + \sin^2(\theta_W)$, $g_R = -1/2 + \sin^2(\theta_W)$. We can rewrite it in the terms of correction to effective temperature of neutrino.

$$\delta T_\nu(p,t) = \left(1 + e^{-\frac{p}{T_\nu}}\right)\frac{T_\nu}{p}\delta_\nu(p,t), \tag{4.185}$$

It is seen from this expression, that if $T_\nu < T_\gamma$, at low energies effective temperature is effectively decreased with negative correction, while at higher energies - increased. This can be understood as follows: hotter EM plasma drags the neutrinos, trying to give it the same temperature, but neutrinos

are getting out of equilibrium, so their population is not restored effectively, especially at low energies, where such neutrinos are already decoupled and such neutrinos are "used" to refill the population at $E_\nu \gtrsim T_\nu$.

To follow this approach we need the temperature of neutrinos T_ν introduced. For this, we use the one from 4.5.2. Namely, the one, defining the energy density of neutrinos $\rho_\nu = \frac{7}{8}\frac{\pi^2}{30}T_\nu^4$. Having the T_ν/T_γ for each moment of time and using Eqn, (4.184) we can find the distorted population.

Naively, we have use the value of $T_\nu + \delta T_\nu(p,t)$ as the effective temperature of neutrinos $\mathcal{T}_{\text{eff}}$. But since our temperature T_ν is basically a neutrino energy density rather than temperature, defining spectra while treatment of [96] corresponds to exact distribution we have to take care about the consistency [6]. For this, we use $T_\nu + \delta T_\nu(p,t)$ as *shape-defining* effective temperature and then re-normalize the distribution such that energy density of neutrino still correspond to T_ν. With this,we have the following spectra for quasi-equilibrium component of neutrino spectra.

$$f_{\nu,\text{quasi-eq}}(p,T) = \frac{\frac{7}{8}\cdot\frac{\pi^2}{30}\cdot T_\nu^4}{\int \frac{p}{e^{p/(T_\nu+\delta T_\nu)}+1}\frac{d^3\mathbf{p}}{(2\pi)^3}} \cdot \frac{1}{\exp\left(\frac{p}{T_\nu+\delta T_\nu}\right)+1} \equiv \frac{1}{\exp\left(\frac{p}{T_{\text{eff}}}\right)+1},$$

(4.186)

With this we can calculate directly the change of conversion rates for any ratio of neutrino to photon temperature, the difference in rates are shown at Fig. 4.25

Low-energy distortions

Although the previously described temperature-driven distortions have also corresponded to low energy (compared to $E_\nu \sim m_N$) contribution, we separate the one, forced by injections. We will concentrate on neutrinos with such energy, that $\Gamma_{\nu,\text{therm}}(E_\nu) \sim H(T)$. Hence, this distortion becomes important only at temperature of neutrino decoupling and below (*e.g.* $T_{\nu,\text{dec}} \sim 2-3$ MeV). The most important difference from high-energy distortions is that there

---

[6]The inconsistency appears since the expression (4.184) contains not only energy redistribution within the neutrino spectra, but also the energy transfer between $EM \leftrightarrow \nu$. At the same time, in the T_ν/T_γ evolution these processes are already incorporated. Hence, we might double account this energy transfer as both T_ν/T_γ and $\delta f_\nu(p,t)$ evolves in the same time.
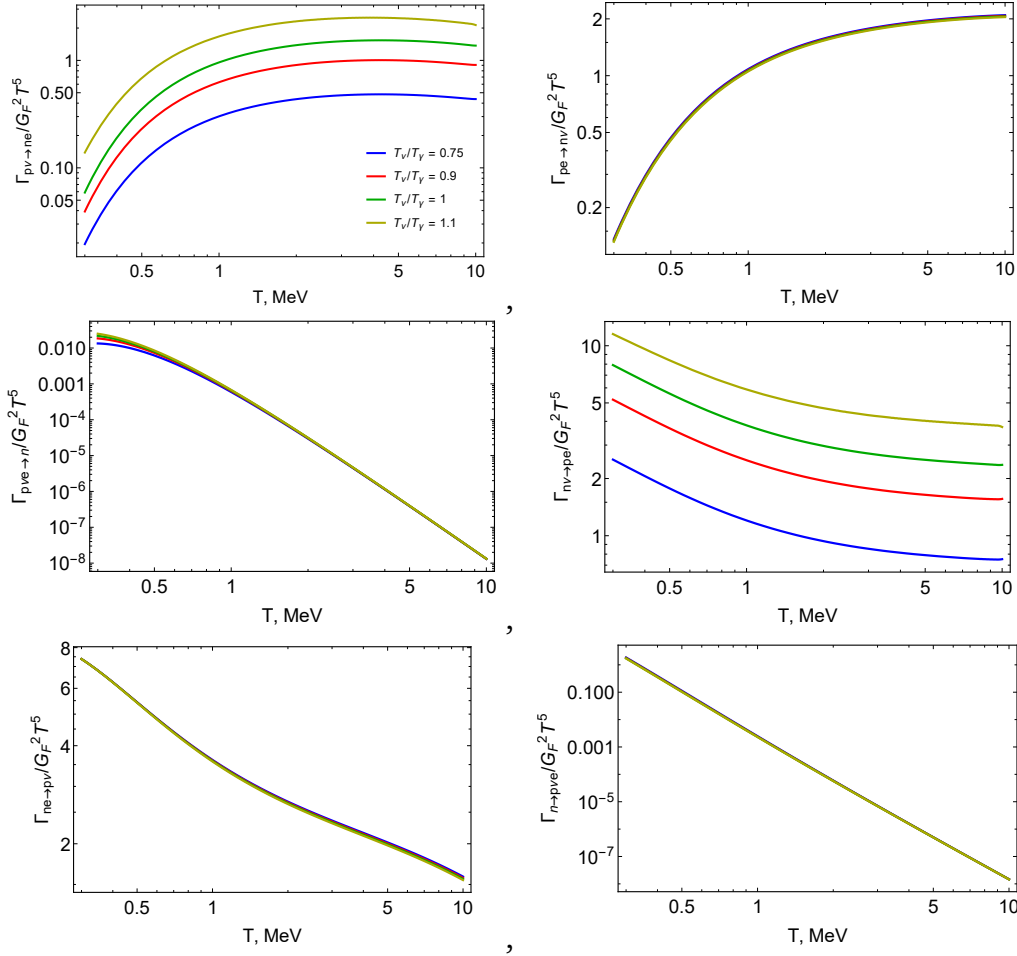
Figure 4.25: All conversion rates $p \leftrightarrow n$ as a function of temperature for different neutrino-to-photon temperature T_{ν_e}/T_γ. Panels from top left to bottom right correspond to the processes: *(i)* $p+\nu \to n+e$, *(ii)* $p+e \to n+\nu$, *(iii)* $p+\nu+e \to n$, *(iv)* $n+\nu \to p+e$, *(v)* $n+e \to p+\nu$, *(vi)* $n \to p+\nu+e$. Obviously, the most sensitive fot temperature changes are the rates, involving neutrinos as initial state, as they are proportional to their number density and energy. Rates, that has neutrinos only as final state, also depend in the neutrino population , but much weaker - through the Pauli blocking

is no dynamic equilibrium anymore, neutrinos during the energy-loss process may go out of equilibrium before getting thermal distribution, so instead of dissolving in the thermal bath, they can "stack" at $E_\nu \gtrsim E_{\nu,\text{thermal}} = 3.15 \cdot T_\nu$. While a total number of high-energy non-equilibrium neutrinos is defined by decay rate and temperature, it does not depend on the total number of HNLs decaying. For low-energy, this is not the case as we can expect, that they all will settle down in form of "slightly hotter than thermal" neutrinos. The more HNL decays, the stronger will be this cumulative effect.

Let us start from estimating the energy , where non-thermal neutrinos will be stacking. For this, let us calculate the energy evolution of a single neutrino injected at temperature $T = T_{\text{inj}}$ with energy $E_\nu = E_{\text{inj}}$. For a simple estimate we can use kinetic equation

$$\frac{dE_{\text{non-eq}}}{dt} + H \cdot E_{\text{non-eq}} \approx \log(2) \cdot \Gamma_{\nu,\text{therm}} \cdot (E_{\text{non-eq}} - E_{\nu,\text{therm}}), \quad E_{\nu,\text{therm}} \equiv 3.15 \cdot T_\nu \tag{4.187}$$

here, $\Gamma_{\nu,\text{therm}}$ - flavour-averaged rate of neutrinos interaction that lead to change of energy of initial neutrino (without annihilation processes) - (see rates from Table 4.1). $E_{\nu,\text{therm}}$ was introduced to represent, that thermalization has to lead to averaged thermal energy. Factor $\text{Log}[2]$ - numeric factor following from the assumption, that when energy of neutrino is high, it has to lose half of it's energy each interaction ($E_\nu \sim 2^{-\Gamma_{\nu,\text{therm}}t}$). Let us for now consider the case $T_\nu = T_\gamma$, such that we can use the same temperature in all rates. Rewriting it with respect to temperature

$$\frac{dE_{\text{non-eq}}}{dT} - \frac{E_{\text{non-eq}}}{T} \approx A \cdot E_{\text{non-eq}} T (E_{\text{non-eq}} - 3.15T), \quad A \equiv \text{Log}2 \frac{M_{pl}}{1.66\sqrt{g_*}} \cdot \Gamma_{\nu,\text{therm}}\big|_{E_{\text{non-eq}}=T=1\text{ MeV}} \tag{4.188}$$

it can be solved explicitly

$$E_{\text{non-eq}}(T) \approx \frac{3.15T}{\left(\frac{3.15\text{Tinj}}{\text{Einj}} - 1\right) e^{\frac{0.11(T^3 - \text{Tinj}^3)}{\text{MeV}^3}} + 1} \tag{4.189}$$

At temperature, close to injection, change of energy is completely driven by fast reactions, while at $T \ll T_{\text{inj}}$ - by expansion factor ($\sim T$). The value $E_{\text{non-eq}}(T)/T$ at small temperatures is frozen-out and depend on the initial injected energy very weakly. Much more important is the temperature of injection. See Fig. 4.26

In more general case, the temperature of neutrinos and photons does not have to be equal. For this, the factor $A \equiv \text{Log}2 \frac{M_{pl}}{1.66\sqrt{g_*}} \cdot \Gamma_{\nu,\text{therm}}$ in the r.h.s. of Eq. 4.188 have to be calculated using rates with different temperatures. Using this equation, we have found that the non-equilibrium neutrinos equilibrates completely (i.e., $\mathcal{T}_{\text{eff}} \to T$) only if the injection temperature $T_{\text{inj}} \gtrsim 3.5$ MeV, see Fig. 4.26. Although this equation was used to describe the evolution of a single neutrino, it can be used to calculate the evolution of *average energy* of neutrinos injected at some temperature (see App. A.1), in assumption, that distribution function of neutrinos, injected at some temperature T_{inj} acquires
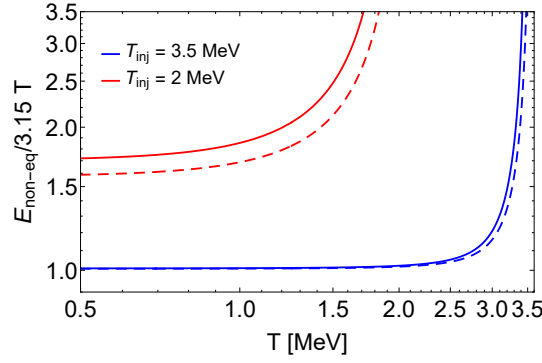
Figure 4.26: The ratio $E_{\text{non-eq}}/3.15T$ for the cascade of non-equilibrium neutrinos for two injection temperatures $T_{\text{inj}} = 3.5$ MeV (blue lines) and $T_{\text{inj}} = 2$ MeV (red lines) and the energy $E_{\nu,\text{inj}}$ of the injected non-equilibrium neutrinos (solid lines: $E_{\text{inj}} = 500$ MeV, dashed lines: $E_{\text{inj}} = 50$ MeV).

FD-shape with the temperature $T_{\text{eff}} = \langle E_\nu \rangle / 3.15$, and normalization factor given by the number density of non-equilibrium neutrinos. In its turn, to find the number density of injected non-equilibrium neutrinos, we follow the approach of multiple-step thermalization and use (4.178), but instead of k-th step of thermalization we use the value of energy obtained from Eqn. (4.188) extrapolating the applicability of F-factor to lower energies

$$n_{\nu,\text{non-eq}}(E_\nu, T) = \left(\frac{a(T_{\text{inj}})}{a(T)}\right)^3 \cdot F_\nu^{\text{Log}_2\left((E_{\text{inj}}/E_\nu)\cdot(T/T_{\text{inj}})\cdot(g_*(T)/g_*(T_{\text{inj}}))^{1/3}\right)} n_{\nu,\text{inj}}(T_{\text{inj}}) \tag{4.190}$$

where $n_{\nu,\text{inj}}(T_{\text{inj}})$ - number density of neturinos, injected at temperature T_{inj} Here we introduced ratio (T/T_{inj}), since power in abundance factor F must correspond to energy change only due to energy-loss reactions but in Eqn. (4.188), the expansion of the Universe is also taken into account. To compensate it we need to add the ratio of scaling factors which is related to temperature and g_* through $s(T)a(T)^3 = const$[7]. Factor $\left(\frac{a(T_{\text{inj}})}{a(T)}\right)^3 \cdot$ corresponds to dilution of injected number density during expansion. We didn't have this two last terms in Eqn. (4.178) as the initial steps of thermalization proceeds much faster, than universe expands. We also do not have factor 2^k since it appeared from dynamical equilibrium. While here, instead of instantaneous number density we introduce total number of neutrinos injected at some temperature.

Let us summarize our approach for treatment of low-energy corrections:

---

[7]If the temperatures of neutrinos and photons are different, this ratio would be slightly modified, as contribution to entropy density will be not even

- Consider, that at temperature T_{inj} high-energy neutrinos were injected with number density n_{inj}

- During the termalization neutrinos acquire FD-shape distribution (normalized to n_{inj}) and increase their number density with factor F_ν.

- Effective temperature of those neutrinos is taken from their average energy evolution as $T_{\text{eff}} = \langle E_\nu \rangle / 3.15$

- We account the expansion of the Universe by diluting the resulting number density with temperature

- $p \leftrightarrow n$ conversion rates from low-energy non-equilibrium neutrinos are calculated using the general formula (5.12)

Let us only make a small additional comment about improving the consistency of our approach. When considering high-energy distortions, their low number density allowed us to avoid taking their effect on the quasi-equilibrium population into account. In the case of low-energy neutrinos, their number density may become significant, since *(i)* HNLs do not have time to decay before $T_{\nu,\text{dec}} \sim 2-3$ MeV, *(ii)* factor F_ν together with branchings into multiple-neutrino decay leads to additional factor ~ 10, that increases number density of neutrinos compared to HNLs. Since equilibrium neutrinos are being dragged out during the thermalization process, we account for it by introducing an additional "depletion" factor for the quasi-equilibrium neutrinos when calculating the final rates.

The resulting neutrino distribution function is

$$f_\nu(p, T) \approx f_{\nu,\text{non-eq}} + \left(1 - \frac{n_{\nu,\text{non-eq}}}{n_{\nu,\text{quasi-eq}}} \right) f_{\nu,\text{quasi-eq}}, \qquad (4.191)$$

where the pre-factor $1 - n_{\nu,\text{non-eq}}/n_{\nu,\text{quasi-eq}}$ corresponds to the fraction of the quasi-equilibrium neutrinos.

4.5.4 Computation of neutron abundance

Now we can finally describe the machinery of our computations.

1. **First step:** We start from calculation of HNL number density-to-entropy ratio $\mathcal{Y}_N(T) \equiv n_N/s$, that will be present in plasma as a function of temperature. For this we use kinetic equation

$$\frac{d\mathcal{Y}_N}{dt} = -\Gamma_N^{\text{int}}(T)(\mathcal{Y}_N - \mathcal{Y}_{N,\text{eq}}), \qquad (4.192)$$

where $\mathcal{Y}_{N,\text{eq}} = n_{N,\text{eq}}/s(T)$ is the abundance at equilibrium (i.e., calculated using the Fermi-Dirac distribution), and Γ_N^{int} is the total rate of processes $A + N \to B + C$:

$$\Gamma_N^{\text{int}} = \sum_{A,B,C} \Gamma_{A+N\to B+C}, \quad \Gamma_{A+N\to B+C}(T) = n_A(T)\cdot\langle\sigma_{NA\to BC}v\rangle \quad (4.193)$$

2. **Second step:** We solve the system of Friedman equations (4.144)-(4.146) to define the evolution of: *(1)* dilution factor $\zeta(T)$, *(2)* neutrino and EM plasma energy density evolution with account of energy injections. At this step, the shape of all distribution is taken as Fermi-Dirac with some temperature.

3. **Third step:** Take the temperature interval for injections starting fro $T_{\text{start}} = 3.5$ MeV (higher values are irrelevant due to perfect thermalization) and until $T_{\text{fin}} = \min(T_{n,\text{dec}}, T(10 \cdot \tau_N))$. Separate the $(T_{\text{fin}}, T_{\text{start}})$ into $\Delta N = 100$ intervals (T_i, T_{i+1}). Suppose, that at each T_i there was an injection of

$$n_{\text{inj},2}^{\text{i-th}} = \text{Br}_{\nu,2-\text{dec}}\left(n_N(T_i) - n_N(T_{i+1})\right) \qquad (4.194)$$

neutrinos with energy $E_{\text{inj}} = \frac{m_N^2 - m_\pi^2}{2m_N}$ from 2-particle decay. Here $\text{Br}_{\nu,2-\text{dec}}$ - 2-particle decay branching into neutrino of HNL, and

$$n_{\text{inj},3}^{\text{i-th}} = \left(\text{Br}_{\nu,3-\text{dec}} + \text{Br}_{3\nu,3-\text{dec}}\right)\left(n_N(T_i) - n_N(T_{i+1})\right) \qquad (4.195)$$

neutrinos with energy $E_{\text{inj}} = m_N/3$. Here $\text{Br}_{\nu,3-\text{dec}}$ and $\text{Br}_{\nu,3-\text{dec}}$ are 3-particle decay branchings with 1 and 3 neutrinos respectively.

4. **Fourth step:** Neutrinos from each of that injection are accounted as separate contribution to non-equilibrium distribution function:

$$f_{\nu,\text{non-eq}}^{\text{i-th}}(p, T) = \left(\frac{a(T)}{a(T_i)}\right)^3 \left(\frac{n_{\text{inj},2}^{\text{i-th}}}{n_{\nu,\text{eq}}(\mathcal{T}_{\text{eff}}^{\text{i-th},2})} \frac{1}{e^{p/\mathcal{T}_{\text{eff}}^{\text{i-th},2}} + 1} + \frac{n_{\text{inj},3}^{\text{i-th}}}{n_{\nu,\text{eq}}(\mathcal{T}_{\text{eff}}^{\text{i-th},3})} \frac{1}{e^{p/\mathcal{T}_{\text{eff}}^{\text{i-th},3}} + 1}\right)$$
(4.196)

Here, $n_{\nu,\text{eq}}$ is the equilibrium number density of neutrinos at given temperature, $\mathcal{T}_{\text{eff}}^{\text{i-th},2}, \mathcal{T}_{\text{eff}}^{\text{i-th},3}$ is an effective temperature of the neutrinos at the temperature T, originated from the injection at T_i from 2- and 3- particle decays, given by solving the Eqn. (5.7) for average energy and taking $\mathcal{T}_{\text{eff}} = \langle E_{\text{non-eq}}\rangle/3.15$.

5. **Fifth step:** Combine all the low-energy non-equilibrium distortions from each injection $f_{\text{non-eq}}(p, T) = \sum_i f_{\nu,\text{non-eq}}^{\text{i-th}}(p, T)$ together with correction from high-energy distortions (4.178) and quasi-equilibrium distribution function (4.186) in a total neutrino distribution. **Sixth step:** Solve the Boltzmann equation (4.22) for neutron abundance X_n with the account of correction to $p \leftrightarrow n$ conversion rates, temperatures of plasma components and correction to Hubble rate from HNLs, starting at temperature $T = 10$ MeV, where SM rates are defining the neutron fraction. We solve this equation untill the moment $T_{\text{BBN}} = 0.084$ keV to compare the final value of $X_n(T_{\text{BBN}})$ with numeric results of [194]

6. **Final step:** Transfer the obtained fraction of neutrons into Helium-4 mass fraction $Y_p \approx 2 \cdot X_n(T_{\text{BBN}})$. Compare it with the SM-driven value we compute without corrections. If the correction is higher, than the constrained error 3.8%, such HNLs would be considered as excluded.

4.6 Results

First of all, we compare our non-meson results with the numeric results in [194] where the same mass range was considered (see Fig. 4.27). This line does not correspond to our final constraint, as it uses a different limit error of $\Delta Y_p/Y_p = 2.5\%$ which we increase to $\sim 4\%$ to be consistent with all observational data. Qualitatively – the shape of the bound, the hierarchy of the bounds for different mixings – the bounds agree well. The discrepancy occurs at low masses $m_n \lesssim m_\pi$.
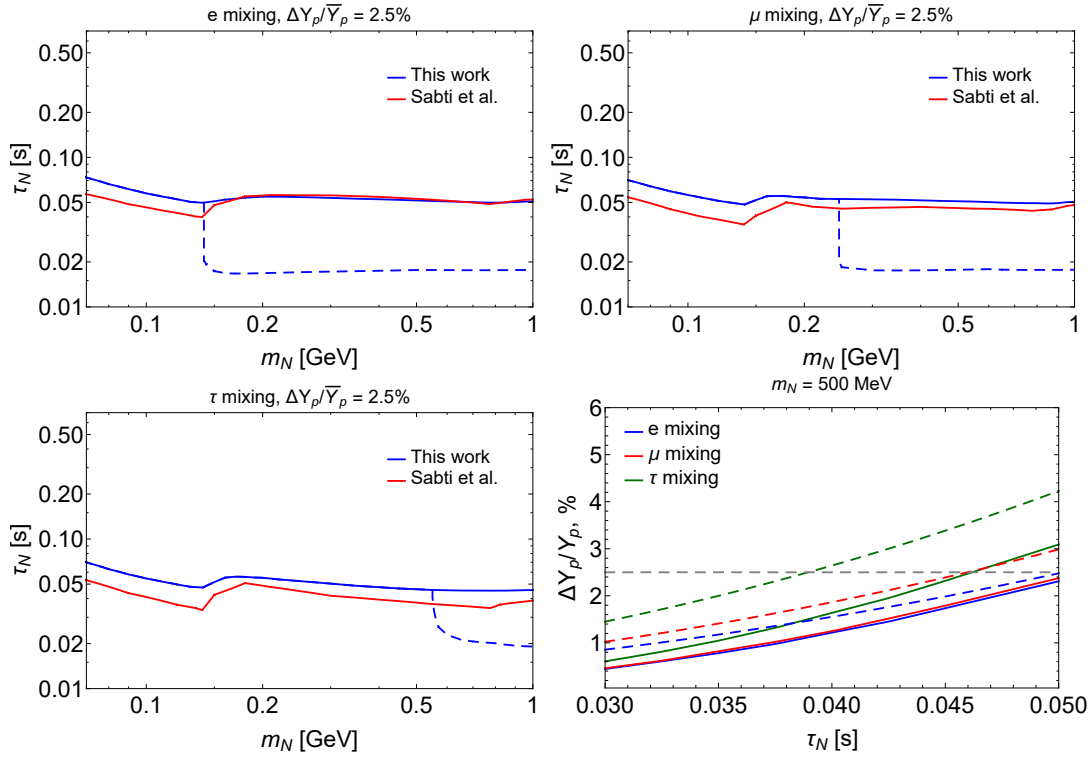
Figure 4.27: *Top panels and down left panel*: constraints on the HNL lifetime from primordial helium abundance measurements assuming the maximal correction $\Delta Y_p/Y_p = 2.5\%$. Blue lines are the results of this work and red lines of [194]. The dashed lines correspond to the constraint with meson effect taken into account, see Sec. 4.4. *Bottom right panel*: The He abundance correction induced by a 1 GeV HNL versus its lifetime (see text for details). Solid lines denote our predictions, while dashed lines correspond to the fitting functions of [194], which have a maximum deviation of 0.4%. The dashed gray line denotes 2.5% correction.

We also present our final constraint for HNL parameters that is related to our pick of maximum error at Fig. 4.28:
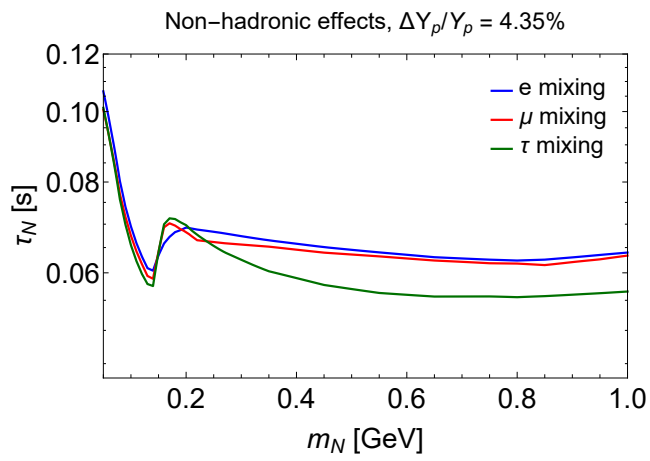
Figure 4.28: Parameter space of HNLs, which non-hadronic contribution to BBN lead to a correction of 4.35% to Helium-4 abundance for three different mixings. HNLs with higher lifetimes are constrained until they reach the non-thermal production, which did not consider.

Discussion and conclusion

Particle physics is at crossroads [202, 106, 205]. On the one hand the latest accelerator experiments have confirmed predictions of the Standard Model with the remarkable precision [see e.g. 146] while failing to discover new physics at electroweak scale [41, see e.g.]. On the other hand BSM phenomena (subject of Chapter 1 of this thesis) unequivocally point towards incompleteness of the Standard Model and existence of new particles. The uniqueness of today's moment is in the absence of any hints regarding the properties of these particles. Their masses, types of interactions, even their numbers are not known. It is possible that only 3 new particles are missing (as in the case of heavy neutral leptons in the νMSM [35, 38, 202, 71]) or that the number of the SM particles will double one day (as in the case of supersymmetric SM [23]). It is even possible that the number of new particles is infinite, as in the case of Kaluza-Klein-like extensions of the SM [30]. The proposed solutions to each of the BSM problems predict particles ranging in masses by many orders of magnitude.

Current situation is perplexing not only from a theoretical viewpoint. It also has drastic practical consequences. There exists no single experiment that could explore all the proposed options. What experiment should we build and in what combination? Which frontier (Figure 1.1) should we explore first? There is no lack of potential ways to go forward [107] and no obvious winner. In this situation any prior knowledge we can obtain about parameter space of hypothetical particles can be of paramount importance, shaping the future of experimental particle physics.

The cosmic frontier is one of the ways to constrain (or even discover) new particles without doing new experiments. It is especially important when one tries to constrain feebly interacting particles. Indeed, interiors of the stars (and especially, supernovae) as well as primordial plasmas early in the Universe's history deliver to us densities of matter where even feebly interacting particles

become noticeable and can affect the existing observables in an essential way.

This thesis uses cosmic frontier to constrain the properties of hypothetical particles – sterile neutrinos with masses ranging from few keV to few GeV. It considers two "test grounds" – proto-neutron stars (interiors of supernovae during the first second after the explosion) and primordial plasma at MeV (billions of degree Kelvin) temperatures.

In the case of exploding supernovae it is demonstrated that the keV-scale sterile neutrinos can be copiously produced in their interior regions via the analog of MSW effect [214]. The reported result presents a self-consistent treatment of such a production, taking into account for the first time back-reaction of sterile neutrinos on the supernova lepton number distribution. The mechanism of production is very efficient and can lead to copious production of keV-scale sterile neutrinos with the couplings many orders of magnitude weaker than *e.g.* those probed by the KATRIN experiment [61]. Surprisingly this does not lead to any competitive bounds on sterile neutrino parameters, contrary to the previous claims in the literature [33]. This is because the experimental data about supernova explosion (e.g. those coming from SN1987A) are scarce and numerical simulations has not yet reached the maturity that would allow to answer detailed questions about the *interiors* of the proto-neutron stars, in particular about the temperature in the inner regions.

In the second part of the thesis, the interaction of sterile neutrinos with primeval plasma is analysed [66, 67]. Our information about the state of primordial plasma at MeV temperatures comes mainly from the measurements of the primordial abundance of Helium-4. It is demonstrated in the thesis that once sterile neutrinos have masses above that of pion mass, their semi-leptonical decays (with one or several mesons in the final state) change neutron-to-proton ratio and thus the Helium-4 abundance to the values incompatible with observations. The effect qualitatively is driven by the large difference between strong and weak rates of proton-to-neutron conversion. The bounds on sterile neutrino lifetime become factor 5 stronger than in the absence of this effect [99, 194]. Next we consider the influence of decaying sterile neutrinos to the overall expansion rate of the Universe (expressed via N_{eff}). While sterile neutrinos can indeed change the expansion rate of the Universe at the early times, they are not able to alleviate fully the so-called Hubble

tension. The limits on the lifetime of sterile neutrinos from the measurements of the anisotropies of Cosmic Microwave Background are also derived.

Unlike most of the previous works, the treatment of sterile neutrinos on BBN is done analytically and this thesis provides necessary details of this treatment. Such treatment not only allows for a simpler cross-check of the results, but also for the exploration of full (4-dimensional) parameter space of sterile neutrinos.

Finally, the cosmic frontier results are confronted with the specific particle physics models in [60] where they provide a "bottom line" for direct intensity frontier searches.

There are two important conclusions of this thesis that go beyond specific results and bounds on sterile neutrino parameters. First, the existing super-novae bounds are prone to high "systematic" uncertainties having to do with the lack of information about the supernovae interiors. This conclusion (that was derived for sterile neutrinos) holds for other types of feebly interacting particles. This result should be kept in mind when "SN1987A bounds" are confronted with direct particle physics searches, as often done in the literature [17].

Second important conclusion is the complementarity of cosmic frontier results to other types of searches. Astrophysical/cosmological bounds often probe the properties of feebly interacting particles in the (very) long-lived regime – the regime that is the hardest for particle physics experiments.

Appendix A

A.1 Equation for $\langle E_{\nu,\text{non-eq}} \rangle$

In this section we derive the equation for evolution of average energy of non-equilibrium neutrinos. In our rough estimates for high-energy neutrino contribution we considered them as having the wide-peak distribution so we can follow it's evolution similar to evolution of a single neutrino with given energy. It is much more natural, though, to expect this distribution to become a Fermi-Dirac shape but with a different temperature. Such that this temperature approaches to the temperature of equilibrium (quasi-equilibrium) neutrinos. We have tested this hypothesis, using the code for [194], injecting neutrinos at different energies and temperatures and comparing the resulting population with Fermi-Dirac distribution function with some effective temperature. We have found, that this assumption is a relatively good approximation for neutrino spectrum. Not that this is true only after few thermalization times after injection, otherwise spectrum is completely non-thermal. The example of such comparison is on the Fig. A.1

With this assumption, evolution of average energy is the same as evolution of effective temperature, as for FD distribution they are related. Quickly after the injection of non-equilibrium neutrinos their distribution function gains the Fermi-Dirac shape with some effective momentum independent temperature $\mathcal{T}_{\text{eff}} > T$:

$$f_\nu \sim \frac{1}{1 + e^{p_\nu/\mathcal{T}_{\text{eff}}}} \tag{5.1}$$

To describe the evolution of this distribution function and in particular, to derive the equation for $\mathcal{T}_{\text{eff}}$ we can consider the Fokker-Planck equation. It
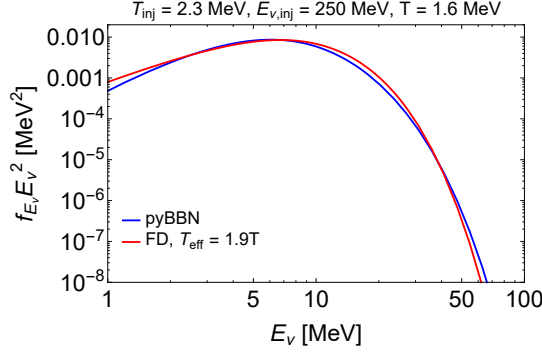
Figure A.1: The energy spectrum at $T = 1.6$ MeV (the blue line) of muon neutrinos injected with monochromatic energy $E_{\text{inj}} = 250$ at $T_{\text{inj}} = 2.3$ MeV, and evolved due to energy loss processes with thermal bath particles $e^{\pm}, \gamma, \nu_{e/\tau}$. All the processes leading to the non-conservation of the ν_{μ} number are turned off. The spectrum is provided by pyBBN simulations [194]. By the red line, we show the Fermi-Dirac spectrum with the effective temperature $\mathcal{T}_{\text{eff}} \approx 1.9 \cdot T$. Main discrepancy appears on the lowest energies as that part of neutrino spectra thermalize the worst.

is applied for the distribution function of non-equilibrium neutrinos $f_{\nu,\text{non-eq}}$ that present are in some thermal bath of temperature T (for now, let us not distinguish, that components of such thermal bath may have different components). We also assume the conservation of number density of neutrinos (co-moving) during this evolution [57], as for the evolution at high temperatures, when number of non-equilibrium neutrino changing a lot (factor F_{ν} (4.166)), FD-distribution approximation is not applicable:

$$\partial_t f_{\nu,\text{non-eq}} - H\mathbf{p}_{\nu}\partial_{\mathbf{p}_{\nu}} f_{\nu,\text{non-eq}} = p_{\nu}\partial_{\mathbf{p}_{\nu}} \left[\gamma(E_{\nu}T\partial_{\mathbf{p}_{\nu}} f_{\nu,\text{non-eq}} + \mathbf{p}_{\nu} f_{\nu,\text{non-eq}}(1 - f_{\nu,\text{non-eq}}))\right] \tag{5.2}$$

Here, H is the Hubble factor, γ is the momentum transfer rate,

$$\gamma(p_{\nu}, T) = \frac{1}{6E_{\nu}T(1 - v_{\nu}^2/3)} \sum_j \int \frac{d^3\mathbf{p}_j}{(2\pi)^3} f_j(1 - f_j) \int_0^{4p_{\text{cm}}^2} dt\, t\frac{d\sigma_{\nu_{\text{non-eq}}+j\to\nu_{\text{non-eq}}+j'}}{dt} v, \tag{5.3}$$

with j denoting $\nu/\bar{\nu}, e^{\pm}$ particles. In our case,

$$\gamma \approx 1.04 G_F^2 T^4 p_{\nu} \approx 1.27 \Gamma_{\text{E loss}}(p_{\nu}, T), \tag{5.4}$$

with $\Gamma_{\text{E loss}} \approx 0.82 G_F^2 T^4 p_{\nu}$ being the energy loss rate averaged over flavors (see Table 4.1). Finally, $t = -(p_{\nu} - p_{j'})^2$ is the squared momentum transfer. The applicability of Eq. (5.2) breaks down in the regime of large energy transfer, i.e. as far as typical energies of neutrinos are much higher than thermal

bath average energy $3.15T$. However, we expect that in the regime when the average energy $\langle E_\nu \rangle$ exceeds the thermal energy at most by a factor of few, which is our case of interest, it describes the evolution properly. To derive the equation for $\mathcal{T}_{\text{eff}}$, we approximate $1 - f_{\nu,\text{non-eq}} \approx 1$ (since the amount of non-equilibrium neutrinos is small), multiplying (5.2) by p_ν and integrating over $d^3\mathbf{p}_\nu/(2\pi)^3$, we get

$$\partial_t \rho_{\nu,\text{non-eq}} + 4H\rho_{\nu,\text{non-eq}} \approx -1.3\gamma(\langle E_{\nu,\text{non-eq}}\rangle, T)\rho_{\nu,\text{non-eq}}(\langle E_{\nu,\text{non-eq}}\rangle - 3.1T) \quad (5.5)$$

Using then the relation

$$\partial_t \rho_{\nu,\text{non-eq}} = \partial_t \mathcal{T}_{\text{eff}}\partial_{\mathcal{T}_{\text{eff}}}\rho_{\nu,\text{non-eq}} = 4\frac{\rho_{\nu,\text{non-eq}}}{\mathcal{T}_{\text{eff}}}\partial_t \mathcal{T}_{\text{eff}} = 4\frac{\rho_{\nu,\text{non-eq}}}{\langle E_{\nu,\text{non-eq}}\rangle}\partial_t\langle E_{\nu,\text{non-eq}}\rangle,$$
$$(5.6)$$

following from the FD shape of the non-equilibrium neutrinos, and taking into account Eq. (5.4), we finally obtain

$$\partial_t\langle E_{\nu,\text{non-eq}}\rangle + H\langle E_{\nu,\text{non-eq}}\rangle \approx -0.4\Gamma_{\text{E loss}}(\langle E_{\nu,\text{non-eq}}\rangle, T)(\langle E_{\nu,\text{non-eq}}\rangle - 3.15 \cdot T)$$
$$(5.7)$$

A.2 Weak $p \leftrightarrow n$ conversion rates

When calculating the $p \leftrightarrow n$ conversion rates we follow the procedure of [194]. Namely, we start from the matrix elements for the process $n + \nu \to p + l$:

$$\mathcal{M}_{n\nu\to pl} = \frac{G_F}{\sqrt{2}}J_\mu^{np}(q)\bar{u}_l(p_l)\gamma^\mu(1-\gamma_5)u_\nu(p_\nu), \quad (5.8)$$

where $q^2 = -(p_p - p_n)^2$ is the squared transferred momentum, $J_\mu^{np}(q)$ is the matrix element of the hadronic charged current,

$$J_\mu^{np} = \cos(\theta_c)\bar{u}_p(p_p)\Gamma_\mu(p_p, p_n)u_n(p_n) \quad (5.9)$$

Following [**Leitner2005**, 240, 155], we write

$$\Gamma_\mu(p_p, p_n) = \gamma_\mu(F_1^V(q^2) - \gamma_5 F^A(q^2)) + \frac{i}{2m_p}\sigma_{\mu\nu}q^\nu F_2^V(q^2) + \frac{q_\mu}{m_p}\gamma_5 F^P(q^2), \quad (5.10)$$

with $\sigma_{\mu\nu} = i[\gamma_\mu, \gamma_\nu]/2$. Having the squared matrix element $\overline{|\mathcal{M}_{n\nu\to pe}|^2}$ in terms of s, t, u invariants, we can calculate the other matrix elements for the $p \leftrightarrow n$ conversion:

$$\overline{|\mathcal{M}_{pe\to n\nu}|^2}(s,t,u) = \frac{1}{2}\overline{|\mathcal{M}_{n\nu\to pe}|^2}(s,t,u),$$

$$\overline{|\mathcal{M}_{p\nu\to ne}|^2}(s,t,u) = 2\overline{|\mathcal{M}_{ne\to p\nu}|^2}(s,t,u) = \overline{|\mathcal{M}_{n\nu\to pe}|^2}(u,t,s) \quad (5.11)$$

Then, we calculate $2 \to 2$ conversion rates under an assumption that incoming nucleons are at rest (as $T \ll m_{n/p}$), but taking into account the non-zero momentum transfer and Coulomb correction:

$$\Gamma_{Nl\to N'l'} = \frac{1}{64\pi^3}\frac{g_l}{m_N}\int f_l(E_l)(1 - f_{l'}(E_{l'}))\overline{|\mathcal{M}_{Nl\to N'l'}|^2}F_c(E_e)dE_l dE_l', \quad (5.12)$$

where N/N' denote nucleons and l' electron (positron) or electron (anti)neutrino, f_l is the distribution function of the lepton l, and F_c is a Coulomb correction being non-zero only if electron and proton are both in the initial or final states:

$$F_c(E_e) = \frac{x}{1 + e^{-x}}, \quad \text{where} \quad x = \frac{2\pi\alpha_{\text{EM}}}{v_e}, \quad (5.13)$$

where E_e and v_e are the electron energy and velocity correspondingly.

The rate $\Gamma_{n\to pe\bar\nu}$ does not give the free neutron decay rate $\Gamma_{n,\text{decay}}^{-1} = 880.2$ s, which is due to unaccounted corrections (see [176]). We multiply it by a constant ≈ 1.047, which calibrates it on $\Gamma_{n,\text{decay}}$ (see also [194]).

A.3 Nucleon form factors

The form factors entering (5.8) are

$$F^A(q^2) = \frac{g_A}{(1 + q^2/m_A^2)^2}, \quad F^P(q^2) = \frac{2m_p^2}{q^2 + m_\pi^2}F_A(q^2), \quad (5.14)$$

$$F_1^V(q^2) = \frac{G_E^p(q^2) - G_E^n(q^2) + \tau(G_M^p(q^2) - G_M^n(q^2))}{1 + \tau}, \quad (5.15)$$

$$F_2^V(q^2) = \frac{G_M^p(q^2) - G_M^n(q^2) - (G_E^p(q^2) - G_E^n(q^2))}{1 + \tau}, \quad (5.16)$$

where $\tau = q^2/(4m_p^2)$, and $G_{E/P}$ are electric and magnetic form factors. In dipole approximation they read

$$G_E^p(q^2) \approx G_D(q^2), \quad G_E^n(q^2) = -\mu_n \frac{a\tau}{1+b\tau} G_D(q^2), \qquad (5.17)$$

$$G_M^p(q^2) \approx \mu_p G_D(q^2), \quad G_M^n(q^2) = \mu_n G_D(q^2), \quad G_D(q^2) = \frac{1}{\left(1 + \frac{q^2}{m_V^2}\right)^2}, \quad (5.18)$$

with $\mu_p = 2.793$, $\mu_n = -1.913$ are magnetic moments of the proton and the neutron. The other phenomenological parameters entering the form factors are given in Table 5.1.

Parameter	a	b	m_A	m_V	g_A
Value	0.942	4.61	1.026 GeV	0.843 GeV	1.26

Table 5.1: Values of parameters entering the form factors (5.14) (5.18).

A.4 Abundance of HNLs

We consider the following equation for the evolution of the HNL number density-to-entropy ratio $\mathcal{Y}_N(T) \equiv n_N/s$:

$$\frac{d\mathcal{Y}_N}{dt} = -\Gamma_N^{\text{int}}(T)(\mathcal{Y}_N - \mathcal{Y}_{N,\text{eq}}), \qquad (5.19)$$

where $\mathcal{Y}_{N,\text{eq}} = n_{N,\text{eq}}/s(T)$ is the abundance at equilibrium (i.e., calculated using the Fermi-Dirac distribution), and Γ_N^{int} is the total rate of processes $A + N \to B + C$:

$$\Gamma_N^{\text{int}} = \sum_{A,B,C} \Gamma_{A+N \to B+C}, \quad \Gamma_{A+N \to B+C}(T) = n_A(T) \cdot \langle \sigma_{NA \to BC} v \rangle \qquad (5.20)$$

We approximate the cross sections by the expression

$$\langle \sigma_{NA \to BC} v \rangle \approx \sigma_{NA \to BC} v \Big|_{s = \langle s_{NA} \rangle}, \qquad (5.21)$$

with $\langle s_{NA} \rangle$ being the average invariant mass of the colliding particles. We assume that rates with light quarks u, d, s in the initial states rapidly turn off at the temperature $T \simeq 150$ MeV of the QCD confinement. For the temperature behavior of g_* we used a fit from [134]. We use the matrix elements of

all relevant processes with HNLs from [194]. The behavior of the rates for particular masses of the HNL is shown in Fig. A.2.
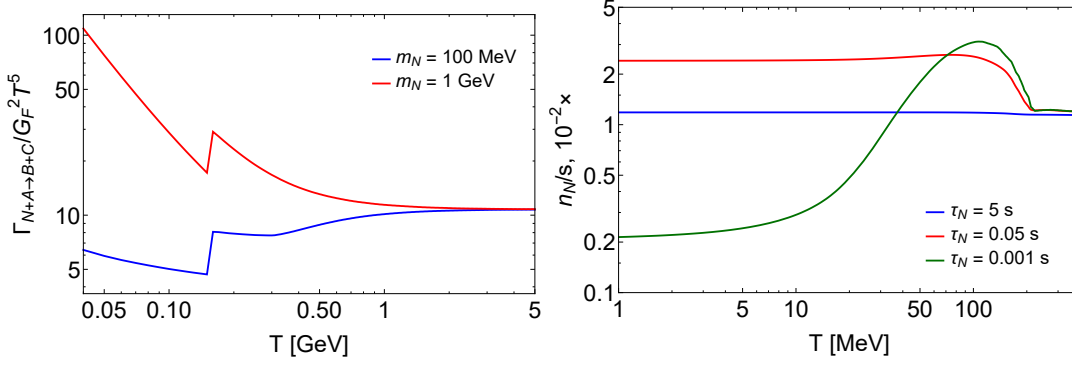
Figure A.2: *Left panel*: the temperature behavior of the ratio $\Gamma^{\text{int}}/G_F^2 T^5$ for HNLs with masses $m_N = 100$ MeV and 1 GeV, where Γ^{int} is the rate keeping HNLs in the equilibrium. The matter suppression of the mixing angle (Eq. (4.51)) is not taken into account here. A sudden jump around $T \simeq 150$ MeV is caused by the disappearance of $u/d/s$ quarks from the primordial plasma due to the QCD confinement. For 100 MeV HNLs, the ratio changed slowly in the considered temperature domain, whereas for 1 GeV HNLs it starts increasing below $T = 1$ GeV since the HNL mass changes the temperature behavior of the rate. *Right panel*: the behavior of the ratio $\mathcal{Y}_N = n_N/s$ versus temperature for the HNL mass $m_N = 150$ MeV and various lifetimes. For large lifetimes (=small couplings) HNLs decouple at $T_- \gg m_N$, and the abundance is given by the UR estimate (4.61). For lower $\tau_N \sim 0.1$ s HNLs decouple in the regime $T_- \simeq m_N$, but the Boltzmann suppression is compensated by the rapid drop of g_*, see Fig. A.3, and the abundance increases. With further decrease the Boltzmann suppression becomes the dominant factor, and the abundance decreases.

The temperature behavior of $\mathcal{Y}_N$ for particular lifetimes is shown in Fig. A.2. Having the solution, we define the HNL abundance as

$$Y_N = \mathcal{Y}_N(T = 5 \text{ MeV}), \tag{5.22}$$

see Fig. 4.12.

In Fig. A.3 we compare our estimates for the temperature behavior of n_N with predictions of pyBBN [194]. For the whole mass range of interest 50 MeV $< m_N < 1$ GeV and the most of lifetimes the agreement between the approaches the abundances differ by at most by a factor of 0.6.
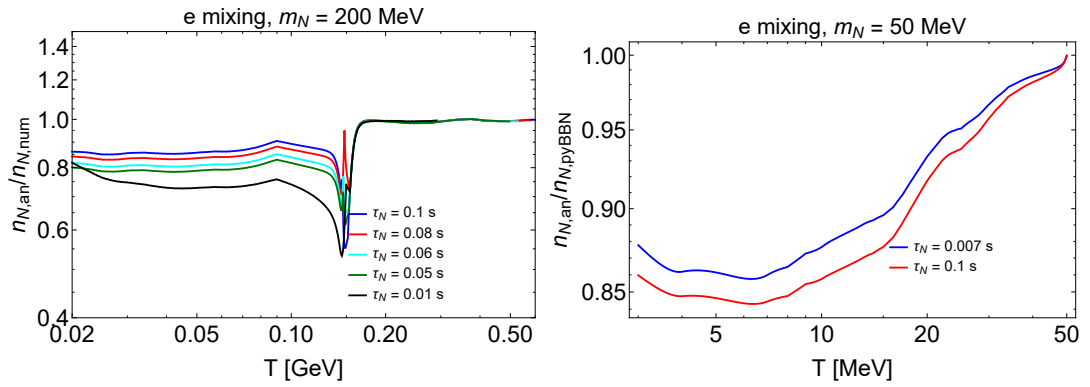
Figure A.3: The behavior of the ratio of the HNL number density obtained in our work and in [194] for masses $m_N = 200$ MeV (left panel) and $m_N = 50$ MeV (right panel). The jump at $T \simeq 150$ MeV for $m_N = 200$ MeV is caused by the implementation of the instant QCD confinement in pyBBN.

Bibliography

[1] Roel Aaij *et al.* „Test of lepton universality in beauty-quark decays". In: (2021). arXiv: `2103.11769 [hep-ex]`.

[2] J. Aalbers, F. Agostini, M. Alfonsi, *et al.* „DARWIN: towards the ultimate dark matter detector". In: *Journal of Cosmology and Astroparticle Physics* 2016.11 (Nov. 2016), pp. 017–017.

[3] A. Abada *et al.* „FCC-hh: The Hadron Collider". In: *Eur. Phys. J. ST* 228.4 (2019), pp. 755–1107.

[4] A. Abada, C. Biggio, F. Bonnet, M.B. Gavela, and T. Hambye. „Low energy effects of neutrino masses". In: *JHEP* 12 (2007), p. 061. arXiv: `0707.4058 [hep-ph]`.

[5] Kevork N. Abazajian. „Sterile neutrinos in cosmology". In: *Phys. Rept.* 711-712 (2017), pp. 1–28. arXiv: `1705.01837 [hep-ph]`.

[6] Kevork N. Abazajian, Maxim Markevitch, Savvas M. Koushiappas, and Ryan C. Hickox. „Limits on the Radiative Decay of Sterile Neutrino Dark Matter from the Unresolved Cosmic and Soft X-ray Backgrounds". In: *Phys. Rev. D* 75 (2007), p. 063511. arXiv: `astro-ph/0611144`.

[7] Kevork Abazajian, George M. Fuller, and Mitesh Patel. „Sterile neutrino hot, warm, and cold dark matter". In: *Phys. Rev.* D64 (2001), p. 023501. arXiv: `astro-ph/0101524 [astro-ph]`.

[8] Kevork Abazajian, George M. Fuller, and Wallace H. Tucker. „Direct detection of warm dark matter in the X-ray". In: *Astrophys. J.* 562 (2001), pp. 593–604. arXiv: `astro-ph/0106002 [astro-ph]`.

[9] K. Abe *et al.* „Indication of Electron Neutrino Appearance from an Accelerator-produced Off-axis Muon Neutrino Beam". In: *Phys. Rev. Lett.* 107 (2011), p. 041801. arXiv: `1106.2822 [hep-ex]`.

[10]   B. Abi *et al.* „Measurement of the Positive Muon Anomalous Magnetic Moment to 0.46 ppm". In: *Phys. Rev. Lett.* 126.14 (2021), p. 141801. arXiv: `2104.03281` [`hep-ex`].

[11]   Babak Abi *et al.* „Deep Underground Neutrino Experiment (DUNE), Far Detector Technical Design Report, Volume II: DUNE Physics". In: (2020). arXiv: `2002.03005` [`hep-ex`].

[12]   P. Abreu *et al.* „Search for neutral heavy leptons produced in Z decays". In: *Z. Phys. C* 74 (1997). [Erratum: Z.Phys.C 75, 580 (1997)], pp. 57–71.

[13]   P. Adamson *et al.* „Improved search for muon-neutrino to electron-neutrino oscillations in MINOS". In: *Phys. Rev. Lett.* 107 (2011), p. 181802. arXiv: `1108.0015` [`hep-ex`].

[14]   P. A. R. Ade *et al.* „Planck 2013 results. XVI. Cosmological parameters". In: *Astron. Astrophys.* 571 (2014), A16. arXiv: `1303.5076` [`astro-ph.CO`].

[15]   N. Aghanim *et al.* „Planck 2018 results. VI. Cosmological parameters". In: *Astron. Astrophys.* 641 (2020), A6. arXiv: `1807.06209` [`astro-ph.CO`].

[16]   M. Aglietta *et al.* „On the event observed in the Mont Blanc Underground Neutrino observatory during the occurrence of Supernova 1987a". In: *Europhys. Lett.* 3 (1987), pp. 1315–1320.

[17]   Prateek Agrawal *et al.* „Feebly-Interacting Particles:FIPs 2020 Workshop Report". In: (Feb. 2021). arXiv: `2102.12143` [`hep-ph`].

[18]   A. Aguilar-Arevalo *et al.* „Improved search for heavy neutrinos in the decay $\pi \to e\nu$". In: *Phys. Rev. D* 97.7 (2018), p. 072012. arXiv: `1712.03275` [`hep-ex`].

[19]   M. Aguilar *et al.* „The Alpha Magnetic Spectrometer (AMS) on the international space station: Part II - Results from the first seven years". In: *Phys. Rept.* 894 (2021), pp. 1–116.

[20]   C. Ahdida *et al.* „Sensitivity of the SHiP experiment to Heavy Neutral Leptons". In: *JHEP* 04 (2019), p. 077. arXiv: `1811.00930` [`hep-ph`].

[21]   C. Ahdida *et al.* „The experimental facility for the Search for Hidden Particles at the CERN SPS". In: *JINST* 14.03 (2019), P03025. arXiv: `1810.06880` [`physics.ins-det`].

[22] J. K. Ahn *et al.* „Observation of Reactor Electron Antineutrino Disappearance in the RENO Experiment". In: *Phys. Rev. Lett.* 108 (2012), p. 191802. arXiv: `1204.0626 [hep-ex]`.

[23] Ian J. R. Aitchison. „Supersymmetry and the MSSM: An Elementary introduction". In: (2005). arXiv: `hep-ph/0505105 [hep-ph]`.

[24] Evgeny K. Akhmedov, V. A. Rubakov, and A. Yu. Smirnov. „Baryogenesis via neutrino oscillations". In: *Phys. Rev. Lett.* 81 (1998), pp. 1359–1362. arXiv: `hep-ph/9803255 [hep-ph]`.

[25] Sergey Alekhin *et al.* „A facility to Search for Hidden Particles at the CERN SPS: the SHiP physics case". In: *Rept. Prog. Phys.* 79.12 (2016), p. 124201. arXiv: `1504.04855 [hep-ph]`.

[26] E. N. Alekseev, L. N. Alekseeva, I. V. Krivosheina, and V. I. Volchenko. „Detection of the neutrino signal from SN 1987A using the INR Baksan underground scintillation telescope". In: *European Southern Observatory Conference and Workshop Proceedings*. Ed. by I. J. Danziger. Vol. 26. European Southern Observatory Conference and Workshop Proceedings. 1987, pp. 237–247.

[27] Dennis Alp *et al.* „The 30-Year Search for the Compact Object in SN 1987A". In: *Astrophys. J.* 864.2 (2018), p. 174. arXiv: `1805.04526 [astro-ph.HE]`.

[28] F. P. An *et al.* „Observation of electron-antineutrino disappearance at Daya Bay". In: *Phys. Rev. Lett.* 108 (2012), p. 171803. arXiv: `1203.1669 [hep-ex]`.

[29] C. D. Anderson. „The Positive Electron". In: *Phys. Rev.* 43 (1933), pp. 491–494.

[30] Thomas Appelquist, Hsin-Chia Cheng, and Bogdan A. Dobrescu. „Bounds on universal extra dimensions". In: *Phys. Rev.* D64 (2001), p. 035002. arXiv: `hep-ph/0012100 [hep-ph]`.

[31] E. Aprile, J. Aalbers, F. Agostini, M. Alfonsi, F. D. Amaro, M. Anthony, B. Antunes, F. Arneodo, M. Balata, and et al. „The XENON1T dark matter experiment". In: *The European Physical Journal C* 77.12 (Dec. 2017).

[32] E. Aprile, K. Arisaka, F. Arneodo, *et al.* „The XENON100 dark matter experiment". In: *Astroparticle Physics* 35.9 (Apr. 2012), pp. 573–590.

[33]   Carlos A. Argüelles, Vedran Brdar, and Joachim Kopp. „Production of keV Sterile Neutrinos in Supernovae: New Constraints and Gamma Ray Observables". In: *Phys. Rev.* D99.4 (2019), p. 043012. arXiv: `1605.00654 [hep-ph]`.

[34]   A.V. Artamonov *et al.* „Search for heavy neutrinos in $K^+ \to \mu^+ \nu_H$ decays". In: *Phys. Rev. D* 91.5 (2015). [Erratum: Phys.Rev.D 91, 059903 (2015)], p. 052001. arXiv: `1411.3963 [hep-ex]`.

[35]   Takehiko Asaka, Steve Blanchet, and Mikhail Shaposhnikov. „The nuMSM, dark matter and neutrino masses". In: *Phys. Lett.* B631 (2005), pp. 151–156. arXiv: `hep-ph/0503065 [hep-ph]`.

[36]   Takehiko Asaka, Mikko Laine, and Mikhail Shaposhnikov. „Lightest sterile neutrino abundance within the nuMSM". In: *JHEP* 01 (2007). [Erratum: JHEP02,028(2015)], p. 091. arXiv: `hep-ph/0612182 [hep-ph]`.

[37]   Takehiko Asaka, Mikko Laine, and Mikhail Shaposhnikov. „On the hadronic contribution to sterile neutrino production". In: *JHEP* 06 (2006), p. 053. arXiv: `hep-ph/0605209`.

[38]   Takehiko Asaka and Mikhail Shaposhnikov. „The νMSM, dark matter and baryon asymmetry of the universe". In: *Phys. Lett.* B620 (2005), pp. 17–26. arXiv: `hep-ph/0505013 [hep-ph]`.

[39]   Anupama Atre, Tao Han, Silvia Pascoli, and Bin Zhang. „The Search for Heavy Majorana Neutrinos". In: *JHEP* 05 (2009), p. 030. arXiv: `0901.3589 [hep-ph]`.

[40]   Erik Aver, Keith A. Olive, and Evan D. Skillman. „The effects of He I $\lambda 10830$ on helium abundance determinations". In: *JCAP* 1507 (2015), p. 011. arXiv: `1503.08146 [astro-ph.CO]`.

[41]   Howard Baer, Vernon Barger, Shadman Salam, Dibyashree Sengupta, and Kuver Sinha. „Status of weak scale supersymmetry after LHC Run 2 and ton-scale noble liquid WIMP searches". In: *Eur. Phys. J. ST* 229.21 (2020), pp. 3085–3141. arXiv: `2002.03013 [hep-ph]`.

[42]   Peter Ballett, Tommaso Boschi, and Silvia Pascoli. „Heavy Neutral Leptons from low-scale seesaws at the DUNE Near Detector". In: *JHEP* 03 (2020), p. 111. arXiv: `1905.00284 [hep-ph]`.

[43]   Philip Bambade *et al.* „The International Linear Collider: A Global Project". In: (2019). arXiv: `1903.01629 [hep-ex]`.

[44]   T. M. Bania, Robert T. Rood, and Dana S. Balser. „The cosmological density of baryons from observations of 3He+ in the Milky Way". In: *Nature* 415 (2002), pp. 54–57.

[45]   Nitsan Bar, Kfir Blum, and Guido D'Amico. „Is there a supernova bound on axions?" In: (2019). arXiv: `1907.05020 [hep-ph]`.

[46]   M. Barkovich, J. C. D'Olivo, and R. Montemayor. „Active sterile neutrino oscillations and pulsar kicks". In: *Phys. Rev.* D70 (2004), p. 043005. arXiv: `hep-ph/0402259 [hep-ph]`.

[47]   J. Beacham *et al.* „Physics Beyond Colliders at CERN: Beyond the Standard Model Working Group Report". In: *J. Phys. G* 47.1 (2020), p. 010501. arXiv: `1901.09966 [hep-ex]`.

[48]   John F. Beacom, R. N. Boyd, and A. Mezzacappa. „Black hole formation in core collapse supernovae and time-of-flight measurements of the neutrino masses". In: *Phys. Rev.* D63 (2001), p. 073011. arXiv: `astro-ph/0010398 [astro-ph]`.

[49]   K. G. Begeman, A. H. Broeils, and R. H. Sanders. „Extended rotation curves of spiral galaxies : dark haloes and modified dynamics." In: *Mon. Not. Roy. Astron. Soc.* 249 (Apr. 1991), p. 523.

[50]   Jack J. Bennett, Gilles Buldgen, Marco Drewes, and Yvonne Y.Y. Wong. „Towards a precision calculation of the effective number of neutrinos N_{eff} in the Standard Model I: The QED equation of state". In: *JCAP* 03 (2020), p. 003. arXiv: `1911.04504 [hep-ph]`.

[51]   Jack J. Bennett, Gilles Buldgen, Pablo F. de Salas, Marco Drewes, Stefano Gariazzo, Sergio Pastor, and Yvonne Y.Y. Wong. „Towards a precision calculation of N_{eff} in the Standard Model II: Neutrino decoupling in the presence of flavour oscillations and finite-temperature QED". In: (Dec. 2020). arXiv: `2012.02726 [hep-ph]`.

[52]   F. Bergsma *et al.* „A Search for Decays of Heavy Neutrinos in the Mass Range 0.5-{GeV} to 2.8-{GeV}". In: *Phys. Lett. B* 166 (1986), pp. 473–478.

[53]   G. Bernardi *et al.* „FURTHER LIMITS ON HEAVY NEUTRINO COUPLINGS". In: *Phys. Lett. B* 203 (1988), pp. 332–334.

[54]   G. Bernardi *et al.* „Search for Neutrino Decay". In: *Phys. Lett. B* 166 (1986), pp. 479–483.

[55]   Gianfranco Bertone and Dan Hooper. „History of dark matter". In: *Rev. Mod. Phys.* 90.4 (2018), p. 045002. arXiv: 1605.04909 [astro-ph.CO].

[56]   S. M. Bilenky. „Neutrino in Standard Model and beyond". In: *Phys. Part. Nucl.* 46.4 (2015), pp. 475–496. arXiv: 1501.00232 [hep-ph].

[57]   Tobias Binder, Laura Covi, Ayuki Kamada, Hitoshi Murayama, Tomo Takahashi, and Naoki Yoshida. „Matter Power Spectrum in Hidden Neutrino Interacting Dark Matter Models: A Closer Look at the Collision Term". In: *JCAP* 1611 (2016), p. 043. arXiv: 1602.07624 [hep-ph].

[58]   Kfir Blum and Doron Kushnir. „Neutrino Signal of Collapse-induced Thermonuclear Supernovae: the Case for Prompt Black Hole Formation in SN1987A". In: *Astrophys. J.* 828.1 (2016), p. 31. arXiv: 1601.03422 [astro-ph.HE].

[59]   Kyrylo Bondarenko, Alexey Boyarsky, Dmitry Gorbunov, and Oleg Ruchayskiy. „Phenomenology of GeV-scale Heavy Neutral Leptons". In: *JHEP* 11 (2018), p. 032. arXiv: 1805.08567 [hep-ph].

[60]   Kyrylo Bondarenko, Alexey Boyarsky, Juraj Klaric, Oleksii Mikulenko, Oleg Ruchayskiy, Vsevolod Syvolap, and Inar Timiryasov. „An allowed window for heavy neutral leptons below the kaon mass". In: (Jan. 2021). arXiv: 2101.09255 [hep-ph].

[61]   A. Boyarsky, M. Drewes, T. Lasserre, S. Mertens, and O. Ruchayskiy. „Sterile Neutrino Dark Matter". In: *Prog. Part. Nucl. Phys.* 104 (2019), pp. 1–45. arXiv: 1807.07938 [hep-ph].

[62]   Alexey Boyarsky, Denys Malyshev, Andrey Neronov, and Oleg Ruchayskiy. „Constraining DM properties with SPI". In: *Mon. Not. Roy. Astron. Soc.* 387 (2008), p. 1345. arXiv: 0710.4922 [astro-ph].

[63]   Alexey Boyarsky, A. Neronov, O. Ruchayskiy, M. Shaposhnikov, and I. Tkachev. „Where to find a dark matter sterile neutrino?" In: *Phys. Rev. Lett.* 97 (2006), p. 261302. arXiv: astro-ph/0603660.

[64]   Alexey Boyarsky, A. Neronov, Oleg Ruchayskiy, and M. Shaposhnikov. „Constraints on sterile neutrino as a dark matter candidate from the diffuse x-ray background". In: *Mon. Not. Roy. Astron. Soc.* 370 (2006), pp. 213–218. arXiv: astro-ph/0512509.

[65] Alexey Boyarsky, A. Neronov, Oleg Ruchayskiy, and Mikhail Shaposhnikov. „Restrictions on parameters of sterile neutrino dark matter from observations of galaxy clusters". In: *Phys. Rev. D* 74 (2006), p. 103506. arXiv: `astro-ph/0603368`.

[66] Alexey Boyarsky, Maksym Ovchynnikov, Oleg Ruchayskiy, and Vsevolod Syvolap. „Improved BBN constraints on Heavy Neutral Leptons". In: (Aug. 2020). arXiv: `2008.00749 [hep-ph]`.

[67] Alexey Boyarsky, Maksym Ovchynnikov, Nashwan Sabti, and Vsevolod Syvolap. „When FIMPs Decay into Neutrinos: The N_{eff} Story". In: (Mar. 2021). arXiv: `2103.09831 [hep-ph]`.

[68] Alexey Boyarsky, Oleg Ruchayskiy, and Dmytro Iakubovskyi. „A Lower bound on the mass of Dark Matter particles". In: *JCAP* 03 (2009), p. 005. arXiv: `0808.3902 [hep-ph]`.

[69] Alexey Boyarsky, Oleg Ruchayskiy, Dmytro Iakubovskyi, and Jeroen Franse. „Unidentified Line in X-Ray Spectra of the Andromeda Galaxy and Perseus Galaxy Cluster". In: *Phys. Rev. Lett.* 113 (2014), p. 251301. arXiv: `1402.4119 [astro-ph.CO]`.

[70] Alexey Boyarsky, Oleg Ruchayskiy, and Maxim Markevitch. „Constraints on parameters of radiatively decaying dark matter from the galaxy cluster 1E0657-56". In: *Astrophys. J.* 673 (2008), pp. 752–757. arXiv: `astro-ph/0611168`.

[71] Alexey Boyarsky, Oleg Ruchayskiy, and Mikhail Shaposhnikov. „The Role of sterile neutrinos in cosmology and astrophysics". In: *Ann. Rev. Nucl. Part. Sci.* 59 (2009), pp. 191–214. arXiv: `0901.0011 [hep-ph]`.

[72] Maruša Bradač, Tim Schrabback, Thomas Erben, *et al.* „Dark Matter and Baryons in the X-Ray Luminous Merging Galaxy Cluster RX J1347.51145". In: *The Astrophysical Journal* 681.1 (July 2008), pp. 187–196.

[73] G.C. Branco, W. Grimus, and L. Lavoura. „The Seesaw Mechanism in the Presence of a Conserved Lepton Number". In: *Nucl. Phys. B* 312 (1989), pp. 492–508.

[74] D.I. Britton *et al.* „Improved search for massive neutrinos in pi+ —> e+ neutrino decay". In: *Phys. Rev. D* 46 (1992), pp. 885–887.

[75] G. E. Brown, S. W. Bruenn, and J. C. Wheeler. „Is There a Black-Hole in Supernova 1987A". In: *Comments on Astrophysics* 16 (1992), p. 153.

[76] Esra Bulbul, Maxim Markevitch, Adam Foster, Randall K. Smith, Michael Loewenstein, and Scott W. Randall. „Detection of An Unidentified Emission Line in the Stacked X-ray spectrum of Galaxy Clusters". In: *Astrophys. J.* 789 (2014), p. 13. arXiv: 1402.2301 [astro-ph.CO].

[77] A. Burrows. „On detecting stellar collapse with neutrinos". In: *Astrophys. J.* 283 (Aug. 1984), pp. 848–852.

[78] Adam Burrows and David Vartanyan. „Core-Collapse Supernova Explosion Theory". In: *Nature* 589.7840 (2021), pp. 29–39. arXiv: 2009.14157 [astro-ph.SR].

[79] Miguel D. Campos and Werner Rodejohann. „Testing keV sterile neutrino dark matter in future direct detection experiments". In: *Phys. Rev.* D94.9 (2016), p. 095010. arXiv: 1605.02918 [hep-ph].

[80] Laurent Canetti, Marco Drewes, and Mikhail Shaposhnikov. „Matter and Antimatter in the Universe". In: *New J. Phys.* 14 (2012), p. 095012. arXiv: 1204.4186 [hep-ph].

[81] Fu-Guang Cao. „Neutrino masses from lepton and quark mass relations and neutrino oscillations". In: *Phys. Rev. D* 85 (2012), p. 113003. arXiv: 1205.4068 [hep-ph].

[82] T. K. Charles *et al.* „The Compact Linear Collider (CLIC) - 2018 Summary Report". In: *CERN Yellow Rep. Monogr.* 2 (2018). Ed. by P. N. Burrows, N. Catalan Lasheras, L. Linssen, M. Petric, A. Robson, D. Schulte, E. Sicking, and S. Stapnes. arXiv: 1812.06018 [physics.acc-ph].

[83] B. T. Cleveland, Timothy Daily, Raymond Davis Jr., James R. Distel, Kenneth Lande, C. K. Lee, Paul S. Wildenhain, and Jack Ullman. „Measurement of the solar electron neutrino flux with the Homestake chlorine detector". In: *Astrophys. J.* 496 (1998), pp. 505–526.

[84] Timothy Clifton, Pedro G. Ferreira, Antonio Padilla, and Constantinos Skordis. „Modified Gravity and Cosmology". In: *Phys. Rept.* 513 (2012), pp. 1–189. arXiv: 1106.2476 [astro-ph.CO].

[85] Douglas Clowe, Marusa Bradac, Anthony H. Gonzalez, Maxim Markevitch, Scott W. Randall, Christine Jones, and Dennis Zaritsky. „A direct empirical proof of the existence of dark matter". In: *Astrophys. J. Lett.* 648 (2006), pp. L109–L113. arXiv: astro-ph/0608407.

[86] Pilar Coloma, Enrique Fernández-Martınez, Manuel González-López, Josu Hernández-Garcıa, and Zarko Pavlovic. „GeV-scale neutrinos: interactions with mesons and DUNE sensitivity". In: (July 2020). arXiv: 2007.03701 [hep-ph].

[87] Eduardo Cortina Gil *et al.* „Search for heavy neutral lepton production in K^+ decays to positrons". In: *Phys. Lett. B* 807 (2020), p. 135599. arXiv: 2005.09575 [hep-ex].

[88] Richard H. Cyburt. „Primordial nucleosynthesis for the new cosmology: Determining uncertainties and examining concordance". In: *Phys. Rev. D* 70 (2004), p. 023505. arXiv: astro-ph/0401091.

[89] Richard H. Cyburt, John R. Ellis, Brian D. Fields, and Keith A. Olive. „Updated nucleosynthesis constraints on unstable relic particles". In: *Phys. Rev. D* 67 (2003), p. 103521. arXiv: astro-ph/0211258.

[90] Sacha Davidson and Alejandro Ibarra. „A Lower bound on the right-handed neutrino mass from leptogenesis". In: *Phys. Lett. B* 535 (2002), pp. 25–32. arXiv: hep-ph/0202239.

[91] Sacha Davidson, Enrico Nardi, and Yosef Nir. „Leptogenesis". In: *Phys. Rept.* 466 (2008), pp. 105–177. arXiv: 0802.2962 [hep-ph].

[92] M. Dhibar, I. Mazumdar, G. Anil Kumar, A. K. Rhine Kumar, S. M. Patel, P. B. Chavan, C. D. Bagdia, and L. C. Trivedi. „Measurement of cross sections and astrophysical S-factors for d(p,gamma)3He reaction at astrophysically relevant energies using a large volume LaBr3:Ce detector". In: (June 2018). arXiv: 1806.05809 [nucl-ex].

[93] Eleonora Di Valentino, Olga Mena, Supriya Pan, Luca Visinelli, Weiqiang Yang, Alessandro Melchiorri, David F. Mota, Adam G. Riess, and Joseph Silk. „In the Realm of the Hubble tension − a Review of Solutions". In: (Mar. 2021). arXiv: 2103.01183 [astro-ph.CO].

[94] Scott Dodelson and Lawrence M. Widrow. „Sterile-neutrinos as dark matter". In: *Phys. Rev. Lett.* 72 (1994), pp. 17–20. arXiv: hep-ph/9303287 [hep-ph].

[95] A. D. Dolgov. „Neutrinos in cosmology". In: *Phys. Rept.* 370 (2002), pp. 333–535. arXiv: hep-ph/0202122.

[96] A. D. Dolgov and M. Fukugita. „Nonequilibrium effect of the neutrino distribution on primordial helium synthesis". In: *Phys. Rev.* D46 (1992), pp. 5378–5382.

[97]   A. D. Dolgov, S. H. Hansen, G. Raffelt, and D. V. Semikoz. „Cosmo-
logical and astrophysical bounds on a heavy sterile neutrino and the
KARMEN anomaly". In: *Nucl. Phys.* B580 (2000), pp. 331–351. arXiv:
`hep-ph/0002223 [hep-ph]`.

[98]   A.D. Dolgov and S.H. Hansen. „Massive sterile neutrinos as warm
dark matter". In: *Astropart. Phys.* 16 (2002), pp. 339–344. arXiv:
`hep-ph/0009083`.

[99]   A.D. Dolgov, S.H. Hansen, G. Raffelt, and D.V. Semikoz. „Heavy sterile
neutrinos: Bounds from big bang nucleosynthesis and SN1987A". In:
Nucl. Phys. B 590 (2000), pp. 562–574. arXiv: `hep-ph/0008138`.

[100]   Mingyi Dong *et al.* „CEPC Conceptual Design Report: Volume 2 -
Physics & Detector". In: (2018). Ed. by Joao Barreiro Guimaraes
da Costa, Yuanning Gao, Shan Jin, Jianming Qian, Christopher G.
Tully, Charles Young, Lian-Tao Wang, Manqi Ruan, Hongbo Zhu, Qun
Ouyang, *et al.* arXiv: `1811.10545 [hep-ex]`.

[101]   M. Drewes *et al.* „A White Paper on keV Sterile Neutrino Dark Matter".
In: *JCAP* 01 (2017), p. 025. arXiv: `1602.04816 [hep-ph]`.

[102]   Marco Drewes, Juraj Klarić, and Philipp Klose. „On Lepton Number
Violation in Heavy Neutrino Decays at Colliders". In: *JHEP* 19 (2020),
p. 032. arXiv: `1907.13034 [hep-ph]`.

[103]   K. Eguchi *et al.* „First results from KamLAND: Evidence for reactor
anti-neutrino disappearance". In: *Phys. Rev. Lett.* 90 (2003), p. 021802.
arXiv: `hep-ex/0212021`.

[104]   S. Eijima, M. Shaposhnikov, and I. Timiryasov. „Parameter space of
baryogenesis in the νMSM". In: *JHEP* 07 (2019), p. 077. arXiv: `1808.`
`10833 [hep-ph]`.

[105]   Shintaro Eijima, Mikhail Shaposhnikov, and Inar Timiryasov. „Freeze-
in generation of lepton asymmetries after baryogenesis in the νMSM".
In: (Nov. 2020). arXiv: `2011.12637 [hep-ph]`.

[106]   John Ellis. „Where is Particle Physics Going?" In: *Int. J. Mod. Phys. A*
32.34 (2017), p. 1746001. arXiv: `1704.02821 [hep-ph]`.

[107]   Richard Keith Ellis *et al.* „Physics Briefing Book: Input for the European
Strategy for Particle Physics Update 2020". In: (Oct. 2019). arXiv:
`1910.11775 [hep-ex]`.

[108] K. Enqvist, K. Kainulainen, and Mark J. Thomson. „Stringent cosmological bounds on inert neutrino mixing". In: *Nucl. Phys.* B373 (1992), pp. 498–528.

[109] Miguel Escudero Abenza. „Precision early universe thermodynamics made simple: N_{eff} and neutrino decoupling in the Standard Model and beyond". In: *JCAP* 05 (2020), p. 048. arXiv: `2001.04466 [hep-ph]`.

[110] P. Esposito, N. Rea, D. Lazzati, M. Matsuura, R. Perna, and J. A. Pons. „Can a bright and energetic X-ray pulsar be hiding amid the debris of SN 1987A?" In: *Astrophys. J.* 857.1 (2018), p. 58. arXiv: `1803.04692 [astro-ph.HE]`.

[111] Ivan Esteban, M.C. Gonzalez-Garcia, Michele Maltoni, Thomas Schwetz, and Albert Zhou. „The fate of hints: updated global analysis of three-flavor neutrino oscillations". In: *JHEP* 09 (2020), p. 178. arXiv: `2007.14792 [hep-ph]`.

[112] Benoit Famaey and Stacy McGaugh. „Modified Newtonian Dynamics (MOND): Observational Phenomenology and Relativistic Extensions". In: *Living Rev. Rel.* 15 (2012), p. 10. arXiv: `1112.3960 [astro-ph.CO]`.

[113] Anthony Fradette and Maxim Pospelov. „BBN for the LHC: constraints on lifetimes of the Higgs portal scalars". In: *Phys. Rev. D* 96.7 (2017), p. 075033. arXiv: `1706.01920 [hep-ph]`.

[114] Y. Fukuda *et al.* „Evidence for oscillation of atmospheric neutrinos". In: *Phys. Rev. Lett.* 81 (1998), pp. 1562–1567. arXiv: `hep-ex/9807003`.

[115] M. Fukugita and T. Yanagida. „Baryogenesis Without Grand Unification". In: *Phys. Lett. B* 174 (1986), pp. 45–47.

[116] George M. Fuller, Alexander Kusenko, Irina Mocioiu, and Silvia Pascoli. „Pulsar kicks from a dark-matter sterile neutrino". In: *Phys. Rev.* D68 (2003), p. 103002. arXiv: `astro-ph/0307267 [astro-ph]`.

[117] George M. Fuller, Alexander Kusenko, and Kalliopi Petraki. „Heavy sterile neutrinos and supernova explosions". In: *Phys. Lett.* B670 (2009), pp. 281–284. arXiv: `0806.4273 [astro-ph]`.

[118] M. B. Gavela, T. Hambye, D. Hernandez, and P. Hernandez. „Minimal Flavour Seesaw Models". In: *JHEP* 09 (2009), p. 038. arXiv: `0906.1461 [hep-ph]`.

[119] Murray Gell-Mann, Pierre Ramond, and Richard Slansky. „Complex Spinors and Unified Theories". In: *Conf. Proc. C* 790927 (1979), pp. 315–321. arXiv: `1306.4669` [`hep-th`].

[120] Graciela B. Gelmini, Masahiro Kawasaki, Alexander Kusenko, Kai Murai, and Volodymyr Takhistov. „Big Bang Nucleosynthesis constraints on sterile neutrino and lepton asymmetry of the Universe". In: *JCAP* 09 (2020), p. 051. arXiv: `2005.06721` [`hep-ph`].

[121] J. Ghiglieri and M. Laine. „Improved determination of sterile neutrino dark matter spectrum". In: *JHEP* 11 (2015), p. 171. arXiv: `1506.06752` [`hep-ph`].

[122] R. Gilmozzi, A. Cassatella, J. Clavel, C. Fransson, R. Gonzalez, C. Gry, N. Panagia, A. Talavera, and W. Wamsteker. „The progenitor of SN1987A". In: *Nature* 328.6128 (July 1987), pp. 318–320.

[123] M.C. Gonzalez-Garcia and J.W.F. Valle. „Fast Decaying Neutrinos and Observable Flavor Violation in a New Class of Majoron Models". In: *Phys. Lett. B* 216 (1989), pp. 360–366.

[124] Dmitry Gorbunov, Igor Krasnov, Yury Kudenko, and Sergey Suvorov. „Heavy Neutral Leptons from kaon decays in the SHiP experiment". In: *Phys. Lett. B* 810 (2020), p. 135817. arXiv: `2004.07974` [`hep-ph`].

[125] Dmitry Gorbunov and Alexander Panin. „On the minimal active-sterile neutrino mixing in seesaw type I mechanism with sterile neutrinos at GeV scale". In: *Phys. Rev.* D89.1 (2014), p. 017302. arXiv: `1312.2887` [`hep-ph`].

[126] Dmitry Gorbunov and Mikhail Shaposhnikov. „How to find neutral leptons of the νMSM?" In: *JHEP* 10 (2007). [Erratum: JHEP11,101(2013)], p. 015. arXiv: `0705.1729` [`hep-ph`].

[127] Evgueni Goudzovski. *Search for heavy neutral lepton production at the NA62 experiment*. Preliminary results presented at ICHEP 2020, 28 July 2020 to 6 August 2020, Prague.

[128] C. Gustavino. „Measurements of nuclear cross sections of interest in BBN with the LUNA experiment". In: *Frontier Objects in Astrophysics and Particle Physics*. Ed. by F. Giovannelli and G. Mannocchi. Jan. 2007, p. 191.

[129]   M. M. Guzzo, J. Bellandi, and V. M. Aquino. „Nonadiabatic neutrino oscillations reexamined“. In: *Phys. Rev. D* 49 (3 Feb. 1994), pp. 1404–1408.

[130]   Jun Hidaka and George M. Fuller. „Dark matter sterile neutrinos in stellar collapse: Alteration of energy/lepton number transport and a mechanism for supernova explosion enhancement“. In: *Phys. Rev.* D74 (2006), p. 125015. arXiv: `astro-ph/0609425 [astro-ph]`.

[131]   Jun Hidaka and George M. Fuller. „Sterile Neutrino-Enhanced Supernova Explosions“. In: *Phys. Rev.* D76 (2007), p. 083516. arXiv: `0706.3886 [astro-ph]`.

[132]   Christopher Hill, Craig Hogan, Steve Holmes, Young-Kee Kim, Joseph Lykken, Chris Quigg, and Katie Yurkewicz. „Fermilab: A plan for discovery“. In: (2011).

[133]   K. Hirata *et al.* „Observation of a Neutrino Burst from the Supernova SN 1987a“. In: *Phys. Rev. Lett.* 58 (1987). [,727(1987)], pp. 1490–1493.

[134]   Lars Husdal. „On Effective Degrees of Freedom in the Early Universe“. In: *Galaxies* 4.4 (2016), p. 78. arXiv: `1609.04979 [astro-ph.CO]`.

[135]   Y. I. Izotov, T. X. Thuan, and N. G. Guseva. „A new determination of the primordial He abundance using the He i λ10830 Å emission line: cosmological implications“. In: *Mon. Not. Roy. Astron. Soc.* 445.1 (2014), pp. 778–793. arXiv: `1408.6953 [astro-ph.CO]`.

[136]   H. -Thomas Janka, Tobias Melson, and Alexander Summa. „Physics of Core-Collapse Supernovae in Three Dimensions: a Sneak Preview“. In: *Ann. Rev. Nucl. Part. Sci.* 66 (2016), pp. 341–375. arXiv: `1602.05576 [astro-ph.SR]`.

[137]   H.-T. Janka. „Neutrino Emission from Supernovae“. In: *Handbook of Supernovae*. Ed. by A. W. Alsabti and P. Murdin. Springer International Publishing AG, 2017, p. 1575. arXiv: `1702.08713 [astro-ph.HE]`.

[138]   Hans-Thomas Janka, Annop Wongwathanarat, and Michael Kramer. „Supernova Fallback as Origin of Neutron Star Spins and Spin-kick Alignment“. In: (Apr. 2021). arXiv: `2104.07493 [astro-ph.HE]`.

[139]   Oliver Just, Robert Bollig, Hans-Thomas Janka, Martin Obergaulinger, Robert Glas, and Shigehiro Nagataki. „Core-collapse supernova simulations in one and two dimensions: comparison of codes and approximations". In: *Mon. Not. Roy. Astron. Soc.* 481.4 (2018), pp. 4786–4814. arXiv: `1805.03953 [astro-ph.HE]`.

[140]   K. Kainulainen, J. Maalampi, and J. T. Peltoniemi. „Inert neutrinos in supernovae". In: *Nucl. Phys.* B358 (1991), pp. 435–446.

[141]   Mathias Th. Keil, Georg G. Raffelt, and Hans-Thomas Janka. „Monte Carlo Study of Supernova Neutrino Spectra Formation". In: *The Astrophysical Journal* 590.2 (June 2003), pp. 971–991.

[142]   Mathias Thorsten Keil. „Supernova neutrino spectra and applications to flavor oscillations". Other thesis. Aug. 2003. arXiv: `astro-ph/0308228`.

[143]   Jörn Kersten and Alexei Yu. Smirnov. „Right-Handed Neutrinos at CERN LHC and the Mechanism of Neutrino Mass Generation". In: *Phys. Rev. D* 76 (2007), p. 073005. arXiv: `0705.3221 [hep-ph]`.

[144]   Juraj Klaric, Mikhail Shaposhnikov, and Inar Timiryasov. „Reconciling resonant leptogenesis and baryogenesis via neutrino oscillations". In: (2021). arXiv: `2103.16545 [hep-ph]`.

[145]   Edward W. Kolb and Michael S. Turner. *The Early Universe*. Vol. 69. 1990.

[146]   Jan Kretzschmar. „Standard Model physics at the LHC". In: *From My Vast Repertoire ...: Guido Altarelli's Legacy*. Ed. by Aharon Levy, Stefano Forte, and Giovanni Ridolfi. 2019. arXiv: `1803.10800 [hep-ex]`.

[147]   Alexander Kusenko, Bhabani Prasad Mandal, and Alok Mukherjee. „Delayed pulsar kicks from the emission of sterile neutrinos". In: *Phys. Rev.* D77 (2008), p. 123009. arXiv: `0801.4734 [astro-ph]`.

[148]   Alexander Kusenko and Gino Segre. „Neutral current induced neutrino oscillations in a supernova". In: *Phys. Lett.* B396 (1997), pp. 197–200. arXiv: `hep-ph/9701311 [hep-ph]`.

[149]   V. A. Kuzmin, V. A. Rubakov, and M. E. Shaposhnikov. „On the Anomalous Electroweak Baryon Number Nonconservation in the Early Universe". In: *Phys. Lett. B* 155 (1985), p. 36.

[150]   M. Laine and M. Shaposhnikov. „Sterile neutrino dark matter as a consequence of nuMSM-induced lepton asymmetry". In: *JCAP* 0806 (2008), p. 031. arXiv: `0804.4543 [hep-ph]`.

[151] Paul Langacker, Jacques P. Leveille, and Jon Sheiman. „On the Detection of Cosmological Neutrinos by Coherent Scattering". In: *Phys. Rev.* D27 (1983), p. 1228.

[152] J. M. Lattimer and M. Prakash. „Neutron star structure and the equation of state". In: *Astrophys. J.* 550 (2001), p. 426. arXiv: `astro-ph/0002232 [astro-ph]`.

[153] James M. Lattimer. „Neutron Stars". In: *eConf* C0507252 (2005), p. L007.

[154] Matthias Liebendoerfer, M. Rampp, H. -Th. Janka, and A. Mezzacappa. „Supernova simulations with Boltzmann neutrino transport: A Comparison of methods". In: *Astrophys. J.* 620 (2005), pp. 840–860. arXiv: `astro-ph/0310662 [astro-ph]`.

[155] C. H. Llewellyn Smith. „Neutrino Reactions at Accelerator Energies". In: *Phys. Rept.* 3 (1972), pp. 261–379.

[156] Michael Loewenstein, Alexander Kusenko, and Peter L. Biermann. „New Limits on Sterile Neutrinos from Suzaku Observations of the Ursa Minor Dwarf Spheroidal Galaxy". In: *Astrophys. J.* 700 (2009), pp. 426–435. arXiv: `0812.2710 [astro-ph]`.

[157] Thomas J. Loredo and Don Q. Lamb. „Bayesian analysis of neutrinos observed from supernova SN-1987A". In: *Phys. Rev.* D65 (2002), p. 063002. arXiv: `astro-ph/0107260 [astro-ph]`.

[158] L. Ma, H. J. Karwowski, C. R. Brune, Z. Ayer, T. C. Black, J. C. Blackmon, E. J. Ludwig, M. Viviani, A. Kievsky, and R. Schiavilla. „Measurements of ^{1}H$(d \to, \gamma)^3$He and ^{2}H$(p \to, \gamma)^3$He at very low energies". In: *Phys. Rev. C* 55 (2 Feb. 1997), pp. 588–596.

[159] Ziro Maki, Masami Nakagawa, and Shoichi Sakata. „Remarks on the unified model of elementary particles". In: *Prog. Theor. Phys.* 28 (1962), pp. 870–880.

[160] Philippe Mermod. „Prospects of the SHiP and NA62 experiments at CERN for hidden sector searches". In: *PoS* NuFact2017 (2017), p. 139. arXiv: `1712.01768 [hep-ex]`.

[161] D. G. Michael *et al.* „Observation of muon neutrino disappearance with the MINOS detectors and the NuMI neutrino beam". In: *Phys. Rev. Lett.* 97 (2006), p. 191801. arXiv: `hep-ex/0607088`.

[162] S. P. Mikheev and A. Yu. Smirnov. „Resonance Amplification of Oscillations in Matter and Spectroscopy of Solar Neutrinos". In: *Sov. J. Nucl. Phys.* 42 (1985). [Yad. Fiz.42,1441(1985)], pp. 913–917.

[163] Peter Minkowski. „$\mu \rightarrow e\gamma$ at a Rate of One Out of 10^9 Muon Decays?" In: *Phys. Lett. B* 67 (1977), pp. 421–428.

[164] R.N. Mohapatra and J.W.F. Valle. „Neutrino Mass and Baryon Number Nonconservation in Superstring Models". In: *Phys. Rev. D* 34 (1986), p. 1642.

[165] Rabindra N. Mohapatra and Goran Senjanovic. „Neutrino Mass and Spontaneous Parity Nonconservation". In: *Phys. Rev. Lett.* 44 (1980), p. 912.

[166] Bernhard Müller. „The Core-Collapse Supernova Explosion Mechanism". In: *IAU Symp.* 329 (2016), pp. 17–24. arXiv: `1702.06940 [astro-ph.SR]`.

[167] K. Nomoto and M. Hashimoto. „Presupernova evolution of massive stars." In: *Phys. Rept.* 163.1 (Jan. 1988), pp. 13–36.

[168] Dirk Notzold and Georg Raffelt. „Neutrino Dispersion at Finite Temperature and Density". In: *Nucl. Phys. B* 307 (1988), pp. 924–936.

[169] H. Nunokawa, J. T. Peltoniemi, Anna Rossi, and J. W. F. Valle. „Supernova bounds on resonant active sterile neutrino conversions". In: *Phys. Rev.* D56 (1997), pp. 1704–1713. arXiv: `hep-ph/9702372 [hep-ph]`.

[170] Evan O'Connor *et al.* „Global Comparison of Core-Collapse Supernova Simulations in Spherical Symmetry". In: *J. Phys.* G45.10 (2018), p. 104001. arXiv: `1806.04175 [astro-ph.HE]`.

[171] Paraficz, D., Kneib, J.-P., Richard, J., Morandi, A., Limousin, M., Jullo, E., and Martinez, J. „The Bullet cluster at its best: weighing stars, gas, and dark matter". In: *A&A* 594 (2016), A121.

[172] Stephen J. Parke. „Nonadiabatic Level Crossing in Resonant Neutrino Oscillations". In: *Phys. Rev. Lett.* 57 (1986), pp. 1275–1278.

[173] P. J. E. Peebles. „Growth of the nonbaryonic dark matter theory". In: *Nature Astron.* 1.3 (2017), p. 0057. arXiv: `1701.05837 [astro-ph.CO]`.

[174] Antonio Peimbert, Manuel Peimbert, and Valentina Luridiana. „The primordial helium abundance and the number of neutrino families". In: *Rev. Mex. Astron. Astrofis.* 52.2 (2016), pp. 419–424. arXiv: `1608.02062 [astro-ph.CO]`.

[175] J. T. Peltoniemi. „Resonance transitions to inert neutrinos in supernovae." In: *Astron. Astrophys.* 254 (Feb. 1992), pp. 121–126.

[176] Cyril Pitrou, Alain Coc, Jean-Philippe Uzan, and Elisabeth Vangioni. „Precision big bang nucleosynthesis with improved Helium-4 predictions". In: *Phys. Rept.* 754 (2018), pp. 1–66. arXiv: `1801.08023` `[astro-ph.CO]`.

[177] B. Pontecorvo. „Mesonium and anti-mesonium". In: *Sov. Phys. JETP* 6 (1957), p. 429.

[178] B. Pontecorvo. „Neutrino Experiments and the Problem of Conservation of Leptonic Charge". In: *Zh. Eksp. Teor. Fiz.* 53 (1967), pp. 1717–1725.

[179] Maxim Pospelov and Josef Pradler. „Big Bang Nucleosynthesis as a Probe of New Physics". In: *Ann. Rev. Nucl. Part. Sci.* 60 (2010), pp. 539–568. arXiv: `1011.1054 [hep-ph]`.

[180] Maxim Pospelov and Josef Pradler. „Metastable GeV-scale particles as a solution to the cosmological lithium problem". In: *Phys. Rev.* D82 (2010), p. 103514. arXiv: `1006.4172 [hep-ph]`.

[181] G. G. Raffelt. *Stars as laboratories for fundamental physics.* Chicago, USA: Univ. Pr. (1996) 664 p, 1996.

[182] G. Raffelt and G. Sigl. „Neutrino flavor conversion in a supernova core". In: *Astropart. Phys.* 1 (1993), pp. 165–184. arXiv: `astro-ph/9209005` `[astro-ph]`.

[183] Georg G. Raffelt. „Astrophysical methods to constrain axions and other novel particle phenomena". In: *Phys. Rept.* 198 (1990), pp. 1–113.

[184] Georg G. Raffelt. „Particle physics from stars". In: *Ann. Rev. Nucl. Part. Sci.* 49 (1999), pp. 163–216. arXiv: `hep-ph/9903472 [hep-ph]`.

[185] Georg G. Raffelt and Shun Zhou. „Supernova bound on keV-mass sterile neutrinos reexamined". In: *Phys. Rev.* D83 (2011), p. 093014. arXiv: `1102.5124 [hep-ph]`.

[186] Tomasz Rembiasz, Martin Obergaulinger, Manuel Masip, M. Ángeles Pérez-Garcia, Miguel-Ángel Aloy, and Conrado Albertus. „Heavy sterile neutrinos in stellar core-collapse". In: *Phys. Rev.* D98.10 (2018), p. 103010. arXiv: `1806.03300 [astro-ph.HE]`.

[187] Signe Riemer-Sørensen, Steen H. Hansen, and Kristian Pedersen. „Sterile neutrinos in the Milky Way: Observational constraints". In: *Astrophys. J. Lett.* 644 (2006), pp. L33–L36. arXiv: `astro-ph/0603661`.

[188] Alejandro Rivero and Andre Gsponer. „The Strange formula of Dr. Koide". In: (May 2005). arXiv: `hep-ph/0505220`.

[189] Matts Roos. „Astrophysical and Cosmological Probes of Dark Matter". In: *Journal of Modern Physics* 03.09 (2012), pp. 1152–1171.

[190] Ananda Roy and Mikhail Shaposhnikov. „Resonant production of the sterile neutrino dark matter and fine-tunings in the [nu]MSM". In: *Phys. Rev. D* 82 (2010), p. 056014. arXiv: `1006.4008 [hep-ph]`.

[191] Valery A. Rubakov and Dmitry S. Gorbunov. *Introduction to the Theory of the Early Universe: Hot big bang theory*. Singapore: World Scientific, 2017.

[192] Oleg Ruchayskiy and Artem Ivashko. „Experimental bounds on sterile neutrino mixing angles". In: *JHEP* 06 (2012), p. 100. arXiv: `1112.3319 [hep-ph]`.

[193] Oleg Ruchayskiy and Artem Ivashko. „Restrictions on the lifetime of sterile neutrinos from primordial nucleosynthesis". In: *JCAP* 10 (2012), p. 014. arXiv: `1202.2841 [hep-ph]`.

[194] Nashwan Sabti, Andrii Magalich, and Anastasiia Filimonova. „An Extended Analysis of Heavy Neutral Leptons during Big Bang Nucleosynthesis". In: *JCAP* 11 (2020), p. 056. arXiv: `2006.07387 [hep-ph]`.

[195] A. D. Sakharov. „Violation of CP Invariance, C asymmetry, and baryon asymmetry of the universe". In: *Pisma Zh. Eksp. Teor. Fiz.* 5 (1967). [JETP Lett.5,24(1967); Sov. Phys. Usp.34,no.5,392(1991); Usp. Fiz. Nauk161,no.5,61(1991)], pp. 32–35.

[196] L. Sbordone *et al.* „The metal-poor end of the Spite plateau. 1: Stellar parameters, metallicities and lithium abundances". In: *Astron. Astrophys.* 522 (2010), A26. arXiv: `1003.4510 [astro-ph.GA]`.

[197] J. Schechter and J.W.F. Valle. „Neutrino Decay and Spontaneous Violation of Lepton Number". In: *Phys. Rev. D* 25 (1982), p. 774.

[198] J. Schechter and J.W.F. Valle. „Neutrino Masses in SU(2) x U(1) Theories". In: *Phys. Rev. D* 22 (1980), p. 2227.

[199] Sezen Sekmen. „Beyond the Standard Model Physics at the High Luminosity LHC". In: *PoS* ICHEP2018 (2019), p. 283. arXiv: `1902.03942 [hep-ex]`.

[200] M. E. Shaposhnikov. „Standard model solution of the baryogenesis problem". In: *Phys. Lett.* B277 (1992). [Erratum: Phys. Lett.B282,483(1992)], pp. 324–330.

[201] Mikhail Shaposhnikov. „A Possible symmetry of the nuMSM". In: *Nucl. Phys.* B763 (2007), pp. 49–59. arXiv: `hep-ph/0605047 [hep-ph]`.

[202] Mikhail Shaposhnikov. „Is there a new physics between electroweak and Planck scales?" In: *Astroparticle Physics: Current Issues, 2007 (APCI07) Budapest, Hungary, June 21-23, 2007*. 2007. arXiv: `0708.3550 [hep-th]`.

[203] X. Shi and G. Sigl. „A Type II supernovae constraint on electron-neutrino - sterile-neutrino mixing". In: *Phys. Lett.* B323 (1994). [Erratum: Phys. Lett.B324,516(1994)], pp. 360–366. arXiv: `hep-ph/9312247 [hep-ph]`.

[204] Xiang-Dong Shi and George M. Fuller. „A New dark matter candidate: Nonthermal sterile neutrinos". In: *Phys. Rev. Lett.* 82 (1999), pp. 2832–2835. arXiv: `astro-ph/9810076 [astro-ph]`.

[205] M. Shifman. „Musings on the Current Status of HEP". In: *Mod. Phys. Lett. A* 35.07 (2020), p. 2030003. arXiv: `2001.00101 [physics.hist-ph]`.

[206] Andrew W. Steiner, Matthias Hempel, and Tobias Fischer. „Core-collapse supernova equations of state based on neutron star observations". In: *Astrophys. J.* 774 (2013), p. 17. arXiv: `1207.2184 [astro-ph.SR]`.

[207] Andrew W. Steiner, James M. Lattimer, and Edward F. Brown. „The Neutron Star Mass-Radius Relation and the Equation of State of Dense Matter". In: *Astrophys. J. Lett.* 765 (2013), p. L5. arXiv: `1205.6871 [nucl-th]`.

[208] L. Stodolsky. „Treatment of neutrino oscillations in a thermal environment". In: *Phys. Rev. D* 36 (8 Oct. 1987), pp. 2273–2277.

[209] Alessandro Strumia and Francesco Vissani. „Neutrino masses and mixings and...". In: (June 2006). arXiv: `hep-ph/0606054`.

[210] Anna M. Suliga, Irene Tamborra, and Meng-Ru Wu. „Lifting the core-collapse supernova bounds on keV-mass sterile neutrinos". In: *JCAP* 08 (2020), p. 018. arXiv: `2004.11389 [astro-ph.HE]`.

[211] Anna M. Suliga, Irene Tamborra, and Meng-Ru Wu. „Tau lepton asymmetry by sterile neutrino emission – Moving beyond one-zone supernova models". In: (2019). arXiv: 1908.11382 [astro-ph.HE].

[212] R. Svoboda, C. B. Bratton, D. Casper, A. Ciocio, and R. Claus. „Neutrinos from SN1987A in the IMB detector". In: *European Southern Observatory Conference and Workshop Proceedings*. Ed. by I. J. Danziger. Vol. 26. European Southern Observatory Conference and Workshop Proceedings. 1987, pp. 229–235.

[213] Jaco de Swart, Gianfranco Bertone, and Jeroen van Dongen. „How Dark Matter Came to Matter". In: (2017). [Nature Astron.1,0059(2017)]. arXiv: 1703.00013 [astro-ph.CO].

[214] Vsevolod Syvolap, Oleg Ruchayskiy, and Alexey Boyarsky. „Resonance production of keV sterile neutrinos in core-collapse supernovae and lepton number diffusion". In: (Sept. 2019). arXiv: 1909.06320 [hep-ph].

[215] Irene Tamborra, Georg G. Raffelt, Lorenz Hudepohl, and Hans-Thomas Janka. „Impact of eV-mass sterile neutrinos on neutrino-driven supernova outflows". In: *JCAP* 1201 (2012), p. 013. arXiv: 1110.2104 [astro-ph.SR].

[216] Irene Tamborra, Georg Raffelt, Florian Hanke, Hans-Thomas Janka, and Bernhard Mueller. „Neutrino emission characteristics and detection opportunities based on three-dimensional supernova simulations". In: *Phys. Rev.* D90.4 (2014), p. 045032. arXiv: 1406.0006 [astro-ph.SR].

[217] M. Tanabashi *et al.* „Review of Particle Physics". In: *Phys. Rev.* D98.3 (2018), p. 030001.

[218] *The Garching Core-Collapse Supernova Archive*. https://wwwmpa.mpa-garching.mpg.de/ccsnarchive.

[219] Todd A. Thompson, Adam Burrows, and Jorge E. Horvath. „Mu and tau-neutrino thermalization and production in supernovae: Processes and time scales". In: *Phys. Rev.* C62 (2000), p. 035802. arXiv: astro-ph/0003054 [astro-ph].

[220] S. Tremaine and J. E. Gunn. „Dynamical Role of Light Neutral Leptons in Cosmology". In: *Phys. Rev. Lett.* 42 (1979), pp. 407–410.

[221] A. Vaitaitis *et al.* „Search for neutral heavy leptons in a high-energy neutrino beam". In: *Phys. Rev. Lett.* 83 (1999), pp. 4943–4946. arXiv: `hep-ex/9908011`.

[222] Mabel Valerdi, Antonio Peimbert, Manuel Peimbert, and Andrés Sixtos. „Determination of the Primordial Helium Abundance Based on NGC 346, an H II Region of the Small Magellanic Cloud". In: *Astrophys. J.* 876.2 (2019), p. 98. arXiv: `1904.01594 [astro-ph.GA]`.

[223] David Vartanyan, Adam Burrows, David Radice, Aaron M. Skinner, and Joshua Dolence. „A Successful 3D Core-Collapse Supernova Explosion Model". In: *Mon. Not. Roy. Astron. Soc.* 482.1 (2019), pp. 351–369. arXiv: `1809.05106 [astro-ph.HE]`.

[224] Francesco Vissani. „Do experiments suggest a hierarchy problem?" In: *Physical Review D* 57.11 (June 1998), pp. 7027–7030.

[225] MacKenzie L. Warren, Matthew Meixner, Grant Mathews, Jun Hidaka, and Toshitaka Kajino. „Sterile neutrino oscillations in core-collapse supernovae". In: *Phys. Rev.* D90.10 (2014), p. 103007. arXiv: `1405.6101 [astro-ph.HE]`.

[226] MacKenzie Warren, Grant J. Mathews, Matthew Meixner, Jun Hidaka, and Toshitaka Kajino. „Impact of sterile neutrino dark matter on core-collapse supernovae". In: *Int. J. Mod. Phys.* A31.25 (2016), p. 1650137. arXiv: `1603.05503 [astro-ph.HE]`.

[227] Casey R. Watson, John F. Beacom, Hasan Yuksel, and Terry P. Walker. „Direct X-ray Constraints on Sterile Neutrino Warm Dark Matter". In: *Phys. Rev. D* 74 (2006), p. 033009. arXiv: `astro-ph/0605424`.

[228] Steven Weinberg. „Baryon and Lepton Nonconserving Processes". In: *Phys. Rev. Lett.* 43 (1979), pp. 1566–1570.

[229] Achim Weiss. „The Progenitor of SN 1987A: Uncertain Evolution of a 20 M Star". In: *Astrophys. J.* 339 (Apr. 1989), p. 365.

[230] Joachim Wolf. „The KATRIN neutrino mass experiment". In: *Nuclear Instruments and Methods in Physics Research Section A: Accelerators, Spectrometers, Detectors and Associated Equipment* 623.1 (Nov. 2010), pp. 442–444.

[231] L. Wolfenstein. „Neutrino Oscillations in Matter". In: *Phys. Rev.* D17 (1978), pp. 2369–2374.

[232] S. E. Woosley and Thomas A. Weaver. „The Evolution and Explosion of Massive Stars. II. Explosive Hydrodynamics and Nucleosynthesis". In: *Astrophys. J. Suppl.* 101 (Nov. 1995), p. 181.

[233] Meng-Ru Wu, Tobias Fischer, Lutz Huther, Gabriel Martinez-Pinedo, and Yong-Zhong Qian. „Impact of active-sterile neutrino mixing on supernova explosion and nucleosynthesis". In: *Phys. Rev.* D89.6 (2014), p. 061303. arXiv: 1305.2382 [astro-ph.HE].

[234] D. Wyler and L. Wolfenstein. „Massless Neutrinos in Left-Right Symmetric Models". In: *Nucl. Phys. B* 218 (1983), pp. 205–214.

[235] Zewei Xiong, Meng-Ru Wu, and Yong-Zhong Qian. „Active-Sterile Neutrino Oscillations in Neutrino-driven Winds: Implications for Nucleosynthesis". In: *Astrophys. J.* 880.2, 81 (Aug. 2019), p. 81. arXiv: 1904.09371 [astro-ph.HE].

[236] T. Yamazaki *et al.* „Search for Heavy Neutrinos in Kaon Decay". In: *Conf.Proc.C* 840719 (July 1984). Ed. by A. Meyer and E. Wieczorek, p. 262.

[237] Tsutomu Yanagida. „Horizontal gauge symmetry and masses of neutrinos". In: *Conf. Proc. C* 7902131 (1979). Ed. by Osamu Sawada and Akio Sugamoto, pp. 95–99.

[238] Naoki Yoshida. *Structure Formation in the Early Universe*. 2009. arXiv: 0906.4372 [astro-ph.CO].

[239] Hasan Yuksel, John F. Beacom, and Casey R. Watson. „Strong Upper Limits on Sterile Neutrino Warm Dark Matter". In: *Phys. Rev. Lett.* 101 (2008), p. 121301. arXiv: 0706.4084 [astro-ph].

[240] G. P. Zeller. „Low-energy neutrino cross-sections: Comparison of various Monte Carlo predictions to experimental data". In: *2nd International Workshop on Neutrino-Nucleus Interactions in the Few GeV Region (NuInt 02) Irvine, California, December 12-15, 2002*. 2003. arXiv: hep-ex/0312061 [hep-ex].

[241] Shun Zhou. „Supernova Bounds on keV-mass Sterile Neutrinos". In: *Int. J. Mod. Phys.* A30.13 (2015). [Adv. Ser. Direct. High Energy Phys.25,243(2015)], p. 1530033. arXiv: 1504.02729 [hep-ph].

[242] P. A. Zyla *et al.* „Review of Particle Physics". In: *PTEP* 2020.8 (2020), p. 083C01.